1506
UNIVERSITÀ
DEGLI STUDI
DI URBINO
CARLO BO

DIPARTIMENTO DI SCIENZE PURE E APPLICATE
(DISPEA)

Corso di Dottorato di Ricerca in Scienze di Base e Applicazioni
Curriculum Chimico
(ciclo XXXIII)

Electron paramagnetic resonance applications: from drug discovery to marine biology studies

Settore Scientifico Disciplinare: CHIM/02

RELATORI:
Chiar.mi Prof. Dr. Fco. Javier de La Mata de al Mata e Prof. Dr. Mauro Formica
CORRELATRICE:
Chiar.ma Prof.ssa Dr.ssa Maria Francesca Ottaviani

DOTTORANDO:
Dott. Riccardo Carloni

Anno accademico 2019-2020

Universidad de Alcalá

DEPARTAMENTO DE QUÍMICA ORGÁNICA Y QUÍMICA INORGÁNICA

Unidad Docente de Química Inorgánica

Electron paramagnetic resonance applications: from drug discovery to marine biology studies

DOCTORADO EN QUÍMICA
2020

Memoria presentada en la Universidad de Alcalá para optar al grado de Doctor en Química por el graduado:

RICCARDO CARLONI

Realizada bajo la supervisión del Prof. Dr. Fco. Javier de la Mata de la Mata y el Prof. Dr. Mauro Formica

To those who suffer, phytoplankton included

List of Abbreviations

The ordered abbreviations that will appear throughout this report are collected in alphabetical order, in order to facilitate the reading of the contents.

Abbreviation	Full Name
CW	Continuous Wave
CAT12	4-(dodecyl dimethyl ammonium)-1-oxyl-2,2,6,6-tetramethyl piperidine bromide
DMF	Dimethylformamide
DMPC	1,2-dimyristoyl-sn-glycero-3-phosphocholine
DMPG	1,2-dimyristoyl-sn- glycero-3-phospho-rac-(1-glycerol) sodium salt
DMSO	Dimethyl sulfoxide
DPH	1,6-diphenyl-1,3,5-hexatriene
DS	Dense Shell
EPR	Electron Paramagnetic Resonance
ESR	Electron Spin Resonance
FTIR	Fourier transform infrared spectroscopy
L	Ligand
LEC	1,2-Diacyl-sn-glycero-3-phosphocholine 3-sn-Phosphatidylcholine
M	Metal
Me	Methyl
MTT	3-(4,5-Dimethylthiazol-2-yl)-2,5-diphenyltetrazolium bromide
MW	Molecular Weight
NMR	Nuclear Magnetic Resonance
OS	Open Shell
PAMAM	Polyamidoamine
PBMC	Peripheral Blood Mononuclear Cells
PBS	Phosphate Buffer Saline

PC3	Human Prostate Cancer cell line
PEG	Polyethylene glycol
PET	Polyethylene Terephthalates
PPI	Polypropilenimine
ppm	Parts per Million
ROS	Reactive Oxygen Species
rpm	Revolutions per Minute
THF	Tetrahydrofuran
TMA-DPH	N,N,N-trimethyl-4-(6-phenyl-1,3,5-hexatrien-1-yl) phenylammonium p-toluenesulfonate
UV-Vis	Ultraviolet–visible spectroscopy
WD	Wilson Disease
τ_c	Correlation Time
Δ**W**	Line Width

GENERAL INTRODUCTION

EPR Spectroscopy and Dendrimers

1 - INTRODUCTION AND GOALS

The main goal of this thesis was the *in-situ* characterization of novel nanomolecules, mainly dendrimers, and the study of the interactions occurring between species of biological interest for biomedical and environmental purposes. The characterization and interactions studies were mainly performed by means of the Electron Spin Resonance (ESR) technique, which provides unique and precious information about paramagnetic systems. With this mindset, we focused on the following objectives:

✓ The synthesis and characterization of novel carbosilane metallodendrimers for the treatment of various types of tumors;

✓ The study of the interaction between novel polyamidoamine glycodendrimers and membrane models in the presence of Cu(II) ions to develop a new treatment for Wilson's disease;

✓ The characterization of the physical interaction of phytoplankton with PET microplastics to explain a particular type of biological pollution in the Mediterranean Sea.

Since this is a thesis by a compendium of publications, chapters 1, 2, and 3 are composed of a dissertation comprising the main goals and conclusions on each topic, followed by the published articles.

This doctoral thesis is therefore developed as follows:

The General Introduction starts with a brief description of Electron Paramagnetic Resonance technique, how it was discovered, its theory, and applications. Math equations used in the computer simulation of the spectra will be shown and discussed, as well as the EPR devices used for this thesis. It follows an introduction about dendrimers, which is meant to be integrated by the detailed review in chapter 1.

- Chapter 1 is about the design, synthesis, characterization, and evaluation of the anticancer activity of carbosilane metallodendrimers. Several articles, here reported, have been published on this topic. This chapter is opened by a detailed review of the world of metallodendrimers, their current applications, and future prospects. Then, three more articles describing the activity of newly synthesized polymers belonging to this class are going to follow.

- Chapter 2 is about a new approach to Wilson's disease treatment. After a brief introduction about this rare pathology, a recently published article is going to describe the synthesis, characterization, and interaction with membrane models of novel glycodendrimers.

- Chapter 3 is about the evaluation of the physical interaction between PET plastics and phytoplankton. After an introduction describing the current issue of biological pollution in the Mediterranean Sea, an article describing our findings on the topic will close this short chapter.

Finally, in the general conclusions section, the most relevant conclusions of this work will be presented.

This thesis was born from the cooperation between Prof. Maria Francesca Ottaviani, Prof. F. Javier de la Mata, and their research groups, which I was lucky enough to take part in.

Moreover, several international groups took part in the development of this work, to whose researchers I direct my sincerest thanks:

- Prof. Dietmar Appelhans and Dr. Silvia Moreno Pinilla, from the Bioactive und responsive Polymers group of Leibniz Institute of Polymer Research, Dresden

- Prof. Vieri Fusi and Prof. Mauro Formica, from the Pure and Applied Sciences Department (DISPEA) of Urbino University

- Prof. Lucchetti, Dr. Barbara Canonico, Dr. Gemma Nasoni, Dr. Caterina Ciacci and Dr. Mariele Montanari, from the Pure and Applied Sciences Department (DISPEA) of Urbino University

- Prof. Penna, Dr. Casablanca and Dr. Samuela Cappellacci, from the Biomolecular Sciences Department (DISB) of Urbino University

2 - ELECTRON PARAMAGNETIC RESONANCE: THEORY AND APPLICATIONS

2.1 EPR

The Electron Paramagnetic Resonance technique is based on the absorption of electromagnetic radiation in the microwave field by a system containing unpaired electrons, immersed in an external magnetic field. It was discovered in the 1940s by Dr. Evgenij Zavojskij, [1] who for the first time observed the absorption of electromagnetic radiation by a $CuCl_2 \cdot 2H_2O$ crystal exposed to a static magnetic field. For many systems of chemical and biological interest, the analysis of EPR spectra is the only observation method capable of:

- ✓ Highlighting variations in the three-dimensional structure of a molecular aggregate;
- ✓ Studying the behavior of specific functional groups;
- ✓ Evaluating the dynamics of paramagnetic species and their environments. [2]

As already mentioned, the microwave radiation is absorbed by a paramagnetic system featuring one or more unpaired electrons ($S \neq 0$), immersed in a static magnetic field. The absorption is due to a degeneration of the electronic spin levels, removed by the static magnetic field, which is registered as a series of absorption bands characteristic for a specific chemical environment. The frequency of these radiations is compatible with the energy differences that characterize the spin levels. The most common paramagnetic systems are free radicals, molecules with an unpaired electron, or transition metal ions, such as Cu^{2+}, Mn^{2+}, Fe^{3+}, Cr^{3+}... displaying unpaired electrons.

The field of application, however, can also be extended to diamagnetic systems through the use of alien paramagnetic species in the form of spin probes or spin labels, sensitive to the surrounding in which they are introduced without perturbing it.

2.2 Electron's Physics

The electron is a charged subatomic particle, characterized by an orbital motion around the nucleus and a rotation movement around its axis. [3] It is therefore characterized by a spin angular momentum (S), represented by a vector whose direction coincides with that of the axis around which the rotation occurs and an orbital angular momentum (L), a vector oriented along the rotation axis and perpendicular to the rotation plane.

2.2.1 Orbital angular momentum

The angular momentum L of a particle mass m that travels a circular orbit of radius r with a velocity v, (Figure 3.2), can be expressed as follows:

$$L = mvr$$

However, since the electron follows the rules of quantum mechanics a more accurate way to express the angular momentum consists in taking into consideration the Schrodinger equation. The wave functions, describing the hydrogen atom, from whose resolution we obtain the orbital

(or azimuthal) quantum number l, ultimately determines the value of the orbital angular momentum L according to the relation:

$$L = \sqrt{l(l+1)}\,\hbar$$

In vector terms it is possible to observe the angular momentum vector that precedes along a z-axis:

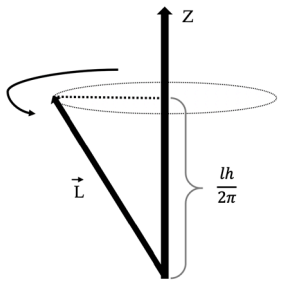

Figure 2.1 Component along the z-axis of the angular momentum vector

The component of the angular momentum vector along the z-axis is quantized and can therefore only take the values allowed for the magnetic quantum number ml (i.e. ml = l, l - 1, …, -L). For example, for l = 2 (orbitals d) we will have ml = +2, +1, 0, -1, -2. Associated with the orbital angular momentum there is an orbital magnetic moment μl which, for a charged particle q rotating on a circumference of radius r, can be expressed μl = I · A, where I is the current intensity and A is the area of the orbit.

2.2.2 Spin angular momentum

The intrinsic angular momentum theory, formulated in 1922 and confirmed in 1925,[4] postulates the existence of an angular momentum independent of electron's orbital characteristics. This introduced the concept of electron spin and therefore the need for a fourth quantum number for fully describing the electrons. These have an electron spin s = 1/2 and a spin angular momentum S:

$$S = \sqrt{s(s+1)}\,\hbar$$

Again, as for the orbital angular momentum, the component of the spin angular along the z-axis vector is quantized, and can assume (in units of ħ) only the values allowed by the spin quantum number $m_s = \pm ½$. As a charged particle, the electron generates an intrinsic magnetic field while rotating around its axis, whose direction depends on the direction of rotation.

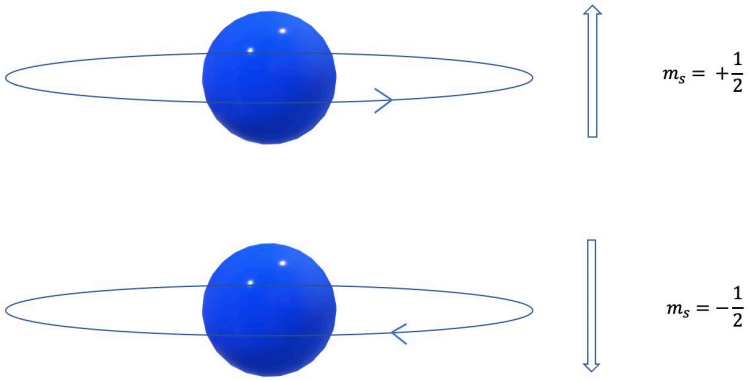

Figure 2.2 Values of the spin quantum magnetic number, m_s, in relation to the direction of rotation of the electron on its axis.

2.4 Interaction of the electron-spin magnetic moment with the applied field

Due to its spin magnetic moment μ_s, the electron interacts with the external magnetic field behaving like a tiny magnet, whose orientation is determined by the value of m_s.[5] This interaction is called Electron Zeeman Interaction, and the two configurations arising from it are the Zeeman levels of unpaired electrons. Therefore, by applying a static magnetic field in the Z direction a torsion force is generated, which produces a precession motion of the vectors m_s around the direction of H_0:

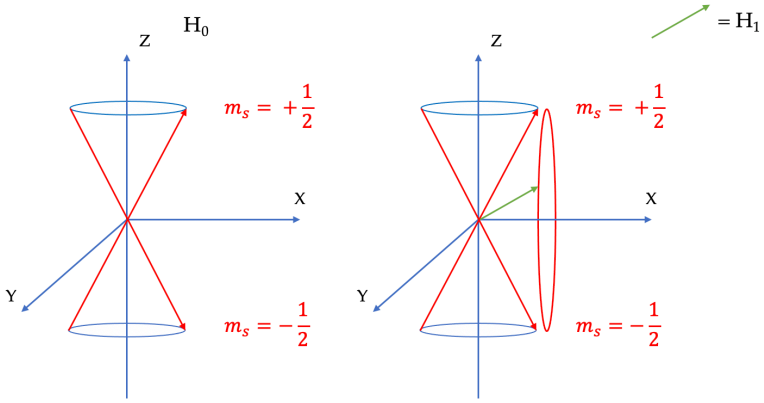

Figure 2.3 Precession motion of the vectors and precession motion around the Z axis that causes the exchange of position between the vectors m_s = + 1/2 and m_s = -1/2.

At all times the magnetic field vector, H_1, of the radiation will produce the same effect that H_0 had on the vectors m_s. A precession motion is generated around the Z-axis which causes the exchange of position between the vectors m_s = + 1/2 and m_s = - 1/2. This effect is referred to as the "state of resonance". Transitions from one state to another can take place in both directions giving rise to absorption ($E_\beta \rightarrow E_\alpha$) or emission ($E_\alpha \rightarrow E_\beta$). The system, as a whole, will absorb or emit energy depending on the number of transitions that occur during the exposure and, since the two

transitions are equally likely to occur, the population of the two energy levels plays a decisive role. Boltzmann's distribution law predicts a slight excess of population in the lower β level, so that we usually exploit the absorption phenomenon.

2.5 Spin Hamiltonian

If we introduce a paramagnetic species containing a nucleus with $I \neq 0$ into a magnetic field, the possible interactions between the external field and the magnetic moments of the two particles are three: [6]

- ✓ Electron Zeeman interaction (EZ_e): between electron spin and external magnetic field;
- ✓ Nuclear Zeeman interaction (EZ_n): between nuclear spin and external field;
- ✓ Hyperfine or Fermi's interaction (E_{hyper}): between electron and nuclear magnetic moments.

So, the total energy of our species can be written as the sum of these three terms:

$$E_{tot} = EZ_e + EZ_n + E_{hyper}$$

Assuming that the axes of the electronic spin and the nuclear spin coincide with the magnetic field, this expression can be expressed through the so-called spin Hamiltonian:

$$H_0 = \beta_e \tilde{\boldsymbol{B}}_0 \boldsymbol{g} \boldsymbol{S} / \hbar + \sum_{k=1}^{m} \tilde{\boldsymbol{S}} \boldsymbol{A}_k \boldsymbol{I}_k - \beta_n \sum_{k=1}^{m} g_{n,k} \tilde{\boldsymbol{B}}_0 \boldsymbol{I}_k / \hbar$$

All of these parameters are experimentally determinable, and allow to obtain information about the distribution of the unpaired electron and the structural properties of the paramagnetic specie.

2.6 Spectrum Parameters and Components

The main spectral components, obtainable through computer simulation, math calculation, or direct measurements on the spectrum are going to be explained in the next sections.

2.6.1 Parameter g

The position of the peak in the EPR spectrum is a function of the parameter g. This is related to the intensity of the coupling between the magnetic moment induced by the electron spin and the magnetic moment induced by the orbital motion. Depending on the molecular structure of the latter, the g factor reflects its anisotropic behavior and gets tensor properties. The parameter g is therefore a property of the paramagnetic specie and is used for its identification.

A system having a single unpaired electron, not interacting with other electrons nor nuclear spins, produces a single row of resonance, with a g value of *2.0023* which we denote by g_e. For any other substance, where there are contributions other than those of the free electron, the deviation of the parameter g from g_e depends on the aptitude of the applied field to induce electron currents in the sample and, therefore, gives information about the structure of the sample itself.

2.6.2 Parameter A: hyperfine interaction

The hyperfine interaction is a significant source of information extractable from an EPR spectrum. Enrico Fermi mentioned it for the first time in his explanation of the origin of the hyperfine structure

in atomic spectra. If the interaction of an unpaired electron with the applied magnetic field only caused the separation of the spin levels, the spectra obtained would all consist of a single line, and the only value obtainable from a spectrum would be the parameter g. However, other interactions enrich an EPR spectrum, such as that determined by the proximity to the electron spin magnetic dipole of the nuclei of the atoms present in the molecule, the "nuclear hyperfine interaction". Some nuclei possess, in fact, an intrinsic angular momentum which, as already mentioned, is associated with a magnetic moment. As a consequence, electrons are affected by the resulting magnetic field, which is also affected by neighboring nuclei. The equation gives the number of lines that are obtained by the interaction of the unpaired electron with *n* equivalent nuclei:

$$number\ of\ lines = 2\ nI + 1$$

Where I is the quantum number of nuclear spin and n is the number of equivalent interacting nuclei.

A nucleus with nuclear spin I = 1/2 causes the resonance peak to split due to the interaction of the electron magnetic moment with the nuclear magnetic moment, giving rise to two lines whose distance is given by the hyperfine constant, at:

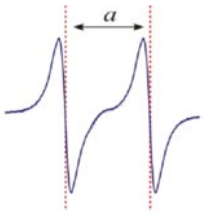

Figure 2.4 Doubling of the resonance peak due to the interaction of the electron magnetic moment with the nuclear magnetic moment, giving rise to two lines whose distance is given by the hyperfine constant A

These interactions are responsible for the separation of the resulting signal into several components, and are represented for each nucleus by the hyperfine tensor A. The tensor consists of an isotropic (or contact) component A° and an anisotropic component.

The anisotropic contribution originates from the classical interaction between two magnetic dipoles whose size depends on the relative orientation between the dipoles and the external field. A characteristic of this interaction is that of canceling itself out if it is averaged over all the possible orientations that the connecting line between the two dipoles can assume with respect to the direction of the applied magnetic field. Therefore, in fluid solutions in which the rotational diffusion motion is fast enough to allow the radical to assume all possible orientations in a short period of time with respect to the reciprocal of the hyperfine anisotropic interaction, the latter results to zero and therefore doesn't affects the position of the spectral lines. In an anisotropic system, the components of the spin magnetic moment are different from each other, so we need a matrix system to define it. In general, the tensors are diagonalized through mathematical methods. And as a result, we will have three components of each (g_{xx}, g_{yy}, g_{zz} and A_{xx}, $A_{yy,}$ and A_{zz}).

In the case of the contact interaction, Fermi has developed an expression to derive the value of A_0 (isotropic hyperfine coupling constant, expressed in Joules) which is a scalar:

$$A_0\ (iso)\ =\ -\frac{2\mu_0}{3}|\psi(0)|^2$$

Where μ_0 is the permeability in vacuum and $|\psi\ (0)|^2$ is the probability of finding the electron at a distance 0 rom the nucleus. It is important to underline that the coupling constant is zero if the unpaired electron is on orbitals other than s, since for all orbitals with a secondary quantum number l> 0 (p, d, f, ..) that have a nodal plane to the nucleus, the value of $|\psi\ (0)|^2$ is equal to 0.

2.6.3 Correlation time

It is possible to identify the probe interaction with its surroundings by taking into consideration the linewidth, expressed as a function of:

- ✓ Correlation time τ_c (linked to the system microviscosity);
- ✓ Steric dimensions, monitored by the paramagnetic probe.

The correlation time expresses the lifetime of the molecular configuration, before it rotates 360°, regaining the initial configuration. Such value is an estimate of the mobility of the radical. For nitroxide radicals in solution, the main relaxation mechanism (which determines the linewidth and therefore the overall shape of the spectrum) is the change in orientation of a given molecular configuration (rotational motion). This gives rise to a modulation in time (and in the rotational space) of the components of the tensors g and A. Depending on the value of τ_c, 3 limit-situations can be distinguished for the motion in solution.

Fast motion conditions, which occur when τ_c <10^{-9} s. In this situation, there are three narrow Lorentzian lines. By replacing the appropriate values, it is possible to use a simplified formula for the calculation of τ_c starting from the experimental spectrum.

$$\tau_c = 6.5 \cdot 10^{-10} \cdot \Delta H_0 \cdot \left(\sqrt{\frac{h_0}{h_{+1}}} + \sqrt{\frac{h_0}{h_{-1}}} - 2 \right)$$

Where ΔH_0 is the line width at half maximum of the central peak and h_0, h_{+1} and h_{-1} are the peaks of the 3, having different values of m_I. The constant multiplicative value contains precisely the components of the tensors which are constant for a certain type of system and can be obtained under conditions of rigid motion when there is a total resolution of the anisotropies.

Slow motion conditions, for correlation times in the range between 10^{-9} s and $5 \cdot 10^{-7}$s, in which the anisotropies of g and A begin to resolve and the spectral parameters can no longer be obtained directly from the spectrum. Appropriate calculation programs are then used to solve the spin Hamiltonian and evaluate the row shape.

For τ_c >10^{-7} s the system appears blocked (rigid motion): in this case it is possible to simulate the spectrum without taking into account the relaxation. For an axial symmetry system, the complete resolution of the parallel and perpendicular components of the tensors A and g is assumed. Different relaxation modes according to the molecular direction considered will prevail, since rotation around the z-axis is favored over rotation around the two perpendicular directions.

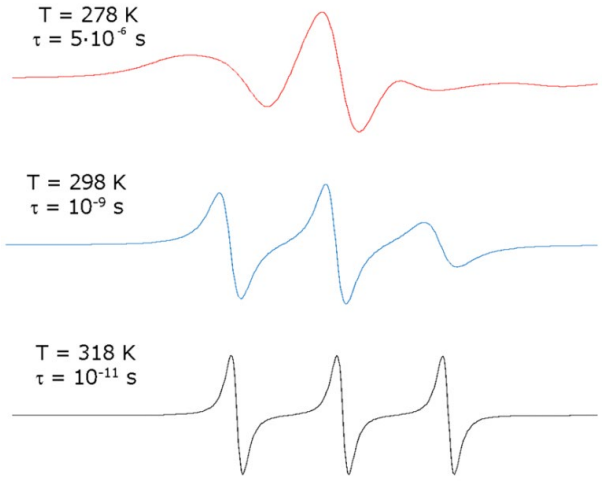

Figure 2.5 EPR absorption spectrum, in derivative form in various mobility conditions

2.6.4 Relaxation and line width

The absorption of microwave radiation causes spin transitions. The lifetime of a spin state is linked to the interaction of the molecule with its surroundings. This gives rise to relaxation phenomena that allow the spin system to transfer the energy previously absorbed to its surroundings and return to the ground state. If this did not happen, or if the speed of the transitions were higher than that of relaxation, a saturation condition would be quickly reached with a consequent total loss of absorption.

Mainly, the relaxation processes are due to local magnetic fields fluctuations generated by the molecular motion. If these fields have oscillation frequencies similar to those of the resonant field, they can cause relaxation. Relaxation processes have a significant influence on linewidth. If the lifetime of a spin system is shortened by relaxation, uncertainty about the real value of the energy increases with consequent line widening, following what is established by the uncertainty principle.

There are therefore two types of relaxation:

- **Longitudinal,** due to spin-lattice interactions (T_1);
- **Transversal,** due to the spin-spin interaction (T_2), corresponding to the time necessary for the spin directions to be redistributed according to all possible angles around z.

The shorter time predominates. When the interaction between the spins creates a series of close energy levels, each of which has indeterminate energy from the Heisenberg principle, then a form of Gaussian line (Lorentzian envelope) is obtained.

2.6.5 Main parameters directly measurable from the EPR spectra

The following values are measurable in the EPR spectrum:

- **$2A_{zz}$ and 2<A>**: for nitroxide radicals in slow motion conditions, $2A_{zz}$ is calculated by subtracting (in Gauss or Tesla) the maximum positive value of the Gaussian peak (h-1) and the negative minimum value referred to the same peak (h+1). For fast motion spectra, the distance between the

two high-field and low-field peaks provides the 2<A> parameter. For nitroxide radicals, these values afford a measure of increases or decreases in polarity in the surroundings, directly from the spectrum.

- **H_s/H_f:** in case the slow (s) motion signal superimposes to a fast (f) motion one, H_s/H_f represents the ratio between the peak heights of the two signals, which may be transformed into the percentage of the interacting probes that give rise to the slow component:

- **ΔW (line width)**: the Heisenberg exchange frequency, W_{ex}, measures the increase in the local radical concentration in a fluid system due to spin-spin interactions. In a system with low motion-freedom, a dipolar interaction between neighboring spins prevails. The main effect of spin-spin interactions, that is, dipolar interaction and low exchange frequency, in the EPR spectrum is reflected by increase in linewidth, ΔW. Therefore, this parameter (distance between peaks maximum and minimum in derivative form) provides a measure of spin-spin interactions, in turn indicating radical local concentration. If strong spin-spin interactions occur, a high W_{ex} provokes linewidth narrowing, while a strong dipolar interaction let the broadening being so large to decrease the spectral intensity.

- **g_{zz} and <g>**: these two parameters, measuring the coupling between the electron spin and the magnetic field, satisfy the equation $h\nu = g\beta H$, where ν is the frequency, β is the Bohr magneton, h is the Plank constant, and H is the magnetic field (H_{zz} or <H>, as the central field in slow motion and fast motion spectra, respectively). For nitroxide radicals, usually these values poorly change, being g_{zz} variable between 2.002-2.003, and <g> around 2.006 (for free electrons, <g>=2.0023).

- **S (order parameter)**: measures the oscillatory motion of the carbon chain bearing the radical group inserted in a structured system, ranging from 0 (completely disordered system) to 1 (perfectly ordered system).

$$S = \frac{a_0}{a_n}\left[\frac{A_{//} - A_{\perp}}{A_{zz} - \frac{1}{2}(A_{xx} + A_{yy})}\right]$$

Where $\frac{a_0}{a_n}$ is the polarity correction factor. The values of the hyperfine tensor are those obtained from computation.

Usually the above described parameters are used in a comparative way, to analyze the properties of related systems. To obtain a more accurate evaluation of the structural and dynamical parameters a spectra computation is needed, using programs taking into account the relaxation process and the resolution of the dynamic Schrodinger equation.

2.7 Paramagnetic systems and EPR instrumentation used in the present thesis work

The use of spin probes has been introduced to further extend the application field of this technique in biological systems, in which paramagnetism occurs very rarely. These are non-perturbative paramagnetic species, allowing the study of the surface of diamagnetic species with whom they interact.

This technique uses two types of strategies, by means of: [7]

- **Spin Probes**: they are paramagnetic probes that are used to investigate structural and dynamic properties. They act as "cameras" capable of providing information about the molecular chemical environment.
- **Spin Labels**: they are stable paramagnetic units linked covalently or through a permanent physical interaction with molecules belonging to the system itself.

The choice between one strategy or another depends on the system and on the type of information to be obtained. In both cases, the probe must be sensitive to the surroundings to be studied, without modifying it.

2.7.1 Nitroxide radical probes

Nitroxide is a radical group, since the oxygen, by binding with nitrogen, places an unpaired electron in a *sp* hybrid orbital. [8] This electron is then delocalized on the whole group, according to two limit forms.

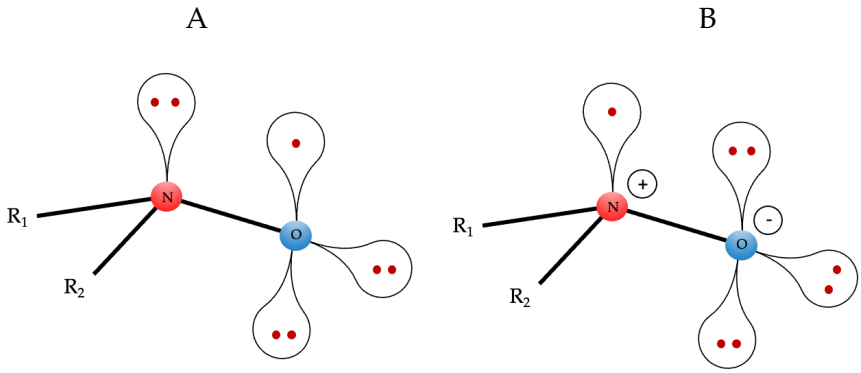

Figure 2.6 Nitroxide radical resonance forms

Since nitrogen has a nuclear spin I = 1, the values that the magnetic quantum number (m_I) can assume are [+1, 0, -1]. Therefore, following the hyperfine interaction between the unpaired electron and the nitrogen nucleus, three transitions are allowed:

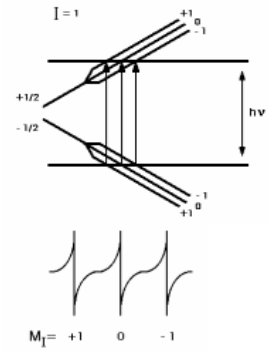

Figure 2.7: EPR spectrum obtained from the analysis of a nitroxide radical. Three lines arise due to the interaction of the unpaired electron with a nucleus having spin I = 1.

In the figure, it is also possible to observe an example of the first derivative EPR spectrum that is obtained from the analysis of a nitroxide radical, with three lines due to the interaction of the unpaired electron with a nucleus having spin I = 1. It is possible to obtain information on the chemical surroundings in which the nitroxide was inserted by observing the variation of certain parameters. A free nitroxide radical is not only sensitive to the rotational motions of the molecule itself, but also to the type of solvent and other solutes used and therefore to its molecular surroundings.

The explanation for this is that the magnetic resonance parameters of any radical species are very sensitive to the electronic distribution in the molecule, and are therefore influenced by perturbations of the surrounding environment. It would be possible to notice a variation of the electron-spin nuclear-spin coupling, (hyperfine coupling A_n), as regards the nitroxide radical in the example given in Figure 2.6: situation B is strongly stabilized by the presence of a polar neighborhood, as in the case of solvation with water, while the situation in A is related to non-polar environments. This variation affects the EPR spectrum by changing the electron-nucleus hyperfine constant.

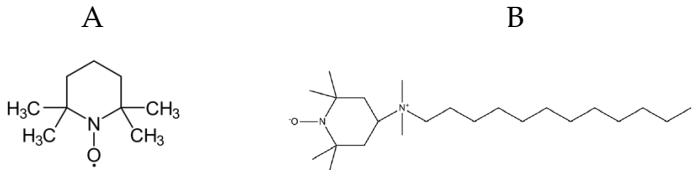

Figure 2.8 Nitroxide radicals exploited in this work: A) TEMPO group B) CAT12 Spin Probe

The evaluation of this constant will allow us, therefore, to ascertain the polarity of the environment experienced by the paramagnetic probe, as shown in paragraph 2.6.2 and already discussed in paragraph 2.6.5.

2.7.2 EPR spectra of Cu(II) ions

The graph of the electronic energy levels for the Cu(II) ion is shown in figure 2.9, which also shows the effect of the electron Zeeman interaction.

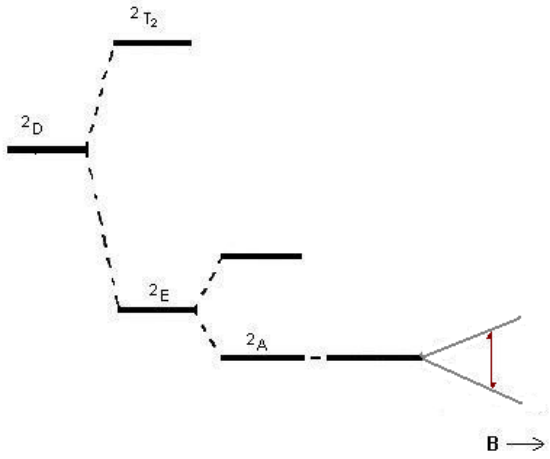

Figure 2.9: Splitting the states of a d9 ion in an Oh ligand field

Copper is an element with a nuclear spin I = 3/2 and therefore consists of four lines (n. lines = 2I + 1). Through the perturbation theory it is possible to calculate the magnetic field values for the four absorption lines:

$$B_z = \frac{h\nu_0 - \frac{m_I}{g_s} \cdot \sqrt{\left(A_{//}^2 \cdot g_{\perp}^2 - A_{\perp}^2 \cdot g_{//}^2\right)} \cdot cos^2\gamma + A_{\perp}^2 \cdot g_{//}^2}{\beta_e \cdot \sqrt{\left(g_{\perp}^2 - g_{//}^2\right) \cdot cos^2\gamma + g_{//}^2}}$$

where

$$g_s = \sqrt{\left(g_{\perp}^2 - g_{//}^2\right) \cdot cos^2\gamma + g_{//}^2}$$

γ is the angle between the z-axis of the laboratory reference system (i.e. the direction of the magnetic field) and the z-axis of the main axis system of g (it has been considered that the main axis systems of A and g coincide).

Fortunately, the relaxation mechanisms of nitroxide radicals and Cu(II) ions coincide. This allowed us to use the same empirical parameters and calculation programs, already described for nitroxide radicals in paragraph 2.6.5. The main difference is the meaning/use of the magnetic parameters g_{zz}/<g> and A_{zz}/<A>. For Cu(II) ions these parameters change in function of the type of complex/coordination (and geometry) formed by the ions with different ligands.

2.8 EPR device used in this work

For this dissertation and all the related papers, it was used a continuous wave (CW) Bruker X Band 9.5 GHz, interfaced with a Bruker microwave bridge, ER 041 XG type (serial number W1702025).

The device is interfaced with a computer to process the signal.

3 - DENDRIMERS

3.1 Introduction and structure

Dendrimers constitute a particular class of polymers that exhibit a high degree of symmetry and monodispersity, deriving from a series of reactions of type AB_x, with $x \geq 2$. The name dendrimer derives from the Greek "Dendron", i.e. tree, in reference to the highly branched structure, reminiscent of a bare shrub.

Their applications are wide ranging: from medicine to material chemistry, as *drug per se* or conjugated to pharmacologically active molecules, ligands for biological targets, fluorescence probes, or as contrast agents for imaging. [9] The family of dendritic macromolecules includes a variety of different compounds, characterized by monodispersity and well-defined symmetry.

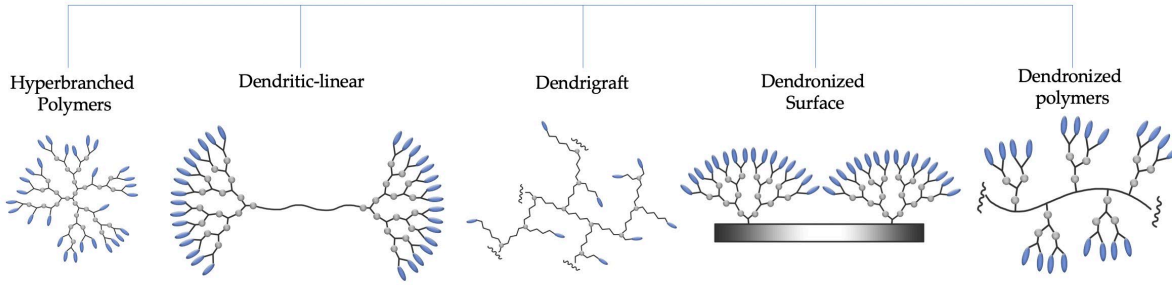

Figure 3.1 Dendritic polymers

Dendrimers have a spherical structure and macromolecular dimensions; these structures should not be confused with the "dendrons", even though often the two terms are used synonymously. It is possible to compare the two structures in Figure 3.2. A dendron only consists of one section of the complete dendrimer, and has different physico-chemical properties.

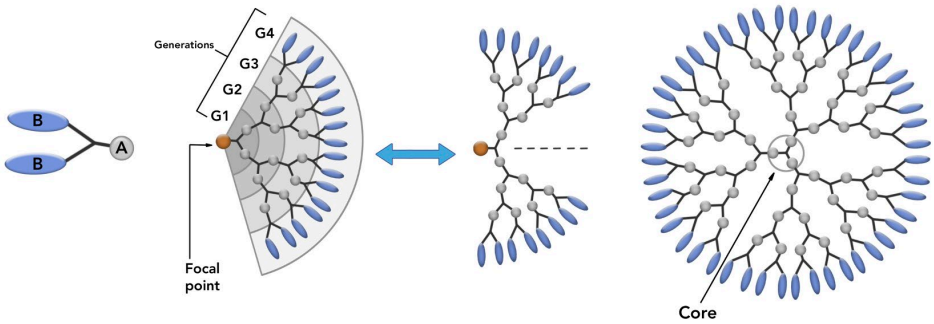

Figure 3.2 Dendrimers vs Dendrons

The skeleton that constitutes the dendrimer can be composed of various types of polymers. It is precisely from the composition of the skeleton that the dendrimer class takes its name, as well as the vast majority of its chemical-physical properties.

The most important skeleta are [10]:

- Polypropylenimine (PPI)
- Polyamidoamine (PAMAM)
- Carbosilane
- Phosphorus Dendrimers
- Polyether

Three components are common to all dendrimers:

- **Central Core:** the innermost core of the structure, composed of an atom or a small molecule which often differs in nature from the rest of the skeleton.
- **Generations:** concentric layers of atoms arranged neatly, linked through cyclic reactions. Starting from generation 0, often corresponding to the central core only, up to generation 12 are reported in literature.
- **External terminal groups:** the last generation is generally decorated with functional groups based on the use designed for the polymer.

Since the diameter of the dendrimer grows linearly while the number of surface groups grows exponentially for each generation, steric hindrance is marked at high generations. Low-generation dendrimers usually have an open and flexible structure, while high-generation ones have a denser structure. [11][12]

The conformational state is different according to the type of skeleton of the dendrimer, many of whom are strongly influenced by the pH of the medium in which they are immersed for the possible establishment of electrostatic interactions between surface groups. Taking PAMAM dendrimers as an example, it has been observed that at low pH values (less than 5) it has an elongated structure, due to electrostatic repulsion between the internal proton tertiary amines. At high pH values, however, we can observe a globular structure, tending to occupy all the available space due to the absence of ionic "bridging" forces between the functional groups. [13]

On the other hand, PPI dendrimers with terminal carboxy units maintain a globular structure at any pH value, with more or less accentuated backfolded conformation.

3.2 History and Synthesis

Initially born as by-products of linear polymer synthesis, dendrimers have attracted increasing interest in the final decades of the last century due to the extreme versatility that distinguishes them. The first example of synthesis dates back to 1978, described by Fritz Vögtle. The procedure was defined as a "cascade", with two reactions repeated cyclically eventually giving birth to the final product. Unfortunately, this cannot be today defined as a dendrimer, given the high degree of impurity, polydispersity, and very low yield achieved by Vögtle.

It was only in 1985 that a PAMAM dendrimer was obtained for the first time, characterized by monodispersity and a well-defined structure, as a result of Tomalia's work. This time, the synthesis protocol adopted was named "divergent": starting from a central amino core, he proceeded outwards, through the reactions between methyl acrylate and ethylenediamine. The subsequent

polymerization of amidoamines led to a sixth-generation dendrimer, which mimicked a histone structure for gene transport.

This type of synthesis, still widely used to date, involves the formation of the central core, on which layers of monomers are cyclically reacted until the desired generation is reached.

The growth of the dendrimer can occur up to a "critical" branching level, beyond which it can no longer increase due to the growing density of the dendron, as direct result of the its steric limitations. The divergent approach is widely used due to its effectiveness for the production of large quantities of dendrimers. However, it is possible that collateral or incomplete reactions may occur, especially for high generations. [18]

In 1993, Vögtle's work was resumed by the research team of Brabander-Van Den Berg and Meijer, who made significant improvements to the synthesis generating the first PPI dendrimer. Finally, Fréchet and Hawker faced the drawbacks encountered by their predecessors, creating a different kind synthesis with a convergent approach. [14] [15]

This starts from the outside of the molecule and proceeds inwards. It was conceived by Fréchet to overcome the drawbacks of divergent synthesis. It foresees two cyclically repeated reactions until the desired generation is formed:

- **Coupling Step:** a type AB multifunctional monomer, with a protected function called "focal point", is reacted by creating the outer layer of the generation
- **Activation Step:** the focal point is activated and reacted with other monomers.

These two reactions are repeated as many times as desired, until a dendron of the suitable generation is created, which is then reacted with the central core to form the dendrimer. It should be emphasized that each activation/coupling cycle requires only a small number of transformations per molecule and therefore only a few excess reagents are needed. [17]

Nowadays, dendrimers are synthesized with step-wise processes in order to avoid non-quantitative reactions or unwanted by-products. For the subsequent external functionalization, the use of click chemistry practices is common. New methods have been recently developed, but to date, these two synthesis methods are still the most widely used. [16][17]

Lately, accelerated growth approaches are becoming more and more popular between chemists, exploiting different mechanisms: the so called “orthogonal strategy” allows, for example, the production of up to 6^{th} generation dendrimers in one day, through the use of activated AB_2C type monomers. Nevertheless, the holy grail of dendrimers, namely the one-pot synthesis system for high generation dendrimers with a single purification step, is far from being achieved. [29][30]

3.3 Applications in the Biomedical Field

Dendrimers find innumerable outlets in the biomedical field. Extreme structural versatility and high biocompatibility are just two of the characteristics that make this class of polymers so special. [20] The globular structure gives them a weak adhesivity to biological membranes, with reduced cytotoxicity. The numerous cavities present in the skeleton allow the complexation/coordination of smaller chemical entities (such as metal ions, genetic material or proper drugs), in a host-guest mechanism. [21]

Dendrimers can therefore act as metallic carriers with low tissue accumulation, when compared with metallic markers. [22] The interior of high-generation dendrimers undergoes little penetration by the solvent: in an aqueous solution they have a micellar-like behavior, maintaining a hydrophobic internal environment.

Thus, they are excellent drug transporters, aligning with modern smart drug-delivery techniques. New and old molecules can be incorporated inside the structure (endo-receptor) or linked to external branches (exo-receptor). This allows the on-site preservation and transfer of poorly soluble drugs, significantly improving the bioavailability of the drug itself. Another supramolecular level application is the use of dendrimers as support for controlled release systems.

Schematizing, the main fields of use in medicine are: [12][18][23][24]

- Drugs per se;
- Pharmacological Carrier;
- Gene Transfection Agents;
- Magnetic Resonance Imaging Agents;

Table 1. *Most successful dendrimers so far:*

Dendrimer	Type	Distributing Company	Applications	Research Status
Vivagel	Poly-L-Lys	StarPharma	*HIV* and *SDS* Transmission Prevention	Clinical Studies Phase III
Stratus CS	PAMAM	Dade Behring	Cardiac diagnostic tests	In commerc.
Superfect	PAMAM	Qiagen	Transfection agent (gene delivery)	In commerc.
Priofect	PAMAM	Starpharma	Transfection agent (gene delivery)	In commerc.
Alert ticket	PAMAM	U.S. army lab	Anthrax detection agent	In commerc.
DEP®Dendrimer-Docetaxel	Poly-L-Lys	Starpharma	Breast cancer treatment	Under Development
Dendrimer-oxaliplatin	Poly-L-Lys	Starpharma	Colon cancer treatment	Preclinical studies

3.3.1 Dendrimers as antimicrobials

The emergency of the drug resistance widespread has shifted research to new molecular targets to be used as antimicrobials.

Dendrimers have been identified as potential new drugs to treat infections. Thanks to the numerous interactions between the dendrimer surface groups and microorganisms, they find a wide range of applications: from antibiotics to antivirals, antifungal agents and more.

In particular, carbosilane dendrimers and metallodendrimers show high activity at low generation as well, as shown in chapter 1.

As regards the use of antivirals, dendrimers demonstrated great potential in the treatment of herpes simplex infections (*HSV*) and *HIV-1* infections, as topical microbicides to be applied rectally and/or vaginally in order to protect the patient from infections. Dendrimer SPL7013 (VivaGel™), distributed by Starpharma Pty Ltd (Melbourne, Australia), is a sulphonated L-Lys based compound. At the moment the drug is in phase III of the clinical trials, and has proven to be well tolerated by both animals and humans. [25]

3.3.2 Dendrimers in the treatment of cancer

In recent years, research in the fields of new chemotherapy agents has turned its attention to drugs with greater cellular selectivity. The major drawback of conventional chemotherapy is the poor cyto-selectivity, which causes countless side effects worsening patients' life expectancy.

Dendrimers have proven to be a good substrate for the development of site-specific chemotherapy, through surface modifications with ligands capable of recognizing and binding to cancer cells only. A few examples of such ligands are folic acid, glycosidic groups, and colchicine. In this last case, the modified dendrimer is recognized by the tumor cells with a good degree of selectivity, inhibiting its mitosis processes following the intracellular release of colchicine. [26]

Frequently, dendrimers designed for this purpose are coordinated with metal ions, to exploit the synergic activity of the two classes of molecules. The outcome of the binding, called metallodendrimers, are described in section 3.4.2.

Despite the high potential of such antitumoral agents, the required degree of potency and selectivity for tumoral cells to replace traditional anticancer drugs hasn't been reached yet. This thesis aims to get one step closer to the discovery of effective metal conjugated dendrimers for the treatment of cancer.

The vast field of metallodendrimers as antitumoral agents will be discussed in chapter 1

3.3.3 Dendrimers in the treatment of neurodegenerative pathologies

Dendrimers have *in vitro* shown the ability to interfere with the formation of amyloid fibrils structures typically linked to the appearance and development of so-called conformational diseases, such as Alzheimer's or prion diseases. [27]

To date, PAMAM dendrimers proved the highest potency in this sense. However, due to the intrinsic toxicity of positively charged dendrimers, research has moved towards the design of more biocompatible molecules such as glycodendrimers, described in section 3.4.1. The use of dendrimers in the treatment of neurodegenerative diseases is one of the most promising fields from a pharmacological point of view, also taken into account that no treatment is currently available, other than symptomatic.

3.4 Structural improvements to classic dendrimers

3.4.1 Glycodendrimers

Dendrimer structures with terminal amino residues can hardly find use in the biomedical field, given their high toxicity.

In fact, the amino groups, protonated at physiological pH, interact with the cell membranes causing lysis as a final effect. This cytotoxic behavior is more marked in the presence of more amino residues. Therefore, the toxicity increases exponentially together with the generation of the dendrimer.

Research has gone in the direction of mitigating this toxicity, through various techniques. One of the most effective is the bonding of oligosaccharide groups on the terminal amines, making the dendrimer completely biocompatible. The most used sugar-coating techniques imply the use of maltose, galactose, or maltotriose. The effect of the addition of carbohydrates is multiple: besides the renewed bioavailability, it allows the dendrimer to interact with a variety of physio/pathological processes, thus making it versatile for use in drug delivery and/or as drug per se.

Based on the degree of substitution of the surface amines, we can divide the resulting structures into:

- **Dense Shell (DS)**, i.e. all the amino hydrogens are replaced by carbohydrate units, resulting in a complete coating of the molecule. For a generation 4 PPI, presenting 64 terminal amino groups, it implies the conjugation of 128 sugar groups.
- **Open Shell (OS)**, i.e. only 50% of the hydrogens in the amino groups are replaced. For a generation 4 PPI, on 64 amino groups, it implies the conjugation of 64 sugar groups.
- **Other,** recently, lesser degrees of substitution are being explored

What differentiates the synthesis of DS and OS is the number of sugar equivalents that are added in reaction: a large excess of oligosaccharides is processed for DS, while in OS the precise number of moles must be added, trying to get a 100% yield. The synthesis of this coating type can be less time-efficient. The coating process performed in this work is carried out under click chemistry conditions. [19]

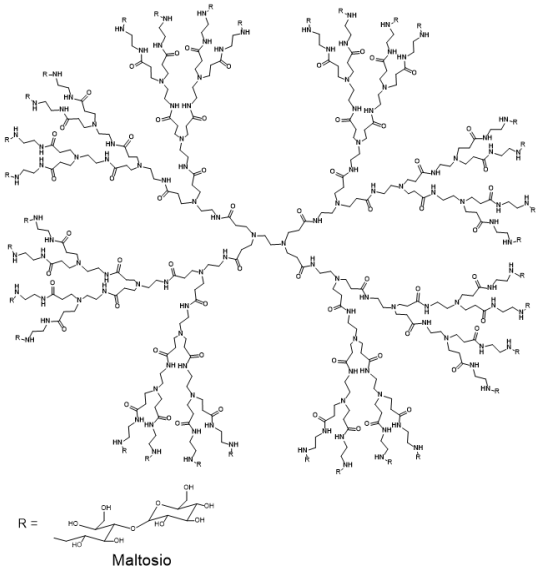

Figure 3.3 Example of PAMAM Dendrimer, coated with maltose groups

Given glycodendrimers extreme biocompatibility, this thesis aims to use them as a well-tolerated metal chelator, for the treatment of metal accumulation pathologies such as Wilson disease.

3.4.2 Metallodendrimers

Metallodendrimers are the combination of dendrimers and metal ions, greatly improving the range of application of this class of molecules. Such metals can be incorporated in a preformed dendrimer, or take part to the dendrimer growth.

They can be: [31]

- Dendrimer core
- Dendrimer termini
- Branching units
- Connectors
- Placed at multiple locations

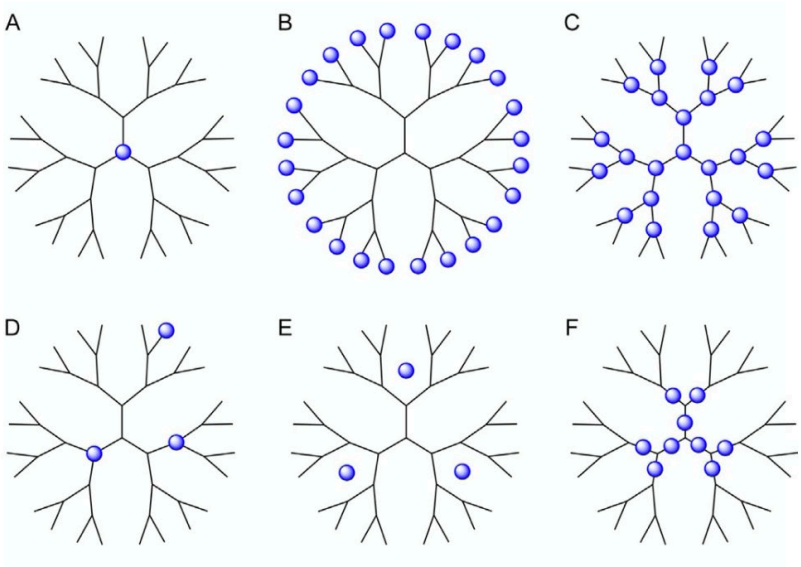

Figure 3.4 Different metal location inside the dendrimer skeleton: (A) Core; (B) Periphery; (C) nodes of ramification; (D) Multiple locations; (E) inside the cavities; (F) as building-blocks. (Review, figure 1)

The possibilities of this emerging class of molecules are wide, both biomedical and non-biomedical. Several examples are reported in literature, for their use as antiviral, antifungal antibacterial agents.

One of their most studied applications is the treatment of cancer, namely the purpose of their application in this thesis. The most exploited metal ion for this purpose is Pt(II), followed by, among the others, Ru(II), Gd(I) and Pd(II). [28]

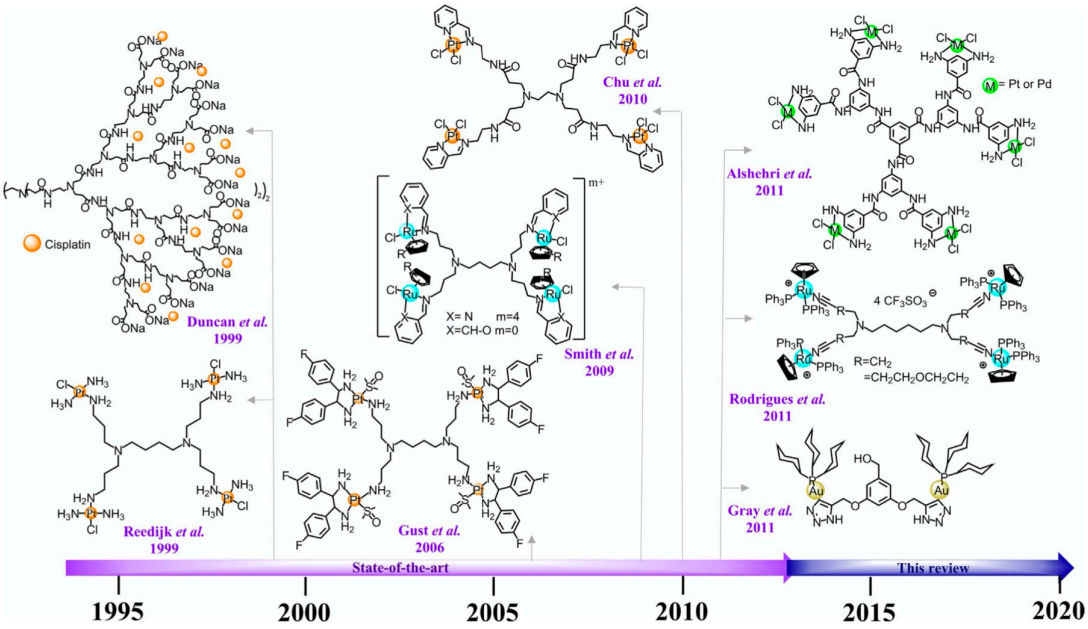

Fig. 3.5 state of the art of antineoplastic metallodendrimers. (Review, figure 3)

The metallodendrimers synthetized for this work are carbosilane, and chelate Cu(II) and Ru(II) ions acting as Schiff-base ligands.

A detailed explanation of the metallodendrimers world and application is present in chapter 1.

4 - BIBLIOGRAPHY

1. Weil J.A., Bolton J.R., "*Electron Paramagnetic Resonance: Elementary Theory and Practical Applications*", Wiley Interscience, John Wiley & Sons, Inc., 2007
2. Atherton N.M., "*Electron Spin Resonance*", Ellis Horwood, Ed. J. Wiley, Press: N.Y., 1973
3. Atkins P. W., "*Chimica Fisica*", Ed. Zanichelli, 1997
4. Eaton G.R., Eaton S.S., Salikhow K.M., "*Foundation of Modern EPR*", Ed. World Scientific, 1998
5. Gerson F., Huber W., "Electron Spin Resonance Spectroscopy of Organic Radicals", Ed. John Wiley & Sons, 2006
6. Aglietto M., Bongiovanni R., Mariani A., "Caratterizzazione di materiali polimerici. Tecniche per polimeri in soluzione", Ed. Nuova Cultura, 2014
7. Berliner L.J., "*Spin Labeling: Theory and Applications*", Academic Press, Inc., 1976
8. Nordio P.L. "*General Magnetic Resonance Theory*", Academic Press, Inc., 1976
9. Carlmark A., Hawker C., Hult A., Malkoch M., *"New methodologies in the construction of dendritic materials"*, Chem. Soc. Rev., 2009, 38, 352–362
10. Schultz J.L., Wilks E.S., "Dendritic and Star Polymers: Classification, Nomenclature, Structure Representation, and Registration in the DuPont SCION Database", J. Chem. Inf. Comput. Sci., 1998, 38, 85-99
11. Lallana E., Fernández-Trillo F., Sousa-Herves A., Riguera R., Fernández-Megia E., *"Click Chemistry with Polymers, Dendrimers, and Hydrogels for Drug Delivery"*, Pharm. Res., 2012, 29, 902–921
12. Mintzer M.A., Grinstaff M.W., "Biomedical applications of dendrimers: a tutorial", Chem. Soc. Rev., 2011, 40, 173–190
13. Maiti P.K., Çağın T., Lin S., Goddard W.A., *"Effect of Solvent and pH on the Structure of PAMAM Dendrimers"*, Macromolecules, 2005, 38, 979-991
14. Gao C., Yan D., "Hyperbranched polymers: from synthesis to applications" Prog. Polym. Sci. 2004, 29, 183-275
15. Tomalia A.D., Fréchet J.M.J., *"Discovery of dendrimers and dendritic polymers. A brief historical perspective"*, J. Polym. Sci. Part A: Polym. Chem., 2002, 40, 2719–2728
16. Hawker C., Fréchet J.M.J., *"A New Convergent Approach to Monodisperse Dendritic Macromolecules"*, J. Am. Chem. Soc., Chem. Commun., 1990, 15, 1001-1068
17. Hawker C., Fréchet J.M.J., "Preparation of Polymers with Controlled Molecular Architecture. A New Convergent Approach to Dendritic Macromolecules", J. Am. Chem. Soc., 1990, 112, 7638-7647
18. Boas U., Heegaard P.M.H., *"Dendrimers in drug research"*, Chem. Soc. Rev., 2004, 33, 43 – 63
19. Kannan A., Saravanan V., Rajakumar P., "Synthesis, Photophysical, Electrochemical Studies, and Antioxidant Properties of Fluorescein-Linked Glycodendrimers", Asian J. Org. Chem. 2016, 5, 1155 – 1163
20. Svenson S., "The dendrimer paradox – high medical expectations but poor clinical translation", Chem. Soc. Rev., 2015, 44, 4131-4144
21. Malik N., Wiwattanapatapee R., Klopsch R., Lorenz K., Frey H., Weener J.W., Meijer E.W., Paulus W., Duncan R., "Dendrimers: Relationship between structure and biocompatibility in vitro, and preliminary studies on the biodistribution of I-125-labelled polyamidoamine dendrimers in vivo", Journal of Controlled Release, 2000, 65, 1/2, 133-148
22. Ambade A.V., Savariar, E.N., Thayumanavan S., *"Dendrimeric micelles for controlled drug release and targeted delivery"*, Molecular Pharmaceutics, 2005, 2, 4, 264-272
23. Guillot-Nieckowski M., Eisler S., Diederich F., *"Dendritic vectors for gene transfection"*, New J. Chem., 2007, 31, 1111–1127
24. Wang D., Zhao T., Zhu X., Yan D., Wang W., "*Bioapplications of hyperbranched polymers*", Chem. Soc. Rev., 2015, 44, 4023-4071
25. Balogh L., Swanson D.R., Tomalia D.A., Hagnauer G.L., McManus A.T., *"Dendrimer-silver complexes and nanocomposites as antimicrobial agents"*, Nano Letters, 2001, 1, 1, 18-21

26. Andreozzi E., Antonelli A., Cangiotti M., Canonico B., Sfara C., Pianetti A., Bruscolini F., Sahre K., Appelhans D., Papa S., Ottaviani M.F., *"Interactions of Nitroxide-Conjugated and Non-Conjugated Glycodendrimers with Normal and Cancer Cells and Biocompatibility Studies"*, Bioconjugate Chem., 2017, 28, 524−538
27. Klajnert B., Cortijo-Arellano M., Cladera J., Bryszewska M., *"Influence of dendrimer's structure on its activity against amyloid fibril formation"*, Biochemical and Biophysical Research Communications, 2006, 345, 1, 21-28
28. Sanz del Olmo N., Carloni R., Ortega P., García-Gallego S., De la Mata F., *"Metallodendrimers as a promising tool in the biomedical field: An overview"*, Advances in Organometallic Chemistry, 2020, Volume 74
29. Malkoch M., García-Gallego S., *"Introduction to Dendrimers and Other Dendritic Polymers*", Dendrimer Chemistry: Synthetic Approaches Towards Complex Architectures, 2020
30. Waltera M.V. Malkoch M., "*Simplifying the synthesis of dendrimers: accelerated approaches*", Chemical Society Reviews, 2012, 41, 4593-4609
31. Hwang S., Shreiner C.D., Moorefield C.N., Newkome G.R., "*Recent progress and applications for metallodendrimers, new journal of chemistry*", New Journal of Chemistry, 2007,31, 1192-1217

CHAPTER 1

Carbosilane metallodendrimers as promising antitumoral agents

1 - INTRODUCTION AND GOALS

1.1 Introduction

1.1.1 Cancer and nanotechnologies

Cancer is a major threat issue humanity has to face, with approximately 9.6 million deaths per year. Among the various types of tumor, lungs, breast and prostate cancer are the deadliest, accounting for over 37% of the total demises, as GLOBOCAN estimated in 2018.

Cis-Platin, by far the most successful metal-conjugated drug ever made, is still used for the treatment of various types of cancer, bladder, lungs, ovarian and more. Its mechanism relies in DNA cross linking, affecting more fast replicating cells, like tumoral ones. However, several side effects come along with the treatment, the most common ones are a decreased immunity to infections, allergic reactions, and kidneys problems.

The biggest problem related with cis-platin though is the induced resistance to the treatment, which pushed physicians to combine it with other drugs to mitigate this effect.

Nanotechnology is addressed as one of the best candidates to overcome old drugs limitations. Its strength relies in the use of various novel techniques, like malignant hyperthermia induced by magnetic nanoparticles, smart drug-delivery with liposomes etc.

Dendrimers, as already described in the introduction of this work, are a very promising class of molecules for the treatment of cancer, being able to deliver traditional drugs as smart carriers or to act as drug-per-se.

Among the various types of dendrimers used for the treatment of cancer, Schiff-base-bearing carbosilane have had a discrete success, thanks to their ability to firmly chelate metals ions and synergically express the antitumoral activity.

1.1.2 Schiff-base carbosilane metallodendrimers

The general synthesis adopted by our group for carbosilane dendrimers is the following:

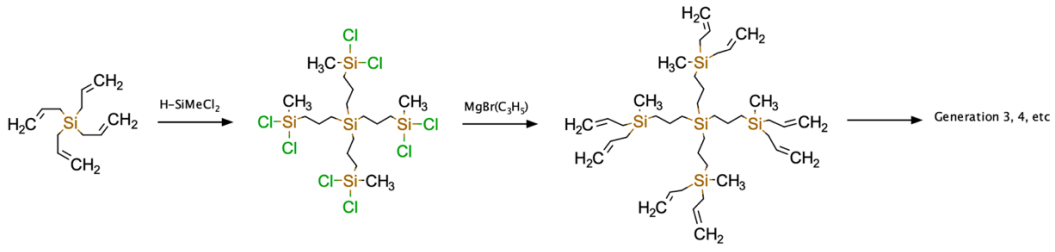

Figure 1.1 General synthesis of carbosilane dendrimers

This way, it's possible to reach the desired generation, achieving high yields and product purity. Carbosilane skeleton grants a high degree of interaction with biological membranes, due to its balanced hydrophobicity, stability and flexibility.[1] It was therefore chosen as a promising starting point for the development of antitumoral agents.

The modification of dendrimer termini with iminopyridine groups makes a Schiff-base bidentate, ligand out of the molecule, allowing it to chelate metal ions. This way it's possible to

bind them the dendrimer skeleton, in a directly proportional number to the dendrimer branches, and therefore to the dendrimer generation.

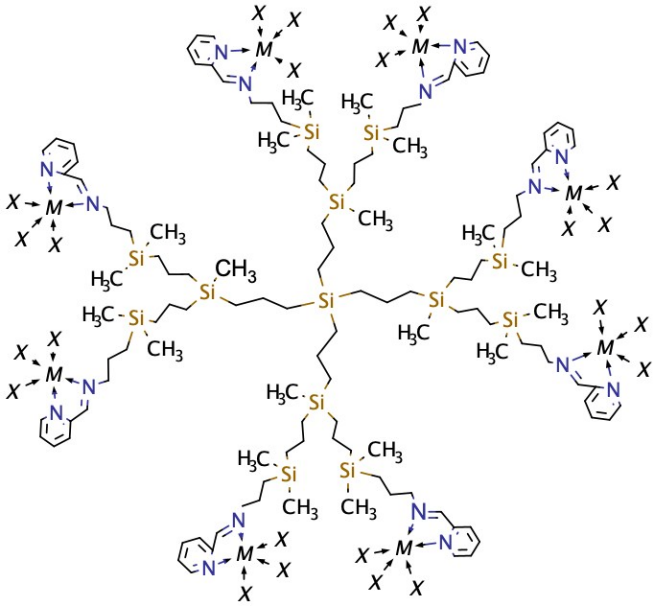

Figure 1.2 An example of generation 2 metallodendrimer, bound to a generic penta-coordinated metal.

The combination of dendrimers and metal ions allows to get access to a wider variety of mechanisms of action for the treatment of cancer, if compared to the dendrimer alone.

The following review describes in details the world of metallodendrimers.

1.2 Objectives

In this chapter, the attention is focused on studies performed on carbosilane metallodendrimers for the treatment of cancer.

Our goals were the following:

- Study and define the state-of-the-art of metallodendrimers for the treatment of cancer and infectious diseases.
- Design, synthetize and characterize novel metallodendrimers with potential as antitumoral agents.
- Study the interaction of the newly synthetized metallodendrimers with biological systems and define their antitumoral activity.

1.3 Methodology

The synthesis and characterization of the molecules was carried out in the laboratories of Alcalá University under the guidance of Prof. de la Mata and Prof. García-Gallego.

In-vitro testing was carried out with both healthy and tumoral cell lines, allowing to compare the results obtained for different kinds of cancer. For one metallodendrimer structure, it was also possible to carry out an *ex-vivo* testing, as shown in the results and discussion section.

The structure-interaction relationship of the newly synthetized structures with model membranes and cells was investigated by means of the EPR technique, by directly analyzing paramagnetic metal ions (when present) and/or inserting spin probes in the biological systems. EPR studies were performed in the physical chemistry laboratory of Urbino University, by the group of Prof. Ottaviani.

1.4 Results

- Our first goal gave birth to a review which presents the current state of the art of metallodendrimers, their uses in the biomedical field and applications for the treatment of the most diverse pathologies. The first half of the review is about the use of metallodendrimers for the treatment of cancer. An historical overlook of the use of metal-conjugated drugs for the treatment of tumors will introduce the topic, followed by a detailed description of the most successful metallodendrimers synthetized for this purpose.

- Our second and third goal resulted in the publication of three papers describing the synthesis and characterization of novel antitumoral carbosilane metallodendrimers. A particular emphasis was given on the effect of different metal ions, dendrimer generations, metal counterions, and structure substitutions on the antitumoral activity. The outcome of these studied is going to be summarized in section 2.

REVIEW

Metallodendrimers as a promising tool in the biomedical field: an overview

Natalia Sanz del Olmo, Riccardo Carloni, Paula Ortega, Sandra García-Gallego, F. Javier de la Mata

Advances in Organometallic Chemistry, Volume 74
https://doi.org/10.1016/bs.adomc.2020.03.001

Metallodendrimers as a promising tool in the biomedical field: an overview

Natalia Sanz del Olmo [a,b,c], Riccardo Carloni [d], Paula Ortega [a,b,c], Sandra García-Gallego [a,b,c] *, F. Javier de la Mata [a,b,c],*

[a]Department of Organic and Inorganic Chemistry, and Research Institute in Chemistry "Andres M. del Rio" (IQAR), University of Alcala´, Madrid, Spain
[b]Networking Research Center on Bioengineering, Biomaterials and Nanomedicine (CIBER-BBN), Spain
[c]Institute "Ramo´n y Cajal" for Health Research (IRYCIS), Spain
[d]Department of Pure and Applied Sciences, University of Urbino "Carlo Bo", Urbino, Italy

*Corresponding authors: e-mail address: sandra.Garcíagallego@uah.es; javier.delamata@uah.es

1. Introduction

Since ancient times, inorganic compounds have been used to treat different diseases. The discovery of Arsfenamin to treat syphilis in 1910 by Paul Ehrlich launched the clinical use of metal-based drugs.[1] Although in some cases the treatment is carried out with inorganic salts of the corresponding metal, in most of them coordination complexes and organometallic derivatives are employed. The metal complexes present the ability to form strong interactions with the target biomolecule thanks to the combination of the coordination ability of metals, through covalent or ionic bond, with the unique stereoelectronic properties of the ligand. Moreover, the complexation of metals ions to organic ligands frequently reduces their toxicity

Table 1 *Overview of common metals used in clinic, including examples of commercially available metallodrugs:*

Metal	Therapeutic/diagnostic application	Metallodrug
Au	Rheumatoid arthritis, gout	Auranofin®
Ag	Antiseptic in burns and wounds	Silvadene®
Cu	Dermatitis, algaecide, fungicide, antioxidant	Copper aspirinate
Pt	Cancer	Cisplatin®
Gd	Contrast agent for Magnetic Resonance Imaging	Magnevist®
Zn	Peptic ulcer disease, dyspepsia	Polaprezinc®
Co	Synthesis of vitamin B_{12}	Cyanocobalamin
Li	Manic depression	Lithobid®
Bi	Stomach discomfort, diarrhea, skin injuries	Pepto-Bismol®
Hg	Antiseptic	Meralein sodium®

and improves both the bioavailability and the absorption of ions in tissues. The versatility of metal complexes, with a great variety of coordination numbers, geometries, structural diversity and kinetics of ligand exchange, places them as promising candidates in biomedicine (Table 1). Many other fields have also benefited from their catalytic properties, redox activities, Lewis acid- ity, magnetic and spectroscopic properties, radioactivity, etc. Nevertheless, the treatment with metallodrugs is often associated with a high toxicity and side effects,[2] thus highlighting the need to develop novel strategies with higher efficiency and selectivity. The potential accumulation of the metal ions in the human body could be harmful, leading to the development of exhaustive studies of their biodistribution and interaction with biological molecules.[3]

Nanotechnology has emerged as a promising alternative to traditional treatments. The nanometric size and the high surface area of these tools often lead to an increase in the therapeutic response and specificity. Since the first conceptualization of molecular machines and nanotechnology in 1959 by Richard Feynman,[4] the field has expanded exponentially and multiple strategies have been reported in the literature, including nanoparticles, liposomes, micelles and dendrimers.[5] Dendrimers and dendritic polymers emerged as a class of macromolecular structures, with an arborescent shape, highly branched and symmetrical, prepared through the repetition of a series of reaction steps that extend from a nucleus to the periphery. Such controlled synthesis, unique among the nanotechnological tools, pro- duces monodisperse molecules with application-driven design. Together with their chemical stability, multivalence and possibility to on-demand attach therapeutic drugs, monitoring tags or other biomolecules, have boosted their use in the last decades not only in the biomedical field, but also in cosmetics,[6] catalysis[7] and photochemistry,[8] among others.

The field of dendritic polymers comprises different topologiesmonodisperse dendrimers and dendrons, polydisperse dendritic polymers and hybrids— and different scaffolds —polyamidoamine (PAMAM), polypropyleneimine (PPI), carbosilane, polyesters, polyether, polyglycerol, and phosphorus dendrimers, among others.[9–11] Traditional synthetic approaches to dendrimers include the divergent, the convergent and the mixed synthesis methods. The divergent approach was described in 1978 by D. A. Tomalia and consists on a sequence of reactions that emerge from the core to the periphery.[12] Later, in 1990 C. Hawker and J. M. J. Frechet developed a new method, in which the synthesis of the dendrimer was carried out in the opposite direction, called convergent synthesis.[13] The syn- thesis is mainly based on the attachment of dendrons to a multifunctional core, building the dendritic macromolecule from outside to inside. While the divergent synthesis might be suitable for large-scale production, the increasing steric hindrance in the growth to higher generations can compromise the purity and monodispersity of the final dendrimers and structural defects may appear. On the other hand, the convergent route reduces the possibility to get structural defects, but it is mainly limited to low-generation dendrimers, considering the steric hindrance in the attachment of big dendrons to the core. Finally, the mixed method emerged as an alternative to the previous two methods with the aim of reducing the disadvantages of both.[14] Recently, accelerated-approaches have remarkably simplified the synthetic routes to dendrimers and rely on the extraordinary properties of chemoselective and orthogonal reactions.[15,16] This growth concept makes the typical usage of activation steps obsolete, reducing the reaction time and increasing the total yield.

Considering their structural perfection, nanometric size and resemblance to proteins, dendrimers have been described as "artificial proteins." Dendrimers are in the size range of other biomolecules like DNA (2.4 nm), insulin (3 nm), hemoglobin (5.5 nm) or membrane lipids (around 5.5 nm).[17]

Furthermore, some dendrimers have the ability of mimicking actions of their biological analogues such as self-assembly, catalysis or light collection.[18] These similarities have led the scientist to conduct studies of these macromolecules in different biomedical applications. Dendrimers can act as therapeutic agents *per se* or as carriers of drugs or biomolecules through encapsulation, electrostatic

interactions or covalent bonds. These macro- molecules have been studied toward different diseases such as HIV infection,[19] malaria,[20] neurodegenerative diseases,[21] bacterial infections,[22] cancer and diagnosis,[23] among others. The reader is referred to excellent reviews in the literature.[17,24]

The combination of metal ions and dendritic scaffolds can lead to enhanced or even new properties, in the so-called metallodendrimers. The multivalency and monodisperse nature of dendrimers enable a con- trolled attachment of multiple metal entities in a single molecule, which has proved to be more effective than their mononuclear counterparts.[25] There are different positions in the dendritic framework susceptible of incorporating metals (Figure 1). The synthetic route will be dictated by the location of the metal ion, being included during the growth of the dendritic scaffold or after, on a preformed dendrimer. Moreover, the location of the metal ion, together with the nature of the metal, will determine the final application. For example, metallodendrimers containing ruthenium, gold, copper, zinc, iron or technetium have been evaluated due to their therapeutic or diagnostic potential. This review summarizes the latest advances in the use of metallodendrimers in the field of biomedicine, focused on the treatment of cancer and infectious diseases as the most widespread uses. The reader is referred to an excellent review published in 2012 by G. Smith to previous state-of-the-art in the field of anticancer agents.[26]

The demand of multipurpose materials is increasingly changing the focus to heterofunctional dendritic molecules, bearing different moieties in a single scaffold. Therapeutic drugs, monitoring tags or targeting moieties can be attached in a single dendrimer and enhance the efficacy of the treatment. Several approaches have been reported in the literature, where the heterofunctionalities are introduced in the periphery or in the scaffold either randomly or in a controlled way (Figure 1G–I). This review will also present different heterofunctional metallodendrimers, based on whether the heterofunctionalization has been performed only with metal complexes or if other molecules have been incorporated to provide additional proper- ties such as water solubility or tracing tools. Surprisingly, despite the numerous possibilities that exist today in herofunctionalized dendrimers, only a few have been used in the field of metallodendrimers.

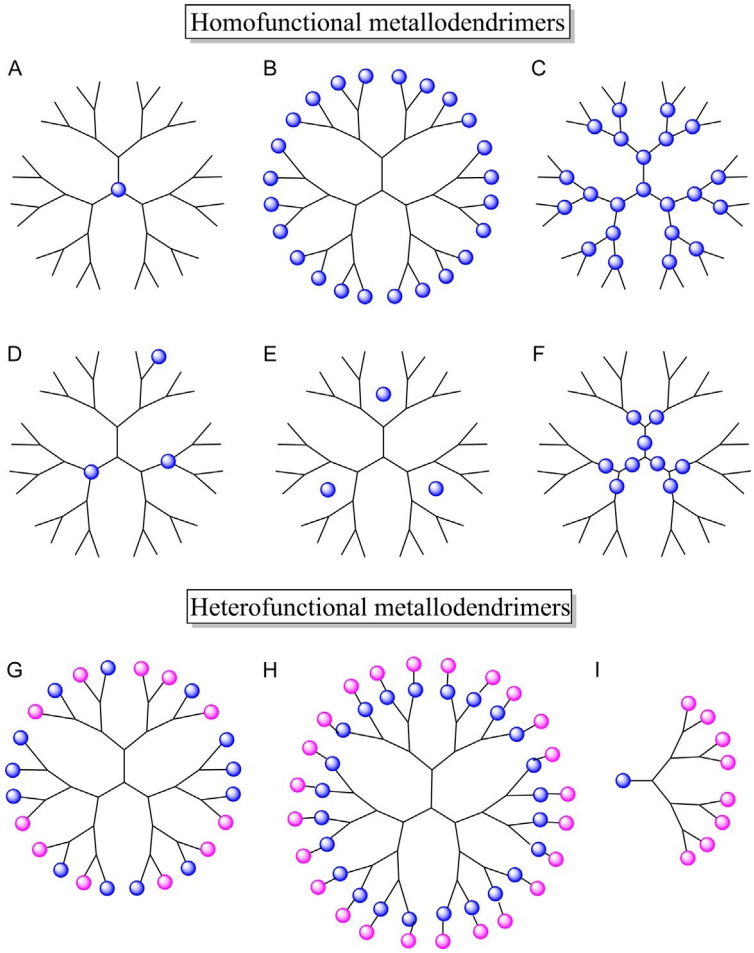

Figure 1 Metallodendrimers classification attending to the metal position in the frame- work. (A) In the center of the skeleton; (B) in the periphery; (C) in the nodes of ramification; (D) in different points of the structure; (E) inside the cavities; (F) as building-blocks; (G) heterofunctional random; (H) heterofunctional layer-block; and (I) heterofunctional dendron.

2. Applications of metallodendrimers in biomedicine

2.1 Metallodendrimers in cancer treatment

Cancer is one of the main causes of death in the world. According to GLOBOCAN estimations for the year 2018, 18.1 million new cases would be diagnosed with cancer and this disease would be responsible of 9.6 millions of deaths.[27] From a biological point of view, cancer arises from an uncontrolled cell proliferation that in some occasions acquires the ability to invade foreign tissues producing what we know today as metastasis, and often leads to the death of the patient. Due to the heterogeneous causes, it is difficult to find an effective and non-toxic treatment for cancer.

The use of metal complexes in cancer treatment started when Rosenberg discovered the potential of cisplatin in 1969.[28] Its mechanism of action resides in its ability of interacting with DNA, which avoids its replication, leading to cell death through apoptosis. Cisplatin and their second- and third-line analogues, carboplatin and oxaliplatin, are currently one of the most used strategies in clinic to treat patients with ovarian, lung, head, neck and bladder cancer. However, they also produce

undesirable side effects and drug resistance related to their non-specificity.[29] In this sense, nanotechnological tools can greatly improve cancer treatment. Due to their nanometric size, these tools benefit from non-specific targeting to solid tumors, known as enhanced permeation and retention effect (Figure 2).[30] The defective anatomy of the vasculature surrounding the tumor, highly disorganized with numerous dilations and pores, together with functional anomalies produce a high permeation and retention of these nanoparticles, thus increasing the therapeutic index.

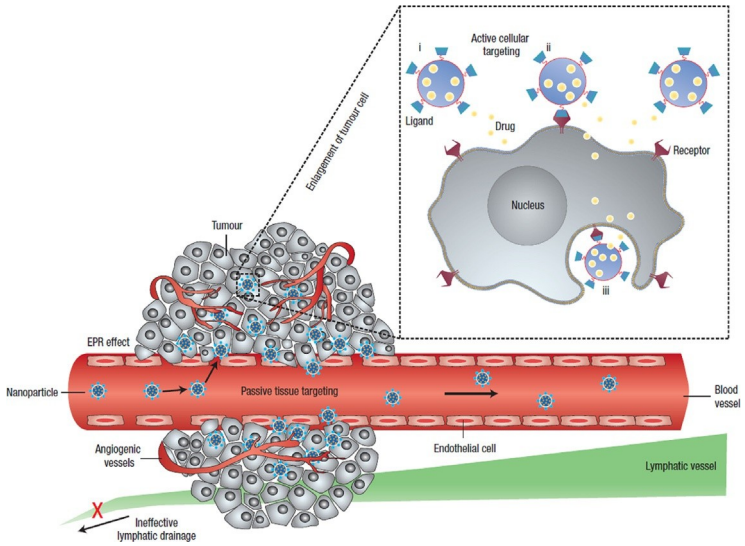

Figure 2 Schematic representation of different mechanisms which nanocarriers use to deliver drugs to tumors, including passive tissue targeting (enhanced permeation and retention effect) and active cellular targeting. Reprinted by permission from Springer Nature, Peer D, Karp JM, Hong S, Farokhzad OC, Margalit R, Langer R. Nanocarriers as an emerging platform for cancer therapy. Nat Nanotechnol. 2007;2 (12):751–760. Copyright 2007.

In the search for new antitumor strategies, the combination of metal complexes and dendritic scaffolds seemed like a logic transition to explore. Different examples have been reported in the literature, where metallodendrimers act directly as drugs, or as carriers of drugs o genetic material in gene therapy. Furthermore, they have been studied as diagnostic tools or even as theranostic agents, combining both therapy and diagnosis. All these applications will be reviewed in the following sections.

2.1.1 Metallodendrimers as anticancer drugs

Considering the potential of platinum complexes as anticancer agents, a popular alternative has been the use of polymeric supports which enable the sustained release of the drug into the extracellular fluid.[31] The first metallodendrimers reported in the literature contained this drug in its structure, providing non-toxic and multivalent platforms. Figure 3 presents the state-of-the-art timeline in the development of anticancer metallodendrimers, as highlighted by Smith in 2012.[26] In 1999, the first metallodendrimers with antitumor properties were presented to the scientific community, when Reedijk et al.[32] and Duncan et al.[33] designed platinum complexes conjugated with PPI and PAMAM dendrimers, respectively, showing high cytotoxic activities in diverse

cancer cell lines. The carboxylate-decorated PAMAM dendrimer showed a high cytotoxicity in cisplatin-resistant cell lines, like an ovarian cancer cell line (SKOV3). However, the PPI metallodendrimer with four metal centers showed a low cytotoxicity in two mouse leukemia cells lines (L1210/0 and L1210/2) and seven human cancer cell lines, probably due to the high steric congestion hindering the cellular uptake. After this starting point, researchers introduced structural modifications with the goal of reducing some of the severe effects involved in the treatment with cisplatin. For example, the efforts of Gust et al.[34] on achieving a more selective system for breast cancer led to platinum G1-PPI metallodendrimers which improved the cellular uptake and DNA binding 20–700 times more than the free drug in breast cancer cells (MCF-7). Besides platinum, other metal ions have been reported in the state-of- the-art of metallodendrimers, such as ruthenium(II), copper(II), gold(I) and palladium(II), as depicted in Figure 3. It is worth highlighting that, in recent years, the research focus has shifted to such alternative metals, with few examples of new platinum metallodendrimers. A summary of the most promising ones and their cytotoxicity indices are included in Table 2 and will be discussed below.

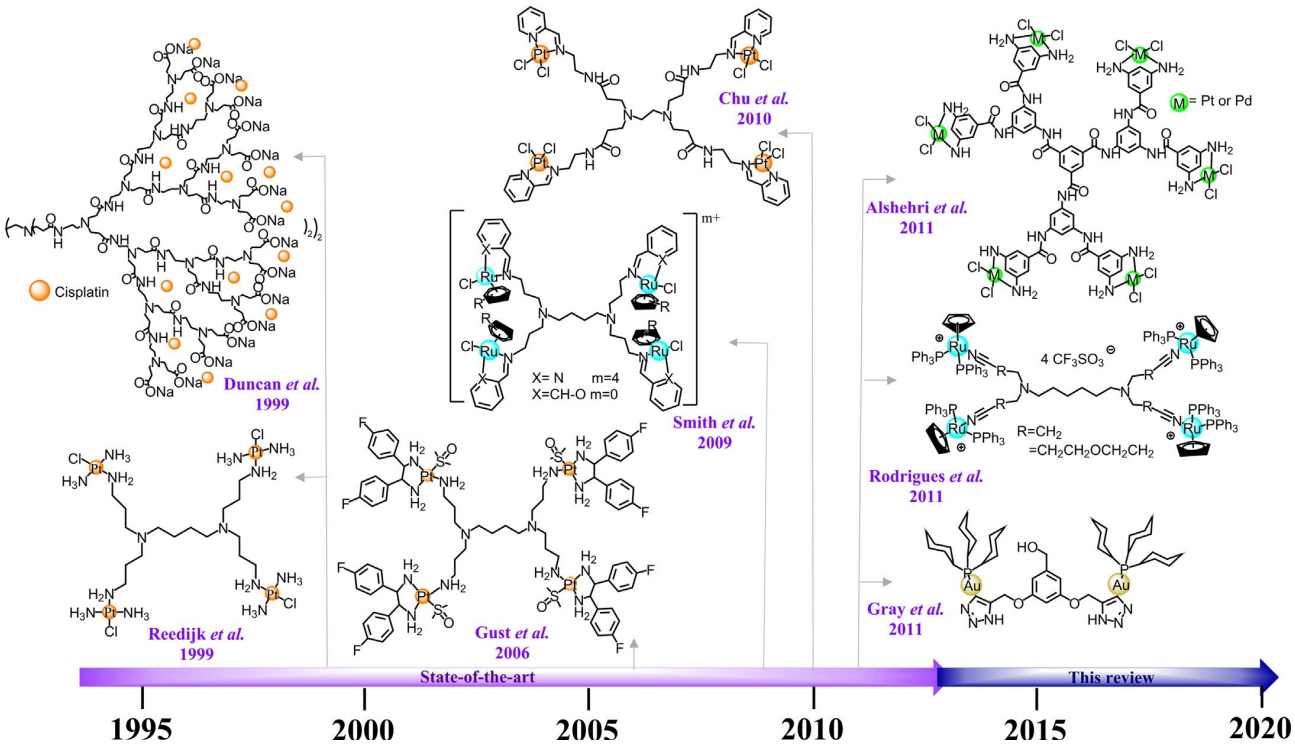

Figure 3 State-of-the-art in anticancer metallodendrimers until 2012, including selected examples.[26]

Table 2 *Overview of selected metallodendrimers including the cytotoxicity index IC_{50} in different tumor and non-tumor cell lines, after 24 h treatment.*

Entry	Metal	Dendritic scaffold	Metal complex	Number metals	Cell line (tumor, *non-tumor)	$IC_{50} \pm SD$ (μM)	Ref.
1	Pt(IV)	G4-PAMAM	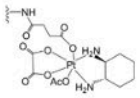	12	CH1/PA-1 A549 SW480	0.009 ± 0.002 0.15 ± 0.03 0.04 ± 0.02	35
2	Ru(II)	G4-PA	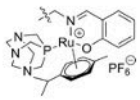	32	A2780 A2780*cis*R *HEK	0.8 ± 0.1 2.7 ± 0.1 2.6	36
3	Ru(II)	G1-CBS	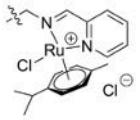	4	HeLa MCF7 HT29 MDA-MB-231 PC-3 HL-60 * HEK-239T	8.1 ± 0.4 6.9 ± 0.5 5.6 ± 0.1 6.1 ± 1.0 7.8 ± 1.4 2.3 ± 0.4 10.7 ± 0.0	37,38
4	Ru(II)	G4-PA	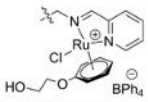	32	A2780 A2780cisR *HEK293	5.0 ± 0.1[a] 17.3 ± 1.5[a] 12.0 ± 0.9[a]	39
5	Ru(II)	G1-PA	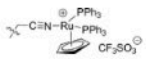	4	Caco-2 CAL-72 MCF-7 A2780 A2780*cis*R hMSC	3.4[a] 0.6[a] 2.5[a] 0.1[a] 0.3[a] <0.05[a]	40
6	Ru(II)	G1-CBS	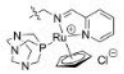	4	HeLa MCF7 HT29 HCC1806 PC-3 *142BR	6.3 ± 0.2 10.3 ± 0.5 11.4 ± 0.4 2.2 ± 0.1 8.3 ± 0.6 19.2 ± 0.2	41
7	Cu(II)	G3-PD	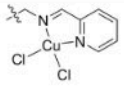	48	KB HL60 HCT116 MCF7 OVCAR8 U87 *EPC *MRC5	0.46[a] 0.58[a] 0.30[a] 0.41[a] 0.65[a] 0.86[a] 1.36[a] 0.80[a]	42
8	Cu(II)	G1-CBS		4	HeLa PC-3 MCF-7 HCC1806 HT29 *142BR	1.7 ± 0.5 3.4 ± 0.2 2.1 ± 0.2 1.9 ± 0.1 9.3 ± 0.5 7.7 ± 0.5	43
9	Fe(II)	G1-PA		3	DLD-1 HT29	17.0 ± 1.2 33.9 ± 1.2	44
10	Re(I)	G1-PA	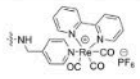	4	A431 DLD-1 A2780 *BJ	14.09 ± 2.23 10.18 ± 0.47 6.38 ± 1.18 17.69 ± 1.5	45
11	Au(III)	G3-PD	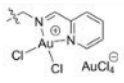	48	KB HL60 *EPC *MRC5	7.5 ± 7.5 3.3 ± 0.6 >1000 12.0 ± 5.0	46
12	Rh(III)	G2-PA	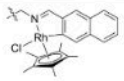	8	A2780 A2780cisR *HEK293	8.0 ± 0.5[a] 3.1 ± 0.3[a] 4.5 ± 0.5[a]	47
13	Ir(III)	G2-PA	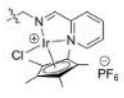	8	A2780 A2780cisR *HEK	0.75 ± 0.01[a] 3.5 ± 0.3[a] 28.6 ± 1.3[a]	47
14	Os(II)	G2-PA	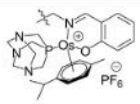	8	A2780 A2780cisR	16.4 ± 12.5[a] 43.5 ± 2.7[a]	48

[a]Values after 72 h treatment. PLL, polylysine dendrimer; PA, polyamine dendrimer; CBS, carbosilane dendrimer; PD, phosphorous dendrimer.

2.1.1.1 Platinum(II, IV) metallodendrimers

Among the recent trends on the design of anticancer platinum metallodendrimers, two different approaches are prevalent. First, the use of dendritic scaffolds as carriers of cisplatin or analogues through electrostatic interactions or encapsulation. In 2013, Palakurthi et al. reported a new family of biotin-conjugated PAMAM metallodendrimers functionalized with amino and carboxylic groups in their periphery with the ability to act as potential carriers of cisplatin.[49] All dendrimers studied showed better anti- cancer activities than cisplatin in a wide variety of tumor cancer cell lines (OVCAR-3, SKOV, A2780, CP70), as well as higher expression of apoptotic genes. All these properties, besides their higher potential to form adducts with DNA, placed them as promising candidates in this field. A similar strategy was recently proposed by Wheate et al., using a cationic PAMAM dendrimer as a carrier of PHENSS, a potent platinum anticancer drug developed by Aldrich-Wright, previously encapsulated with *p*-sulfonatocalix[4]arene.[50] Unfortunately, the final dendritic nanocomplex did not potentiate the anti- cancer properties but placed it as a possible vehicle to increase the selectivity of the drug and decrease the side effects.

The second prevalent approach relies on the covalent attachment of platinum complexes to the dendritic scaffold, leading to new metallodendrimers with anticancer activity *per se*. In 2016, Xu et al. developed three different generations (G1, G2 and G3) of poly-L-lysine dendrimers with platinum coordinated to selenium in the core and amino groups in the periphery (Figure 4A).[51] The coordination of platinum was carried out through the replacement of the chloro and amino ligands in the cisplatin complex leading to the formation of a selenium–platinum active site. These dendrimers showed better cellular uptake than cisplatin allowing the reduction of the dosage, as well as better anticancer activities *in vitro*. Importantly, the increase in generation led to a decrease in the anticancer activity due to the reduced availability of the metal center. *In vivo* experiments carried out in Balb/c mice with breast cancer showed that all metallodendrimers had similar activity than cisplatin but did not affect the mouse weight, unlike cisplatin (Figure 4B). In the same year, Keppler et al. conjugated an oxaliplatin analogue to G2 and G4 PAMAM dendrimers decorated with amino groups, which showed improved cytotoxicity in some cell lines (CH1/PA-1, A549 and SW480) (Table 2, Entry 1).[35]

2.1.1.2 Ruthenium(II) metallodendrimers

In pursuit of new mechanisms of action that overcome cancer cell resistance to drugs, ruthenium has stood out during the last years. The main reason is the wide variety of oxidation states (+2, +3, +4) and the ability to reduce systemic toxicity through the mimicking of iron behavior and binding to some biological molecules, including transferrin. Taking into account that some cancer cells have the transferrin receptor overexpressed a high level of ruthenium complexes will be delivered preferentially to these cells.

Currently, there are two ruthenium complexes in clinical trials, namely NAMI-A H_2Im[trans-$RuCl_4$(DMSO)(Him)] (Him ¼ imidazole) and KP1019 H_2Ind[trans-$RuCl_4(Hind)_2$] (Hind¼ indazole), both comprising Ru(III). Ru(III) complexes can behave as prodrugs, being reduced to

Ru(II) in the solid tumor where a reducing environment is created due to the low oxygen content. On the contrary, only Ru(II) metallodendrimers have been reported in the literature, probably due to the protective nature of the dendrimer which enables a direct delivery of the active metal.

In the search of new metallodendritic structures, the imine-type ligands have become popular, since these can act as anchor points of various metals centers. In 2013, PPI metallodendrimers functionalized with RAPTA (ruthenium(II)-arene-1,3,5-triaza-7-phosphatricyclo) complexes were developed and evaluated as anticancer agents.[36] Smith et al. presented a library

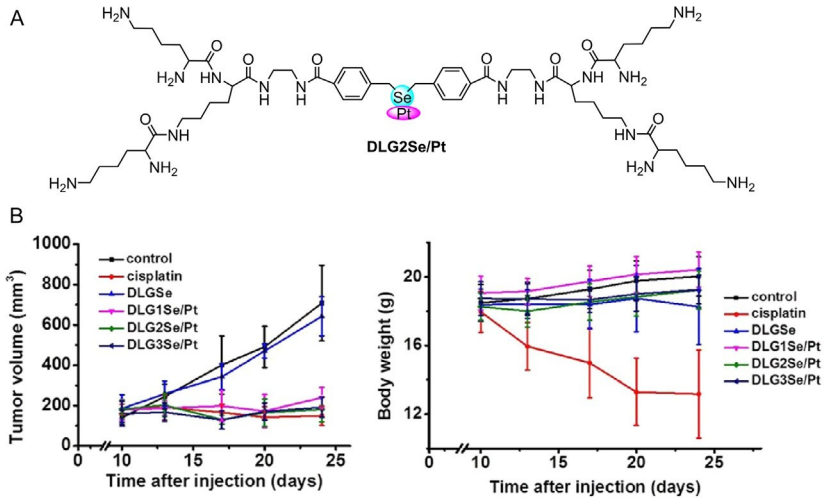

Figure 4 Antitumor activity of Pt(II) poly-L-lysine metallodendrimers.[51] (A) Structure of the second-generation metallodendrimer. (B) Changes in tumor volume and body weight in breast (4T1) cancer mice models after the treatment with cisplatin, dendrimer and three different generations of metallodendrimers. Reprinted with permission from Li T, Smet M, Dehaen W, Xu H. Selenium–platinum coordination dendrimers with controlled anti-cancer activity. ACS Appl Mater Interfaces. 2016;8(6):3609–3614. Copyright 2016 American Chemical Society.

of dendrimers from first to fourth generation and functionalized with *N*-monodentate, specifically pyridine, and *N,O*-, *N,N*-chelating imine ligands and complexes with ruthenium(II)-arene-PTA where the arene derivate can be *p*-cymene or hexamethylbenzene. They found a correlation between the size of the metallodendrimer and the activity, being the complex with 32 phenol-imine ligands and *p*-cymene the most active, with IC_{50} values in the low μM range in two ovarian cancer cell lines (A2780 and A2780*cis*R) (Table 2, Entry 2). The dendritic scaffolds improved the selectivity *in vitro* toward tumor cell lines, compared to their mononuclear analogues. In addition, they demonstrated that the presence of PTA ligands in the metal complexes improved the overall activity probably due to a better interaction with DNA.

Using the same chelating ligands but supported on a carbosilane scaffold, de la Mata et al. presented in 2016 different families of Ru(II) carbosilane metallodendrimers employing [Ru(η^6-*p*-cymene)Cl_2]$_2$ as precursor and evaluated their anticancer activity in a wide variety of tumor cell lines.[37] The influence of the lipophilic dendrimer was clearly observed, being the first-generation dendrimer with four functional groups the most efficient, activity that did not improve even if the number of metal centers doubled in the second generation. The reported studies of reactivity toward some biomolecules like Human Serum Albumin (HSA), Cathepsin-B and DNA confirmed a different mechanism of action, compared to cisplatin, and *in vitro* antimetastasic activity. In 2019, further *in vitro* studies— proliferation, cell cycle, cytotoxicity, cell adhesion—were performed on selected first-generation metallodendrimers. Overall, the assays concluded that the metallodendrimer with iminopyridine ligands G1-[[NCPh (*o*-N)Ru(η^6-*p*-cymene)Cl]Cl]$_4$ was an outstanding molecule with IC_{50} values in the range 5.6–8.1 μM in different human cancer cell lines

(Table 2, Entry 3). The authors evaluated the antitumor behavior of this metallodendrimer in an *ex vivo* mice model of human prostate cancer, inoculating untreated or treated PC-3 cells subcutaneously into two different groups of immunodepressed mice. A remarkable 82% smaller tumor size was observed in the treated mice, compared to non-treated group, at the end of the experiment (Figure 5A). An *in vivo* mice model was later established, using athymic male nude mice nu/nu with subcutaneously injected PC-3 cells, in order to use a scenario as closer to clinical practice as possible. In this case, the subcutaneous treatment with this metallodendrimer at a daily dose of 5 mg/kg inhibited up to 36% of the tumor growth (Figure 5A)and no appreciable negative effect in mice health was observed

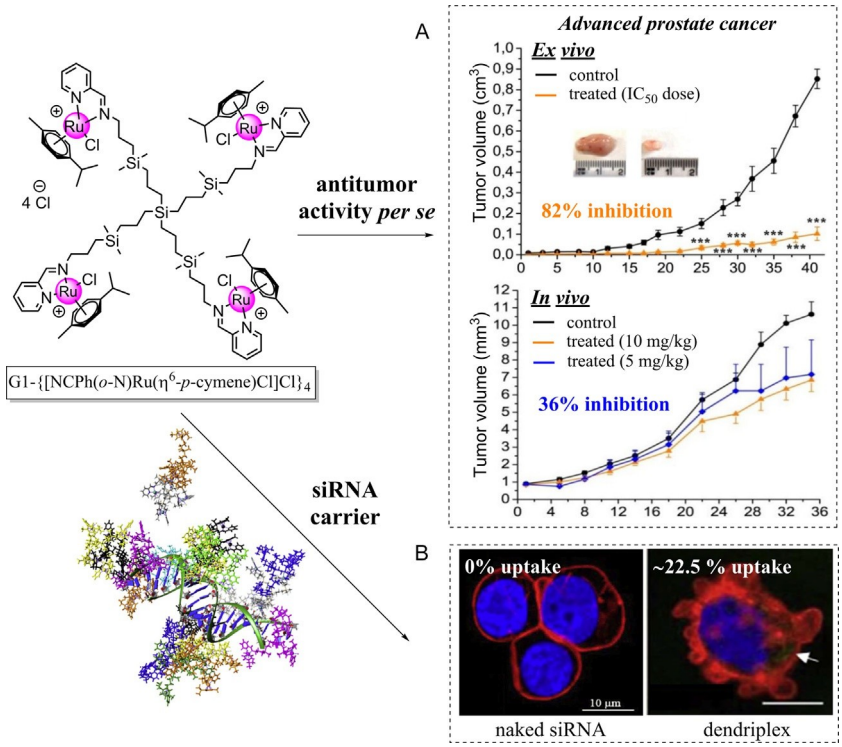

Figure 5 Reported anticancer strategies employing the Ru(II) carbosilane metallodendrimer G1-[[NCPh(o-N)Ru(η⁶-p-cymene)Cl]Cl]₄. (A) Antitumor activity per se in advanced prostate cancer mice models. (B) Carrier of antitumor siRNA. Panel (A): Figures adapted from Maroto-Díaz M, Sanz del Olmo N, Muñoz-Moreno L, et al. In vitro and in vivo evaluation of first-generation carbosilane arene Ru(II)-metallodendrimers in advanced prostate cancer. Eur Polym J. 2019;113:229–235. Copyright 2019, with permission from Elsevier; Panel (B) Figures adapted from Michlewska S, Ionov M, Maroto M, et al. Ruthenium dendrimers as carriers for anticancer siRNA. J Inorg Biochem. 2018;181:18–27. Copyright 2018, with permission from Elsevier.

during the treatment.[52] Aiming to provide insight into the mechanism of action of these Ru(II) carbosilane metallodendrimers, Bryszewska et al. evaluated their antitumor effect in the human leukemia cell line HL-60.[38] Again, they observed a remarkable cytotoxicity for the first-generation metallodendrimer G1-[[NCPh(*o*-N)Ru(η⁶-*p*-cymene)Cl]Cl]₄ (Table 2, Entry 3). Circular dichroism studies using TMA-DPH and DPH probes showed the metallodendrimers interaction with the hydrophobic and hydrophilic regions of the cell membranes. Moreover, the first-generation metallodendrimer increased the production of Reactive Oxygen Species (ROS) and decreased the

mitochondria potential, confirming the activation of apoptosis pathway, as well as the DNA damage and the increase in caspase level. The treatment with this metallodendrimer produced visible changes in the cell structure, and they observed a chromatin condensation with changes in mitochondrial shape and appearance of multivesicular and lamellar bodies, characteristic of early apoptosis.

Other dendritic scaffolds used by Smith et al. in 2015 to anchor Ru(II)-ethylene-glycol complexes were G1–G4 pyridylimine-based poly(propylene)dendrimers.[39] The antiproliferative effect was evaluated *in vitro* in two ovarian cancer cell lines (the cisplatin sensitive A2780 and the cisplatin-resistant A2780cisR) and compared with monometallic complexes. The results showed that the monomer and low generation dendrimers were inactive, whereas the higher generation analogues exhibited antitumor activity (Table 2, Entry 4).

As an alternative cancer treatment, metallodendrimers have also been used as siRNA carriers to selectively silence aberrantly activated oncogenes. The lack of effective and cheap carriers of siRNA remains a major problem in gene silencing, where the use of dendrimers has shown promising results.[53] Cationic PAMAM, phosphorous and carbosilane dendrimers, among others, efficiently interact with negatively charged siRNA through electrostatic interactions.[54] Nonetheless, there are very few examples in which the nanocarrier contains metals in its structure. In 2018, Bryszewska and co-workers studied the interactions between ruthenium(II) carbosilane metallodendrimers and small siRNA,[55] aiming to observe an enhanced anti- cancer activity arising from the combination of the metallodendrimer and the siRNA. Two different families of ruthenium metallodendrimers were studied, comprising pyridine or iminopyridine ligands. The authors con- firmed the *in vitro* interaction between the metallodendrimers and the siRNA, the protection from nucleases degradation as well as the transfection in human promyelocytic leukemia cell line (HL60), observing that the dendriplexes crossed the cell membrane and penetrated into the cell, unlike naked siRNA (Figure 5B). The dendriplex uptake was more efficient for iminopyridine-bearing dendrimers, due to their cationic nature, and for second-generation counterparts, finding up to 30% loaded cells for the most efficient metallodendrimer G2-[[NCPh(o-N)Ru(η6-p-cymene)Cl] Cl]8, compared to the ca. 23% of the first-generation counterpart.

Besides the dendritic scaffold and the peripheral moieties, the ligands on the metal coordination sphere clearly influence the antitumor activity of the final metallodendrimer. Among the different arene ligands on the Ru(II) ion, cyclopentadienyl (Cp or η^5-C_5H_5) showed promising results. Continuing their work on poly(alkylidenimine) dendrimers functionalized with the metal complex [Ru(η^5-C_5H_5)(PPh_3)$_2$]$^+$,[56] in 2018 Rodrigues and co-workers evaluated the antitumor activity in a broad variety of tumor cells, including colorectal, osteosarcoma, breast and ovarian (Table 2, Entry 5).[40] The metallodendrimers exhibited high cytotoxicity, with IC_{50} values in the range 0.1–3.4 μM after 72 h treatment, higher than the precursor dendrimers, the complex [Ru(η^5-C_5H_5)(PPh_3)$_2$Cl] and cisplatin. In addition, promising activity was observed in primary human mesenchymal stem cells (hMSCs), involved in tumor progression and drug resistance, with IC_{50} < 0.05 μM.

The organometallic ligand cyclopentadienyl and the phosphine, 1,3,5-Triaza-7-phosphatricyclo[3.3.1.13.7]decane (PTA), were included in a new family of Ru(II) carbosilane metallodendrimers in order to improve the activity, solubility and stability.[41] Both families shared the carbosilane dendritic scaffold and peripheral *N*,*N*-chelating imine ligands, as well as similarly potent cytotoxic activity toward multiple cancer cell lines, including advanced prostate, breast, colorectal and cervix, higher than the activity observed toward non-tumor fibroblasts (Table 2, Entry 6). In order to corroborate the antitumor activity of this ruthenium dendrimer, an *in vivo* experiment was designed in athymic mice with advanced prostate cancer injecting a dose of 10

mg/kg intravenously once a week and achieving 25% of inhibition of the tumor growth compared to the non-treated mice. No negative symptoms, such as weight loss, were observed during the experiment (Figure 6).

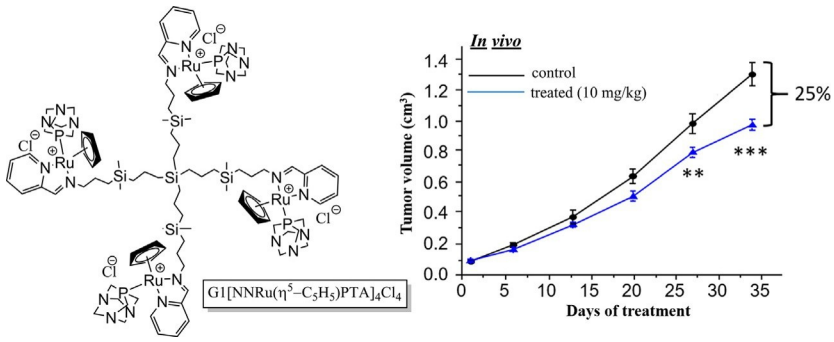

Figure 6 Antitumor activity of Ru(II) carbosilane metallodendrimer G1{[NNRu(5-C_5H_5) PTA]Cl}$_4$in an in vivo advanced prostate cancer mice model.[41]

2.1.1.3 Copper(II) metallodendrimers

Copper is a biocompatible metal, endogenously present in the human body. Copper(II) mononuclear complexes have been explored as anticancer agents showing promising results.[57] Its cytotoxicity is related to the high redox activity and the alteration of Reactive Oxygen Species (ROS) balance.[58] Copper is also involved in tumor angiogenesis at early stages. In 2013, Majoral and co-workers demonstrated the anticancer activity of new Cu(II)-conjugated phosphorus dendrimers.[42] Three different families were prepared bearing ligands with nitrogen donor atoms, i.e., *N*-(pyridin-2- ylmethylene) ethanamine, *N*-(di(pyridin-2-yl)methylene)ethanamine and 2-(2-(methylenehydrazinyl)pyridine, able to coordinate $CuCl_2$. The resultant first-, second- and third-generation metallodendrimers presented 12, 24 and 48 bound Cu(II) ions, respectively. Overall, the study concluded that both the nature and the number of the peripheral groups play a major role in the antitumor potency of the dendrimers and the metal coordination boosted this effect. The metallodendrimers produced an increasing inhibition of the proliferation of human promyelocytic leukemia cells (HL60) when the number of functional groups increased, being the third-generation dendrimer the most promising one. Interestingly, the third-generation metallodendrimer decorated with *N*-(pyridin-2-ylmethylene)ethanamine and 48 Cu(II) ions exhibited certain preference for cancer cells, such as HL60 and human cervical cancer derivative cell line (KB), compared to the non-cancer cells used as control, after 72 h treatment (Table 2, Entry 7).

The promising results obtained with Ru(II) carbosilane metallodendrimers decorated with *N*,*N*- and *N*,*O*-chelating ligands encouraged de la Mata and co-workers to generate the Cu(II) analogues and evaluate their antitumor activity. In 2017, the dendritic scaffolds were used to chelate $CuCl_2$.[43] Unlike the phosphorous Cu(II) metallodendrimers, the first- generation carbosilane metallodendrimers—with four metal ions—exhibited the highest antitumor activity among the different dendritic generations. This behavior is consistent with that observed for the Ru(II) carbosilane counter- parts and confirms the dramatic influence of the lipophilic scaffold. In order to improve the water solubility of the Cu(II) metallodendrimers, in 2019

the dendritic scaffolds were used to chelate $Cu(NO_3)_2$.[59] The NO_3^- groups are more labile than the Cl^- ligands, and are susceptible to be released after dissolution in water creating an overall positive charge in the metallodendrimer. The study showed that the exchange from chloride to nitrate ligands increased not only the water solubility but also the general cyto- toxic activity (Table 2, Entry 8), probably due to the positive charge of the new metallodendrimers, which interact and consequently destabilize the cell membrane, according to Electron Paramagnetic Resonance (EPR) studies. Further *ex vivo* studies in an advanced prostate cancer mice model (athymic male nude mice nu/nu) demonstrated that the first- generation carbosilane dendrimer functionalized with $Cu(NO_3)_2$ produced a significant inhibition of the tumor growth, reaching up to 37% smaller tumor size compared to non-treated mice. Copper metallodendrimers open new avenues in cancer treatment being more economic and more biocompatible than traditional metallodrugs.

2.1.1.4 Iron(II) metallodendrimers

Similar to copper, iron is also found in traces in the human body and takes part in numerous biological processes. This metal has shown interesting anticancer properties; in fact, ferrocene was the first organometallic com- pound reported for its antiproliferative effect.[60] Ferrocenyl derivatives might be oxidized in the cell via Fenton pathway generating free radicals that lead to DNA damage and final cell apoptosis as a possible mechanism of action.[61]

Despite the interest in including ferrocene moieties in a multivalent scaffold, surprisingly, only few examples are found in the literature. In recent years, Smith and co-workers presented tri- and tetrametallic systems comprising polypropylenimine tetramine or tris(2-aminoethyl)amine cores functionalized with a ferrocenyl aldehyde by Schiff condensation followed by reductive amination.[44] The Fe(II) metallodendrimers exhibited moderate IC_{50} values in human colorectal cancer cell lines (Table 2, Entry 9). Both compounds were capable of penetrating inside the cell and producing early apoptosis, but only the trinuclear metallodendrimer increased the ROS level in tumor cells.

2.1.1.5 Rhenium(I) metallodendrimers

Recently, rhenium has attracted a widespread attention from the biomedical field due to the high variety of oxidation states and geometries, and the ability of coordinating different ligands.[62] In particular, the stable Re(I) tricarbonyl complexes have become quite popular,[63] inducing cell death in a different manner compared to cisplatin and many other drugs, suggesting a novel mode of action different from the traditional apoptosis, necrosis, paraptosis and autophagy. In 2018, Smith and co-workers presented two different first-generation Re(I) PPI metallodendrimers,[45] comprising 3 and 4 $[Re(bpy)(CO)_3]$ complexes bound to the dendrimer through a pyridine moiety. The cytotoxicity of these metallodendrimers against epithelial, colon and ovarian carcinoma was moderate, with IC_{50} values in the micromolar range and selectivity toward cancer cells in comparison to the mononuclear counterpart used as a control (Table 2, Entry 10). The tetranuclear metallodendrimer exhibited higher cyto- toxicity than cisplatin in all cell lines tested. Mechanistic studies demonstrated that these rhenium metallodendrimers boost apoptotic cell death by modulating the expression of Bax-α, being the tetranuclear dendrimer the most efficient.

2.1.1.6 Gold(III) metallodendrimers

Gold has been used from ancient times, and its potential as anticancer agent has been proved in *in vitro* and *in vivo* experiments.[64] Despite sharing the same electronic configuration and similar properties, gold(III) and platinum(II) complexes frequently follow different mechanism of action. Gold complexes exhibit better selectivity and potency against cancer cells due to their weaker DNA-binding activity and higher affinity to protein targets through sulfhydryl, thiol and selenocysteine groups.[65]

Majoral and co-workers published in 2017 an original third-generation phosphorous metallodendrimer comprising 48 iminopyridine end groups complexing Au(III), namely $1G_3$-$[Au_{48}][AuCl_4]_{48}$.[46] This metallodendrimer showed IC_{50} values in the nanomolar range in different tumor cell lines, while a very weak effect was observed against non-cancer cells (Table 2, Entry 11). In order to corroborate that the activity arised from the metallodendritic complex, $AuCl_3$ was also studied, and it was observed that it retained a low intrinsic activity. In addition, the physical mixture of $AuCl_3$ and the precursor dendrimer did not potentiate the intrinsic anti- proliferative effect of the dendrimer compared to that of the metallodendrimer $1G_3[Au_{48}][AuCl_4]_{48}$. Moreover, the authors expanded the study performing different structural modifications, including the evaluation of non-complexed dendrimers with iminopyridine and PEG, gold metallodendrimers with PEG and dendrimers with free iminopyridine without metal, showing the best results with the metallodendrimer

2.1.1.7 Osmium(II), Iridium(III), Rhodium(III) metallodendrimers

Recently, metals such as iridium, osmium and rhodium have caught the attention in the search for new metallodrugs due to their intrinsic anticancer activity.[66–68] In 2014 Smith et al. reported new families of rhodium(III) and iridium(III) metallodendrimers of first- and second-generation naphthaldimine-decorated PPIscaffolds and with Cp* (pentamethylcyclo- pentadienyl) as ligand of the metal complex. The anticancer activity was measured *in vitro* in two different ovarian cancer cell lines (A2780 and A2780cisR) where the second-generation complexes with eight functional groups stood out as the most promising ones, being Rh(III) complexes bet- ter than their Ir(III) counterparts (Table 2, Entries 12 and 13).[47] The activity found for the new rhodium and iridium derivatives is comparable with the antitumor activity of arene-ruthenium(II) complexes attached to similar dendritic scaffolds.[69]

Osmium analogues of potent anticancer drugs, such as Ruthenium- NAMI-A, present moderate antiproliferative activity *in vitro* in colon carcinoma (HT-29) and breast carcinoma (SK-BR-3).[70] With the objective to implement the activity of these derivatives, in 2015 Smith et al.[48] synthetized new families of neutral and cationic half-sandwich Os(II)-arene DAB-PPI metallodendrimers, namely [DAB-PPI-{(η^6-*p*-cym)Os((C_7H_5NO)-κ^2-N,O) Cl}$_n$], [DAB-PPI-{(η^6-*p*-cym)Os(($C_6H_5N_2$)-κ^2-N,N)Cl}$_n$][PF_6]$_n$ and

[DAB-PPI-{(η^6-*p*-cym)Os((C_7H_5NO)-κ^2-N,O)PTA}$_n$]. *In vitro* studies against the cisplatin sensitive (A2780) and cisplatin-resistant (A2780cisR) ovarian cancer cell lines showed that neutral dendrimers were inactive while cationic metallodendrimers displayed moderate activity which improved when the counterion was PTA and not Cl (Table 2, Entry 14).

2.1.1.8 Heterofunctional metallodendrimers

An effective strategy in cancer treatment relies on combination therapy. It has been shown that the administration of several drugs with different mechanisms of action, used in their optimal dose, has a better effect than if they are administrated independently. In this sense, dendrimers are optimal

platforms to provide a precise and controlled combination therapy in a single scaffold, in the so-called heterofunctional dendrimers.

Despite the multiple advantages of designing heterofunctional metallodendrimers with antitumor activity, very few examples can be found in the literature. In 2014, Smith et al. presented the synthesis of first- and second- generation PPI metallodendrimers bearing heterometallic ferrocenyl-derived *N,O-p*-cymene-Ru(II)-PTA-salicylaldimine and *N,N-p*-cymene-Ru(II)-2-pyridylimine (Figure 7A).[71] Preliminary biological studies revealed that most of the compounds at equiiron concentrations of 5 μM decreased the growth of the ovarian human cancer cell lines A2780 and A2780cisR by more than 50% and showed certain selectivity for these ovarian cancer cell lines,

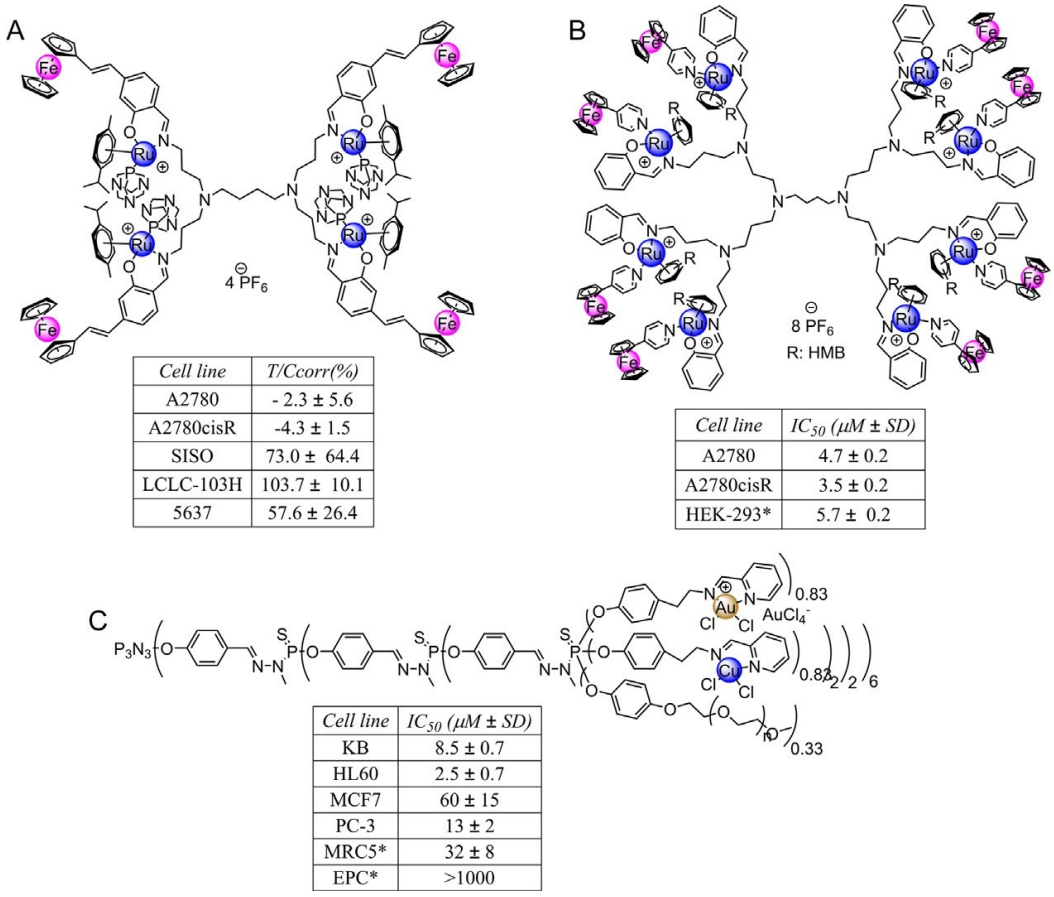

Cell line	*T/Ccorr(%)*
A2780	- 2.3 ± 5.6
A2780cisR	-4.3 ± 1.5
SISO	73.0 ± 64.4
LCLC-103H	103.7 ± 10.1
5637	57.6 ± 26.4

Cell line	*IC_{50} (μM ± SD)*
A2780	4.7 ± 0.2
A2780cisR	3.5 ± 0.2
HEK-293*	5.7 ± 0.2

Cell line	*IC_{50} (μM ± SD)*
KB	8.5 ± 0.7
HL60	2.5 ± 0.7
MCF7	60 ± 15
PC-3	13 ± 2
MRC5*	32 ± 8
EPC*	>1000

Figure 7 Examples of heterometallic dendrimers and cytotoxicity indices in cancer and non-cancer cells, expressed as (A) T/Corr (%) at 96 h exposure to compound at 5 μM Fe relative to untreated control,[71] and (B and C) IC_{50} after 72 h treatment.[46,72]

compared to other cancer cell lines. Higher cytotoxicity was observed with metallodendrimers with *N,O-p*-cymene ligands. Using a similar strategy but expanding the number of metal atoms, in 2016 new ferrocenyl PPI metallodendrimers were reported containing ruthenium(II)-*p*-cymene, ruthenium(II)–HMB (where HMB hexamethylbenzene), rhodium(III)– Cp* or iridium(III)–Cp* moieties.[72] The cytotoxicity of these systems was studied against A2780 and A2780cisR cells and non-tumorigenic human embryonic kidney cells (HEK-293), observing an increase in the activity in the highest generations. Particularly the second-generation dendrimer with ruthenium(II)-HMB

emerged as the most promising candidate, being less toxic in non-cancer cells (Figure 7B). UV–Vis studies showed that these metallodendrimers produce a non-covalent interaction with DNA as a possible mechanism of action. In 2017, Majoral and co-workers also explored the heterometallic strategy in the cancer field. As an expansion of their work in Au(III) phosphorous metallodendrimers,[46] they reported a third-generation metallodendrimer bearing 20 gold(III) complexes and 20 copper(II) complexes, to evaluate a possible synergistic effect, and 8 PEG molecules to improve the water solubility and biocompatibility (Figure 7C). The authors ruled out any additive effect, suggesting the existence of a threshold in the anticancer activity of Au(III) metallodendrimers.

The design of heterofunctional metallodendrimers goes beyond the heterometallic strategy, and the metal complexes can further be combined with other antitumor moieties or tracing moieties (Figure 8). For example, Grabchev et al. have developed several families of Cu(II) and Zn(II) poly(propyleneamine) metallodendrimers decorated with different 1,8- naphtalimides,[73–77] where the metal coordination is performed via the tertiary amine groups at the dendrimer inner shell and the outer naphtalimide shell is available for additional therapeutic or fluorescent response. Even though they were mainly evaluated as antibacterial agents as it will be described in Section 2.2.1, some of these metallodendrimers also exhibited antitumor activity. For example, the second-generation metallodendrimers,[75] decorated with four 4-bromo-1,8-napthtalimide peripheral moieties and two metal ions in the internal shell, presented enhanced cytotoxicity toward human non-small cell lung cancer (A549), triple negative breast cancer (MDA-MB-231) and carcinoma of the uterine cervix (HeLa), compared to the precursor dendrimer. The metallodendrimers exhibited IC_{50} values in the range 15–30 μM after 72 h treatment, with slightly lower values for the Zn(II) derivative (Figure 8A).

The inclusion of tracing moieties in a heterofunctional dendrimer can simplify the challenge of unraveling its mechanism of action and provide accurate and complete information about their behavior in a biological environment. In 2019, de la Mata, Bryszewska and co-workers presented a first-generation ruthenium(II) carbosilane metallodendrimer with fluorescein statistically attached in one of the branches.[78] The attachment of a single fluorochrome enables the monitoring within the cell but at the same time maximizing the antitumor activity arising from the Ru(II) complexes. The uptake by two different cancer cell lines, leukemia HL60 [78] and human prostate PC-3,[52] was evaluated through confocal microscopy, con- firming the ability of this compound to cross the cell membrane and remain in the cytoplasm even 24 h after treatment, unlike the well-known DNA-binding mechanism of platinum complexes (Figure 8B1). A similar strategy was used to attach the spin-label 2,2,6,6-tetramethylpiperidine-1-oxyl (TEMPO) to carbosilane Ru(II) metallodendrimers and conduct a complete study by EPR to analyze the affinity of these metallodendrimers for cell membranes.[79] Two different types of model membranes were used:

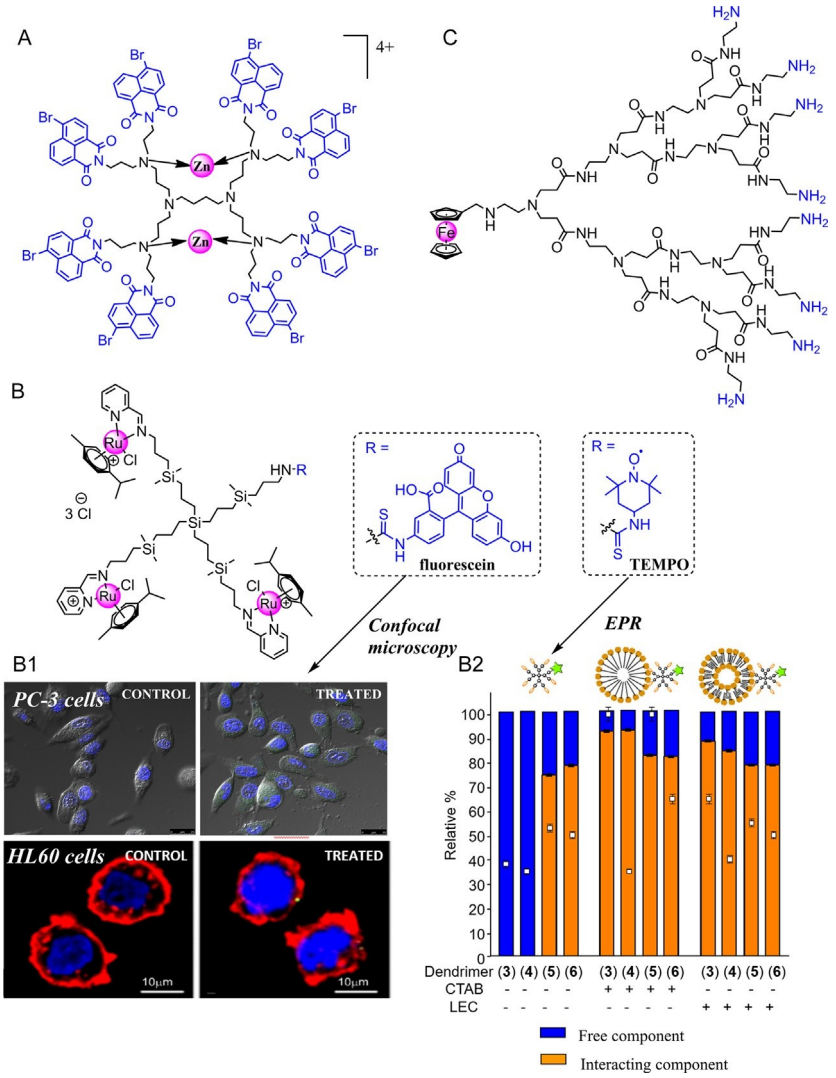

Figure 8 Examples of heterofunctional metallodendrimers combining a cytotoxic metal complex and additional moieties for improvement of activity, traceability or solubility. Layered-block Zn(II) metallodendrimer.[75] (B) Random Ru(II) metallodendrimer, including a fluorescein moiety for confocal microscopy (B1) or a TEMPO label for EPR evaluation (B2). (C) Ferrocene metallodendron.[80] Panel (B1): Figures adapted from Maroto-Díaz M, Sanz del Olmo N, Muñoz-Moreno L, et al. In vitro and in vivo evaluation of first-generation carbosilane arene Ru(II)-metallodendrimers in advanced prostate cancer. Eur Polym J. 2019;113:229–235. Copyright 2019, with permission from Elsevier and Michlewska S, Kubczak M, Maroto-Díaz M, et al. Synthesis and characterization of FITC labelled ruthenium dendrimer as a prospective anticancer drug. Biomolecules 2019;9(9): E411. Copyright 2019, with permission from MDPI. Panel (B2): Figures adapted from Carloni R, Sanz del Olmo N, Ortega P, et al. Exploring the interactions of ruthenium (II) carbosilane metallodendrimers and precursors with model cell membranes through a dual spin-label spin-probe technique using EPR. Biomolecules. 2019;9(10):540. Copyright 2019, with permission from MDPI

cetyltrimethylammonium bromide micelles (CTAB) and lecithin liposomes (LEC). The study provided complementary information from (1) the metallodendrimer point of view, containing the TEMPO label; and (2) the model membrane point of view, using 4-(*N*,*N*-dimethyl-*N*-dodecyl) ammonium-2,2,6,6-tetramethylpiperidine-1-oxyl bromide (CAT12), probe that can be inserted in the membrane. The authors confirmed the partial insertion of the surface groups attached to the

dendrimer skeleton into the model membranes, mainly CTAB micelles, and the presence of both types of interactions (hydrophilic and hydrophobic) whereas, in the case of LEC, it is possible to observe a prevalence of polar interactions (Figure 8B2). Any change in the dendritic structure can modify their ability of interacting with membranes, and, therefore, their anticancer activity.

The inherent heterofunctional nature of dendrons has also been employed to design metallodendrons with improved antitumor activity. In 2013, Şenel and co-workers presented a family of PAMAM dendrons with ferrocene in the focal point and amine groups in the periphery (Figure 8C).[80] The dendrons inhibited the proliferation of stomach adeno- carcinoma cells (AGS) via apoptosis and necrosis, increasing with the dose and the generation of the dendron. A similar strategy was recently reported by de la Mata and co-workers, where carbosilane dendrons comprised a [Ru(η^6-*p*-cymene)] fragment at the focal point coordinated through a *N*-monodentate, a *N*,*N*-chelate or an *N*,*O*-chelate ligand, and multiple – NMe_2 groups in the periphery.[81] These dendrons could potentially be evaluated as antitumor agents in future assays.

2.1.2 Metallodendrimers in the diagnosis and treatment monitoring

Imaging techniques are the mainstay in the diagnosis of numerous diseases. The exclusive properties provided by modern imaging methods in the study of the composition of the human body placed them among the most relevant advances of the century. There are a large number of imaging techniques,[82] and some of them provide remarkable information in the field of cancer. For example, the differences between tumor and normal tissues can be established by Magnetic Resonance Imaging (MRI). In order to improve the MRI signal, contrast agents are often used such as gadolinium chelates. Other techniques, like Single-Photon Emission Computed Tomography (SPECT) and Positron Emission Tomography (PET), involve the use of radiometals. Different metallodendrimers have been developed as diagnostic tools for MRI, optical and nuclear medical imaging, as described below.

In 2014, Shen et al. reported a tumor-targeting biodegradable polyester dendrimer conjugated with gadolinium and functionalized with PEG and folic acid as a MRI contrast agent, namely FA-PEG-G2-DTPA-Gd.[83] The PEG increased the blood circulation time whereas the folic acid increased the tumor selectivity, due to the overexpressed folate receptors in most tumors. This metallodendrimer exhibited a much higher contrast enhancement for longer times than Magnevist®, which is currently used in clinic as a gadolinium contrast agent. Whereas Magnevist® contrast signal starts decreasing 5 min post injection, the dendrimer prolongs it up to 15 min before its biodegradation and excretion in urine. In addition, 60 min post injection a weak contrast was observed between tumor and other tissues in mice using Magnevist® or the non-targeting metallodendrimer PEG-G2-DTPA-Gd; however, the contrast in mice treated with FA-PEG-G2-DTPA-Gd was strong, while in normal tissues the signal deceased with the excretion of the contrast agent (Figure 9A).

Aiming for improved SPECT imaging, Adronov and co-workers reported in 2015 a fifth-generation polyester dendrimer functionalized with mPEG chains of different molecular weights at the periphery and dipicolylamine technetium(I) at the core.[84] *In vivo* experiments in healthy rats showed that this metallodendrimer circulated in blood for up 24 h. Moreover, the inoculation of mice with Human Lung Squamous Cell Carcinoma (H520) showed that the dendrimer could accumulate in the tumor for 6 h post injection, probably due to the enhanced permeation and retention effect that characterize these systems (Figure 9B1). In parallel, Felder-Flesch and co-workers reported the synthesis of ^{111}In labeled PAMAM dendrons derived from DOTA and functionalized with PEG and with a melanin-targeting ligand, and studied the *in vitro* and *in vivo* targeting efficacy in murine melanoma models.[85] They found a correlation

between the multivalence of the dendrimers and the tumor uptake, the highest being 12.7 T 1.6% of the total injected dose per gram of tissue (ID/g) at 4 h post intravenous injection of the second-generation probe, compared to the 1.5 T 0.5 ID/g for a non-dendritic counterpart (Figure 9B2). The authors highlight the importance of multivalent small

nanoprobes for imaging sensitivity enhancement and increased delivery of radiation doses to tumors.

2.1.3 Metallodendrimers as theranostic agents

Current trends in the biomedical field focus on the design of new theranostic agents, which combine diagnostic and therapeutic agents in a single

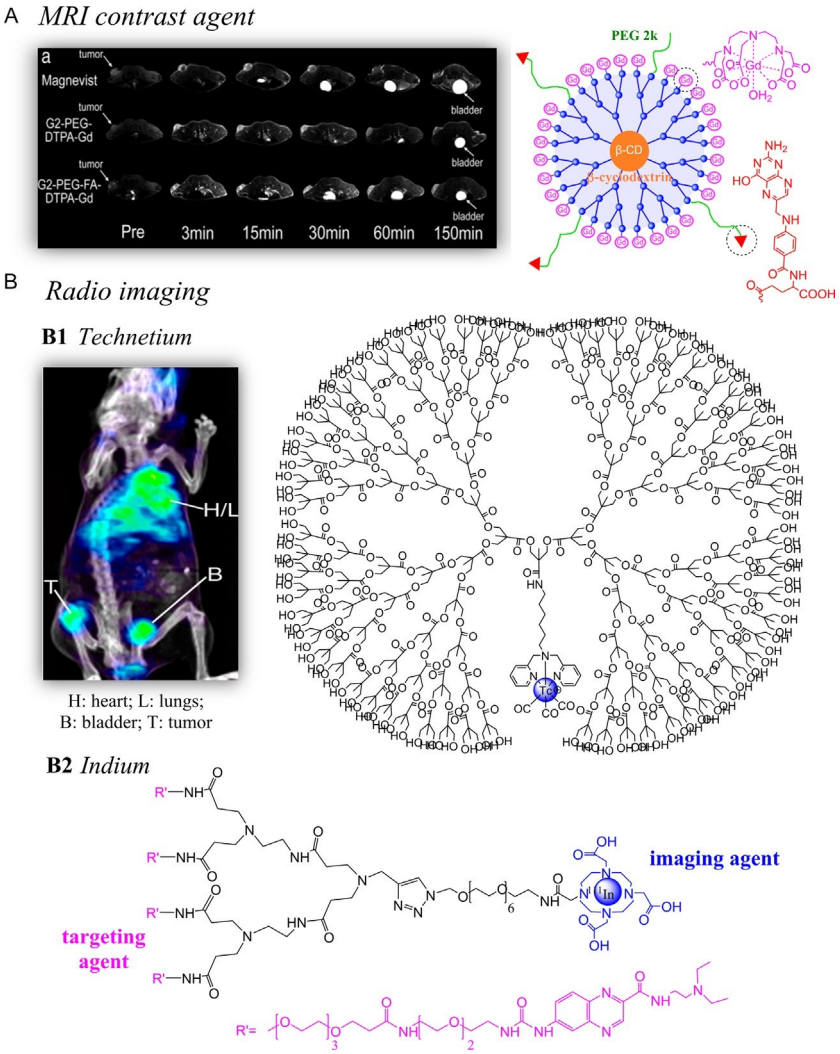

Figure 9 Recent examples of metallodendrimers as imaging agents. (A) Bis-MPA polyester Gd metallodendrimer as contrast agent for MRI, including 2D axial images contrast to noise ratio (CNR) and tumors in mice injected with FA-PEG-G2-DTPA-Gd or Magnevist at 0.1 mmol/kg.[83] (B1) Bis-MPA polyester Tc metallodendrimer for Scintigraphic-CT image of H520 tumor model 6 h post injection of [99mTcDPA-G5-(PEG750)] + (9.2 MBq).[84] (B2)[111] In labeled PAMAM dendron bearing melanin-targeting ligands.[85] Panel (A): Figures adapted from Ye M, Qian Y, Tang J, Hu H, Sui M, Shen Y. Targeted bio- degradable dendritic MRI contrast agent for enhanced tumor imaging. J Control

Release. 2013;169(3):239–245. Copyright 2013, with permission from Elsevier, McNelles SA, Knight SD, Janzen N, Valliant JF, Adronov A. Synthesis, radiolabeling, and in vivo imaging of PEGylated high-generation polyester dendrimers. Biomacromolecules 2015;16 (9):3033–3041. Copyright 2015, with permission from ACS.

platform. In these smart systems, each agent works synergistically and efficiently. Dendrimers are ideal nanoplatforms for this purpose, enabling a con- trolled and precise conjugation of the different moieties. In 2015, Chen et al. used cationic Ru(II) metallodendrimers to coat selenium nanoparticles dec- orated with anionic L- and D-arginine, which provided a chiral nature to the nanoparticle (Figure 10A).[86] The multifunctional nanoparticle was evaluated as carrier of MDR-siRNA (Ru@L-SeNPs-siRNA) into tumor cells, observing that the intravenous injection each 3 days in a mice model bearing adenocarcinoma human alveolar basal epithelial tumor cells (A549R) produced 79.4% inhibition of tumor growth. Furthermore, the intrinsic fluorescence of the multivalent Ru(II) complexes enabled a real-time monitoring in a xenograft mice model, observing a higher intensity in the tumor compared to the rest of the organs 4 h after the last injection. Another recent example of a powerful theranostic nanosystem has been reported by Shi, Majoral et al. and consists on a fifth-generation Cu(II) PAMAM metallodendrimer (G5.NHAc-Pyr/Cu(II)) (Figure 10B).[87] In addition to the promising anticancer properties of Cu(II), the presence of unpaired electrons in its outermost orbital has proposed Cu(II) as an alternative T1-weighted MR contrast agent. The authors confirmed the anticancer properties of this metallodendrimer, which increased the ROS levels, then produced a cell cycle S-phase arrest, apoptosis and finally induced cell death *in vitro*. Furthermore, two *in vivo* experiments—a xenografted subcutaneous tumor model and lung metastatic nodules in a bloodstream metastasis model- confirmed the compound accumulation in the tumor through enhanced permeation and retention effect and the suitability of this metallodendrimer as MRI agent. Nowadays, it is well known that radiotherapy changes the tumor vasculature and favors the accumulation of nanoparticles in the tumor. This fact has been also observed with G5.NHAc-Pyr/Cu(II), where the MRI performance in tumor-bearing mice can be significantly improved after the radiation of tumors observing an increment in the accumulation of this compound in the tumor environment (Figure 10B).

2.2 Metallodendrimers as antimicrobial agents

Ever since Alexander Fleming discovered penicillin in 1928, the antibiotic consumption has grown worldwide at neck-breaking speed. Undoubtedly, the discovery of this seeming panacea represented a milestone of medicine for the whole humanity but has ultimately led to a serious problem of multidrug-resistant bacteria. As an example, 14% of *S. aureus* hospital strains

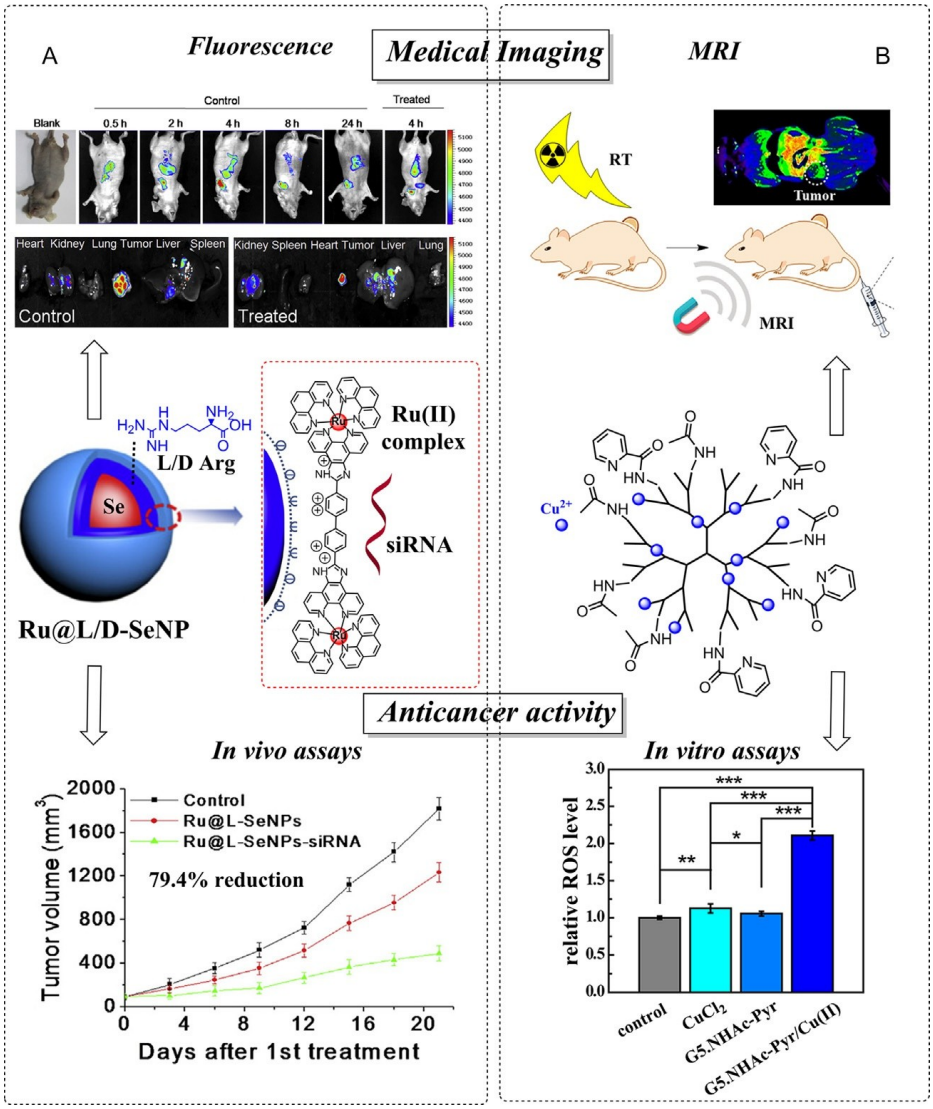

Figure 10 Dual activity of two metallodendritic-based theranostic agents. (A) Selenium NPs (Ru@L-SeNPs-siRNA).[86] (B) Copper(II) metallodendrimers G5.NHAc Pyr/Cu(II).[87] Panel (A): Figure adapted from Chen Q, Qianqian Y, Liu Y, et al. Multifunctional selenium nanoparticles: chiral selectivity of delivering MDR-siRNA for reversal of multidrug resistance and real-time biofluorescence imaging. Nanomedicine (N Y, NY, US). 2015;11 (7):1773–1784. Copyright 2015, Elsevier. Panel (B): Figure adapted from Fan Y, Zhang J, Shi M, et al. Poly(amidoamine) dendrimer-coordinated copper(II) complexes as a theranostic nanoplatform for the radiotherapy-enhanced magnetic resonance imaging and chemotherapy of tumors and tumor metastasis. Nano Lett 2019;19(2):1216–1226. Copyright 2019, ACS.

became resistant 4 years after penicillin started to be used in clinic, and the percentage increased to 59% just 4 years later. Between the 1980s and 90s, resistance exceeded 80% in non-clinical environment and reached 95% in the majority of hospitals.[88] It is estimated that by 2050, 10 million people per year will die due to untreatable infections. The development of new antibacterial agents is therefore one of the most important and challenging tasks that the pharmaceutical field is currently facing. Biofilm formation is one of the main hurdles that new antimicrobial drugs need to overtake.[89] This bacterial mode of growth, highly involved in human infections, con- sists of a matrix made of extracellular polymeric substance produced by microbes, exhibiting an altered

phenotype. The biofilm acts as a barrier hindering the penetration of antimicrobial agents and offering a favorable environment for microbial growth.

The interest in the antimicrobial activity of dendrimers has boosted in the last 20 years.[90] Their versatility and multivalency enable an accurate and application-oriented design to reach maximum efficiency. In most cases, antibacterial dendrimers rely on an adequate cationic charge distribution and amphiphilicity to disrupt the negatively charged microbe membrane in both Gram-positive and Gram-negative bacteria.[91–93] A major issue arises on the high toxicity displayed also toward mammalian cells. On the contrary, antiviral dendrimers mainly exhibit anionic, sugar or peptide moieties which can interfere in the virus-host interaction and avoid the infection at early stages of the viral cycle.[94,95]

To overcome dendrimer limitations and further improve the therapeutic response, researchers have shifted the focus to the combination of metals and dendrimers. The attachment of metal atoms into biologically active molecules has been widely reported as a useful strategy to overcome microbial resistance and improve activity.[96] In this field, the first metal complex dates back to the last century, when Paul Ehrlich and his co-workers developed an organoarsenic compound to treat syphilis. The following sections will provide a complete overview of the different metallodendrimers reported as antimicrobial agents in the literature, toward bacteria, yeast, virus and parasite infections.

2.2.1 Metallodendrimers as antibacterial agents

Even though the inclusion of antibacterial metals in dendritic scaffolds dates back to 2000s, few examples have been described during this 20-year period. An overview of selected metallodendrimers is presented in Table 3, including indices of the antimicrobial activity such as the Minimum Inhibitory Concentration (MIC), the Minimum Bactericidal Concentration (MBC) and the Minimum Biofilm Inhibitory Concentration (MBIC). These indices represent the minimal concentration that inhibits the growth of the microorganisms (MIC), kills the microorganism (MBC) or inhibits the formation of biofilm but not the growth (MBIC).

Table 3 *Overview of selected metallodendrimers and their antibacterial activity indicated as Minimum Inhibitory Concentration (MIC) and Minimum Bactericidal Concentration (MBC) values on different bacterial strains.*

Entry	Metal	Dendritic scaffold	Metal complex	Number metals	Bacteria	MIC/MBC (mg/L)	Ref.
1	Ag(I)	G5-PAMAM	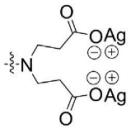	[a]	*S. aureus* *P. aeruginosa* *E. coli*	12.0[a,b] 10.5[a,b] 8.7[a,b]	97
2	Ag(I)	G1-PETIM	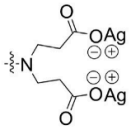	6	*S. aureus* *MRSA*	41.7/– 26.0/–	98
3	Cu(II)	G1-CBS	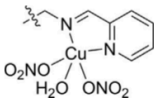	4	*E. coli* *S. aureus* *S. aureus (BF)*[c]	4/4 4/8 8/4[d]	99
4	Ru(II)	G1-CBS	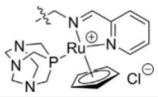	4	*E. coli* *S. aureus* *S. aureus (BF)*[c]	16/16 4/4 32/32[d]	99
5	Pd(II)	G2-Polyamide	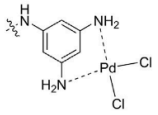	6	*E. coli* *S. typhi* *B. subtilis* *S. aureus*	70/– 102/– 84/– 82/–	100

[a]*Not reported.*
[b]*Sensitivity indicated as inhibition area (in mm).*
[c]*BF stands for biofilm mode of growth.*
[d]*For biofilm-forming bacteria, the Minimum Biofilm Inhibitory Concentration (MBIC) is reported.*

2.2.1.1 Silver(I) metallodendrimers

Silver is probably the most ancient antibacterial agent ever used by humans. Nowadays, different antibacterial drugs to treat external wounds or antibiotic coatings in medical devices rely on silver-based metallodrugs. It has been described that Ag(I) ions interfere with the nutrient transport chain in microorganisms, as well as bind to bacteria's genetic material.[101] Despite this excellent and specific mechanism of action, microorganisms have developed resistance to silver drugs[102] and demand new approaches to treat infections.

The first antibacterial metallodendrimers, described in 2000 by Balogh et al. comprised polyamidoamine scaffolds which complexed Ag(I) ions, forming stable and well characterized bonds (Table 3, Entry 1).[97] Generation 4 and 5 PAMAM dendrimers decorated with 192 hydroxyl and 256 carboxylate groups respectively were complexed with silver acetate. The dendrimers enabled an extremely high local concentration of silver cations within a relatively thin shell at the periphery while the internal tertiary nitro- gen atoms could form stable silver complexes. Nevertheless, the authors indicate that the metallodendrimers slowly photolyze into Ag(0) containing dendrimer-silver nanocomposites (Figure 11A). Using a standard agar overlay method, the diffusible antimicrobial activity was evaluated against plank- tonic *P. aeruginosa*, *E. coli* and *S. aureus*. Both metallodendrimers and nanocomposites exhibited comparable or higher antibacterial

activity than the $AgNO_3$ used as control. Interestingly, the antimicrobial activity was superior in carboxylate-functional dendrimers, due to the higher surface

concentration of silver ions—256 carboxylate groups around a 54 A° sphere—eager to interact with the bacterial membranes. The study also revealed the need for accessibility to silver, considering that those dendrimers with mostly internally conjugated silver ions produced a lower activity.

A similar strategy was recently used by Govender et al. to generate the silver salts of propyletherimine (PETIM) dendrimers (Table 3, Entry 2).[98] The low-generation dendron and dendrimers comprised carboxylate moieties at the surface with Ag(I) counterions (Figure 11B). The PETIM silver salts exhibited lower toxicity toward healthy cells than a comparable concentration of $AgNO_3$, probably due to the reduced net surface charge. The authors

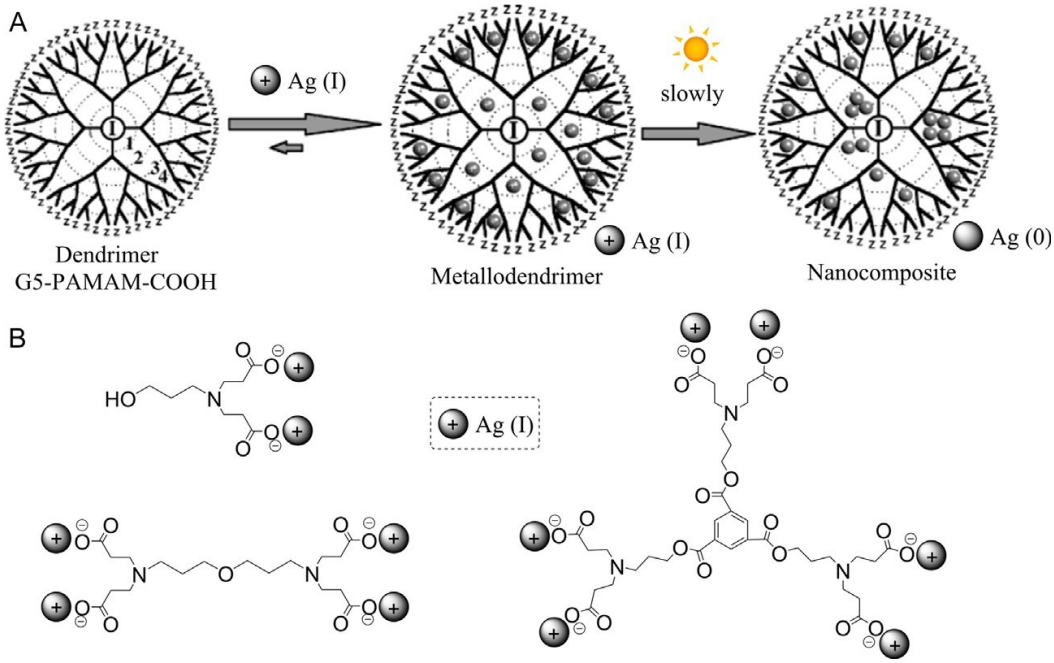

Figure 11 Examples of Ag(I) metallodendrimers. (A) PAMAM metallodendrimers and slow conversion to nanocomposites.[97] (B) PETIM metallodendrimers.[98] Panel (A): With permission from American Chemical Society. Balogh L, Swanson DR, Tomalia DA, Hagnauer GL, McManus AT. Dendrimer–silver complexes and nanocomposites as antimicrobial agents. Nano Lett. 2001;1(1):18–21. Copyright 2001.

demonstrated a direct relation between the number of Ag(I) ions and the antibacterial activity; the more potent response was observed with the aromatic cored metallodendrimer—featuring six Ag(I) ions bound on its surface—which decreased for the oxygen cored metallodendrimer—with only four ions—and even more for the metallodendron with only two ions. In order to analyze the combined effects of the dendritic compounds and silver nitrate, the Fractional Inhibitory Concentration index (ΣFIC) was calculated. The index showed no antagonist effects and, remarkably, synergist effect toward *S. aureus* for the aromatic cored metallodendrimer and toward *MRSA* for the oxygen cored counterpart. Overall, they presented a promising approach considering that the low dendritic generation simplifies the synthetic route, thus reducing time, costs and potential toxicity due to the low number of metal ions.

The antibacterial properties of silver, enhanced by the fine control of dendrimer scaffold, seemed indeed like the best route to get new drugs to overcome the problems of the traditional class of

antimicrobial agents. However, like many similar compounds, these fell into the "dendrimer paradox" of very high medical expectation which fades away due to the hurdles arising during the development of new drugs.[103] Indeed, since this first example of antibacterial metallodendrimers in 2000, the focus has shifted to the use of dendrimer/silver composites due to the synthetic simplicity, the inclusion of alternative metals which provide additional properties and the design of heterofunctional systems that expand the properties and applications of metal-based dendrimers, as it will be described in Section 2.2.1.5.

2.2.1.2 Copper(II) metallodendrimers

Copper is a very promising metal, biocompatible, versatile and cheap, featuring potent antimicrobial activity against viruses, yeasts and bacteria.[104,105] The use of copper in medicine expanded in the last two centuries, with a variety of inorganic copper compounds used to treat eczemas, tubercular infections, syphilis and antibacterial infections.[106] Furthermore, the intrinsic paramagnetic activity of its +2 oxidation state enables the study and monitoring of Cu(II) complexes through Electron Paramagnetic Resonance (EPR), resulting in an accurate chemico-physical characterization.

The attractive properties of copper—cost-effective, antimicrobial and easy to monitor—encouraged de la Mata et al. to evaluate in 2019 the antibacterial properties of Cu(II) carbosilane metallodendrimers bearing iminopyridine ligands (Table 3, Entry 3), previously reported as antitumoral agents.[43,59] The study not only showed the promising antibacterial activity toward Gram-positive and Gram-negative bacteria—including biofilm mode of growth—but most importantly confirmed the positive influence of the following parameters on the antibacterial activity[99]: (1) The *metal complexation* to the ligand, unlike other metallodrugs which exhibit antibacterial activity only after the metal release; (2) the *lipophilic scaffold*, being the first- generation metallodendrimers the most potent members in the family unlike most other dendritic scaffolds which require higher generations; (3) structural parameters such as the *metal ion and counterion*, exhibiting different activity between Ru(II) vs Cu(II) complexes and chloride vs nitrate counterion, confirming additional mechanisms besides the one related to the cationic charge at the dendrimer surface (Figure 12). Furthermore, the authors proved that carbosilane metallodendrimers did not produce hemolysis at the MIC concentrations and can be safely used as antibacterial agents.

2.2.1.3 Ruthenium(II) metallodendrimers

Ruthenium has long proved to be one of the most promising metals to be incorporated in antimicrobial agents, due to its interaction with DNA.[107] Ruthenium complexes exhibit different mechanisms of action,[108] including the interaction to DNA and the inhibition of DNA processing enzymes. In general, Ru(II) complexes exhibit more potent antibacterial activity toward Gram-positive than Gram-negative bacteria, being highly influenced by the charge and lipophilicity of the complex.

The first antibacterial Ru(II) metallodendrimers reported were part of a broader study carried out by de la Mata et al.[99], aiming to evaluate the influence of different structural parameters on the antibacterial activity (Figure 12). Similar to their copper counterparts described in the previous section, the Ru(II) complexes were chelated through the iminopyridine ligands at the periphery of the carbosilane dendrimers.[41] The first- generation Ru(II) metallodendrimer showed potent antibacterial activity against planktonic *S. aureus* and *E. coli* (Table 3, Entry 4), even higher than the analogous Cu(II) metallodendrimers. Furthermore, it inhibited the formation of *S. aureus*

biofilm at low concentrations (MBIC 32 mg/L) but even lower values were accomplished with the Cu(II) metallodendrimers (MBIC 8 mg/L).

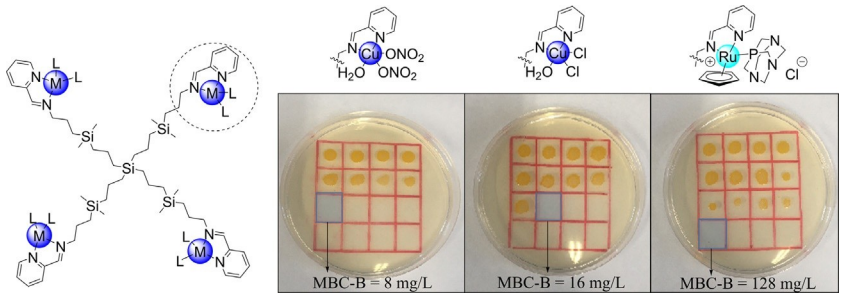

Figure 12 Effect of different first-generation carbosilane metallodendrimers in preventing the formation of S. aureus biofilms, calculating the Minimum Bactericidal Concentration for Biofilms (MBC-B). Figure adapted from Lamazares C, Sanz Del Olmo N, Ortega P, Gomez R, Soliveri J, de la Mata FJ, García-Gallego S and Copa-Patiño JL. Antibacterial effect of carbosilane metallodendrimers in planktonic cells of gram-positive and gram-negative bacteria and Staphylococcus aureus biofilm. Biomolecules 2019;9(9):E405. Copyright 2019, MDPI.

2.2.1.4 Platinum(II) and Palladium(II) metallodendrimers

Platinum and palladium complexes have been widely described as efficient antitumor agents.[109,110] However, fewer reports appear on the antimicrobial activity of these metallodrugs.

In 2012, Alshehri et al. reported the synthesis of platinum(II) and palladium(II) aromatic polyamide metallodendrimers.[100] Each metal ion was coordinated through two amino groups at the dendrimer periphery, a total of three metal ions in first-generation dendrimers and six metal ions in second-generation counterparts. The metallodendrimers exhibited potent antibacterial activity against different Gram-positive and Gram-negative strains, higher than the non-complexed dendrimer, and especially high for Pd(II) derivatives. Indeed, the second-generation Pd(II) metallodendrimer exhibited the most potent activity, comparable to the commercially available antibiotic streptomycin (Table 3, Entry 5).

2.2.1.5 Heterofunctional metallodendrimers and metallodendrons

The field of antibacterial treatments has also benefited from attaching different moieties in a single molecule. Enhancing the therapeutic response, reducing bacteria resistance or increasing the solubility are among the different aims of these multipurpose materials. Several approaches have been reported so far and are described in this section, with relevant examples depicted in Figure 13.

Since 2009, Grabchev et al. have developed several families of Cu(II) and Zn(II) poly(propyleneamine) metallodendrimers decorated with different 1,8-naphtalimides (unsubstituted,[73] 4-bromo-,[74,75] 4-amino-[76]; 4-(*N*,*N*- dimethylaminoethoxy)[77]; and acridine,[111] all biologically active moieties with promising antibacterial activity and fluorescent properties. Similarly to copper, the antimicrobial properties of zinc have been known for long time. For example, ZnO fine particles have deodorizing and antibacterial activity and are therefore exploited in the production of cotton fabrics and oral products.[114] These properties come in handy in the treatment of skin conditions, like sunburn or rush, due to Zn antiseptic activity.

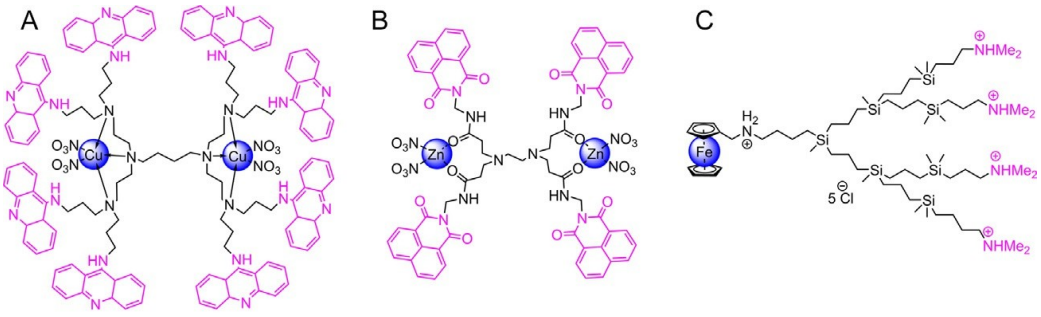

	MIC
B. cereus	10 mg/L
P. aeruginosa	80 mg/L
C. lipolytica	40 mg/L

	MIC
B. subtilis	6.23 mg/L
C. lipolytica	6.23 mg/L

	MIC	MBC
E. coli	2 mg/L	2 mg/L
S. aureus	2 mg/L	2 mg/L

Figure 13 Selected examples of heterofunctional metallodendrimers (A and B)[111,112] and metallodendron (C),[113] including MIC and MBC values in different bacterial strains.

The poly(propyleneamine) complexes are clear examples of heterofunctional metallodendrimers, considering that the metal coordination is performed via the tertiary amine groups at the dendrimer inner shell, comprising 1, 2 or 4 metal ions in G1, G2 and G3 dendrimers, respectively, being the outer shell available for further therapeutic response. The authors evaluated the antibacterial effect toward different Gram-positive bacteria (*B. subtilis*, *B. cereus*, *S. lutea* and *M. luteus*), Gram-negative bacteria (*P. aeruginosa*, *E. coli*, *A. johnsonii* and *Xanthomonas oryzae*) and yeast strains (*C. lipolytica* and *S. cerevisiae*). In general, Zn(II) complexes exhibited slightly higher antibacterial effect compared to the Cu(II) counterparts and superior activity to antimicrobial drugs such as tetracycline and nystatin. The authors also demonstrated the influence of the substituent at the 1,8-naphthalimide ring: the –Br group in the second-generation metallodendrimer [Zn_2(D)$(NO_3)_4$] reveals MIC values in the range 500–2000 μg/mL, while the –NH_2 in the first-generation metallodendrimer [Zn(D)$(NO_3)_2$] produces values in the range 50–200 μg/mL. The third-generation counterpart [Zn_4(D)$(NO_3)_8$] decreases MIC values even further and displayed the highest inhibition

toward *B. subtilis*, *E. coli* and *P. aeruginosa* with MIC ~50 μg/mL. Similarly to 1,8-naphtalimides, acridine moieties have also been attached to a second-generation poly(propyleneamine) dendrimer and used as plat- forms for antimicrobial Cu(II) metallodendrimers. Compared to the dendrimer alone, the Cu(II) complex exhibited an enhanced antimicrobial activity against *B. cereus*, *P. aeruginosa* and *C. lipolytica* (Figure 13A). Deposition of dendrimers on the surface of cotton fabric increased the hydrophobicity of the textile and prevented the formation of bacterial biofilm—inhibiting about 90% of the growth of *B. cereus* and more than 50% of the growth of

P. aeruginosa.[111] The authors explain the enhanced antimicrobial activity of these metallodendrimers through the Overtone's concept of cell permeability and the Tweedy's chelation theory.[76] The chelation reduces the polarity of the metal ion, increases the delocalization of electrons over the chelate ring and thus increases the lipophilicity of the metallodendrimers, favoring the penetration into the lipid cell membrane.

The influence of the dendritic scaffold was also evaluated, decorating PAMAM scaffolds with 1,8-naphtalimides and generating the corresponding Cu(II) and Zn(II) metallodendrimers (Figure 13B).[112] In this case, the metal coordination is produced through the either the carbonyl groups of the internal amide bonds, in the case of Zn(II), or the ethylenediamine core of two different

molecules, in the case of Cu(II), as evidenced through EPR analysis. SEM analysis indicated that the metal coordination

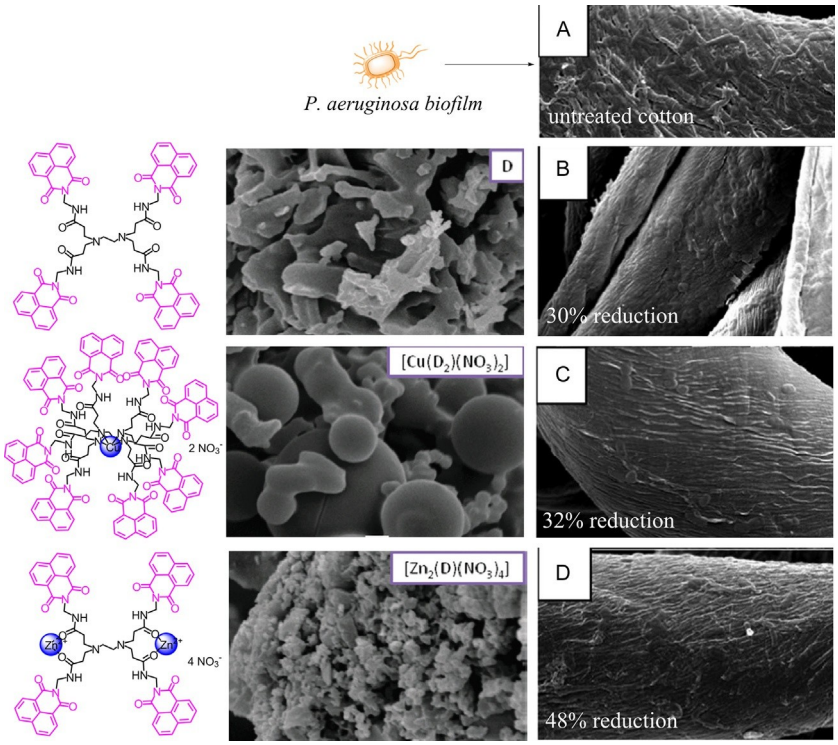

Figure 14 Antibacterial effect of PAMAM metallodendrimers on cotton fabrics. On the left, SEM micrographs of the dendrimer and the corresponding metallodendrimers. On the right, SEM images of cotton fabrics tested against P. aeruginosa biofilm.[112] *Used with permission of The Royal Society of Chemistry, from Impact of Cu(II) and Zn(II) ions on the functional properties of new PAMAM metallodendrimers, Copyright 2018.*[112]

to the dendrimer significantly changed the surface morphology (Figure 14). The smooth and thick laminar structure of the dendrimer is exchanged for a microspherical structure in the copper complex with some agglomerates and for a highly porous rod structure in the zinc derivative, which is later translated into an increased antibacterial activity due to an easier penetration into the cell walls. Again, the Zn(II) complex exhibited slightly higher antibacterial effect compared to the Cu(II) counterpart, with MIC values at the low mg/L range for Gram-positive bacteria. The negligible inhibition toward Gram-negative bacteria can be explained considering the additional outer membrane and slightly different cell wall structure of these bacteria,[115] as well as the different nature of the little holes in intact phospholipidic bilayer where non-charged dendrimers are adsorbed.[116]

The authors also reported the antimicrobial efficacy of cotton fabrics treated with the dendrimers, arising from both slow diffusion of the dendrimers from the cotton fabrics to the medium, a direct contact with the microbes as well as an increase in hydrophobicity that prevents the formation and proliferation of bacterial biofilms. As example, the Zn(II) metallodendrimer reduced the growth of *C. lipolytica* (100%), *B. cereus* (60%) and *P. aeruginosa* (48%) (Figure 14).

A different strategy relies on the use of dendrons, as the most simple heterofunctional dendritic entity. The first antibacterial metallodendron, reported in 2015, comprised a poly(propyl ether imine) scaffold bearing a hydroxyl group in the focal point and two Ag(I) carboxylate moieties. As previously described in Section 2.2.1.1, this metallodendron displayed moderate antibacterial activity

against *S. aureus* and methicillin-resistant *S. aureus*, only observing an additive effect between the dendron and $AgNO_3$ in the first case. The antibacterial effect was clearly improved using the metallodendrimer counterparts bearing 4 or 6 Ag(I) complexes.

In parallel, Gomez et al. designed a carbosilane dendron comprising a ferrocene moiety in the focal point and multiple ammonium groups in the periphery (Figure 13C).[113] Ferrocene is a Fe(II) "sandwich" complex, where the metal ion is coordinated between two cyclopentadienyl anions ($Fe(\eta^5\text{-}C_5H_5)_2$), with antimicrobial activity. Even though the mechanism of action is not clearly defined, it might be related to the triggering of Fenton's reaction and the production of ROS from hydrogen peroxide in biological environments.[117] Unlike the previous silver dendron, the metal is now located in the focal point and anchored through a covalent bond in a real organometallic complex. Furthermore, the antibacterial activity of the ferrocene is reinforced by the multiple cationic groups in the periphery. The Fe(II) metallodendrons exhibited a potent antibacterial activity toward Gram-negative (*E. coli*) and Gram-positive (*S. aureus*) bacteria, especially remarkable for the first-generation complex, which exhibited one of the lowest MIC (2 mg/L) for the examined strains of the whole metallodendrimer field. Surprisingly, the activity decreased when increasing the generation, and NMR DOSY experiments suggested that the large hydrodynamic volume of the G3 metallodendron reduced the interactions with the bacteria membrane. The high activity in both types of bacteria confirm the potential broad-spectrum antibacterial activity of these metallodendrons, unlike many other organometallic compounds featuring ferrocene,[118] highlighting once again the importance of the dendritic scaffold.

2.2.2 Metallodendrimers as antiviral agents

Antiviral metallodendrimers aim to combine the activity of the peripheral anionic, sugar or peptide moieties, with the promising properties of the metals, in order to interfere in the different steps of the virus cycle.[94,119] Despite the few examples reported in the literature in the field of antiviral metallodendrimers, the rationale behind the design of these metallodrugs provides useful insight into most important parameters influencing the antiviral behavior.

2.2.2.1 Copper(II) metallodendrimers

Polyanionic microbicides are known to interfere in the first steps of the HIV replicative cycle, inhibiting the adsorption and fusion of the virus to the cell. Dendrimers decorated with anionic moieties have been widely evaluated as antiviral agents against HIV, such as carbosilane[120–122] and the polylysine-based SPL7013 (VivaGel®).[123] Considering that several metal complexes are known to interfere in this process as well as in subsequent steps of the cycle, such as the viral DNA integration or viral protein processing by HIV protease, de la Mata et al. combined both strategies developing Cu(II) carbosilane metallodendrimers with carboxylate and sulfonate peripheral groups (Figure 15A).[124] In order to evaluate a possible synergic inhibitory effect between the metal atoms and the anionic groups, the dendrimers were modified with both stoichiometric and sub-stoichiometric amounts of copper, the latter leading to statistically functionalized metallodendrimers with an overall negative charge. The UV–Vis and EPR study revealed that carboxylate decorated dendrimers chelate the Cu(II) ion in a square planar $CuNO_3$ geometry, while the sulfonate decorated counter- parts probably form dimers at the internal–external dendrimer layer and at the higher copper concentrations the ions are coordinated by the sulfonate groups and water at the external layer. Second-generation dendrimers showed preventive and therapeutic activity against HIV infection, as revealed the study performed in HEC-1A cells—as a

model for the first cellular barrier in vaginal epithelia—and PBMC—as main target of HIV and second barrier model. The authors concluded that the carboxylate systems are more efficient and the metal coordination can further enhance the inhibitory effect of the anionic dendrimer, and this effect is more important as the metal amount is increased.

The exchange of the dendritic scaffold from carbosilane to poly(propyleneimine) with ethylenediamino core revealed a remarkable strategy to precisely control the heterofunctionalization of the anionic den- drimers.[125] In this case, an accurate specific pattern in the coordination of metal atoms was discovered using Cu(II) as a probe: at 1:1 M ratio between Cu(II) and the dendrimer, the metal exhibits a CuN_2O_2 pattern at the core of the dendrimer, while the increase in Cu(II) concentration indicated a peripheral $CuNO_3$ coordination in a square planar coordination which ultimately forms CuO_4 complexes at the highest concentrations tested. The authors demonstrated a different interaction for sulfonate dendrimers, with a weaker interaction toward nitrogen sites and stronger interaction with the oxygen in the sulfonate group. The antiviral effect toward HIV-1 was dependent upon the number, type and location of the metal within the dendritic scaffold (Figure 15B).[126] Importantly, the highest activity was obtained with the Cu(II) metallodendrimer comprising a single metal ion in the core, considering that all anionic groups were available for the interaction instead of being blocked by chelating the metal atoms. A remarkable increase from 30% to 90% inhibition of HIV-1 infection in Hec-1A was produced by complexing a single Cu(II) ion to the second-generation dendrimer bearing 16 carboxylate groups.

A

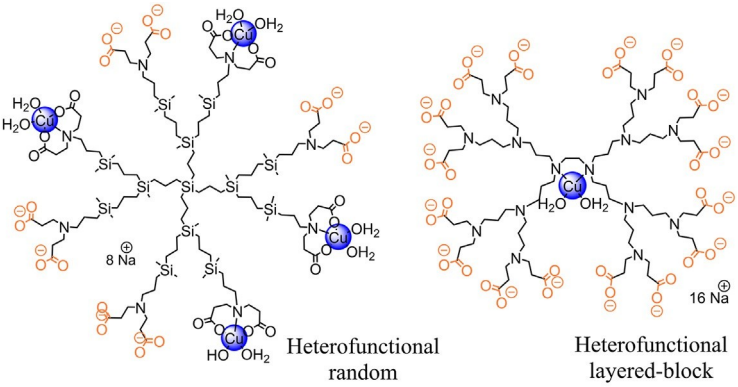

Cell line	*Treatment*	*CBS-G2C*	*CBS-G2C-Cu$_4$*	*PPI-G2C*	*PPI-G2C-Cu$_1$*
Hec-1A	Pre	25%	40%	30%	90%***
PBMC	Pre	20%	45%	15%	50%
PBMC	Post	-	-	15%	25%***

B

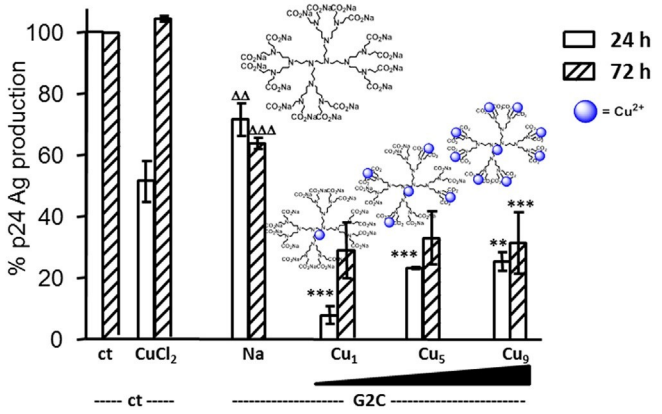

Figure 15 (A) Selected examples of heterofunctional Cu(II) metallodendrimers with antiviral activity against HIV-1. The inserted table shows the percentage of inhibition of HIV-1 infection after 1 h pre/post-treatment with the compounds at 10 μM. Decrease in inhibitory action when increasing the metal content, at different dendrimer:metal ratio 1:0 (Na), 1:1 (Cu$_1$), 1:5 (Cu$_5$) and 1:9 (Cu$_9$). Figure (B) reprinted with permission from García-Gallego S, Díaz L, Jiménez JL, Gómez R, de la Mata FJ, Muñoz- Fernández MÁ. HIV-1 antiviral behavior of anionic PPI metallodendrimers with EDA core. Eur J Med Chem 2015;98:139–148. Copyright 2015, with permission from Elsevier.

2.2.2.2 Nickel(II), Cobalt(II) and Zinc(II) metallodendrimers

As part of the study regarding anionic PPI metallodendrimers with ethylenediamine core,[126] the influence of the nature of the metal ion on the antiviral activity against HIV was evaluated. Accordingly, the carboxylate and sulfonate dendrimers were reacted with Ni(II), Co(II), Cu(II) and Zn(II) in different dendrimer:metal ratios and the resultant metallodendrimers were studied as antiviral agents. Hec-1A and VK-2 cell lines were used as model of the first barrier against HIV-1 infection and PBMC as model of the second barrier, and both preventive and therapeutic behaviors were studied. Important conclusions were drawn from this study, stating the positive influence of the following parameters on the antiviral activity:

(a) the *metal coordination* to the dendritic scaffold, significantly increasing the biocompatibility of the free metal ions as well as the antiviral effect of the precursor dendrimer; (b) the *low metal:dendrimer ratio* (1:1), enabling a cooperative effect between the metal and the free anionic groups and increasing the inhibition from the anionic dendrimer (e.g., 50% for sulfonate and 30%

for carboxylate in Hec-1A cells at 24 h) to the metallodendrimer (40–60% for sulfonate and 80–90% for carboxylate in Hec-1A cells). (c) The *nature of the metal* ion, determining the inhibitory action (especially high for Co(II), Cu(II) and Zn(II), negative for Ni(II)) and even certain HIV-1 strain and co-receptor specificity. Overall, the PPI metallodendrimers showed a high preventive inhibitory action in the first barrier model, avoiding virus internalization inside cells and inhibiting different viral strains, as well as a dual preventive-therapeutic behavior in the second barrier model. A rational design of such metallodendrimers opens new avenues for the production of versatile and efficient treatments against HIV-1 infection.

2.2.3 Metallodendrimers as antiparasitic agents

The multivalent nature of metallodendrimers has also been employed to treat parasite infections, enabling an increased interaction to a multi- receptor target. Malaria is a highly prevalent infectious disease produced by the parasite *Plasmodium falciparum*, which has evolved to generate resistance to traditional antimalarial drugs such as chloroquine. Aiming to alternative treatments with novel modes of action, different metallodrugs have emerged, such as ferroquine, a ferrocene-containing analogue of chloroquine.[127] This metallodrug combines the inhibitory action of the hemozoin formation from the chloroquine moiety and the ferrocenyl production of toxic OH radicals via a Fenton-like reaction.

Smith and co-workers have broad experience in the development of anti-parasitic poly(propyleneimine) metallodendrimers. In 2011, they reported the synthesis of first-generation PPI dendrimers decorated with ferrocenyl- thiosemicarbazones.[128] The conjugation of this motif to the PPI scaffold is presumed to enhance the accumulation of the thiosemicarbazone drug into parasite-infected erythrocytes, due to the recognition of the polyamine scaffold by specific polyamine transporters.[129] The ferrocenyl metallodendrimers showed high antiplasmodial activity against the chloroquine-resistant W2 strain of *P. falciparum*, in the range 2–7 μM, compared to the 20 μM of the non-conjugated ligands. Furthermore, at 10 μM concentration, they inhibited up to 62% the growth of the parasite *Trichomonas vaginalis*, a protozoan responsible for the sexually transmitted disease trichomoniasis. The presence of the lipophilic ferrocene moiety may contribute to the enhanced activity but still the activity was not comparable to the drug metronidazole, producing 100% inhibition.[130] In 2016, a new family of ferrocenyl metallodendrimers was reported, bearing an aromatic extension of the thiosemicarbazone moiety (Figure 16A).[131] First- and second- generation metallodendrimers were screened against the H37Rv strain of *Mycobacterium tuberculosis* and the chloroquine-sensitive NF54 of *P. falciparum*, displaying moderate activity compared to commercial drugs.

The second-generation complex performed slightly better, with MIC_{90} values of 41.7 μM toward *M. tuberculosis* and IC_{50} 32.8 μM toward *P. falciparum*. Recently, Smith et al. developed a PPI dendrimer comprising a single ferroquine moiety in one of the branches, which exhibited IC_{50} of 0.634 T 0.043 μM and 0.545 T 0.030 μM toward the NF54 and K1 strains of *P. falciparum*, respectively. This is an appreciable activity, though lower than chloroquine, and maintains the activity even in the chloroquine-resistant strain, suggesting the influence of the polyamine or ferrocenyl moiety on the improvement of the resistance indices.[132]

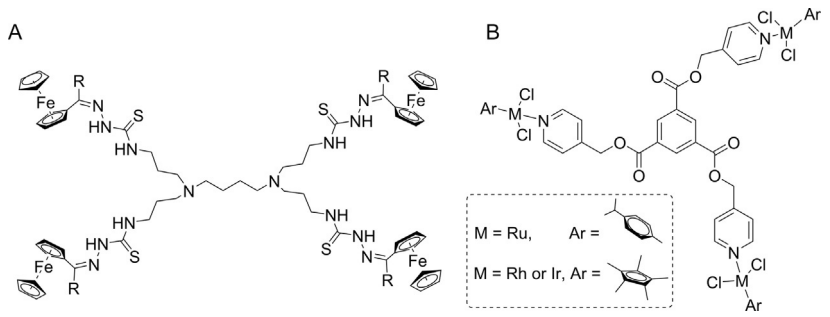

Figure 16 Examples of antiparasite metallodendrimers. (A) Polynuclear ferrocenylthiosemicarbazone complexes[131] and (B) polynuclear organometallic Ru(II), Rh(III) and Ir(III) pyridyl ester complexes.[133]

Smith's group has also explored alternative organometallic complexes of Ru(II), Rh(II) and Ir(II) using first-generation aromatic polyester dendrimers bearing pyridine ligands (Figure 16B). The obtained trinuclear metallodendrimers exhibited moderate to high antiplasmodial activities toward the chloroquine-sensitive strain NF54 of *P. falciparum* (IC_{50} 5–10 μM) and G3 strain of *Trichomonas vaginalis* (34–67% inhibition at 25 μM, 45–96% inhibition at 50 μM).[133]

3. Conclusions

Metallodendrimers have proven to be an original and powerful tool to fight cancer or infectious diseases. The inclusion of several metals centers in one single molecule enhances the effect produced by their mononuclear analogues. Although platinum was a trend in the cancer treatment, recently, other alternatives have emerged which involve the use of other metals such as ruthenium, copper, gold, among others, that have shown very promising activities together with less toxicity. The strategies that have stood out recently in the cancer field have been the use of metallodendrimers as anticancer drugs, as carriers of genetic material or as diagnostic agents. There are different parameters that have a strong influence in the final activity of these metallodendrimers, not only the nature of the metal center, its number and its oxidation state, but also the type of ligands surrounding it, the skeleton of the dendritic systems and the topology of these compounds. In general, the multivalency in metallodendrimers help to improve the activity of these compounds compared to the metallic mononuclear complexes.

In the fight against infectious diseases, dendritic scaffolds decorated with silver, copper, ruthenium, palladium or platinum complexes have shown their possibilities to act as antibacterial agents. In many cases the antibacterial activity is determined not only by the metal but also by the dendritic structure, where its nature and topology play an important role. In these cases, it seems that the hydrophilic/hydrophobic balance in the different parts of these metallodendrimers is crucial for their activity. An important recent achievement is that the use of combination therapy, that is, combination of dendritic structures with traditional antibiotic drugs or other molecules with antimicrobial activity, could be a new therapeutic approach that might help to reduce resistance to conventional antibiotics.

The multivalence present in dendrimers has been exploited to design innovative heterofunctional systems bearing different types of metal complexes or other interesting molecules. Such are the advances that have taken place in recent years that theranostic systems have been designed with application in both areas diagnostic and treatment, showing very promising results that open up a very interesting line of research.

Acknowledgments

Authors thanks funding by grants from CTQ2017-86224-P (MINECO), consortiums IMMUNOTHERCAN-CM B2017/BMD-3733 and NANODENDMED II-CM ref.

B2017/BMD-3703, the Comunidad de Madrid Research Talent Attraction Program 2017-T2/IND-5243, project SBPLY/17/180501/000358 Junta de Comunidades de Castilla-la Mancha (JCCM). CIBER-BBN is an initiative funded by the VI National R&D&i Plan 2008-2011, Iniciativa Ingenio 2010, the Consolider Program, and CIBER Actions and financed by the Instituto de Salud Carlos III with assistance from the European Regional Development Fund. This work has been supported partially by a EUROPARTNER: Strengthening and spreading international partnership activities of the Faculty of Biology and Environmental Protection for interdisciplinary research and innovation of the University of Lodz Programme: NAWA International Academic Partnership Programme. This publication is based upon work from COST Action CA 17140 "Cancer Nanomedicine from the Bench to the Bedside" supported by COST (European Cooperation in Science and Technology).

References

1. Sakurai H. Overview and frontier for the development of metallopharmaceutics. J Health Sci. 2010;56(2):129–143.
2. Slobodan N, Isidora S, Katarina R, Maja S, Jovana J. Toxic effects of metallopharmaceuticals. Serb J Exp Clin Res. 2017;18(3):191–194.
3. Huang Y, Havert M, Gavin D, et al. Biodistribution studies: understanding international expectations. Mol Ther Methods Clin Dev. 2016;3:16022.
4. FeynmanR.ThereisplentyolroomatthebottomIn:GilbertHD,ed.Miniaturization. Reinhold; 1961:282–296.
5. SharmaA,KakkarA.Designingdendrimerandmiktoarmpolymerbasedmulti-tasking nanocarriers for efficient medical therapy. Molecules. 2015;20(9):16987–17015.
6. RajS,JoseS,SumodUS,SabithaM.Nanotechnologyincosmetics:opportunitiesand challenges. J Pharm Bioallied Sci. 2012;4(3):186–193.
7. Caminade A-M. Inorganic dendrimers: recent advances for catalysis, nanomaterials, and nanomedicine. Chem Soc Rev. 2016;45(19):5174–5186.
8. Sakurai H, Maruyama T, Arai T. Photochemistry and aggregation behavior of tri- ethylene glycol (TEG) terminated stilbene dendrimers. Photochem Photobiol Sci. 2017;16(10):1490–1494.
9. Dufe`s C, Uchegbu IF, Sch€atzlein AG. Dendrimers in gene delivery. Adv Drug Deliv Rev. 2005;57(15):2177–2202.
10. GilliesE,FrechetJMJ.Dendrimersanddendriticpolymersindrugdelivery.DrugDiscov Today. 2005;10(1):35–43.
11. Scherrenberg R, Coussens B, van Vliet P, et al. The molecular characteristics of poly(propyleneimine) dendrimers as studied with small-angle neutron scattering, viscosimetry, and molecular dynamics. Macromolecules (Washington DC, US). 1998; 31(2):456–461.
12. Tomalia D, Baker H, Dewald JR, et al. A new class of polymers: Starburst-dendritic macromolecules. Polym J (Tokyo, Jpn). 1985;17:117–132.
13. Hawker CJ, Frechet JMJ. Preparation of polymers with controlled molecular architecture. A new convergent approach to dendritic macromolecules. J Am Chem Soc. 1990;112(21):7638–7647.
14. Inoue K. Functional dendrimers, hyperbranched and star polymers. Prog Polym Sci. 2000;25(4):453–571.
15. García-Gallego S, Andren OCJ, Malkoch M. Accelerated chemoselective reactions to sequence-controlled heterolayered dendrimers. J Am Chem Soc. 2020;142(3): 1501–1509.
16. 16. Walter MV, Malkoch M. Simplifying the synthesis of dendrimers: accelerated approaches. Chem Soc Rev. 2012;41(13):4593–4609.
17. Svenson S, Tomalia D. Dendrimers in biomedical applications—reflections on the field. Adv Drug Deliv Rev. 2006;57(15):2106–2129.
18. Yang X, Shang H, Ding C, Li J. Recent developments and applications of bioinspired dendritic polymers. Polym Chem. 2015;6(5):668–680.
19. Relano-RodriguezI, Juarez-Sanchez R, Pavicic C ,Muñoz E, Muñoz-Fernández M.A. Polyanionic carbosilane dendrimers as a new adjuvant in combination with latency reversal agents for HIV treatment. J Nanobiotechnol. 2019;17(1):69.
20. Movellan J, Urban P, Moles E, et al. Amphiphilic dendritic derivatives as nano- carriers for the targeted delivery of antimalarial drugs. Biomaterials. 2014;35(27): 7940–7950.
21. Florendo M, Figacz A, Srinageshwar B, et al. Use of polyamidoamine dendrimers in brain diseases. Molecules. 2018;23(9):E2238.
22. Meyers S.R., Juhn F.S., Griset A.P., Luman N.R., Grinstaff M.W. Anionic amphiphilic dendrimers as antibacterial agents. J Am Chem Soc. 2008;130(44):14444–14445.
23. Sampathkumar SG, Yarema K. Dendrimers in cancer treatment and diagnosis. In: Kumar CSSR, ed. Nanotechnologies for the Life Sciences. Wiley-VCH; 2007:vol 7.
24. Klajnert B, Peng L, Cena V, eds. Dendrimers in Biomedical Applications. RSC Publishing; 2013.
25. Shingu T, Chumbalkar V, Gwak H-S, et al. The polynuclear platinum BBR3610 induces G2/M arrest and autophagy early and apoptosis late in glioma cells. Neuro- Oncology (Cary, NC, US). 2010;12:1269–1277.

26. Govender P, Therrien B, Smith G. Bio-metallodendrimers—emerging strategies in metal-based drug design. Eur J Inorg Chem. 2012;2012(17):2853–2862.
27. Bray F, Ferlay J, Soerjomataram I, Siegel R, Torre L, Jemal A. Global cancer statistics 2018: GLOBOCAN estimates of incidence and mortality worldwide for 36 cancers in 185 countries. Ca-Cancer J Clin. 2018;68(6):394–424.
28. RosenbergB,VancampL,TroskoJE,MansourVH.Platinumdompounds:anewclass of potent antitumor agents. Nature (London, UK). 1969;222(5191):385–386.
29. OunR,MoussaY,WheateN.Thesideeffectsofplatinum-basedchemotherapydrugs: a review for chemists. Dalton Trans. 2018;47(19):6645–6653.
30. Maeda H, Wu J, Sawa T, Matsumura Y, Hori K. Tumor vascular permeability and the EPR effect in macromolecular therapeutics: a review. J Control Release. 2000; 65:271–284.
31. Howell B, Fan D, Rakesh L. Nanoscale dendrimer-platinum conjugates as multivalent antitumor drugs. In: Abd-El-Aziz AS, Carraher CE, Pittman CU, Zeldin M, eds. Inorganic and Organometallic Macromolecules. New York, NY: Springer; 2008:269–294.
32. Jansen BAJ, van der Zwan J, Reedijk J, den Dulk H, Brouwer J. A tetranuclear platinum compound designed to overcome cisplatin resistance. Eur J Inorg Chem. 1999;1999(9):1429–1433.
33. Malik N, Evagorou EG, Duncan R. Dendrimer-platinate. Anticancer Drugs. 1999;10(8):767–776.
34. Kapp T, Dullin A, Gust R. Platinum(II)-dendrimer conjugates: synthesis and investigations on cytotoxicity, cellular distribution, platinum release, DNA, and protein binding. Bioconjug Chem. 2010;21:328–337.
35. Sommerfeld NS, Hejl M, Klose MHM, et al. Low-generation polyamidoamine dendrimers as drug carriers for platinum(IV) complexes. Eur J Inorg Chem. 2017;2017(12): 1713–1720.
36. GovenderP,SuddingLC,ClavelCM,DysonPJ,TherrienB,SmithGS.Theinfluence of RAPTA moieties on the antiproliferative activity of peripheral-functionalised poly(salicylaldiminato) metallodendrimers. Dalton Trans. 2013;42(4):1267–1277.
37. Maroto-Dıaz M, Elie BT, Gomez-Sal P, et al. Synthesis and anticancer activity of carbosilane metallodendrimers based on arene ruthenium(II) complexes. Dalton Trans. 2016;45(16):7049–7066.
38. Michlewska S, Ionov M, Maroto-Díaz M, et al. Ruthenium dendrimers against acute promyelocytic leukemia: in vitro studies on HL-60 cells. Future Med Chem. 2019;11(14):1741–1756.
39. Govender P, Riedel T, Dyson PJ, Smith GS. Higher generation cationic N,N- ruthenium(II)-ethylene-glycol-derived metallodendrimers: synthesis, characterization and cytotoxicity. J Organomet Chem. 2015;799–800:38–44.
40. GouveiaM,FigueiraJ,JardimM,etal.Poly(alkylidenimine)dendrimersfunctionalized 5+ with the organometallic moiety [Ru(η -C5H5)(PPh3)2] as promising drugs against cisplatin-resistant cancer cells and human mesenchymal stem cells. Molecules. 2018;23(6):E1471.
41. de la Mata FJ, Gomez R, Ortega P, et al. Inventors; PCT/ES2019/070416, 14 June, assignee. Metalodendrımeros de naturaleza carbosilano conteniendo rutenio y cobre coordinados a ligandos base de Schiff, su preparacion y sus usos. 2019.
42. El Brahmi N, El Kazzouli S, Mignani SM, et al. Original multivalent copper(II)-conjugated phosphorus dendrimers and corresponding mononuclear copper(II) complexes with antitumoral activities. Mol Pharm. 2013;10(4):1459–1464. .
43. Sanz del Olmo N, Maroto-Díaz M, Gomez R, et al. Carbosilane metallodendrimers based on copper (II) complexes: synthesis, EPR characterization and anticancer activity. J Inorg Biochem. 2017;177:211–218.
44. Baartzes N, Szabo C, Cenariu M, et al. In vitro antitumour activity of two ferrocenyl metallodendrimers in a colon cancer cell line. Inorg Chem Commun. 2018;98:75–79.
45. Giffard D, Fischer-Fodor E, Vlad C, Achimas-Cadariu P, Smith G. Synthesis and antitumour evaluation of mono- and multinuclear [2 + 1] tricarbonylrhenium(I) complexes. Eur J Med Chem. 2018;157:773–781.
46. Mignani S, El Brahmi N, El Kazzouli S, et al. Original multivalent gold (III) and dual gold(III)-copper(II) conjugated phosphorus dendrimers as potent antitumoral and antimicrobial agents. Mol Pharm. 2017;14(11):4087–4097.

47. SuddingLC,PayneR,GovenderP,etal.Evaluationoftheinvitroanticanceractivityof cyclometalated half-sandwich rhodium and iridium complexes coordinated to naphthaldimine-based poly(propyleneimine) dendritic scaffolds. J Organomet Chem. 2014;774:79–85.
48. Govender P, Edafe F, Makhubela BCE, Dyson PJ, Therrien B, Smith GS. Neutral and cationic osmium(II)-arene metallodendrimers: synthesis, characterisation and anticancer activity. Inorg Chim Acta. 2014;409:112–120.
49. Yellepeddi VK, Vangara KK, Palakurthi S. Poly(amido)amine (PAMAM) dendrimer–cisplatin complexes for chemotherapy of cisplatin-resistant ovarian cancer cells. J Nanopart Res. 2013;15(9):1897.
50. Pang CT, Ammit AJ, Ong YQE, Wheate NJ. Para-Sulfonatocalix[4]arene and polyamidoamine dendrimer nanocomplexes as delivery vehicles for a novel platinum anti- cancer agent. J Inorg Biochem. 2017;176:1–7.
51. Li T, Smet M, Dehaen W, Xu H. Selenium–platinum coordination dendrimers with controlled anti-cancer activity. ACS Appl Mater Interfaces. 2016;8(6):3609–3614.
52. Maroto-Díaz M, Sanz del Olmo N, Muñoz-Moreno L, et al. In vitro and in vivo evaluation of first-generation carbosilane arene Ru(II)-metallodendrimers in advanced prostate cancer. Eur Polym J. 2019;113:229–235.
53. Wu J., Huang W., He Z., Dendrimers as carriers for siRNA delivery and gene silencing: a review. Sci World J. 2013;2013:630654.
54. Ionov M, Lazniewska J, Dzmitruk V, et al. Anticancer siRNA cocktails as a novel tool to treat cancer cells. Part (A). Mechanisms of interaction. Int J Pharm (Amsterdam, Neth). 2015;485(1–2):261–269.
55. Michlewska S, Ionov M, Maroto M, et al. Ruthenium dendrimers as carriers for anticancer siRNA. J Inorg Biochem. 2018;181:18–27.
56. Rodrigues J, Jardim MG, Figueira J, Gouveia M, Tomas H, Rissanen K. Poly(alkylidenamines) dendrimers as scaffolds for the preparation of low-generation ruthenium based metallodendrimers. New J Chem. 2011;35(10):1938–1943.
57. Santini C, Pellei M, Gandin V, Porchia M, Tisato F, Marzano C. Advances in copper complexes as anticancer agents. Chem Rev. 2014;114(1):815–862.
58. Hussain A, Al Ajmi M.F, Rehman M.T., et al. Copper(II) complexes as potential anticancer and Nonsteroidal anti-inflammatory agents: in vitro and in vivo studies. Sci Rep. 2019;9(1):5237.
59. Sanz del Olmo N, Carloni R, Bajo A, et al. Insight into the antitumor activity of carbosilane Cu(II)-metallodendrimers through their interaction with biological membrane models. Nanoscale. 2019;11(28):13330–13342.
60. Kopf-Maier P, Kopf H, Neuse EW. Ferrocenium salts—the first antineoplastic iron compounds. Angew Chem Int Ed Engl. 1984;23(6):456–457.
61. Neuse E. Macromolecular ferrocene compounds as cancer drug models. J Inorg Organomet Polym Mater. 2005;15:3–31.
62. Konkankit C.C., Marker S.C., Knopf K.M., Wilson J.J. Anticancer activity of complexes of the third-row transition metals, rhenium, osmium, and iridium. Dalton Trans. 2018;47(30):9934–9974.
63. Lee LC-C, Leung K-K, Lo KK-W. Recent development of luminescent rhenium(I) tricarbonyl polypyridine complexes as cellular imaging reagents, anticancer drugs, and antibacterial agents. Dalton Trans. 2017;46(47):16357–16380.
64. Nardon C, Boscutti G, Fregona D. Beyond platinums: gold complexes as anticancer agents. Anticancer Res. 2014;34:487–492.
65. Yeo CI, Ooi KK, Tiekink ERT. Gold-based medicine: a paradigm shift in anti-cancer therapy? Molecules (Basel, Switzerland). 2018;23(6):1410.
66. Buchel G.E., Stepanenko I.N., Hejl M., Jakupec M.A., Keppler B.K., Arion V.B. Enrouteto osmium analogues of KP1019: synthesis, structure, spectroscopic properties and antiproliferative activity of trans-[Os(IV)Cl4(Hazole)2]. Inorg Chem. 2011;50(16): 7690–7697.
67. Domotor O., Aicher S., Schmidlehner M., et al. Antitumor pentamethylcyclopentadienyl rhodium complexes of maltol and allomaltol: synthesis, solution speciation and bioactivity. J Inorg Biochem. 2014;134:57–65.
68. Liu Z, Sadler PJ. Organoiridium complexes: anticancer agents and catalysts. Acc Chem Res. 2014;47(4):1174–1185.

69. Govender P, Renfrew AK, Clavel CM, Dyson PJ, Therrien B, Smith GS. Antiproliferative activity of chelating N,O- and N,N-ruthenium(II) arene functionalised poly(propyleneimine) dendrimer scaffolds. Dalton Trans. 2011;40(5):1158–1167.
70. Cebrian-Losantos B., Krokhin A.A., Stepanenko I.N., et al. OsmiumNAMI-Aanalogues: synthesis, structural and spectroscopic characterization, and antiproliferative properties. Inorg Chem. 2007;46(12):5023–5033.
71. Govender P, Lemmerhirt H, Hutton AT, Therrien B, Bednarski PJ, Smith GS. First- and second-generation heterometallic dendrimers containing ferrocenyl–ruthenium(II)–arene motifs: synthesis, structure, electrochemistry, and preliminary cell proliferation studies. Organometallics. 2014;33(19):5535–5545.
72. Govender P, Riedel T, Dyson PJ, Smith GS. Regulating the anticancer properties of organometallic dendrimers using pyridylferrocene entities: synthesis, cytotoxicity and DNA binding studies. Dalton Trans. 2016;45(23):9529–9539.
73. Refat MS, El-Deen IM, Grabchev I, Anwer ZM, El-Ghol S. Spectroscopic characterizations and biological studies on newly synthesized Cu2+ and Zn2+ complexes of first- and second-generation dendrimers. Spectrochim Acta A. 2009;72(4):772–782.
74. Staneva D, Vasileva-Tonkova E, Makki MSI, et al. Synthesis and spectral characterization of a new PPA dendrimer modified with 4-bromo-1,8-naphthalimide and in vitro antimicrobial activity of its Cu(II) and Zn(II) metal complexes. Tetrahedron. 2015;71(7):1080–1087.
75. Grabchev I., Staneva D., Vasileva-Tonkova E., et al. Antimicrobialandanticanceractivity of new poly(propyleneamine) metallodendrimers. J Polym Res. 2017;24:210.
76. Grabchev I, Yordanova S, Vasileva-Tonkova E, Bosch P, Stoyanov S. Poly(propylenamine) dendrimers modified with 4-amino-1,8-naphthalimide: synthesis, characterization and in vitro microbiological tests of their Cu(II) and Zn(II) complexes. Inorg Chim Acta. 2015;438:179–188.
77. Staneva D, Grabchev I, Bosch P, Vasileva-Tonkova E, Kukeva R, Stoyanova R. Synthesis, characterisaion and antimicrobial activity of polypropylenamine metallo- dendrimers modified with 1,8-naphthalimides. J Mol Struct. 2018;1164:363–369.
78. Michlewska S, Kubczak M, Maroto-Díaz M, et al. Synthesis and characterization of FITC labelled ruthenium dendrimer as a prospective anticancer drug. Biomolecules. 2019;9(9):E411.
79. Carloni R, Sanz del Olmo N, Ortega P, et al. Exploring the interactions of ruthenium (II) carbosilane metallodendrimers and precursors with model cell membranes through a dual spin-label spin-probe technique using EPR. Biomolecules. 2019;9(10):E540.
80. Sagır T, I ş ık S, Şenel M. Ferrocene incorporated PAMAM dendrons: synthesis, characterization, and anti-cancer activity against AGS cell line. Med Chem Res. 2013; 22(10):4867–4876.
81. Maroto-Díaz M, Sanz del Olmo N, García-Gallego S, Gomez R, Ortega P, de la Mata FJ. Synthesis and structural characterization of carbosilane ruthenium(II) metallodendrons containing cymene units. J Organomet Chem. 2019;901:120942.
82. Kherlopian AR, Song T, Duan Q, et al. A review of imaging techniques for systems biology. BMC Syst Biol. 2008;2:74.
83. Ye M, Qian Y, Tang J, Hu H, Sui M, Shen Y. Targeted biodegradable dendritic MRI contrast agent for enhanced tumor imaging. J Control Release. 2013;169(3):239–245.
84. McNelles SA, Knight SD, Janzen N, Valliant JF, Adronov A. Synthesis, radiolabeling, and in vivo imaging of PEGylated high-generation polyester dendrimers. Biomacromolecules. 2015;16(9):3033–3041.
85. Parat A., Kryza D., Degoul F., et al. Radiolabeled dendritic probes as tools for high in-vivo tumor targeting: application to melanoma. J Mater Chem B. 2015;3(12):2560–2571.
86. Chen Q., Qianqian Y., Liu Y., et al. Multifunctional selenium nanoparticles: chiral selectivity of delivering MDR-siRNA for reversal of multidrug resistance and real-time biofluorescence imaging. Nanomedicine (NY, US). 2015;11(7):1773–1784.
87. Fan Y, Zhang J, Shi M, et al. Poly(amidoamine) dendrimer-coordinated copper(II) complexes as a theranostic nanoplatform for the radiotherapy-enhanced magnetic resonance imaging and chemotherapy of tumors and tumor metastasis. Nano Lett. 2019;19(2):1216–1226.

88. Heymann D.L., Prentice T., Reinders LT. The World Health Report 2007: A Safer Future: Global Public Health Security in the 21st Century. Geneva, Switzerland: WHO; 2007.
89. Denyer S.P., Gorman S.P., Sussman M. Microbial Biofilms: Formation and Control. London, UK: Wiley-Blackwell Scientific Publications LTD; 1993.
90. García-Gallego S., Franci G, Falanga A., et al. Function oriented molecular design: dendrimers as novel antimicrobials. Molecules. 2017;22(10):E1581.
91. Castonguay A, Ladd E, van de Ven TGM, Kakkar A. Dendrimers as bactericides. New J Chem. 2012;36(2):199–204.
92. TuluM, Erturk A.S., Bobbarala V., ed. Dendrimers as Antibacterial Agents. In tech Open; 2012.
93. Lind TK, Polcyn P, Zielinska P, Ca´rdenas M, Urbanczyk-Lipkowska Z. On the anti-microbial activity of various peptide-based dendrimers of similar architecture. Molecules. 2015;20(1):738–753.
94. Rosa Borges A, Schengrund CL. Dendrimers and antivirals: are view. Curr Drug Targets Infect Disord. 2005;5(3):247–254.
95. Jimenez J.L, Pion M., de la Mata F.J., et al. Dendrimers as topical microbicides with activity against HIV. New J Chem. 2012;36(2):299–309.
96. Scott P. Antimicrobial metallodrugs. In: Simpson DH, Lo KK-W, eds. Inorganic and Organometallic Transition Metal Complexes with Biological Molecules and Living Cells. Academic Press; 2017:205–243.
97. Balogh L., Swanson D.R., Tomalia D.A., Hagnauer G.L., McManus A.T. Dendrimer silver complexes and nanocomposites as antimicrobial agents. Nano Lett. 2001;1(1):18–21.
98. Suleman N, Kalhapure RS, Mocktar C, Rambharose S, Singh M, Govender T. Silver salts of carboxylic acid terminated generation 1 poly (propyl ether imine) (PETIM) dendron and dendrimers as antimicrobial agents against S. aureus and MRSA. RSC Adv. 2015;5(44):34967–34978.
99. Llamazares C., Sanz Del Olmo N., Ortega P., Gomez R., Soliveri J., de la Mata F.J., García-Gallego S., Copa-Patino J.L. Antibacterial effect of carbosilane metallodendrimers in planktonic cells of Gram-positive and Gram-negative bacteria and Staphylococcus aureus biofilm. Biomolecules. 2019;9(9):E405.
100. Ahamad T, Mapolie SF, Alshehri SM. Synthesis and characterization of polyamide metallodendrimers and their anti-bacterial and anti-tumor activities. Med Chem Res. 2012;21(8):2023–2031.
101. Maillard J.Y., Hartemann P., Silver as anantimicrobial: facts and gaps in knowledge. Crit Rev Microbiol. 2013;39(4):373–383.
102. Panacek A., Kvitek L., Smekalova M, et al. Bacterial resistance to silver nanoparticle sand how to overcome it. Nat Nanotechnol. 2018;13(1):65–71.
103. Svenson S. The dendrimer paradox–high medical expectations but poor clinical translation. Chem Soc Rev. 2015;44(12):4131–4144.
104. Vincent M, Hartemann P, Engels-Deutsch M. Antimicrobial applications of copper. Int J Hyg Environ Health. 2016;219(7, pt A):585–591.
105. Grass G., Rensing C., Solioz M., Metallic copper as anantimicrobial surface. Appl Environ Microbiol. 2011;77(5):1541–1547.
106. Dalecki A.G., Crawford C.L., Wolschendorf F. Copper and antibiotics: discovery, modes of action, and opportunities for medicinal applications. In: Poole RK, ed. Advances in Microbial Physiology. Academic Press; 2017:193–260. vol 70.
107. Li F, Collins J.G., Keene FR. Ruthenium complexes as antimicrobial agents. Chem Soc Rev. 2015;44(8):2529–2542.
108. Brabec V, Kasparkova J. Ruthenium coordination compounds of biological and biomedical significance. DNA binding agents. Coord. Chem Rev. 2018;376:75–94.
109. Katarzyna M, Anna S, Zielinska-Blizniewska H, Ireneusz M. An evaluation of the antioxidant and anticancer properties of complex compounds of copper (II), platinum (II), palladium (II) and ruthenium (III) for use in cancer therapy. Mini-Rev Med Chem. 2018;18(16):1373–1381.
110. Abu-Surrah AS, Kettunen M. Platinum group antitumor chemistry: design and development of new anticancer drugs complementary to cisplatin. Curr Med Chem. 2006;13(11):1337–1357.

111. Bosch P., Staneva D., Vasileva-Tonkova E., et al. Newpoly(propyleneimine)dendrimer modified with acridine and its Cu(II) complex: synthesis, characterization and antimi- crobial activity. Materials. 2019;12(18):3020.
112. Grabchev I, Vasileva-Tonkova E, Staneva D, Bosch P, Kukeva R, Stoyanova R. Impact of Cu(II) and Zn(II) ions on the functional properties of new PAMAM metallodendrimers. New J Chem. 2018;42(10):7853–7862.
113. Lozano-Cruz T, Ortega P, Batanero B, et al. Synthesis, characterization and antibacterial behavior of water-soluble carbosilane dendrons containing ferrocene at the focal point. Dalton Trans. 2015;44(44):19294–19304.
114. Lallo da Silva B, Abucafy MP. Relationship between structure and antimicrobial activity of zinc oxide nanoparticles: an overview. Int J Nanomedicine. 2019;2019(14): 9395–9410.
115. Denyer SP, Maillard J-Y. Cellular impermeability and uptake of biocides and antibiotics in Gram-negative bacteria. J Appl Microbiol. 2002;92(s1):35S–45S.
116. Mecke A, Uppuluri S, Sassanella TM, et al. Direct observation of lipid bilayer disruption by poly(amidoamine) dendrimers. Chem Phys Lipids. 2004;132(1):3–14.
117. Acevedo-Morantes CY, Melendez E, Singh SP, Ramirez-Vick JE. Cytotoxicity and reactive oxygen species generated by ferrocenium and ferrocene on MCF7 and MCF10A cell lines. J Cancer Sci Ther. 2012; 4:271–275.
118. Scutaru D, Mazilu I, Vata M, et al. Heterodisubstituted derivatives of ferrocene. Ferrocene-containing penicillins and cephalosporins. J Organomet Chem. 1991; 401(1):87–90.
119. Sepulveda-Crespo D, Gomez R, de la Mata FJ, Jimenez JL, Muñoz-Fernández MA. Polyanionic carbosilane dendrimer-conjugated antiviral drugs as efficient microbicides: recent trends and developments in HIV treatment/therapy. Nanomedicine (NY, US). 2015;11(6):1481–1498.
120. Rasines B, Sanchez-Nieves J, Maiolo M, et al. Synthesis, structure and molecular modelling of anionic carbosilane dendrimers. Dalton Trans. 2012;41(41):12733–12748.
121. Arnaiz E., Vacas-Cordoba E., Galan M, et al. Synthesis of anionic carbosilane dendrimers via "click chemistry" and their antiviral properties against HIV. J Polym Sci A Polym Chem. 2014;52(8):1099–1112.
122. Galan M, Sanchez Rodriguez J, Jimenez JL, et al. Synthesis of new anionic carbosilane dendrimers via thiolene chemistry and their antiviral behaviour. Org Biomol Chem. 2014;12(20):3222–3237.
123. Price CF, Tyssen D, Sonza S, et al. SPL7013 Gel (VivaGel(R)) retains potent HIV-1 and HSV-2 inhibitory activity following vaginal administration in humans. PLoS One.2011;6(9):e24095.
124. Galan M, Sanchez-Rodrıguez J, Cangiotti M, et al. Antiviral properties against HIV of water-soluble copper carbosilane dendrimers and their EPR characterization. Curr Med Chem. 2012;19(29):4984–4994.
125. García-Gallego S, Cangiotti M, Fiorani L, et al. Anionic sulfonated and carboxylated PPI dendrimers with the EDA core: synthesis and characterization of selective metal complexing agents. Dalton Trans. 2013;42(16):5874–5889.
126. 126. García-Gallego S, Díaz L, Jimenez JL, Go´mez R, de la Mata FJ, Muñoz Fernández MA. HIV-1 antiviral behavior of anionic PPI metallo-dendrimers with EDA core. Eur J Med Chem. 2015;98:139–148.
127. Biot C, Glorian G, Maciejewski LA, Brocard JS. Synthesis and antimalarial activity in vitro and in vivo of a new ferrocene-chloroquine analogue. J Med Chem. 1997;40(23):3715–3718.
128. Khanye S.D., Gut J., Rosenthal P.J., Chibale K., Smith G.S. Ferrocenyl thiosemicarbazones conjugated to a poly(propyleneimine) dendrimer scaffold: synthesis and in vitro antimalarial activity. J Organomet Chem. 2011;696(21):3296–3300.
129. Muller IB, Das Gupta R., Luersen K, Wrenger C, Walter R.D. Assessing the polyamine metabolism of Plasmodium falciparum as chemotherapeutic target. Mol Biochem Parasitol. 2008;160(1):1–7.
130. Stringer T, Taylor D, de Kock C, et al. Synthesis, characterization, antiparasitic and cytotoxic evaluation of thioureas conjugated to polyamine scaffolds. Eur J Med Chem. 2013;69:90–98.
131. Baartzes N, Stringer T, Okombo J, et al. Mono- and polynuclear ferrocenylthio semicarbazones: synthesis, characterisation and antimicrobial evaluation. J Organomet Chem. 2016;819:166–172.
132. Stringer T, Wiesner L, Smith GS. Ferroquine-derived polyamines that target resistant Plasmodium falciparum. Eur J Med Chem. 2019;179:78–83.

133. Chellan P, Land KM, Shokar A, et al. Synthesis and evaluation of new polynuclear organometallic Ru(II), Rh(III) and Ir(III) pyridyl ester complexes as in vitro antiparasitic and antitumor agents. Dalton Trans. 2014;43(2):513–526.

2 - RESULTS AND DISCUSSION

2.1 Ru(II)-conjugated metallodendrimers: EPR study

The antitumor activity of Ruthenium(II) has been widely studied for over two decades, with the aim of overcoming cisplatin limitations in the treatment of cancer. Ru(II) strength relies in the similarity with iron, being quickly bond to serum transferrin and therefore delivered through a non-toxic mechanism to tumoral cells. [2]

Ru(II) was therefore chosen as a promising candidate to be coordinated on a carbosilane skeleton, to improve its biodistribution, antitumoral mechanism, and ADME parameters.

To better understand the role of the resulting metallodendrimer in the interaction with tumoral cells, an EPR study was carried out using model membranes as a cell substitute. The unreliability of an *in-vitro* system, with different cell size and unprecise number of specimens doesn't indeed allow the precision that an initial study requires.

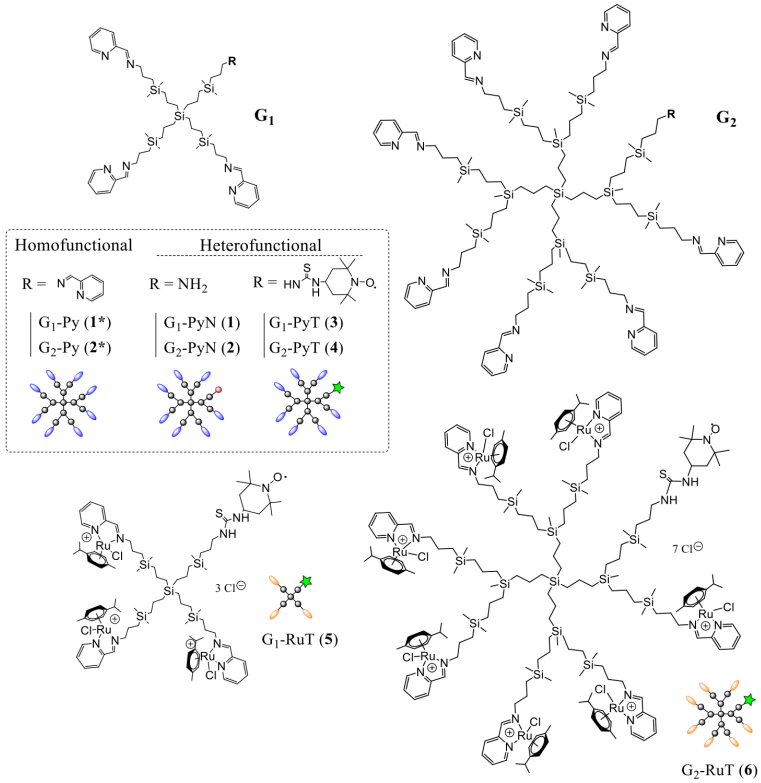

Figure 2.1 dendrimer and metallodendrimers synthetized for the EPR study (article 1, figure 1)

As shown in figure 2.1, both generation 1 and 2 metallodendrimers were synthetized. To better highlight the skeleton role, little variations were made during the synthesis, resulting in three different classes of dendrimer:

- **Homofunctional**, featuring perfect symmetry. All the branches are equal. (G_n-Py/G_n-Ru)
- **Heterofunctional**, -NH_2 terminated. One branch is not conjugated with an iminopyridine, ending instead with an -NH_2 group (protonated at physiological pH). (Gn-PyN/Gn-RuN)
- **Heterofunctional**, TEMPO terminated. One branch is conjugated with a TEMPO molecule through the formation of a thiourea group. (Gn-PyT/Gn-RuT)

The TEMPO group allows a direct EPR study of the molecule, since it features paramagnetic activity. The other dendrimers were monitored with a spin probe (CAT12). The comparison of the two studies allowed to gain a lot of information about the system properties.

Model membranes were prepared from CTAB and egg lecithin: in the first case, micelles were the outcome of the procedure, allowing to study the simplest membrane model possible. In the second case, the produced liposomes allowed to study the approach of metallodendrimers with a double-layered membrane model.

2.1.1 TEMPO-labelled study

TEMPO-labelled molecules studies allowed to gain information from the point of view of dendrimers and metallodendrimers, which were in this case carrying the paramagnetic species.

The extracted parameters of the EPR study in the absence and in the presence of model membranes are reported in table 1.

***Table 1**. Extracted parameters (article 1, table 1)*

Entry	Sample	Components	A_{zz} (G)	τ (ns)
1	G_1-PyT (**3**)	Free (single)	39.21/-	0.014/-
2	G_2-PyT (**4**)	Free (single)	39.12/-	0.017/-
3	G_1-PyT (**3**) + CTAB	Free + Interacting	38.72/37.68	0.21/0.87
4	G_2-PyT (**4**) + CTAB	Free + Interacting	38.68/37.70	0.25/0.73
5	G_1-PyT (**3**) + LEC	Free + Interacting	39.01/38.07	0.050/2.35
6	G_2-PyT (**4**) + LEC	Free + Interacting	38.98/38.20	0.055/3.05
7	G_1-RuT (**5**)	Free + Interacting	38.82/39.00	0.22/3.31
8	G_2-RuT (**6**)	Free + Interacting	38.85/39.00	0.22/3.35
9	G_1-RuT (**5**) + CTAB	Free + Interacting	38.82/37.40	0.22/1.90
10	G_2-RuT (**6**) + CTAB	Free + Interacting	38.85/37.41	0.22/1.38
11	G_1-RuT (**5**) + LEC	Free + Interacting	38.82/34.60	0.22/6.45
12	G_2-RuT (**6**) + LEC	Free + Interacting	38.85/35.00	0.22/7.00

From such parameters, and in also from the interacting/free component ratio analysis, it was found that:

- Metal-free dendrimers partially entered into the micelles, but not into the liposomes, with whom interacted on the external surface.
- Generation 1 samples better interacted with micelles, generation 2 with liposomes.
- The metal-bearing samples show the same behavior, showing little effect of the metal itself on the interaction. The Ru(II) coordination to the skeleton slightly lowers the interaction, but at the

same time improves dendrimer solubility as shown by augment of the total intensity of the spectrum.

Such results were then integrated with the spin-probes study.

2.1.2. CAT12 studies

Spin probe studies allowed to gain information from the point of view of the membranes themselves, taken into account CAT12 ability to insert into biological membranes with its hydrophobic tail.

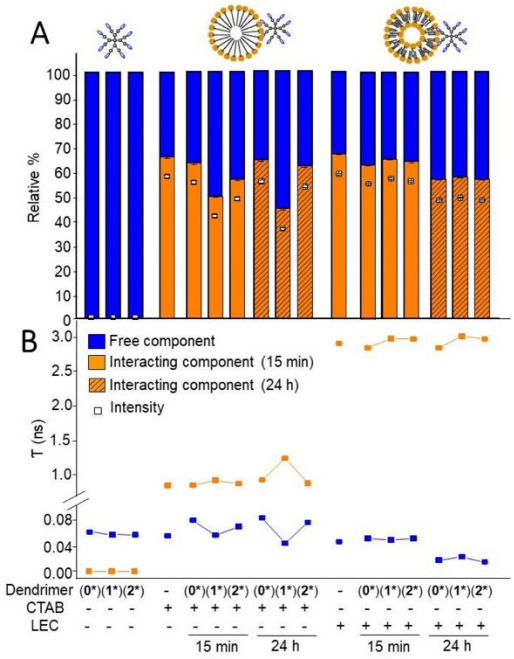

Figure 2.2 CAT12 spectra of unlabeled dendrimers in the absence and in the presence of model membranes A) relative percentage of interacting and free components B) microviscosity parameter (article 1, figure 3)

Results confirm the mode of interaction highlighted for TEMPO labelled samples: generation 1 better interacts with micelles and generation 2 with liposomes.

The presence of -NH_2 group completely changes the interaction: dendrimers and metallodendrimers don't penetrate anymore into the micelles, and establish instead an electrostatic superficial interaction with all model membranes. This would certainly lead to in vivo toxicity, due to the disruption of negatively charged cell membranes.

More details on the experiments conducted can be found in paper 1.

2.2 Cu(II)-conjugated metallodendrimers

Imino-terminated carbosilane skeleton gave a very promising interaction with membrane models, so we exploited it for further studies, with a different metal ion.

Cu(II) was in fact selected in place of Ru(II), for various reasons:

- It has a great anticancer potential, triggering apoptosis in tumoral cells via ROS generation, as shown by many studies. [3]

- It's very biocompatible and toxic at high doses only. Most microorganisms show in fact a complicated system of homeostasis for this ion, granting a clearance of excessive Cu(II). Solid tumors are particularly affected by Cu(II) accumulation due to the enhanced permeation retention effect. [4]
- It's significantly cheaper and less toxic than Ru(II), making a future scaled-up production easier to plan. The synthesis protocol is also considerably simpler.
- It's natively paramagnetic, allowing a direct study of the complexes and molecules interaction by means of EPR analysis.

Therefore Cu(II)-conjugated metallodendrimers were synthetized and characterized by various techniques, including EPR. A particular emphasis was given to the choice of copper counter-ion/ligand: two different ones were chosen to monitor their physico-chemical properties and effect on the antitumoral activity.

- -Cl had already proved to be a good candidate in previous experiments, featuring a ligand character and forming stable complexes with Cu(II). [5]
- $-NO_3$ was chosen to improve metallodendrimer solubility, featuring a counter-ion character.

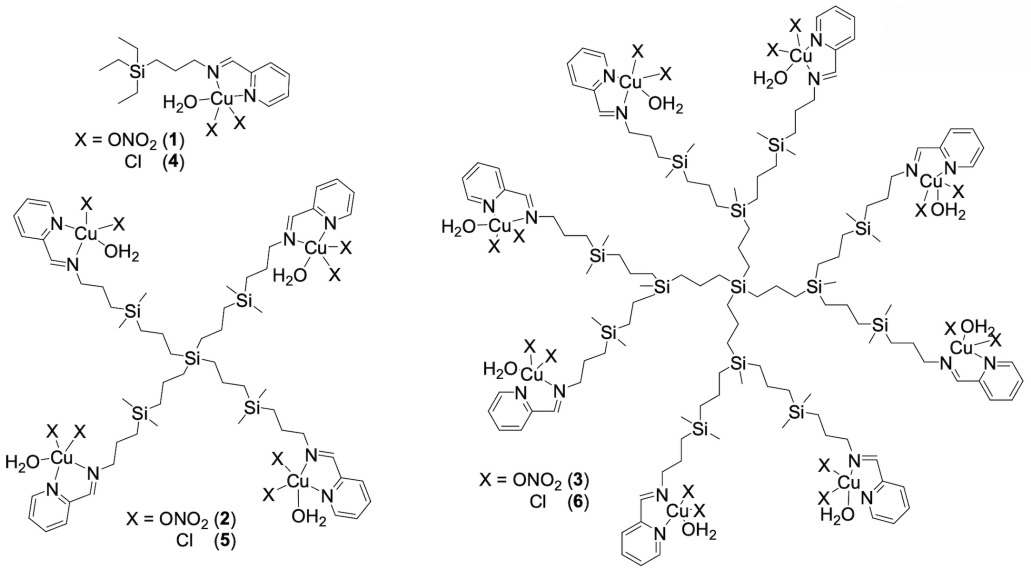

Figure 2.3 Cu(II)-conjugated metallodendrimers synthetized for this work (article 3, figure 1)

Details about the synthesis of such metallodendrimers are reported in paper 3,

They were tested against both tumoral and healthy cells, and finally their ex-vivo activity was evaluated with mice models.

2.2.1 EPR experiments and results

For starters, the interaction with model membranes was studied by EPR technique, similarly of what done in paper 1 for Ru(II)-conjugated metallodendrimers.

Model membranes were prepared from CTAB and egg lecithin, and studied by EPR by means of both CAT12 spin probe and tuning the instrument on copper frequency itself.

Once again, it was found that the increase in dendrimer generation augments the strength of interaction with the model membranes: magnetic parameters suggest that the interactions are mainly electrostatic and ion-dipole. The most stable complexes were formed, as previously hypothesized, with chloride ligands, which gave to the molecule a more hydrophobic character if compared to nitrate.

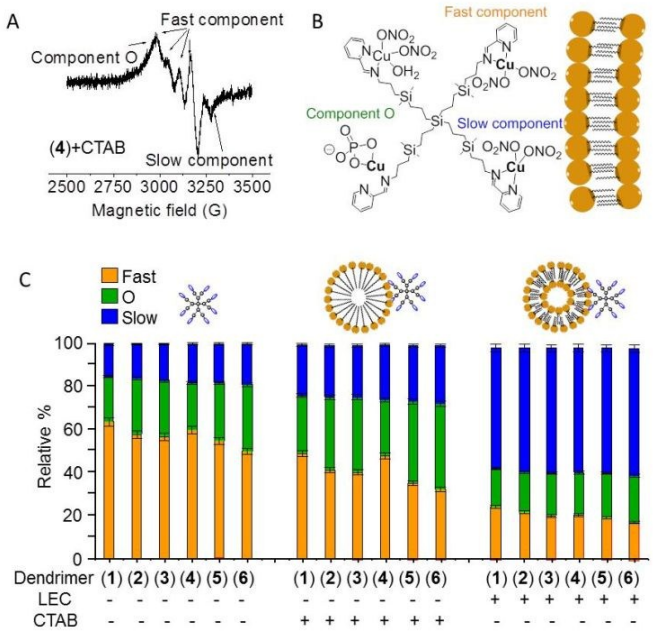

Figure 2.4 EPR study overview (article 3, figure 4)

Cu(II) analysis showed three different components constituting the spectrum:

- A fast Cu-N_2O_2 component, relative to poorly interacting copper ions. Two nitrogens from the iminopyridine directly bind copper acting like a Schiff-base ligand, and two oxygens from either the solvent or nitrate complete the complex;
- A slow Cu-N_2O_2 component, relative to highly interacting copper ions;
- An unexpected Cu-O_4 component, with four oxygens coordinating a completely solvated Cu(II) ion, "component O".

The Cu-N_2O_2 coordination prevailed in the presence of model membranes, mainly for chloride samples. Cu-O_4 arose mainly for nitrate compounds, highlighting the perfect solubility of such metallodendrimers, yet leading to a different path inside the biological system.

Metallodendrimers were then tested with real cells, tumoral line U937 and healthy PBMC. Nitrate- and chloride- conjugated samples act very differently, as EPR results show: chloride complexes feature a more stable copper complex if compared to nitrate ones, and leading to a different interaction with cell membranes. -Cl complex is more hydrophobic, making possible for metallodendrimers to penetrate inside cell membranes, especially at low generations. The resulting interaction is very strong, especially after 24h, and persistent in time.

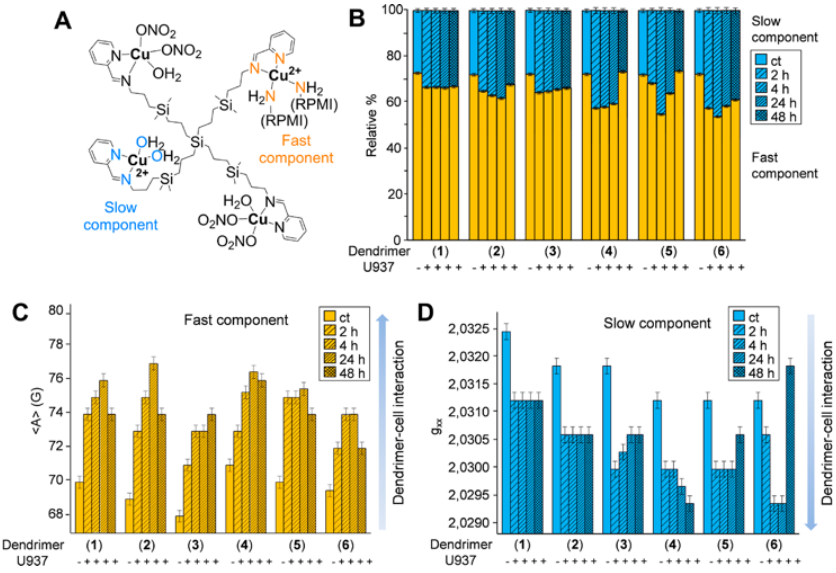

Figure 2.5 EPR parameters, mirroring the cell-dendrimer interaction (article 2, figure 2)

Low generation nitrate compounds interact on a more superficial level, with a rapid yet short lasting effect on cells. Comparison with biological results show how they get internalized mainly by phagocytosis, while -Cl ones could simply diffuse inside cells, without exploiting a specific transportation mechanism.

The situation changes at high dendrimer generations, where all compounds seem to exploit phagocytosis to penetrate inside cells, due to their bigger size and higher superficial groups density.

2.2.2 Biological studies

Cu(II)-conjugated metallodendrimers antitumoral activity and selectivity was evaluated with both tumoral (U937) and healthy (PBMC) cells. First generation ones were active already at 24h, inducing an initial pro-oxidative effect, followed by a mitochondrial membrane potential collapse at 72h.

First generation nitrate compounds, due to their previously described internalization mechanism, provoked a mixed necrosis/necroptosis cytotoxicity, in a faster and more effective way than chloride counterparts.

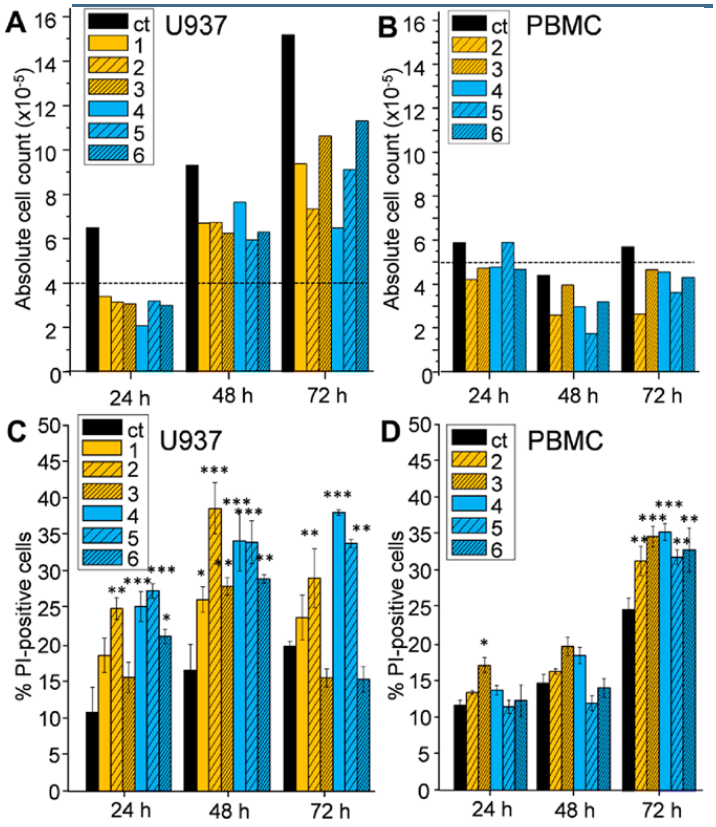

Figure 2.6 toxicity evaluation on tumor and healthy cells (article 2, figure 3)

A promising degree of selectivity was found for all metallodendrimers, with a significantly less marked cytotoxic effect for PBMC cells.

After assessing metallodendrimers selectivity towards U937, a screening of the antitumoral activity on more tumor cell lines was performed to better direct the following ex-vivo experiments.

Compound	*Cu(II) atoms*	*Cytotoxicity* [IC_{50} (μM) ± SD]					
		HeLa	MCF7	PC3	HCC1806	HT29	142BR
1	1	47.3 ± 3.8	30.2 ± 5.1	21.8 ± 2.0	17.3 ± 2.5	32.7 ± 0.9	60.9 ± 0.3
2	4	1.7 ± 0.5	2.1 ± 0.2	3.4 ± 0.2	1.9 ± 0.1	9.3 ± 0.5	7.7 ± 0.4
3	8	5.2 ± 0.3	9.6 ± 1.4	2.5 ± 0.3	0.69 ± 0.03	12.3 ± 0.2	6.1 ± 0.1
4	1	7.6 ± 0.3[a]	44.9 ± 5.1	9.7 ± 3.1[a]	13.9 ± 1.2	44.9 ± 1.8	>100
5	4	10.5 ± 0.3[a]	5.4 ± 0.1	4.5 ± 0.9[a]	2.2 ± 0.1	0.5 ± 0.1	73.4
6	8	10.0 ± 2.6[a]	7.7 ± 0.4	12.5 ± 0.3[a]	7.3 ± 0.1	1.8 ± 0.9	83.6

Figure 2.7 Antitumoral activity screening. [a] Previously published results.[5] (article 3, table 2)

Figure 2.7 shows the outcome of the screening. Notably, the IC_{50} values for PC3 cells are lower than analogous Ru(II)-conjugated metallodendrimers.

- Generation 1 compounds proved once again the most active against the majority of tumors, balancing flexibility and superficial groups density. Such feature is typical of carbosilane skeletal, which are active even at low generation if compared to other types of skeletal, like phosphorus dendrimers; [6]

- Chloride samples proved less cytotoxic than nitrate which also had better technological properties, like improved solubility.

Compound G_1-Cu-(ONO_2) **2** was the most performing against the majority of the tested tumoral cell lines, and poorly non-aggressive towards healthy PBMC cells. It was therefore chosen for the subsequent ex-vivo studies.

2.2.3 Ex-vivo experiments

Mice models of resistant prostate cancer were used to prove metallodendrimer G_1-Cu-(ONO_2) **2** potency in-vivo.

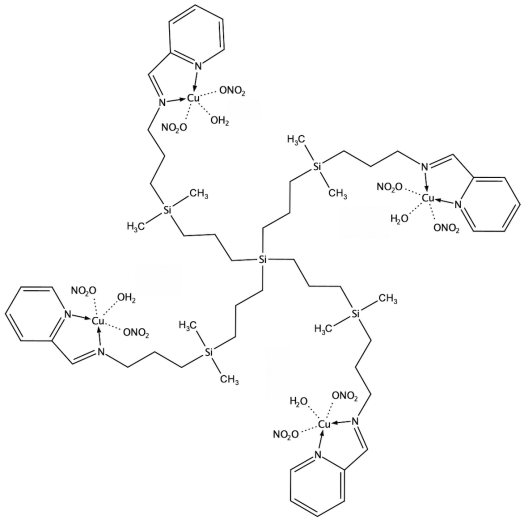

*Figure 2.8 Chosen candidate for ex-vivo testing G_1-Cu-(ONO_2) **2***

The experiment lasted for 55 days, and the antitumoral effect started to be evident since day 25. If compared to non-treated mice, selected specimen experienced up to 37% reduction of tumor size. Notably, no mice significantly lost weight during the treatment, nor signs of acute toxicity were found. Needless to say, no mice died during the 55 days of the experiment.

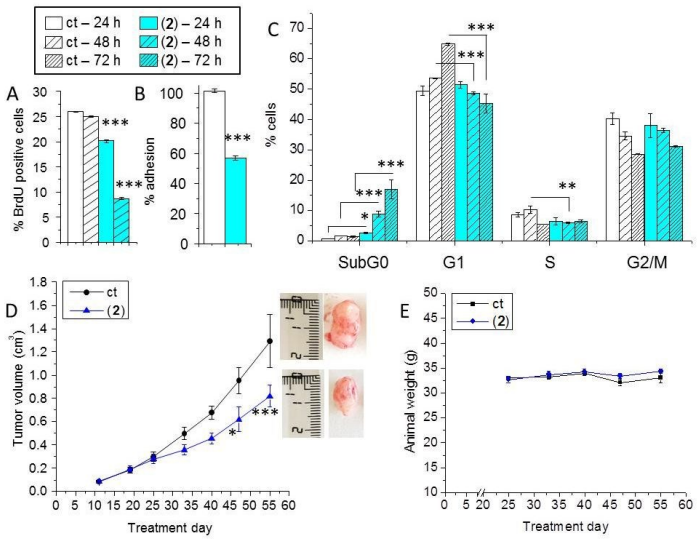

Figure 2.9 Ex-vivo experiment outcome (article 3, figure 5)

Such results are quite promising, given the absence of any treatment for resistant prostate cancer. In future experiments we might consider upping the doses, given the exceptionally good response of mice to the chemotherapy.

3 - BIBLIOGRAPHY

1. Wrobela D., Kłysb A., Ionova M., Vitovicc P., Waczulikowac I., Hianikc T., Gomez-Ramirez R., de la Mata J., Klajnerta B., Bryszewskaa M., *"Cationic carbosilane dendrimers–lipid membrane interactions"*, 2012, Chemistry and Physics of Lipids, 165(4):401-407.
2. Motswainyana W.M., Ajibade P.A., "*Anticancer Activities of Mononuclear Ruthenium(II) Coordination Complexes*", 2015, Advances in Chemistry, 1-21
3. Hussain A., AlAjmi M.F., Rehman M.T., Amir S., Husain F.M., Alsalme A., Siddiqui M.A., AlKhedhairy A.A., Khan R.A., *"Copper(II) complexes as potential anticancer and Nonsteroidal anti-inflammatory agents: In vitro and in vivo studies"* 2019, Scientific reports, 9, 5237
4. Gaetke, L.M., Chow-Johnson, H.S. & Chow, C.K., "*Copper: Toxicological relevance and mechanisms*" 2014, Archives of Toxicology, 88, 1929–1938.
5. Sanz del Olmo N., Maroto-Díaz M., Gomez R., Ortega P., Cangiotti M., Ottaviani M. F., de la Mata F. J., *"Carbosilane metallodendrimers based on copper (II) complexes: Synthesis, EPR characterization and anticancer activity"*, 2017, Journal of Inorganic Biochemistry, 177, 211−218.
6. El Brahmi N., El Kazzouli S., Mignani S. M, Essassi E. M., Aubert G., Laurent R., Caminade A.-M, Bousmina M. M., Cresteil T., Majoral J.-P., *"Original Multivalent Copper(II)-Conjugated Phosphorus Dendrimers and Corresponding Mononuclear Copper(II) Complexes with Antitumoral Activities"*, 2013, Molecular Pharmaceutics, 10, 1459-1464.

PAPER 1

Exploring the Interactions of Ruthenium (II) Carbosilane Metallodendrimers and Precursors with Model Cell Membranes through a Dual Spin-Label Spin-Probe Technique Using EPR

Riccardo Carloni, Natalia Sanz del Olmo, Paula Ortega, Alberto Fattori, Rafael Gómez, Maria Francesca Ottaviani, Sandra García-Gallego
Michela Cangiotti, and F. Javier de la Mata

Biomolecules 2019, 9, 540
https://doi.org/10.3390/biom9100540

Exploring the Interactions of Ruthenium (II) Carbosilane Metallodendrimers and Precursors with Model Cell Membranes through a Dual Spin-Label Spin-Probe Technique Using EPR

Riccardo Carloni [1,†], Natalia Sanz del Olmo [2,3,4,†], Paula Ortega [2,3,4], Alberto Fattori [1], Rafael Gómez [2,3,4], Maria Francesca Ottaviani [1], Sandra García-Gallego [2,3,4], Michela Cangiotti [1,*] and F. Javier de la Mata [2,3,4,*]

[1] Department of Pure and Applied Sciences, University of Urbino "Carlo Bo", 61029, Urbino, Italy
[2] Department of Organic and Inorganic Chemistry, and Research Institute in Chemistry "Andrés M. del Río" (IQAR), University of Alcalá, 28805, Madrid, Spain
[3] Networking Research Center on Bioengineering, Biomaterials and Nanomedicine (CIBER-BBN), 28029, Madrid, Spain
[4] Institute Ramón y Cajal for Health Research (IRYCIS), 28034, Madrid, Spain
* Correspondence: michela.cangiotti@uniurb.it (M.C.) and javier.delamata@uah.es (J.M.).
† Both authors contributed equally to this work

Abstract: Dendrimers exhibit unique interactions with cell membranes, arising from their nanometric size and high surface area. To a great extent, these interactions define their biological activity and can be reported in situ by spin-labelling techniques. Schiff-base carbosilane ruthenium (II) metallodendrimers are promising antitumor agents with a mechanism of action yet to explore. In order to study their in-situ interactions with model cell membranes occurring at a molecular level, namely cetyltrimethylammonium bromide micelles (CTAB) and lecithin liposomes (LEC), electron paramagnetic resonance (EPR) was selected. Both a spin probe, 4-(N,N-dimethyl-N-dodecyl)ammonium-2,2,6,6-tetramethylpiperidine-1-oxyl bromide (CAT12), able to enter the model membranes, and a spin label, 2,2,6,6-tetramethylpiperidine-1-oxyl (TEMPO) covalently attached at newly synthesized heterofunctional dendrimers, were used to provide complementary information on the dendrimer–membrane interactions. The computer-aided EPR analysis demonstrated a good agreement between the results obtained for the spin probe and spin label experiments. Both points of view suggested the partial insertion of the dendrimer surface groups into the surfactant aggregates, mainly CTAB micelles, and the occurrence of both polar and hydrophobic interactions, while dendrimer–LEC interactions involved more polar interactions between surface groups. We found out that subtle changes in the dendrimer structure greatly modified their interacting abilities and, subsequently, their anticancer activity.

Keywords: electron paramagnetic resonance; dendrimer; metallodendrimer; ruthenium; cell membrane; spin probe; cancer

1. Introduction

Current anticancer therapies are poorly efficient because of the non-specific drug distribution, the development of multidrug resistance, and the intrinsic heterogeneity of cancer.

In the cancer field, and in many other fields, nanotechnology provides new tools that increase the therapeutic efficiency and minimize side-effects. Nanotechnology provides multifunctional platforms to be used either as therapeutic agents, as drug delivery systems [1,2], or as contrast agents with longer circulation time for the early detection and diagnosis of diseases [3]. These multifunctional platforms may further be designed to simultaneously present two or more activities in a single molecule, the so-called nanotheranostics. Nanotheranostics are cutting-edge nanoparticles (NPs) designed for simultaneously providing accurate diagnosis together with effective therapeutic activity, monitoring drug release and distribution in real time, and have been already used in different fields including cancer [4,5] and neurological disorders [6]. The different nanotheranostic agents reported in the literature [7]—metal nanoparticles, polymeric nanoparticles, and dendrimers—are useful tools for optimizing treatment outcomes in cancer and other diseases.

In particular, dendrimers are excellent platforms for accurate heterofunctionalization. They are the flagship of precision nanoparticles, whose monodisperse scaffold enables a controlled design of the groups located at the periphery or within the interior [8]. They allow a precise structure-to-activity relationship, unattainable by other nanoparticles, exhibiting different biological activity depending on both their functional groups and the nature of their scaffold. As an example, carbosilane dendrimers rely on a hydrophobic scaffold, comprising multiple C–C and C–Si bonds, which provide extraordinary flexibility and stability and enhance the interaction with biological membranes. Many biomedical applications have been reported for this dendritic family, such as antiviral and antibacterial agents, non-viral vectors for nucleic acid delivery, and antitumor drugs, among others [9].

Dendrimers interact well with membranes and cells [10,11], and thus trigger multiple biological activities. The nanoparticle–cell interactions are modulated by both the physicochemical properties of the NPs and cell-specific parameters [12], and a thorough understanding of this interaction can provide valuable information for the design of effective drugs. Among the available tools for studying nanoparticle–cell interactions, electron paramagnetic resonance (EPR) spectroscopy has excelled in providing on-site structural and dynamical information. The spin-probe/spin-label-based EPR technique has already been demonstrated to be a powerful tool in characterizing the interactions of dendrimers with model membranes and cells [10,13–24], and has even been used in living systems [25]. Importantly, EPR spectroscopy shares many of the features of magnetic resonance imaging (MRI), including the underlying principles, and exhibits superior detection sensitivity. The recent developments in EPR instrumentation, probes, and methods offer opportunities in potential areas of clinical application [26], such as oximetry and dosimetry [27].

We have recently reported the use of Schiff-base containing carbosilane dendrimers as efficient chelators of copper (II) [28,29] and ruthenium (II) [30,31] complexes. The inclusion of metallodrugs in nanostructures improves their delivery and penetration—mainly by endocytosis—thus increasing the concentration in cells and subsequently the anticancer effect [32]. Accordingly, the carbosilane metallodendrimers exhibited promising antitumor activity in both in vitro and in vivo assays. Further insight into the antitumor activity of the Cu(II) metallodendrimers was obtained through the EPR analysis of the dendrimers' interaction with model membranes [29]. We found out that the dendritic generation, as well as the metal counter-ion, tuned the strength of interaction of the dendrimer with the membrane and affected the toxicity and selectivity towards cancer cells.

With the aim of obtaining more information about the interactions occurring at a molecular level in the biological environment of Schiff-base carbosilane dendrimers and their Ru(II) complexes, we selected the EPR technique to study the site–site interactions between the dendrimers and model cell membranes, namely cetyltrimethylammonium bromide micelles (indicated as CTAB) and lecithin liposomes (indicated as LEC). To characterize these interactions in situ, both a spin probe, 4-(*N*,*N*-

dimethyl-*N*-dodecyl)-ammonium-2,2,6,6-tetramethylpiperidine-1-oxyl bromide (CAT12) able to enter the model membranes, and a spin label, 2,2,6,6-tetramethylpiperidine-1-oxyl (TEMPO) covalently attached to the dendrimer surface, were used to provide complementary information on the dendrimer–model membrane interactions from both sides. A comparative EPR analysis was performed on the labelled dendrimers in the absence and presence of the model membranes. Relevant insight was obtained related to the influence of different parameters—generation, equilibration time, peripheral groups, and presence of heterofunctional ligands—on the nanoparticle–membrane interactions, which can explain their biological activity.

2. Materials and Methods

2.1. Dendrimers and Metallodendrimers

In order to evaluate the dendrimer–membrane interactions from the dendrimer point of view, novel labelled iminopyridine dendrimers were prepared (Figure 1). The three-step synthetic route included the preparation of the heterofunctional dendrimers G_n-{[NCPh(*o*-N)]$_{m-1}$[NH_2]} [17] (for simplicity G_n-PyN; n = 1, m = 4 (**1**); n = 2, m =8 (**2**)), G_n-{[NCPh(*o*-N)]$_{m-1}$[NHC(S)NH-TEMPO]} (G_n-PyT, n = 1, m = 4 (**3**); n = 2, m = 8 (**4**)), and G_n-{[NCPh(*o*-N)Ru(η^6-*p*-cymene)Cl_2]$_{m-1}$[NHC(S)NH-TEMPO]} (G_n-RuT; n = 1, m = 4 (**5**); n = 2, m = 8 (**6**)). The synthetic protocols and characterization details are described below for each dendrimer.

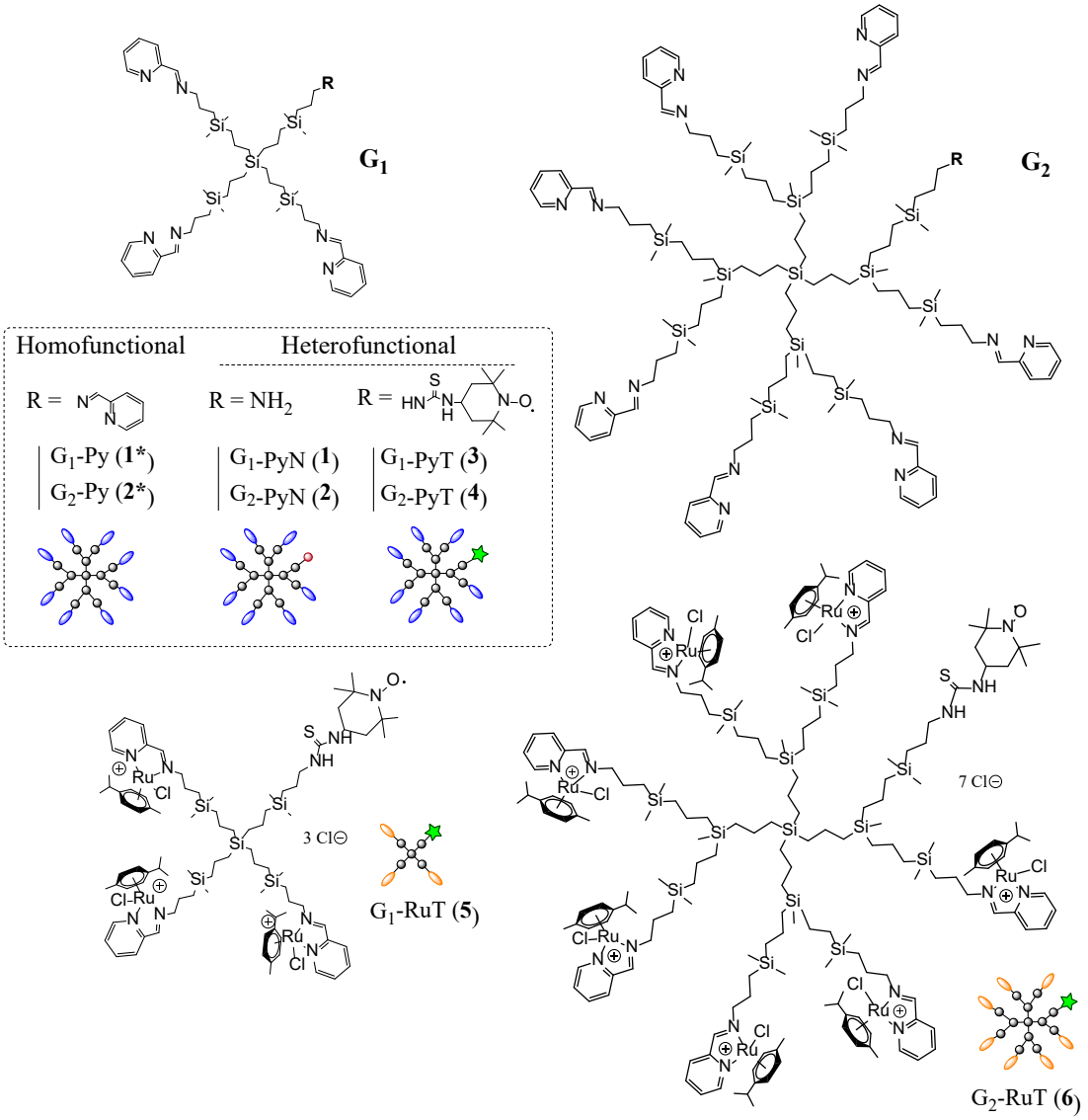

Figure 1. *Structural representation of dendrimers and metallodendrimers used in the electron paramagnetic resonance (EPR) study. Homofunctional dendrimers: Gn-Py (**1***, **2***); heterofunctional dendrimers: Gn-PyN (**1**,**2**) and Gn-PyT (**3**,**4**); heterofunctional metallodendrimers: Gn-RuT (**5**,**6**).*

For comparison, iminopyridine homofunctional dendrimers Gn-{[NCPh(*o*-N)]m (Gn-Py; n = 1, m = 4 (**1***); n = 2, m = 8 (**2***) and the mononuclear counterpart n = 0, m = 1 (**0***)) were used in EPR evaluation. Overall, these dendrimers provided information about the effect of dendritic generation (G1 vs. G2), the functional groups (Gn-Py vs. Gn-PyN), the labelling (Gn-Py vs. Gn-PyT) and the metal complexation (Gn-PyT vs. Gn-RuT), the latter known to enhance anticancer drug properties [32].

G1-{[NCPh(o-N)*]3[NH2]} (**G1-PyN**, **1**)*. To a solution of precursor G1-[NH2]4 (**I**) (313.1 mg, 0.47 mmol) in anhydrous tetrahydrofuran (THF), 2-pyridinecarboxaldehyde (152.1 mg, 1.42 mmol) was added. The mixture was stirred under inert atmosphere at room temperature in the presence of anhydrous $MgSO_4$ for 12 h. Subsequently, the solution was filtered and the solvent was evaporated to obtain compound **1** as brown oil in quantitative yield. ^{1}H-NMR ($CDCl_3$): δ -0.06 (s, 24H, -(C*H*$_3$)$_2$Si-); 0.43 (m, 2H, (-C*H*$_2$CH$_2$CH$_2$NH$_2$); 0.51 (m, 24H, -SiC*H*$_2$-); 1.29 (m, 8H, -SiCH$_2$C*H*$_2$CH$_2$Si); 1.37 (m, 2H, (-SiCH$_2$C*H*$_2$CH$_2$NH$_2$); 1.68 (m, 6H, -SiCH$_2$C*H*$_2$CH$_2$NCPh); 2.62 (m, 2H, (-C*H*$_2$NH$_2$); 3.62 (m, 6H,-C*H*$_2$NCPh); 7.28 (m, 3H, Ar); 7.70 (m, 3H, Ar); 7.95 (m, 3H, Ar); 8.60 (m, 3H, Ar); 8.33 (s, 3H, -

N=CH^{imine}). ^{13}C{^{1}H}-NMR ($CDCl_3$): δ -3.33 (-(CH_3)$_2$Si-); 1.00 (-(CH_3)$_2$SiCH$_2$CH$_2$CH$_2$NH$_2$); 12.1 (-SiCH$_2$CH$_2$CH$_2$NH$_2$); 13.1 (-SiCH$_2$CH$_2$CH$_2$NCPh); 17.5, 18.5, 20.2 (-SiCH$_2$CH$_2$CH$_2$Si-); 25.3 (-SiCH$_2$CH$_2$CH$_2$NCPh); 28.3 (-SiCH$_2$CH$_2$CH$_2$NH$_2$); 45.5 (-CH$_2$NH$_2$); 52.9 (-CH$_2$NCPh); 121.2, 124.5, 136.5, 149.3, 161.7 (CAr); 161.7 (-N=CH^{imine}). Elemental analysis (%): calculated for $C_{50}H_{89}N_7Si_5$ (928.7 g/mol): C, 64.66; H, 9.66; N, 10.56; found: C, 64.30; H, 9.00; N, 10.48.

*G$_2$-{[NCPh(*o*-N)]$_7$[NH$_2$]} (**G$_2$-PyN**, **2**).* Dendrimer G$_2$-PyN was prepared through the same procedure as compound **1,** using the following reagents: G$_2$-[NH$_2$]$_8$ (**II**) (113.0 mg, 0.069 mmol), 2-pyridinecarboxaldehyde (51.73 mg, 0.483 mmol). Dendrimer **2** was isolated as brown oil in quantitative yield. ^{1}H-NMR ($CDCl_3$): δ -0.12 (s, 12H, -(C*H*$_3$)Si(CH$_2$CH$_2$CH$_2$Si)$_2$); -0.06 (s, 48H, -(C*H*$_3$)$_2$Si-); 0.51 (m, 64H, -SiC*H*$_2$-); 1.26 (m, 24H, -SiCH$_2$C*H*$_2$CH$_2$Si- and -SiCH$_2$C*H*$_2$CH$_2$NH$_2$); 1.68 (m, 16H, (-SiCH$_2$C*H*$_2$CH$_2$NCPh); 2.62 (m, 2H, (-C*H*$_2$NH$_2$); 3.63 (m, 14H,-C*H*$_2$NCPh); 7.28 (m, 7H, Ar); 7.71 (m, 7H, Ar); 7.97 (m, 7H, Ar); 8.62 (m, 7H, Ar); 8.35 (s, 7H, -N=CH^{imine}). Elemental analysis (%): calculated for $C_{122}H_{217}N_{15}Si_{13}$ (2259.3 g/mol): C, 64.86; H, 9.68, N, 9.30; found: C, 64.28; H, 8.51; N, 8.62.

*G$_1$-{[NCPh(o-N)]$_3$[NHC(S)NH-TEMPO]} (**G$_1$-PyT**, **3**).* To a solution of G$_1$-PyN (**1**) (41.8 mg, 0.045 mmol) in methanol, the radical 4-isothiocyanate-TEMPO (7.7 mg, 0,036 mmol) was added. The mixture was stirred under inert atmosphere and protected from light at room temperature for 12 h. Subsequently, the solvent was evaporated to obtain dendrimer **3** as brown oil in quantitative yield. ^{1}H-NMR (CD_3OD): δ 0.00 (s, 24H, -(C*H*$_3$)$_2$Si-); 0.60 (m, 24H, -SiC*H*$_2$-); 1.39 (m, 10H, -SiCH$_2$C*H*$_2$CH$_2$Si- and -SiCH$_2$C*H*$_2$CH$_2$NH-TEMPO); 1.74 (m, 6H, (-SiCH$_2$C*H*$_2$CH$_2$NCPh); 3.68 (m, 6H,-C*H*$_2$NCPh); 7.48 (m, 3H, Ar); 7.90 (m, 3H, Ar); 8.02 (m, 3H, Ar); 8.62 (m, 3H, Ar); 8.37 (s, 3H, -N=CH^{imine}). Elemental analysis (%): calculated for $C_{60}H_{106}N_9OSSi_5$ (1142.1 g/mol): C, 63.10; H, 9.36; N, 11.04; S, 2.81; found: C, 61.46; H, 8.59; N, 10.00; S, 2.72.

*G$_2$-{[NCPh(*o*-N)]$_7$[NHC(S)NH-TEMPO]} (**G$_2$-PyT**, **4**).* Dendrimer G$_2$-PyT was prepared through the same procedure as compound **3**, using the following reagents: G$_2$-PyN (**2**) (56.0 mg, 0.025 mmol), 4-isothiocyanate-TEMPO (4.2 mg, 0.020 mmol). Dendrimer **4** was isolated as brown oil in quantitative yield. ^{1}H-NMR ($CDCl_3$): δ -0.05 (s, 12H, -(C*H*$_3$)Si(CH$_2$CH$_2$CH$_2$Si)$_2$); -0.02 (s, 48H, -(C*H*$_3$)$_2$Si-); 0.61 (m, 64H, -SiC*H*$_2$-); 1.42 (m, 26H, -SiCH$_2$C*H*$_2$CH$_2$Si- and -SiCH$_2$C*H*$_2$CH$_2$NH-TEMPO); 1.75 (m, 14H, (-SiCH$_2$C*H*$_2$CH$_2$NCPh); 3.68 (m, 14H,-C*H*$_2$NCPh); 7.46 (m, 7H, Ar); 7.89 (m, 7H, Ar); 8.00 (m, 7H, Ar); 8.61 (m, 7H, Ar); 8.35 (s, 7H, -N=CH^{imine}). Elemental analysis (%): calculated for $C_{132}H_{234}N_{17}OSSi_{13}$ (2472.6 g/mol): C, 64.12; H, 9.54; N, 9.63; S, 1.30; found: C, 62.99; H, 8.70; N, 8.62; S, 0.82.

*G$_1$-{[NCPh(*o*-N)Ru(η^6-*p*-cymene)Cl$_2$]$_3$[NHC(S)NH-TEMPO]} (**G$_1$-RuT**, **5**).* To a solution of [Ru(η^6-*p*-cymene)Cl$_2$]$_2$ (59.8 mg, 0.052 mmol) in methanol, G$_1$-PyT (**3**) (48.1 mg, 0.16 mmol) was added dropwise at 0 °C. The mixture was stirred under inert atmosphere at room temperature for 12 h and protected from light. Subsequently, the solvent was evaporated to obtain dendrimer **5** as brown oil in quantitative yield. ^{1}H-NMR (CD_3OD): δ 0.04 (s, 24H, -(C*H*$_3$)$_2$Si-); 0.64 (m, 24H, -SiC*H*$_2$-); 1.03 (d, 9H, -(C*H*$_3$)$_2$CH^{cym}); 1.15 (d, 9H, -(C*H*$_3$)$_2$CH^{cym}); 1.39 (m, 10H, -SiCH$_2$C*H*$_2$CH$_2$Si- and -SiCH$_2$C*H*$_2$CH$_2$NH-TEMPO); 1.82 (m, 3H, (-SiCH$_2$C*H*$_2$CH$_2$NCPh); 2.02 (m, 3H, (-SiCH$_2$C*H*$_2$CH$_2$NCPh); 2.29 (s, 9H, -(C*H*$_3$)^{cym}); 2.69 (s, 3H, -(CH$_3$)$_2$C*H*^{cym}); 4.27 (m, 3H,-C*H*$_2$NCPh); 4.69 (m, 3H,-C*H*$_2$NCPh); 5.84 (m, 7H, Ar^{cym}); 6.08 (m, 3H, Ar^{cym}); 6.19 (m, 3H, Ar^{cym}); 7.80 (m, 3H, Ar); 8.20 (m, 6H, Ar); 9.50 (s, 3H, Ar); 8.69 (s, 3H, -N=CH^{imine}). Elemental analysis (%): calculated for $C_{90}H_{148}Cl_6N_9ORu_3SSi_5$ (2060.6 g/mol): C, 52.46; H, 7.24; N, 6.12; S, 1.56; found: C, 52.08; H, 7.12; N, 6.60; S, 1.62.

*G$_2$-{[NCPh(*o*-N)Ru(η^6-*p*-cymene)Cl$_2$]$_7$[NHC(S)NH-TEMPO]} (**G$_2$-RuT**, **6**).* Dendrimer G$_2$-RuT was prepared through the same procedure as for compound **5**, using the following reagents: G$_2$-PyT (**4**) (29.3 mg, 0.012 mmol), [Ru(η^6-*p*-cymene)Cl$_2$]$_2$ (25.7 mg, 0.084 mmol).

Dendrimer **6** was isolated as brown oil in quantitative yield. ^{1}H-NMR (CD_3OD): δ -0.02 (s, 12H, -(CH_3)Si($CH_2CH_2CH_2Si$)$_2$); 0.06 (s, 48H, -(CH_3)$_2$Si-); 0.64 (m, 64H, -SiCH_2-); 1.05 (m, 21H, -(CH_3)$_2$CH^{cym}); 1.15 (m, 21H, -(CH_3)$_2$CH^{cym}); 1.41 (m, 26H, -Si$CH_2CH_2CH_2$Si- and -Si$CH_2CH_2CH_2$NH-TEMPO); 1.88 (m, 7H, (-Si$CH_2CH_2CH_2$NCPh); 2.01 (m, 7H, (-Si$CH_2CH_2CH_2$NCPh); 2.29 (s, 21H, -(CH_3)^{cym}); 2.70 (s, 7H, -(CH_3)$_2$CH^{cym}); 4.28 (m, 7H,-CH_2NCPh); 4.69 (m, 7H,-CH_2NCPh); 5.84 (m, 14H, Ar^{cym}); 6.08 (m, 7H, Ar^{cym}); 6.18 (m, 7H, Ar^{cym}); 7.79 (s, 7H, Ar); 8.19 (m, 14H, Ar); 9.49 (s, 7H, Ar); 8.68 (s, 7H, -N=CH^{imine}).Elemental analysis (%): calculated for $C_{202}H_{332}Cl_{14}N_{17}ORu_7SSi_{13}$ (4615.9 g/mol): C, 52.56; H, 7.25; N, 5.16; S, 0.69; found: C, 52.11; H, 7.04; N, 5.68; S, 0.65.

2.2. Nuclear Magnetic Resonance

Proton and carbon nuclear magnetic resonance (^{1}H-NMR, ^{13}C-NMR) experiments were performed on Varian Unity-500, Unity Plus-300, and Mercury Plus-300 instruments (Varian, Palo Alto, CA, USA). Deuterated chloroform ($CDCl_3$) and deuterated methanol (CD_3OD) were used as solvents. Total correlation spectroscopy (TOCSY) experiments were performed on selected compounds for further characterization insight.

2.3. Fourier-Transform Infrared Spectroscopy

Fourier-transform infrared (FT-IR) spectra were measured using a PerkinElmer Frontier spectrometer (Waltham, MA, USA) over KBr solid samples in the range 4000–400 cm^{-1}.

2.4. Elemental Analysis

C, H, and N elemental analysis were performed in a microanalyzer LECO CHNS-932 (LECO, St. Joseph, MI, USA).

2.5. Sample Preparation for Electron Paramagnetic Resonance Analysis

2.5.1. Dendrimer Stock Solution

Each dendrimer was dissolved in 1 mL of dimethyl sulfoxide DMSO:distilled water (1:9). This solution was then diluted in water to obtain a 1 mM stock solution with final 1% DMSO.

2.5.2. Liposome Stock Solution

Egg lecithin was dissolved in chloroform under magnetic stirring at room temperature (r.t.) for 15 min. After chloroform evaporation, a water:phosphate buffered saline (PBS) mixture (1:1, pH = 7.2) was added to obtain a solution at a concentration of 0.05 M. The evaporated sample was added with 10 mL of distilled water in a thermostatic bath at 37 °C under stirring for 15 min. Then, 10 mL of PBS was added and stirred for 45 min. Finally, the mixture was sonicated.

2.5.3. Micelle Stock Solution

Cetyltrimethylammonium bromide micelles (CTAB) were dissolved in a water/PBS buffer solution under stirring at 37 °C for 15 min.

2.5.4. Final Mixtures

Final molar ratios: Dendrimer in surface groups 0.5 mM (in distilled water 0.5% DMSO), CTAB or lecithin 25 mM in buffer (PBS; pH = 7.2), and CAT12 0.125 mM in distilled water. Each sample was prepared mixing 250 μL of dendrimer stock solution and 250 μL of membrane model (CTAB/LEC)

stock solutions, then stirred at 37 °C overnight and finally analyzed. We verified the low impact of the spin probe and the spin label on the system properties by changing the spin probe and the spin label concentrations and, consequently, controlling the invariability of the spectral line shape. Furthermore, the CAT12 probe was specifically synthesized and selected to mimic the surfactant structure of the CTAB and lecithin used to make the membrane models. Therefore, the eventual line shape modifications were considered informative on the system properties.

2.6. Electron Paramagnetic Resonance Instrumentation

Electron paramagnetic resonance spectra were recorded by means of an EMX-Bruker spectrometer operating at X band (9.5 GHz) and interfaced with a PC software WinEPR for spectra acquisition and handing, from Bruker (Bruker BioSpin, Rheinstetten, Germany). The temperature was controlled with a Bruker ST3000 variable-temperature assembly cooled with liquid nitrogen. The spectra were recorded at 37 °C ± 1. The spectra were considered valid if reproducible in at least three repeated experiments on the same sample.

2.7. Computation and Analysis of the Electron Paramagnetic Resonance Spectra

The computational procedure proposed by Budil et al. [33] allowed us to obtain the following main parameters of computation:

(a) The Azz component of the A tensor for the coupling between the electron spin and the nuclear spin of the nitrogen nucleus of the nitroxide group. Axx = Ayy = 6 G were assumed constant for simplicity. The increase in Azz reflected an increase in the polarity of the nitroxide environment. For this reason, this parameter was henceforth called the polarity parameter. The error was in the second decimal and was calculated by computation; values exceeding the error produced a worse fitting between the experimental and the computed spectra, that is, we visually saw a discrepancy between the experimental line shape and the spectrum computed by using the NLSL program by Budil et al. [33]

(b) The correlation time for the rotational motion of the nitroxide group, τ, measured the microviscosity of the nitroxide environment, and, in turn, evaluated the strength of interaction occurring at the nitroxide site. This parameter was henceforth called the microviscosity parameter. The error was ± 0.001 ns for a narrow-lines spectrum and ± 0.01 ns for a broad spectrum, and was calculated by computation, that is, as indicated in (a), with values exceeding the error producing a worse fit between the experimental and the computed spectra.

In most cases, the EPR spectra were constituted by two components due to nitroxide radicals in different environments. In these cases, the experimental spectra containing the two components in different relative amounts were subtracted from each other to extract each of the components and also evaluate, by double integration of the components, their relative percentages. Then, each component was analyzed as described above.

Finally, the total intensity of well reproducible EPR spectra was evaluated by the double integral of the spectra and scaled to 100, assuming intensity = 100 for the spectrum at the highest intensity. Quantitative EPR measurements of spin concentration cannot be performed in the absence of an internal reference, but, in the present case, we trusted the intensity values only in a comparative way for a series of samples, for an indirect measure of the spin-probe solubility, and of the effect of antioxidants.

3. Results and Discussion

Schiff-base carbosilane dendrimers, especially those with the N,N-chelating 1-(2-pyridinyl)methanimine ligand, represent a promising tool for the synthesis of nanosized metallodrugs [28–31]. These dendrimers are air stable and stable in organic solvents for months; however, they are insoluble in water, methanol, and DMSO, preventing their biological evaluation through common techniques. After binding the metal complexes, they become water-soluble and biologically active. The resultant Ru(II) metallodendrimers exhibited promising antitumor activity in both in vitro and in vivo assays.

Herein, we pursue a thorough understanding about the site-site interactions between the dendrimers and the model membranes from two different points of view: the dendrimer point of view, by attaching the TEMPO spin label at the dendrimer surface; and the membrane point of view using the spin probe CAT12 that is able to enter the model membrane with the C12 chain, while the positively charged CAT group remains at the membrane surface, monitoring the interactions.

3.1. Synthesis and Characterization of Heterofunctional TEMPO-Labelled Ru(II) Metallodendrimers

In order to study the interactions between the dendrimers and membrane models by means of EPR, a paramagnetic species had to be introduced into the system, and a good approach was to spin label the dendritic molecule. The synthesis of the heterofunctional ruthenium metallodendrimers of carbosilane nature with the paramagnetic probe TEMPO was carried out using a three-step strategy (Scheme 1).

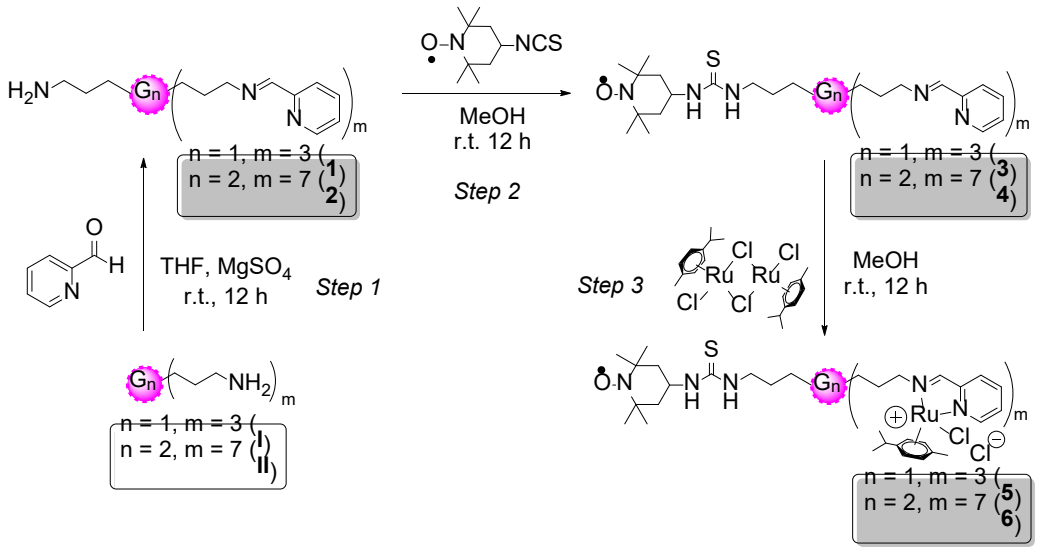

Scheme 1. Three-step synthetic strategy to accomplish the 2,2,6,6-tetramethylpiperidine-1-oxyl (TEMPO)-labelled heterofunctional metallodendrimers Gn-RuT (5,6).

In the first step, we synthesized new heterofunctional dendrimers comprising multiple iminopyridine ligands, able to coordinate Ru(II) complexes, and a primary amino group, available for TEMPO binding. We decided to attach a single nitroxide group per dendrimer, regardless of the dendritic generation, for two reasons: a single radical can provide valuable information about the system, and rules out the possibility of spin–spin interactions between two proximal radicals. Furthermore, we wanted to maximize the number of iminopyridine groups and their metal complexes on the dendritic surface, and subsequently the anticancer activity. Using a statistical approach for the heterofunctionalization of the precursor dendrimers G_n-$[NH_2]_m$ (n = 1, m = 4 (**I**), n =

2, m = 8 (**II**))[34], a condensation reaction was carried out between the amino groups present in the precursor dendrimers and 2-pyridinecarboxaldehyde, in a 1:3 ratio for the first-generation derivative, and a 1:7 ratio for the second-generation analogue, resulting in the formation of G_n-{[NCPh(*o*-N)]$_{(m-1)}$[NH_2]}, (n = 1, m = 4 (G_1-PyN, **1**); n = 2, m = 8 (G_2-PyN, **2**)) with one free -NH_2 group (Scheme 1) [30].

To control the partial functionalization of the precursor dendrimers, the reactions were monitored by ^{1}H-NMR, adding the aldehyde portion-wise until the signal corresponding to the –CH_2NH_2 methylene group at 2.62 ppm integrated 25% in the case of the first-generation dendrimer and 12.5% for the second-generation compound, compared to the beginning of the reaction. The reactions were carried out under inert atmosphere using dry THF as solvent, and in the presence of $MgSO_4$ as drying agent. It is important to note that the addition of the aldehyde produces a reaction color change, indicative of the formation of the new imine bond (-C=N). Once the reaction was completed, the mixture was filtered and the solvent was evaporated in vacuo obtaining G_n-PyN dendrimers **1** and **2** as brown oils in quantitative yields. The ^{1}H-NMR spectra of the Schiff-base containing heterofunctional dendritic systems confirmed the presence of a new signal from the new methinic group bound to the iminopyridine at 3.62 ppm and another new signal at 8.34 ppm corresponding to the new imine formed (Figure S1). Moreover, it was possible to observe one signal at 2.62 ppm corresponding to the methinic group attached to the amino group of the non-functionalized branch. The presence of two different types of dendritic branches was corroborated also by NMR in the first-generation dendrimer **1** spectrum because of the presence of unfolded signals, which were assigned through TOCSY-1D experiments (Figure S2). Regarding G_2-PyN (**2**), the higher number of branches hindered the observation of unfolded signals, but it was confirmed through the –CH_2NH_2 signal.

In the second step, a covalent thiourea bond was formed through the reaction between the -NH_2 group in G_n-PyN dendrimers **1** and **2** and the isothiocyanate moiety in the TEMPO, leading to the labelled dendrimers G_n-{[NCPh(*o*-N)]$_{(m-1)}$[NHC(S)NHTEMPO]} (n = 1, m = 4 (G_1-PyT, **3**); n = 2, m = 8 (G_2-PyT, **4**)). In order to rule out the presence of non-bound TEMPO, which could hinder a clear EPR analysis, a 1:0.8 stoichiometry (dendrimer:radical) was used. This reaction was carried out under inert atmosphere, protected from light, and using methanol as solvent. After 12 h stirring at r.t., the solvent was evaporated and G_n-PyT dendrimers **3** and **4** were obtained as brown oils in quantitative yields.

The structural characterization of compounds **3** and **4** was carried out by ^{1}H-NMR using CD_3OD as a solvent and FT-IR. The most relevant signals in the ^{1}H-NMR spectrum confirmed the binding of TEMPO radical by the attenuation of the methylene group signal closest to the amino group (Figure S3). As previously reported in the literature [35], the NMR signals assigned to the TEMPO radical could not be identified because of the paramagnetic nature of this molecule. Probably for the same reason, it was not possible to identify the new signal corresponding to the methylene groups directly bound to the thiourea group. In order to compare the signal of the –CH_2NH_2 properly, the characterization of the ligand precursors in methanol was needed, due to the fact that these compounds were previously characterized in $CDCl_3$ because of the great resolution of the signals that we observed in this solvent. With the aim of corroborating the completion of this reaction, FT-IR experiments were performed. The high-intensity broad bands belonging to the isothiocyanate groups (-N=C=S), which appeared around 2188.43 cm^{-1} in the reagent 4-isothiocyanate TEMPO, disappeared once attached to our dendrimers (Figure S5).

In the final step, the ruthenium precursor [Ru(η^6-*p*-cymene)Cl_2]$_2$ was coordinated to the *N,N*-chelate ligands present at the periphery of the dendrimers. G_n-PyN dendrimers **3** or **4** were slowly added to a methanol solution of the Ru(II) precursor at 0 °C. The reaction mixture was stirred for 12 h and then evaporated in vacuo, obtaining, in quantitative yields, the labelled metallodendrimers G_n-{[NCPh(*o*-N)]$_{(m-1)}$[NHC(S)NHTEMPO]} (n = 1, m = 4 (G_1-RuT, **5**); n = 2, m = 8 (G_2-RuT, **6**)) as water-soluble brown solids (Scheme 1).

The ^{1}H-NMR spectra of final Ru(II) complexes, G_1-RuT and G_2-RuT (indicated as **5** and **6** in Scheme 1), revealed the formation of two new Ru–N bonds by the shift towards higher frequencies of the signal assigned to the methylene group closer to the imine nitrogen, the proton of the imine itself, as well as of the methinic groups present in the pyridine ring (Figure S4). The addition of the Ru(II) precursor was completely controlled by NMR in order to avoid having an excess of the metal precursor.

3.2. Electron Paramagnetic Resonance Study of TEMPO-Labelled Dendrimers in the Absence and Presence of Model Membranes

The spin-labelling technique is a very useful tool that offers an in situ reporter at the dendrimer surface about the eventually occurring interactions. An accurate computer-aided analysis of the EPR spectra allowed us to obtain specific information about the type and strength of interactions and the structural variations at the Gn-PyT and Gn-RuT dendrimer/model membrane interface.

Figure 2A shows, as an example, the EPR spectrum of G1-RuT (5) in PBS buffer. The arrows in the figure indicate the main features of the two components constituting the spectra. The first component is composed of three narrow lines, which are characteristic of fast moving nitroxide radicals, and it is henceforth called the Free component. The second broader component shows a partial resolution of the anisotropies, evidenced by the shift of the main peaks. The resolution of the anisotropies arose in the case of slow motion of the nitroxide group, due to an increase of the local microviscosity, which, in turn, was related to interactions occurring at the nitroxide environment. For these reasons, this component is henceforth called Interacting component. The occurrence of both these components for the labelled dendrimers in the absence of membrane models indicated that the free and interacting labels were already present at the surface of the labelled dendrimers, due to a different location of the labels themselves, one more external and the other more internal at the dendrimer interface; however, as we will discuss later, both components were affected by the interactions with the model membranes.

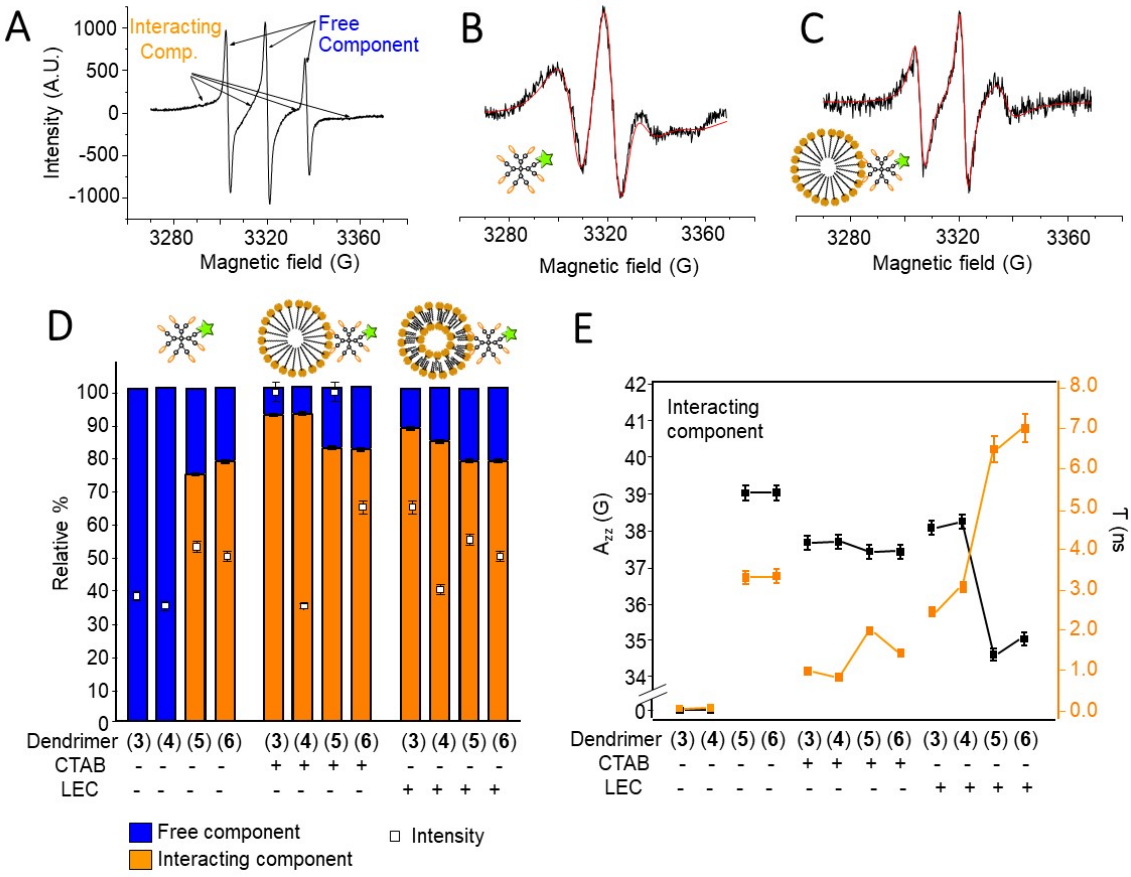

Figure 2. Experimental spectra and computation spectra/parameters for the EPR spectra of the labelled dendrimers Gn-PyT and Gn-RuT 3–6 in the absence and presence of the model membranes (cetyltrimethylammonium bromide micelles (CTAB) and lecithin liposomes (LEC)). (A) Experimental EPR spectrum of G1-RuT (5) in Phosphate Buffered Saline , selected as an example. Arrows indicate the main features of the two components constituting the spectra (termed Free and Interacting); (B,C) experimental and computed Interacting components of G1-RuT (5) alone or in the presence of CTAB, obtained after subtraction of the Free component. The spectra are normalized in height. (D) Total intensity of the EPR spectra (squares, assuming I = 100% for the spectrum of the labelled dendrimers in the absence of model membranes) and relative percentage of Interacting component (bars). (E) Polarity parameter, Azz, and microviscosity parameter, τ, for the Interacting component.

The occurrence of both components allowed us to perform subtractions between spectra to extract each of the components and also evaluate, by double integration of the components, their relative percentages. The components were then also computed to extract parameters providing structural and dynamical information (Table 1, see the experimental section for details). Figure 2B,C show as examples the experimental and computed Free and Interacting components for G1-RuT (5) alone and in the presence of CTAB. Further examples of experimental and computed spectra of labelled dendrimers are shown in Figure S6.

Table 1. Main parameters of computation for the labelled dendrimers Gn-PyT and Gn-RuT in the absence and presence of model membranes.

Entry	Sample	Components	A_{zz} (G)	τ (ns)
1	G_1-PyT (**3**)	Free (single)	39.21/-	0.014/-
2	G_2-PyT (**4**)	Free (single)	39.12/-	0.017/-
3	G_1-PyT (**3**) + CTAB	Free + Interacting	38.72/37.68	0.21/0.87
4	G_2-PyT (**4**) + CTAB	Free + Interacting	38.68/37.70	0.25/0.73
5	G_1-PyT (**3**) + LEC	Free + Interacting	39.01/38.07	0.050/2.35
6	G_2-PyT (**4**) + LEC	Free + Interacting	38.98/38.20	0.055/3.05
7	G_1-RuT (**5**)	Free + Interacting	38.82/39.00	0.22/3.31
8	G_2-RuT (**6**)	Free + Interacting	38.85/39.00	0.22/3.35
9	G_1-RuT (**5**) + CTAB	Free + Interacting	38.82/37.40	0.22/1.90
10	G_2-RuT (**6**) + CTAB	Free + Interacting	38.85/37.41	0.22/1.38
11	G_1-RuT (**5**) + LEC	Free + Interacting	38.82/34.60	0.22/6.45
12	G_2-RuT (**6**) + LEC	Free + Interacting	38.85/35.00	0.22/7.00

TEMPO-labelled dendrimers Gn-PyT (3 and 4, entries 1 and 2 in Table 1, Figure 2D) only showed a Free component, since the radical group was free to move at the dendrimer surface. The computation revealed a very polar environment and a high mobility (low microviscosity), almost equivalent to that found for TEMPO radicals in water. The minor differences in Azz and τ between these two dendrimers can be ascribed to the larger size of G2-PyT, which produced a small increase in microviscosity. The addition of CTAB micelles to these dendrimers (entries 3 and 4 in Table 1) altered the Free component, inducing a decrease of the polarity and mobility (increase in the microviscosity parameter τ) in agreement with a partial insertion of the nitroxide label into the micellar structure. Unexpectedly, the addition of liposomes provoked a lower change of the Free component (entries 5 and 6 in Table 1), indicating that the fast moving labels interact weakly with the liposome structure and mainly remained confined at the interface.

The attachment of Ru(II) complexes to the labelled dendrimers revealed a different interacting behavior. In TEMPO-labelled metallodendrimers Gn-RuT (5 and 6, entries 7 and 8 in Table 1, Figure 2D), the Free component already showed, in the absence of model membranes, a slightly lower polarity and a higher microviscosity if compared to Gn-PyT. The addition of the micelles and the liposomes poorly modified these values (Entries 9–12 in Table 1). Therefore, for the Ru-containing dendrimers, the external free labels were already partially hindered in their rotational mobility at the dendrimer surface, and the interactions with the model membranes provided only small changes in the microviscosity and polarity of the radical environment.

A different but complementary story was told by the computation parameters (the polarity parameter, Azz, and the microviscosity parameter, τ) of the Interacting component (Table 1 and Figure 2E). It is useful to discuss these parameters together with other parameters, i.e., (a) the total intensity, evaluated by the double integral of the spectra and scaled to 100 (assuming I = 100% for the labelled dendrimers in the absence of model membranes), reported in Figure 2D, squares; and (b) the relative percentage of the Interacting component, reported in Figure 2D, bars.

The total intensity of the EPR spectra measured the dendrimer solubility. In the absence of model membranes, the intensities for Gn-PyT were quite low, and slightly increased for Gn-RuT. However, the intensity increased in the presence of CTAB, revealing a significant improvement of solubility due to the interactions with micelles, mainly for first-generation dendrimers. Conversely, the presence of LEC showed no significant changes on the dendrimers' solubility, except for G1-PyT.

The relative percentage of Interacting component (Figure 2D, bars) quantifies the interacting capacity of the dendrimers. As previously mentioned, the Interacting component was absent for Gn-PyT when the model membranes are not present. Conversely, it appeared at a quite high relative extent in the presence of model membranes, mainly for CTAB. The Ru-containing dendrimers, Gn-RuT 5 and 6, showed an Interacting component already in the absence of model membranes, due to the interaction of the TEMPO label with the Ru complex. This percentage slightly increased by adding model membranes, especially CTAB micelles, monitoring the dendrimer/membrane interactions.

As shown in Figure 2E, the environmental polarity measured by Azz decreased from the Free to the Interacting component, and from the absence to the presence of model membranes, indicating that the label responsible of the Interacting component was partially inserted into the lipid core of the aggregate. This effect was quite significant for Gn-RuT with LEC, while the Gn-PyT dendrimers showed a better insertion into CTAB with respect to LEC. A perfect agreement was observed for the microviscosity parameter τ, giving the highest values for the Ru-metallodendrimers in the presence of LEC. Conversely, the CTAB micelles provided a more fluid environment with respect to the liposomes for the dendrimer surface groups partially entering the lipid structure, confirming a better interaction with the micelles.

3.3. Electron Paramagnetic Resonance Study of Unlabelled Dendrimers Using CAT12 Probe in the Absence and Presence of Model Membranes: Comparison with TEMPO-Labelled Dendrimers

In order to gain further insight into the interacting abilities of the dendrimers, we selected the family of homofunctional dendrimers comprising iminopyridine groups in the periphery Gn-Py (first- and second-generation dendrimers 1* and 2*, Figure 1, as well as the mononuclear ligand 0*) [30]. Considering their diamagnetic properties, the use of a spin probe was required to analyze by EPR the interactions occurring between the dendrimers and the model membranes. The CAT12 probe was selected to provide complementary information with respect to those obtained by using labelled dendrimers. CAT12, being a surfactant, was expected to enter the model membrane with the carbon chain, while the positively charged CAT group localized at the membrane surface. This location allowed us to obtain information about the interactions between the dendrimer and the model membrane from the membrane side, while the labels at the dendrimer surface obviously provided information from the other side, the dendrimer surface.

The selection of the CAT12 probe was also based on the similarity between the EPR spectra obtained from the labelled dendrimers and CAT12 in the presence of both the dendrimer and the model membrane. The same line shape was obtained by using the homofunctional Gn-Py family and the heterofunctional Gn-PyN family, and, as shown in Figure 2A, the spectra were again constituted by the two components, Free and Interacting. In both cases, labelled and unlabelled dendrimers, the subtraction procedure between spectra allowed us to extract the two components, evaluate their relative percentages, and compute both of them to obtain the mobility and polarity parameters, which provided information about the dendrimer–model membrane interactions, as described above for the TEMPO-labelled dendrimers. Similarly, the same computation parameters were analyzed for the CAT12 probe as for the labelled dendrimers. In this case, we also found spectral variations over the equilibration time, and, therefore, results are shown and discussed for spectra recorded both after a short time (15 min) and a longer time (24 h) of mixture equilibration. The equilibration time impact was similar for the homofunctional Gn-Py and the heterofunctional Gn-PyN

dendrimers. Then, the equilibration time effect will only be discussed for the homofunctional Gn-Py dendrimers, while, for simplicity, the results for the heterofunctional Gn-PyN dendrimers are only shown for the 15 min spectra to underline the differences between the two series of dendrimers. Further examples of experimental and computed spectra of non-labelled dendrimers in the absence and presence of model membranes are shown in Figure S7.

3.3.1. CAT12 Electron Paramagnetic Resonance Study of the Interactions between Homofunctional G_n-Py Dendrimers and Model Membranes

The relative intensity and relative percentage of interacting component of CAT12 in CTAB and LEC samples in the absence and presence of the G_n-Py dendrimers are shown in Figure 3A. The CAT12 probe is quite soluble in the PBS solution (intensity about 85%), but in the absence of model membranes the intensity decreased by adding G_0-Py and G_2-Py and increased by adding G_1-Py, which was assumed as 100% of intensity. This behavior helped to clarify some properties of the different generation dendrimers in respect to their interacting ability, since CAT12 was interacting by means of both polar and hydrophobic interactions with the dendrimers, as already described in previous studies, and therefore followed the fate of the dendrimers [36]. It can be concluded that G_1-Py showed the highest solubility and interacting ability with the medium, while G_0-Py had the lowest solubility, probably due to the higher hydrophobicity. The opposite experiment, using a solution of model membranes in the absence of the dendrimers, revealed a decrease in the intensity with respect to the CAT12 probe in PBS. It can be explained by the entry and high concentration of the probes at the interface of the aggregates provoking strong spin–spin interactions, which led to very broad lines, no more visible in the spectra. The decrease in intensity was higher for LEC with respect to CTAB, probably due to the high packing of the LEC structure.

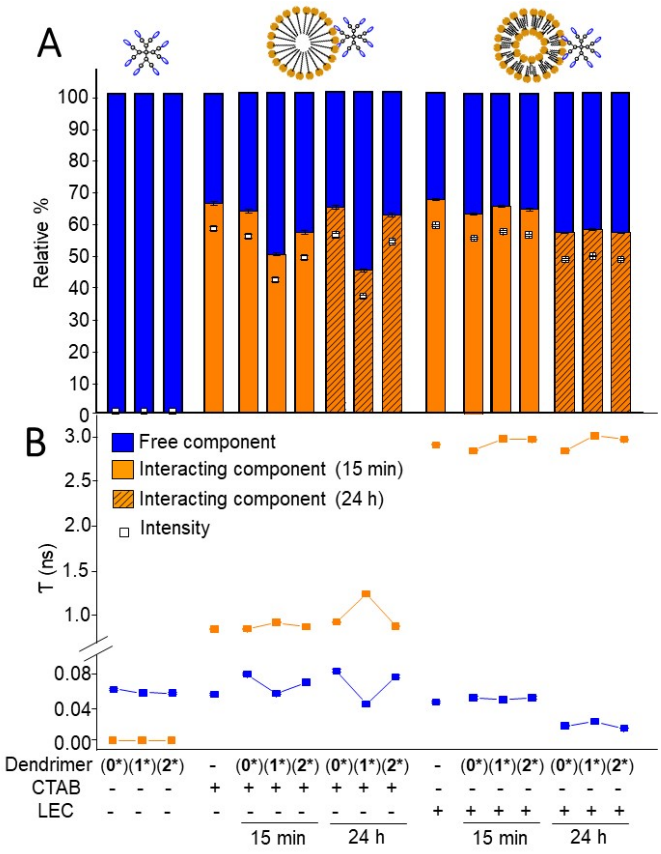

Figure 3. Parameters obtained from the analysis of CAT12 EPR spectra of the unlabeled dendrimers Gn-Py in the absence and presence of the model membranes (CTAB micelles and LEC liposomes). (A) Relative percentages of interacting component (bars) for CTAB and LEC samples in the absence and presence of Gn-Py dendrimers at 15 min and 24 h equilibration times, and intensity values (squares), in percentages, assuming 100% as the highest intensity. (B) Microviscosity parameter, τ, for both the Free and Interacting components.

In the presence of both the dendrimer and the model membrane, the trend found by changing generation was also maintained in the presence of CTAB and LEC and at the different equilibration times. For CTAB dendrimer samples, the intensity was in between the ones for the dendrimer alone and for the CTAB alone in the case of G1-Py and G2-Py, while for G0-Py, the two components' mixture further decreased the solubility. For LEC dendrimer samples, the intensity decreased (~30% maximum) as the radicals were concentrated at the dendrimer/liposome interface. The significant decrease in intensity from 15 min to 24 h in the presence of LEC indicated that the radicals progressively approached each other at the aggregate/dendrimer interface, while the opposite happened in CTAB micelles, where the radicals redistributed better over time into the micelles because of their fluidity when compared to the highly packed liposomes.

Figure 3A also shows the relative percentages of interacting components for CTAB and LEC samples in the presence of the various dendrimers at 15 min and 24 h equilibration times. While the dendrimers alone only showed a Free component, the probe in the model membranes in the absence and presence of the dendrimers showed both the Free and the Interacting components. For CTAB samples, the variation in relative percentage of Interacting component followed an opposite trend with respect to the intensity variation, being the lowest for G1-Py and the highest for G0-Py. The high solubility of CAT12 with G1-Py dendrimer well justified the low interacting component percentage, as this dendrimer, when interacting with the micelles, extracted the probes from the CTAB interface and promoted their solubilization, with this effect continuing over time. The percentage of Interacting component was the highest for G0-Py, almost comparable to the percentage for CTAB alone,. G1-Py showed an intermediate situation, however, for G0-Py and furthermore for G2-Py, the percentage of interacting component in the presence of CTAB increased over time, suggesting a progressive increase of interactions over time.

Similarly to CTAB, the relative percentage of interacting probes for LEC decreased from the absence to the presence of the dendrimers; however, in this case, G1-Py dendrimer showed a higher percentage with respect to the other generations. The LEC liposomes were well packed and the dendrimer–LEC interactions were poorly able to modify the liposome structure. However, over time, the percentage of interacting probes further decreased in line with the decrease in intensity, indicating an increased dendrimer/liposome interaction, which provided an increased local concentration of probes at the interface with consequent strong spin–spin interactions and the disappearance of these probes from contributing to the EPR spectrum.

Further information comes from the parameters Azz and τ obtained by spectral computation (Figure 3E, S8). First of all, we noted that the Free component showed almost equivalent τ and Azz values for CTAB in the absence of the dendrimers and for the dendrimers in the absence of CTAB. This meant that the CAT12 heads were at the external surface of the micelles and the dendrimers, feeling the same environment (the water solution). The polarity for the Free probes almost did not change in function of generation and equilibration time. Conversely, the microviscosity for the Free probes increased for CTAB samples in the presence

of G0-Py and G2-Py, while it decreased in the presence of G1-Py samples, mainly at 24 h. Since for G1-Py + CTAB samples the intensity was higher than for the other generations and the relative percentage of interacting probes decreased, it was clear that the interaction between G1-Py dendrimer and the micelles provoked the extraction of probes from the micelles to the solution, thus increasing both the relative quantity of Free probes and their freedom of motion. This behavior may be accounted for by a modification of the micellar structure due to interactions with G1-Py. The fact that the microviscosity of the Interacting component for G1-Py + CTAB increased, mainly after 24 h, and that the polarity decreased, further demonstrated the structural variations of the micelles when interacting with G1-Py. A higher packing of the surfactants accounted well for the extrusion of some probes from the micelles while the probes remaining inside the micelles more strongly interacted with the dendrimer surface, also partially approaching the less polar region. A quite different behavior was found for G0-Py and G2-Py—for them, the relative percentage of Interacting component changed poorly with respect to the micelles in the absence of the dendrimers, and the Free probes increased their microviscosity since they remained trapped at the dendrimer–micelle interphase. The interactions were weaker with G0-Py and G2-Py if compared to G1-Py because of an unfavorable balance between polar and hydrophobic forces, and the interacting probes showed a smaller decrease in polarity, more significant for G0-Py than for G2-Py.

For LEC liposomes, the differences as a function of generation were much lower. The LEC structure was preserved after 15 min, but after 24 h all the dendrimers provoked a decrease of both the percentage of interacting probes and the microviscosity of free probes, indicating a structural variation connected with the extraction of probes from the liposomes to the solution due to the dendrimer/liposome interactions. The interaction strength of the CAT group at the liposome interface with G0-Py was quite low, while it increased with both G1-Py and G2-Py because of the higher density of polar surface groups.

3.3.2. Electron Paramagnetic Resonance Study of the Interactions between Heterofunctional G_n-PyN Dendrimers and Model Membranes Using CAT12 as Spin Probe

Once we had established the interactions between homofunctional iminopyridine dendrimers G_n-Py and the model membranes, we addressed the influence of leaving one $–NH_2$ group unmodified (Figure 1, compounds **1** and **2**). Interesting variations of the EPR parameters were observed for the heterofunctional dendrimers G_n-PyN, compared to the homofunctional counterparts G_n-Py.

For a matter of clarity, an example of EPR spectrum obtained for CAT12 in G_1-PyN+LEC is shown in Figure 4A, again constituted by the two components, Free and Interacting. Examples of computations of the interacting components are shown in Figure 4B,C, while the main parameters obtained from the analysis of the EPR spectra are shown in Figure 4D,E.

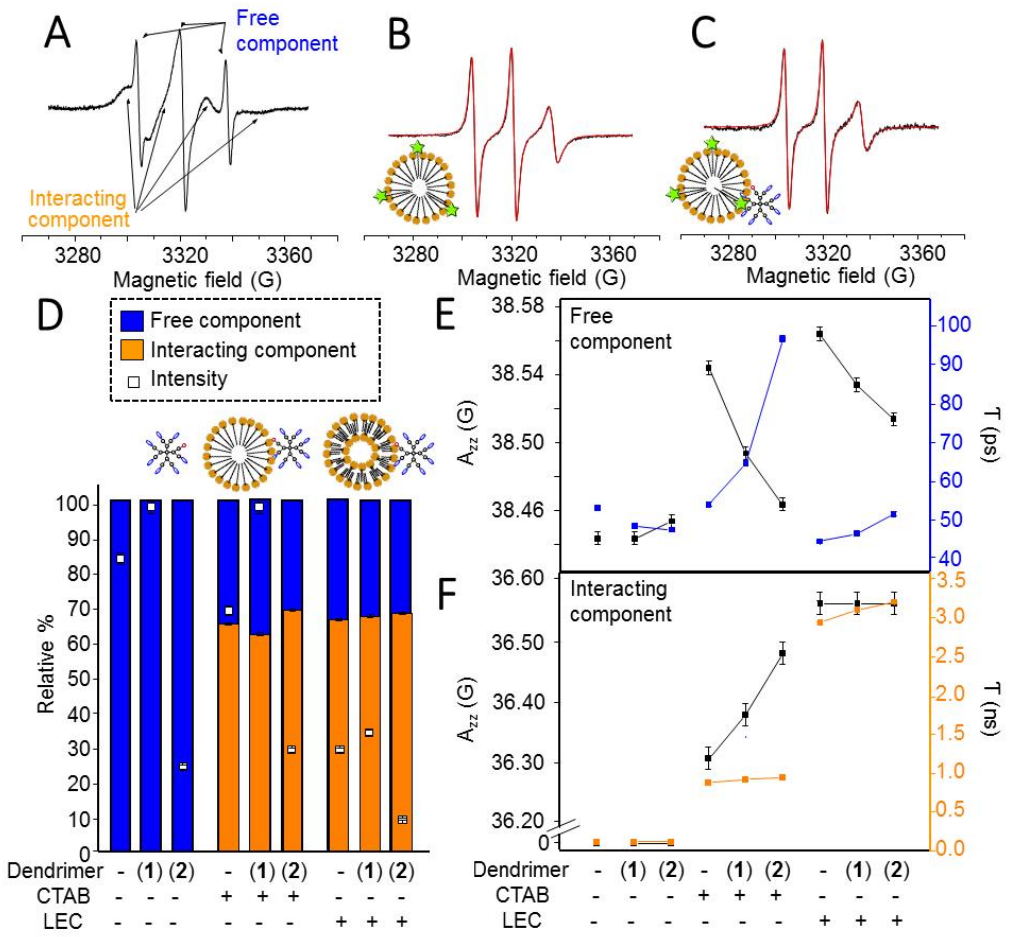

*Figure 4. Experimental spectra and computation spectra/parameters for the CAT12 EPR spectra of the unlabeled heterofunctional dendrimers G_n-PyN in the absence and presence of the model membranes (CTAB micelles and LEC liposomes). (**A**) EPR spectrum of CAT12 for G_1-PyN (**1**) in the presence of LEC; (**B, C**) experimental (black) and computed (red) spectra of the interacting component for CAT12 in CTAB sample, alone and in the presence of G_2-PyN (**2**); (**D**) Relative percentage of Interacting component (bars), and total intensity (squares) as a percentage, where 100% intensity was ascribed to the spectrum at the highest intensity; (**E, F**) A_{zz} values (left axis) and τ values (right axis) for the Free and the Interacting components. PBS sample was evaluated in the absence of dendrimers and model membranes.*

As already found for Gn-Py dendrimers, the intensity (Figure 4D, squares) measuring the probe solubility, was higher for the first-generation dendrimer when compared to the other generations. The solubility of CAT12 probes increased in the presence of G1-PyN because of a good balance between polar and hydrophobic interactions. This effect was maintained for G1-PyN in the presence of CTAB micelles. However, the absence of G1-PyN (CTAB alone) decreased the intensity, probably because some probes concentrated into the micelles provoking strong spin–spin interactions, which led to significant line broadening and the spectral contribution being no longer visible in the spectra. A similar effect may justify the significant decrease in intensity found for the liposomes in the absence of dendrimers, as already discussed in the previous section. For G2-PyN, the CAT12 solubility was low both in the absence and in the presence of CTAB, and reached a very low value (below 10%) in the presence of LEC. The interactions between G2-PyN and LEC provoked a further local increase in probe concentration, increasing spin–spin interactions.

After CAT12 aggregation into the micelles, which led to the intensity decrease in the presence of G2-PyN, the remaining non-aggregated probes showed an increase in the relative percentage of interacting component due to G2-PyN-micelle interactions (Figure 4D, bars). This effect, not observed for G2-Py, was undoubtedly due to the presence of the -NH2 group. Conversely, G1-PyN showed a decrease in the percentage of the interacting component, even if not as low as for G1-Py. Therefore, also in this case, G1-PyN interactions with CTAB produced an extraction of probes from the micelles to the solution, related to a restructuration of the micelles upon interaction with the dendrimer. However, the presence of the -NH2 group, instead of another iminopyridine ligand, decreased this effect, and promoted the dendrimer–micelle interactions preserving the micellar structure.

For LEC liposomes, the presence of the -NH2 group inverted the trend for the variation of the percentage of interacting component. Indeed, for Gn-Py dendrimers, the percentage diminished in the series LEC > LEC+G1-Py > LEC+G2-Py, while for Gn-PyN dendrimers the interacting percentage slightly increased in the series LEC < LEC+G1-PyN < LEC+G2-PyN. The interactions were preferentially at the polar surface of the liposomes, as also demonstrated by the polarity parameter Azz (Figure 4F).

For the polarity and microviscosity parameters, the Free component was also informative (Figure 4E). This Free component arose from probes in solution, but was affected by the surface of dendrimers and model membranes. By adding the dendrimers to CTAB micelles, the polarity decreased because of the approaching of the less polar dendrimer to the model membrane. This approaching partly reduced the mobility (increasing the microviscosity). For LEC, by adding the dendrimers, the freedom of motion and the polarity were reduced because of dendrimer/membrane interactions, and this effect was stronger by increasing generation.

In respect to the Interacting component (Figure 4F), both polarity and microviscosity increased for the model membranes from the absence to the presence of the dendrimers, by increasing generation, and from CTAB to LEC. Also in this case, some trends were inverted with respect to Gn-Py dendrimers. For instance, the microviscosity, measuring the strength of interaction, decreased from G1-Py to G2-Py, while it increased from G1-PyN to G2-PyN; in detail, in respect to CTAB, G1-Py was more interactive than G1-PyN, while G2-Py was less interactive than G2-PyN. For the polarity, G1-Py showed lower polarity than G1-PyN, while G2-Py showed higher polarity than G2-PyN. These results revealed a different interaction mechanism between the different dendrimers and CTAB micelles, being G1-Py able to partially enter the micelles, approaching less polar sites and providing a stronger interaction with the micelles. The presence of -NH2 at the G1-PyN surface hindered the penetration into the micelle, favoring interactions at the charged external surface. For G2-Py, the higher density of surface groups, the lower availability of the low polar dendrimer core, and the higher structural rigidity impeded the penetration into the micelles. Therefore, the interaction was only at the external surface, and the presence of -NH2 at the G2-PyN surface favored polar and electrostatic interactions with the micelles.

The higher Azz and τ parameters for LEC with respect to CTAB were due to the more dense and viscous liposome structure at the interface. The increased microviscosity and polarity parameters in the presence of the dendrimers were clearly reporting the occurrence of electrostatic interactions between the dendrimers and the liposome surface, which became stronger by increasing generation due to the higher density of surface groups for the higher generation. If compared to Gn-Py, Gn-PyN dendrimers showed higher strength of interaction and higher polarity. Furthermore, G2-PyN showed stronger interactions with respect to G1-PyN, while the opposite held for Gn-Py dendrimers. This confirmed that the dendrimer–liposome interactions were mainly polar/electrostatic between the polar/charged surfaces. Therefore, the -NH2 group favored these kinds of interactions.

The last interesting finding was the agreement between the results obtained for the labelled dendrimers (3–6) and for the unlabeled ones (1–2, 1*–2*). Both points of view suggested the partial insertion of the dendrimer surface groups into the surfactant aggregates, mainly CTAB micelles, and the occurrence of both polar and hydrophobic interactions, while dendrimer–LEC interactions involved more polar interactions between surface groups. Finally, the G1-Py interactions were significantly favored, mainly with CTAB, but both the presence of -NH2 and TEMPO moieties perturbed these interactions, partially preventing the entry of dendrimer surface groups into the micellar core.

4. Conclusions

A selective and efficient anticancer therapy requires an efficient uptake of the drug by cancer cells, which in turn depends on the ability of the drug to interact and penetrate the cell membrane. Using model cell membranes (CTAB and LEC), we evaluated in situ the interactions performed by a new family of differently decorated carbosilane dendrimers through a computer-assisted EPR analysis. The analysis of the EPR spectra provided parameters informative of the interacting ability of the dendrimers, and the type and strength of interactions in function of the effect of a metal (Ru(II)), the type of model membrane, a partial functionalization, and generation.

In order to report the interactions from the dendrimer point of view, we synthesized new heterofunctional Ru(II) metallodendrimers labelled with a TEMPO radical. The new nanotheranostic G_n-RuT dendrimers can potentially exhibit an antitumor effect while monitoring in real time drug release and distribution. In the synthetic route, interesting precursors were prepared—The G_n-PyN family, with multiple iminopyridine ligands and a single $–NH_2$ group, and the G_n-PyT family, with multiple iminopyridine ligands and a TEMPO label. These subtle changes of a single group later revealed important differences regarding the interactions between the dendrimers and the CTAB and LEC models. Initially, a comparative EPR study was performed on the labelled dendrimers G_n-PyT and G_n-RuT in the absence and presence of the model membranes. It was found that the G_n-PyT dendrimers partially penetrated the micelle structure, with G_1-PyT being more interactive than G_2-PyT. In the liposomes the interactions occurred at the external surface, with G_2-PyT being more interactive than G_1-PyT. In the metallodendrimers, the TEMPO group interacted with Ru(II) ions but gained freedom entering the micellar structure; otherwise their mobility was slowed down by interacting with the LEC surface. Therefore, for both G_n-PyT and G_n-RuT, the interactions were perturbative of the CTAB micellar structure, but preserve the LEC structure, mainly occurring at the external interface.

The EPR results from the spin-labelled dendrimers were compared and integrated with those obtained by both the unlabeled dendrimer precursors (G_n-PyN) and the homofunctional iminopyridine dendrimers (G_n-Py). In these last cases, the CAT12 probe demonstrated the provision of complementary information with respect to those obtained with the labelled dendrimers. Also in this case, the computer aided EPR analysis allowed us to extract similar parameters as those obtained by means of the TEMPO label, but the point of view provided by CAT12 was on the model membrane side, since this spin probe is deeply inserted into the surfactant aggregates. It was found, similar to G_n-PyT, that G_1-Py interacts better with CTAB, while G_2-Py interacts better with LEC. G_1-Py and G_1-PyN interactions with CTAB produced an extraction of probes from the micelles to the solution, which was related to a restructuration of the micelles in agreement with the results from the labelled dendrimers. The presence of the

NH_2 group at the G_2-PyN surface promoted polar and electrostatic interactions with the micelles instead of penetration of dendrimer branches into the micellar structure. Therefore, the presence of NH_2 at the G_1-PyN dendrimer surface impeded the penetration into the micelle, favoring interactions at the charged external surface.

Clearly the EPR analysis demonstrated itself to be very useful in providing detailed information on the mechanism of interactions of the dendrimer with a model cell membrane, in view of the use of these new dendrimers as anticancer drugs. A second manuscript containing comparative EPR experiments and biological tests using both healthy and tumor cells in the absence and presence of the dendrimers is currently in preparation.

Supplementary Materials: The following are available online at www.mdpi.com/xxx/s1, Figure S1: 1H- and 13C{1H}-NMR spectra of compound 1. Figure S2: TOCSY 1D spectrum of compound 1. Figure S3: 1H-NMR spectrum of compound 3. Figure S4: 1H-NMR spectrum of compound 5. Figure S5: FT-IR spectra of precursor 4-isothiocyanateTEMPO and compound 3. Figure S6: Examples of experimental and computed spectra of labelled dendrimers in the absence and presence of model membranes. Figure S7: Examples of experimental and computed spectra of non-labelled dendrimers in the absence and presence of model membranes. Figure S8: Azz values obtained by computing the Free and the Interacting components for CTAB for homofunctional dendrimers Gn-Py.

Author Contributions: conceptualization, M.F.O. and J.M.; methodology, P.O. and S.G.G.; formal analysis, A.F. and M.C.; investigation, R.C., N.S.O., and A.F.; resources, M.F.O., R.G., and J.M.; data curation, R.C., N.S.O., and M.C.; writing—original draft preparation, S.G.G. and M.C.; writing—review and editing, M.F.O., S.G.G., and P.O.; supervision, M.C., R.G., and J.M.; funding acquisition, M.F.O., R.G., and J.M.

Funding: This research was funded by grants from CTQ2017-86224-P (MINECO), consortiums IMMUNOTHERCAN-CM B2017/BMD-3733 and NANODENDMED II-CM ref. B2017/BMD-3703, project SBPLY/17/180501/000358 Junta de Comunidades de Castilla-la Mancha (JCCM) and the Comunidad de Madrid Research Talent Attraction Program 2017-T2/IND-5243. CIBER-BBN is an initiative funded by the VI National R&D&I Plan 2008–2011, Iniciativa Ingenio 2010, Consolider Program, CIBER Actions and financed by the Instituto de Salud Carlos III with assistance from the European Regional Development Fund. N.S.O. wishes to thank JCCM for a predoctoral fellowship. M.F.O., M.C., R.C., and A.F. thank DiSPeA at the University of Urbino for funding. This article is based upon work from COST Action CA17140 "Cancer Nanomedicine from the Bench to the Bedside" supported by COST (European Cooperation in Science and Technology).

Conflicts of Interest: The authors declare no conflict of interest. The funders had no role in the design of the study; in the collection, analyses, or interpretation of data; in the writing of the manuscript, or in the decision to publish the results.

Supporting Information:

Figures

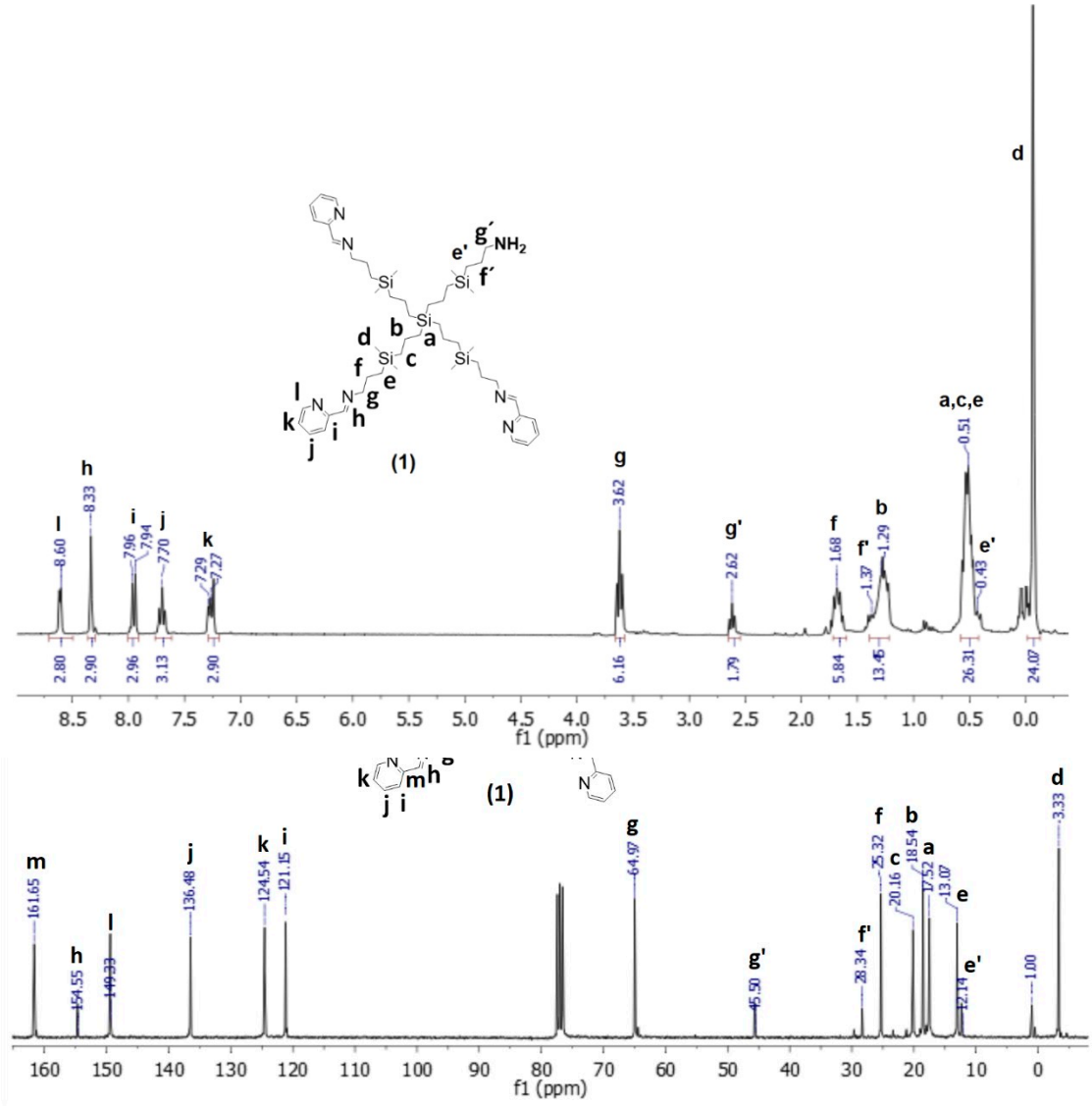

Figure S1. ^{1}H- and $^{13}C\{^{1}H\}$-NMR spectra of compound 1 in CDCl3.

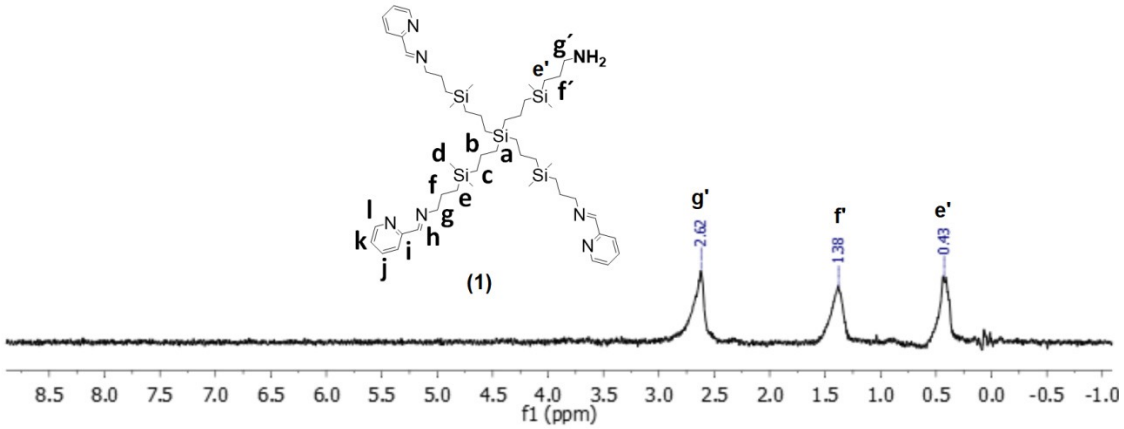

Figure S2. TOCSY 1D spectrum of compound 1 in CDCl3.

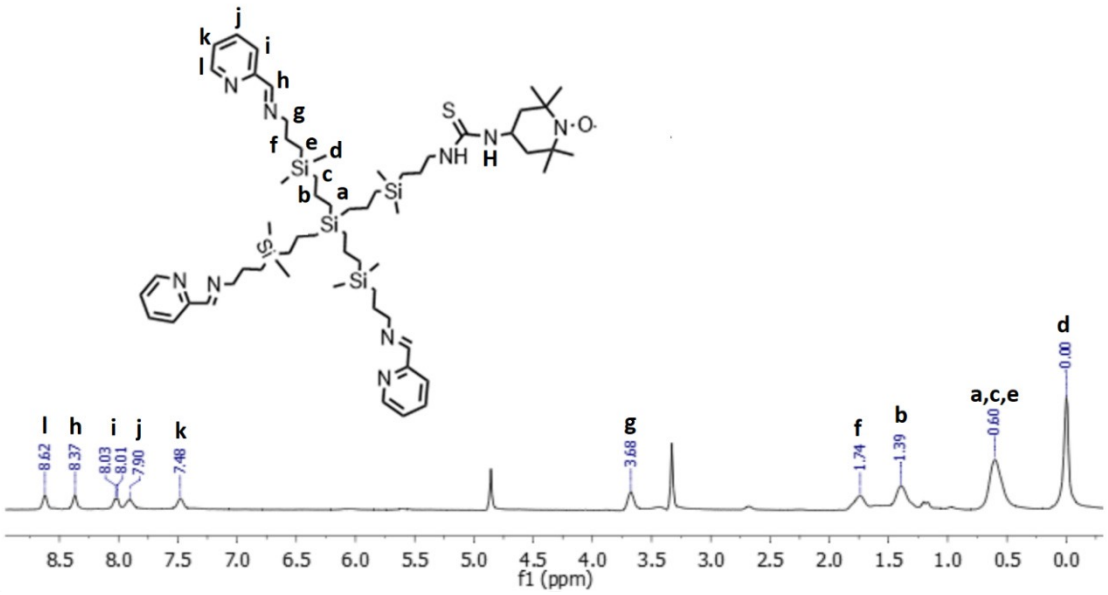

Figure S3. ^{1}H-NMR spectrum of compound 3 in CD3OD.

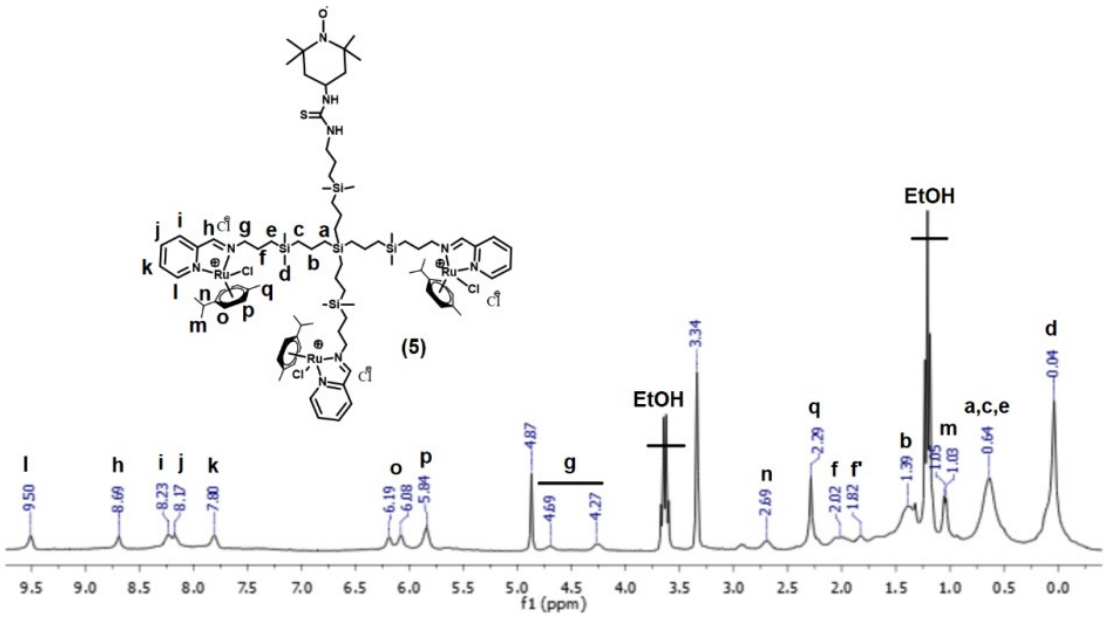

Figure S4. ^{1}H-NMR spectrum of compound 5 in CD3OD.

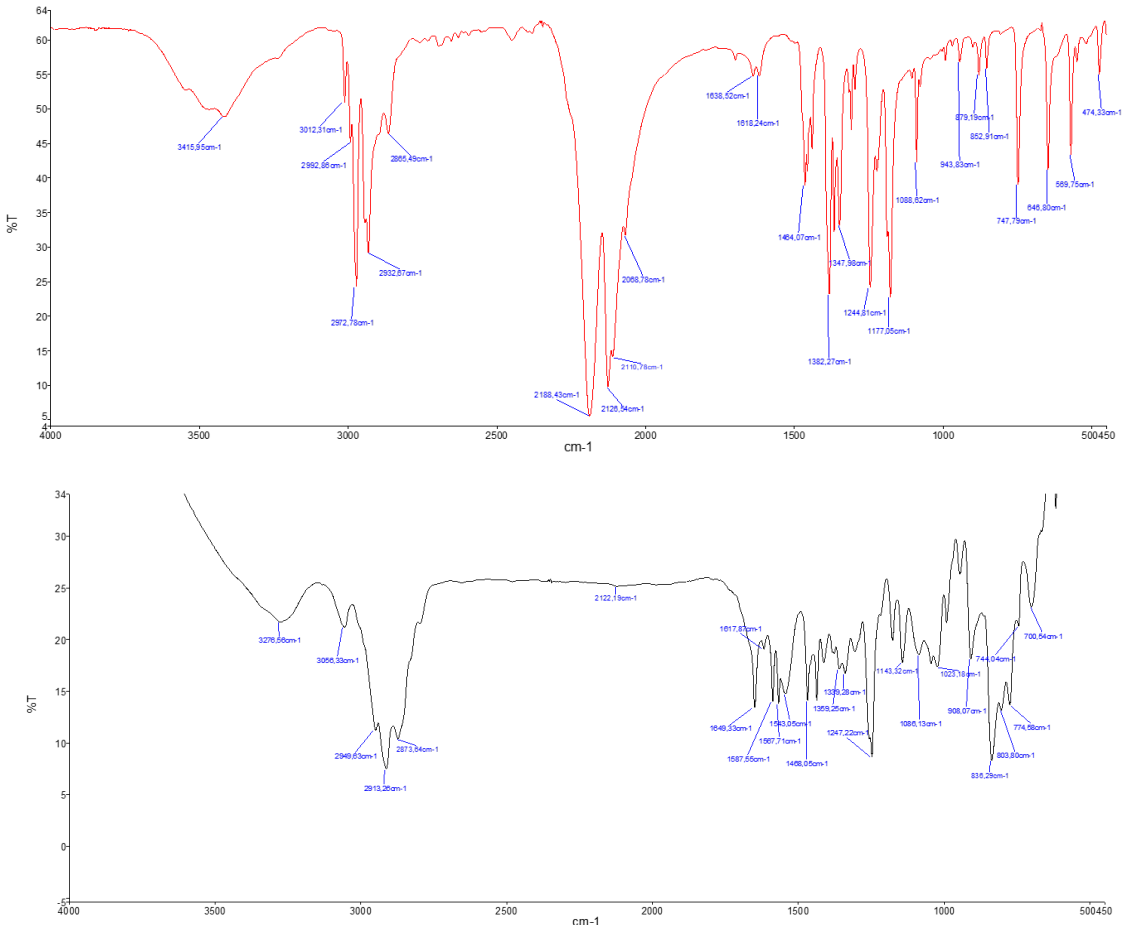

Figure S5. FT-IR spectra of precursor 4-isothiocyanateTEMPO (top) and compound 3 (bottom) in KBr.

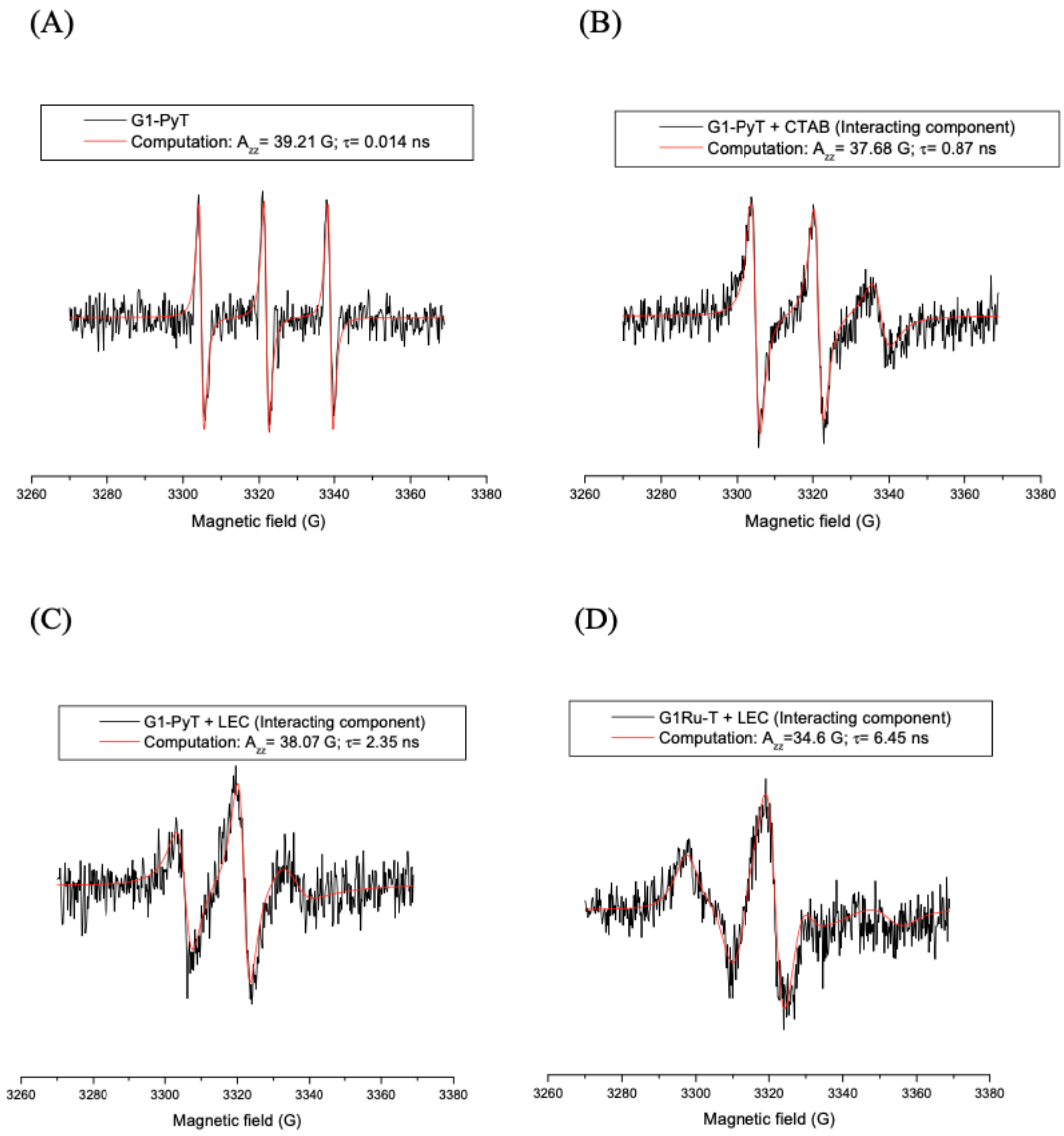

Figure S6. Examples of experimental and computed spectra of labelled dendrimers in the absence and presence of model membranes. Experimental and computed spectra of G1-PyT, only constituted by the Free component (A). Experimental and computed Interacting component, obtained after subtraction of the Free component, of: (B) G1- PyT+CTAB; (C) G1-PyT+LEC; (D) G1-RuT+LEC. The spectra are normalized in height.

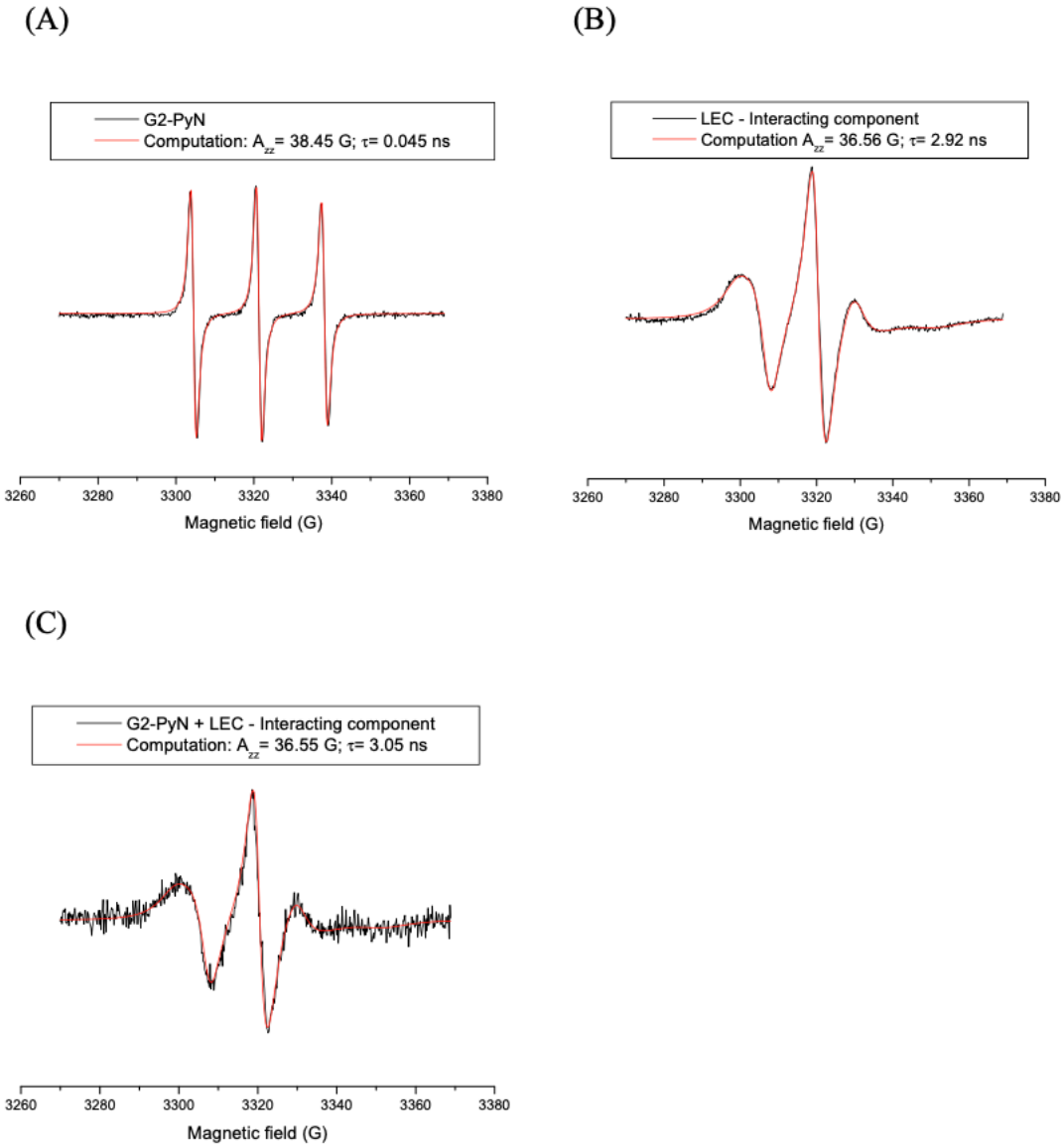

Figure S7. Examples of experimental and computed spectra of non-labelled dendrimers in the absence and presence of model membranes. Experimental and computed spectra of CAT12 in G2-PyN, only constituted by a free component (A). Examples of computations of the interacting component for CAT12 in: LEC (B); and G2-PyN+LEC (C).

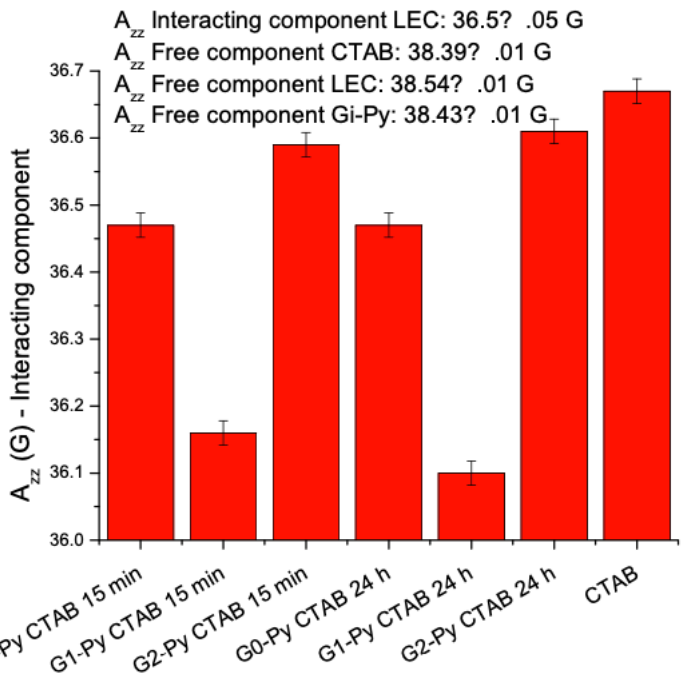

Figure S8: Azz values obtained by computing the Free and the Interacting components for CTAB for homofunctional dendrimers Gn-Py.

References

1. Mi, P.; Cabral, H.; Kataoka, K. Ligand-installed nanocarriers toward precision therapy. *Adv. Mater.* **2019**, e1902604.
2. Sk, U.H.; Kojima, C. Dendrimers for drug delivery of anticancer drugs. In *Frontiers in Clinical Drug Research - Anti-Cancer Agents*, FRS, A.-u.-R., Ed. Bentham Science: UK, 2015; Vol. 2, pp. 3–25.
3. Han, X.; Xu, K.; Taratula, O.; Farsad, K. Applications of nanoparticles in biomedical imaging. *Nanoscale* **2019**, *11*, 799–819.
4. Nabil, G.; Bhise, K.; Sau, S.; Atef, M.; El-Banna, H.A.; Iyer, A.K. Nano-engineered delivery systems for cancer imaging and therapy: Recent advances, future direction and patent evaluation. *Drug Discov. Today* **2019**, *24*, 462–491.
5. Zhao, C.-Y.; Cheng, R.; Yang, Z.; Tian, Z.-M. Nanotechnology for Cancer Therapy Based on Chemotherapy. *Mol*. **2018**, *23*, 826.
6. Sharma, M.; Dube, T.; Chibh, S.; Kour, A.; Mishra, J.; Panda, J.J. Nanotheranostics, a future remedy of neurological disorders. *Expert Opin. Drug Deliv.* **2019**, *16*, 113–128.
7. Mura, S.; Couvreur, P. Nanotheranostics for personalized medicine. *Adv. Drug Deliv. Rev.* **2012**, *64*, 1394–1416.
8. Sowinska, M.; Urbanczyk-Lipkowska, Z. Advances in the chemistry of dendrimers. *New J. Chem.* **2014**, *38*, 2168–2203.
9. Sánchez-Nieves, J.; Ortega, P.; Cano, J.; Gómez, R.; Mata, F.J.d.l. Poly(carbosilane) dendrimers and other silicon-containing dendrimers. In *Dendrimer Chemistry: Synthetic approaches towards complex architectures*, Malkoch, M., García-Gallego, S., Eds. Royal Society of Chemistry: 2019.
10. Andreozzi, E.; Antonelli, A.; Cangiotti, M.; Canonico, B.; Sfara, C.; Pianetti, A.; Bruscolini, F.; Sahre, K.; Appelhans, D.; Papa, S., et al. Interactions of nitroxide-conjugated and non-conjugated glycodendrimers with normal and cancer cells and biocompatibility studies. *Bioconjug. Chem.* **2017**, *28*, 524–538.
11. Ottaviani, M.F.; El Brahmi, N.; Cangiotti, M.; Coppola, C.; Buccella, F.; Cresteil, T.; Mignani, S.; Caminade, A.M.; Costes, J.P.; Majoral, J.P. Comparative EPR studies of Cu(II)-conjugated phosphorous-dendrimers in the absence and presence of normal and cancer cells. *RSC Adv.* **2014**, *4*, 36573–36583.
12. Shang, L.; Nienhaus, K.; Nienhaus, G.U. Engineered nanoparticles interacting with cells: size matters. *J. Nanobiotechnol.* **2014**, *12*, 5.
13. Rokach, S.; Ottaviani, M.F.; Shames, A.I.; Aserin, A.; Garti, N. Behavior of PPI-G2 dendrimer in a microemulsion. *J. Phys. Chem. B* **2017**, *121*, 2339–2349.
14. Perlstein, M.; Ottaviani, M.F.; Aserin, A.; Garti, N. Structural effects on cosolubilization of dendrimer and propofol in water dilutable microemulsions as delivery vehicle. *Colloids Surfaces A: Physicochem. Eng. Asp*. **2016**, *497*, 257–264.
15. Lidich, N.; Ottaviani, M.F.; Hoffman, R.E.; Aserin, A.; Garti, N. Docosahexaenoic acid triglyceride-based microemulsions with an added dendrimer – Structural considerations. *J. Colloid Interface Sci*. **2016**, *483*, 374–384.
16. Rokach, S.; Ottaviani, M.F.; Shames, A.I.; Nir, I.; Aserin, A.; Garti, N. W/O microemulsions as dendrimer nanocarriers: an EPR study. *J. Phys. Chem. B* **2012**, *116*, 12633–12640.
17. Bitan-Cherbakovsky, L.; Libster, D.; Ottaviani, M.F.; Aserin, A.; Garti, N. Structural behavior and interactions of dendrimer within lyotropic liquid crystals, monitored by EPR spectroscopy and rheology. *J. Phys. Chem. B* **2012**, *116*, 2420–2429.
18. Ottaviani, M.F.; Favuzza, P.; Sacchi, B.; Turro, N.J.; Jockusch, S.; Tomalia, D.A. Interactions between starburst dendrimers and mixed DMPC/DMPA-Na vesicles studied by the Spin Label and the Spin Probe techniques, supported by Transmission Electron Microscopy. *Langmuir* **2002**, *18*, 2347–2357.
19. Ottaviani, M.F.; Matteini, P.; Brustolon, M.; Turro, N.J.; Jockusch, S.; Tomalia, D.A. Characterization of Starburst Dendrimers and Vesicle Solutions and Their Interactions by CW- and Pulsed-EPR, TEM, and Dynamic Light Scattering. *J. Phys. Chem. B.* **1998**, *102*, 6029–6039, doi:10.1021/jp980715c.
20. Ottaviani, M.F.; Daddi, R.; Brustolon, M.; Turro, N.J.; Tomalia, D.A. Structural modifications of DMPC vesicles upon interaction with Poly(amidoamine) dendrimers studied by CW-Electron Paramagnetic Resonance and Electron Spin−Echo techniques. *Langmuir* **1999**, *15*, 1973–1980.

21. Ottaviani, M.F.; Andechaga, P.; Turro, N.J.; Tomalia, D.A. Model for the interactions between anionic dendrimers and cationic surfactants by means of the spin probe method. *J. Phys. Chem. B.* **1997**, *101*, 6057–6065.
22. Ottaviani, M.F.; Daddi, R.; Brustolon, M.; Turro, N.J.; Tomalia, D.A. Interaction between starburst dendrimers and SDS micelles studied by continuous-wave and pulsed electron spin resonances. *Appl. Magn. Reson.* **1997**, *13*, 347–363.
23. Ottaviani, M.F.; Turro, N.J.; Jockusch, S.; Tomalia, D.A. Aggregational process of the positively charged surfactants CTAC and CAT16 in the presence of starburst dendrimers: an Electron Paramagnetic Resonance spectroscopic study. *Colloids Surf. A* **1996**, *115*, 9–21.
24. Ottaviani, M.F.; Turro, N.J.; Jockusch, S.; Tomalia, D.A. Characterization of starburst dendrimers by EPR. 3. Aggregational processes of a positively charged nitroxide surfactant. *J. Phys. Chem.* **1996**, *100*, 13675–13686.
25. Lin, Y.; Yokoyama, H.; Ishida, S.-i.; Tsuchihashi, N.; Ogata, T. *In vivo* Electron Spin Resonance analysis of nitroxide radicals injected into a rat by a flexible surface-coil-type resonator as an endoscope- or a stethoscope-like device. *Magn. Reson. Mater. Phy.* **1997**, *5*, 99–103.
26. Galimzyanovich Saifutdinov, R.; Ivanovna Larina, L.; Il'inichna Vakul´skaya, T.; Grigor´evich Voronkov, M. *Electron Paramagnetic Resonance in Biochemistry and Medicine*; Kluwer Academic Publishers: New York, 2002.
27. Swartz, H.M.; Williams, B.B.; Zaki, B.I.; Hartford, A.C.; Jarvis, L.A.; Chen, E.Y.; Comi, R.J.; Ernstoff, M.S.; Hou, H.; Khan, N., et al. Clinical EPR: unique opportunities and some challenges. *Acad. Radiol.* **2014**, *21*, 197–206.
28. Sanz del Olmo, N.; Maroto-Díaz, M.; Gómez, R.; Ortega, P.; Cangiotti, M.; Ottaviani, M.F.; de la Mata, F.J. Carbosilane metallodendrimers based on copper (II) complexes: Synthesis, EPR characterization and anticancer activity. *J. Inorg. Biochem.* **2017**, *177*, 211–218.
29. Sanz del Olmo, N.; Carloni, R.; Bajo, A.M.; Ortega, P.; Fattori, A.; Gómez, R.; Ottaviani, M.F.; García-Gallego, S.; Cangiotti, M.; de la Mata, F.J. Insight into the antitumor activity of carbosilane Cu(II)–metallodendrimers through their interaction with biological membrane models. *Nanoscale* **2019**, *11*, 13330–13342.
30. Maroto-Diaz, M.; Elie, B.T.; Gomez-Sal, P.; Perez-Serrano, J.; Gomez, R.; Contel, M.; de la Mata, F.J. Synthesis and anticancer activity of carbosilane metallodendrimers based on arene ruthenium(ii) complexes. *Dalton Trans.* **2016**, *45*, 7049–7066.
31. Maroto-Diaz, M.; Sanz del Olmo, N.; Muñoz-Moreno, L.; Bajo, A.M.; Carmena, M.J.; Gómez, R.; García-Gallego, S.; de la Mata, F.J. *In vitro* and *in vivo* evaluation of first-generation carbosilane arene Ru(II)-metallodendrimers in advanced prostate cancer. *Eur. Polym. J.* **2019**, *113*, 229–235.
32. Zeng, L.; Gupta, P.; Chen, Y.; Wang, E.; Ji, L.; Chao, H.; Chen, Z.S. The development of anticancer ruthenium(II) complexes: from single molecule compounds to nanomaterials. *Chem. Soc. Rev.* **2017**, *46*, 5771–5804.
33. Budil, D.E.; Lee, S.; Saxena, S.; Freed, J.H. Nonlinear-least-squares analysis of slow-motion EPR spectra in one and two dimensions using a modified Levenberg–Marquardt algorithm. *J. Magn. Reson.* **1996**, *120*, 155–189.
34. Bermejo, J.F.; Ortega, P.; Chonco, L.; Eritja, R.; Samaniego, R.; Mullner, M.; de Jesus, E.; de la Mata, F.J.; Flores, J.C.; Gomez, R., et al. Water-soluble carbosilane dendrimers: synthesis biocompatibility and complexation with oligonucleotides; evaluation for medical applications. *Chemistry (Weinheim an der Bergstrasse, Germany)* **2007**, *13*, 483–495, doi:10.1002/chem.200600594.
35. Huang, L.; Yan, C.; Cui, D.; Yan, Y.; Liu, X.; Lu, X.; Tan, X.; Lu, X.; Xu, J.; Xu, Y., et al. Organic radical contrast agents based on polyacetylenes containing 2,2,6,6-Tetramethylpiperidine 1-Oxyl (TEMPO): Targeted Magnetic Resonance (MR)/Optical Bimodal Imaging of folate receptor expressing HeLa tumors *in vitro* and *in vivo*. *Macromol. Biosci.* **2015**, *15*, 788–798.
36. Ottaviani, M.F.; Cossu, E.; Turro, N.J.; Tomalia, D.A. Characterization of starburst dendrimers by Electron Paramagnetic Resonance. 2. Positively charged nitroxide radicals of variable chain length used as spin probes. *J. Am. Chem. Soc.* **1995**, *117*, 4387–4398.

PAPER 2

Fine-tuning the interaction and therapeutic effect of Cu(II)-carbosilane metallodendrimers in cancer cells An in vitro Electron Paramagnetic Resonance study

Barbara Canonico, Riccardo Carloni, Natalia Sanz del Olmo, Stefano Papa, Maria Gemma Nasoni, Alberto Fattori, Michela Cangiotti, F. Javier de la Mata, Maria Francesca Ottaviani, and Sandra García-Gallego

Mol. Pharmaceutics, 02 Jun 2020
https://doi.org/10.1021/acs.molpharmaceut.0c00396

Fine-Tuning the Interaction and Therapeutic Effect of Cu(II) Carbosilane Metallodendrimers in Cancer Cells: An In Vitro Electron Paramagnetic Resonance Study

Barbara Canonico,[a] Riccardo Carloni,[b] Natalia Sanz del Olmo,[c] Stefano Papa,[a] Maria Gemma Nasoni,[a] Alberto Fattori,[b] Michela Cangiotti,[b] F. Javier de la Mata,[cde] Maria Francesca Ottaviani[b] and Sandra García-Gallego.*[cde]*

a. *Department of Biomolecular Science (DiSB), University of Urbino "Carlo Bo", Urbino, Italy.*
b. *Department of Pure and Applied Sciences, University of Urbino "Carlo Bo", Urbino, Italy.*
c. *Department of Organic and Inorganic Chemistry, and Research Institute in Chemistry "Andrés M. del Río" (IQAR), University of Alcalá, Madrid, Spain.*
d. *Networking Research Center on Bioengineering, Biomaterials and Nanomedicine (CIBER-BBN), Spain.*
e. *Institute Ramón y Cajal for Health Research (IRYCIS).*

* Corresponding authors.

Table of contents graphic

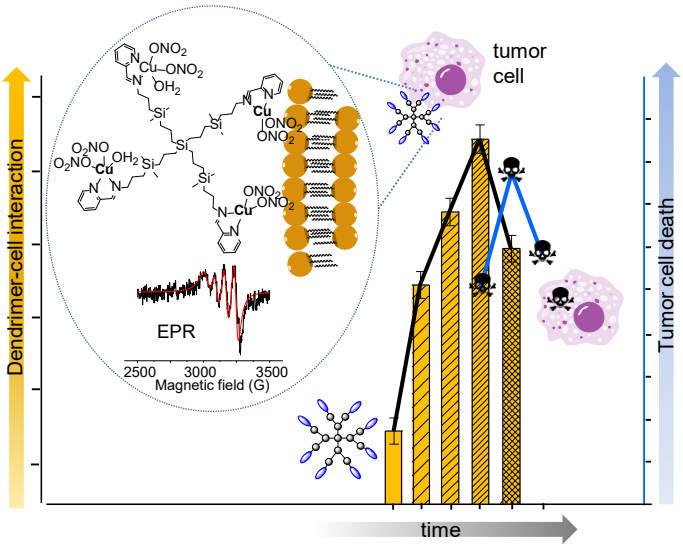

Abstract

Copper(II) carbosilane metallodendrimers are promising nanosized anticancer metallodrugs. The precise control on their design enables an accurate structure-to-activity study. We hypothesized that different structural features, such as the dendrimer generation and metal counterion, modulate the interaction with tumor cells, and subsequently, the effectivity and selectivity of the therapy. A computer-aided analysis of the electron paramagnetic resonance (EPR) spectra allowed us to obtain dynamical and structural details on the interactions over time between the dendrimers and the cells, the myeloid U937 tumor cells and peripheral blood mononuclear cells (PBMC). The intracellular fate

of the metallodendrimers was studied through a complete in vitro evaluation, including cytotoxicity, cytostaticity, and sublethal effects regarding mitochondria function, lysosomal compartments, and autophagic organelle involvement. EPR results confirmed a higher membrane stabilization for chloride dendrimers and low generation complexes, which ultimately influence the metallodrug uptake and intracellular fate. The in vitro evaluation revealed that Cu(II) metallodendrimers are cytostatic and moderate cytotoxic agents for U937 tumor cells, inducing death processes through the mitochondria−lysosome axis as well as autophagic vacuole formation, while barely affecting healthy monocytes. The study provided valuable insight into the mechanism of action of these nanosized metallodrugs and relevant structural parameters affecting the activity.

Keywords: metallodendrimer, copper, cancer cell, EPR, interaction

1. Introduction

Cancer is a multifactorial disease with an alarming incidence worldwide, accounting for 18.1 million new cases and 9.6 million deaths in 2018.1 According to the World Health Organization, the global cancer burden keeps rising due to different factors, such as population growth and aging, or the prevalence of certain causes of cancer linked to social and economic development. [2] The complexity of this disease is related to the unique fingerprint in each tumor, which hinders the development of a universal therapeutic approach. Furthermore, current treatments present serious drawbacks, including the development of drug resistance and the severe side effects, due to the lack of selectivity to tumor tissues. Overall, these reasons are continuously fueling the development of new antitumor strategies, providing unique approaches for the early diagnosis, prevention or personalized therapy of cancer.[3-4] The success of this strategy, compared to traditional cancer therapeutics, is based on two main properties: (i) the nanometric size of the nanoparticles (NPs) enables a preferential accumulation in solid tumors through the enhanced permeability and retention effect, thus bypassing traditional drug resistance mechanisms; (ii) the large surface area of the NPs is available for conjugating a large therapeutic payload of a single or multiple drugs, targeting moieties or diagnostic agents. Primarily, the design of safe and efficient nanomedicines requires a thorough understanding of uptake and trafficking within the cell. While most nanoparticles employ endocytic pathways to enter the cells, the interaction with biological membranes[5] depends on the physicochemical features of the NPs – size, shape, surface properties- as well as on cellular parameters – the phase of the cycle or the type of cell. After internalization, NPs first encounter the early-endosomes, membrane-bound intracellular vesicles that carry the cargo to the target cellular destination. However, NPs can also enter two different degradation routes: The *endolysosomal pathway*, where the early-endosomes mature to late-endosomes and then integrate with lysosomes capable of degrading the trapped NPs; or the *autophagosome pathway*, where cytoplasmic contents are surrounded by the autophagosome and delivered to the lysosome for degradation. Thus, the particular characteristics of the nanoparticle will dictate its biological fate.

Dendrimers are the ultimate precision NPs with promising potential in many different biomedical applications, including cancer.[6-8] Their monodispersed and highly branched structure enables on-demand and controlled attachment of anticancer drugs, tumor-targeting moieties, diagnostic agents, or even a combination of them into the so-called theranostic nanoparticles.[9-10] Unlike other types of nanoparticles, the accurate control on the dendrimer synthesis provides ideal

testbeds for studying the influence of the different structural parameters on the biological activity. Multiple studies have focused on revealing dendrimers mode of action, analyzing their interaction with membranes and cells[11-12] as well as their cell uptake and internal trafficking.[13-14] For example, cationic dendrimers are generally internalized into the cells through endocytosis. As a result, they can suffer endosomal escape and interact with different organelles, affect cellular processes and induce apoptotic cell death.[15-17] Nevertheless, important differences arise depending on the nature of the dendritic scaffold. For example, cationic poly(amidoamine) (PAMAM) and poly(propylenimine) (PPI) dendrimers induced apoptosis in murine neural cells,[18, 19] while cationic phosphorous dendrimers induced necrosis,[20] considering the much higher number of positive charges at the surface for the same generation. Cationic carbosilane dendrimers, comprising a more hydrophobic scaffold, have shown an enhanced interaction with cell membranes, altering the membrane fluidity.[21] The presence of metal complexes at the surface of carbosilane dendrimers can further tune their interaction with cell membranes, as previously observed with copper (II) and ruthenium (II) complexes.[22] Previous studies from our group have shown that nanosized metallodrugs can overcome current limitations of antitumor therapies.[23] In particular, copper(II) carbosilane dendrimers are promising antitumor agents considering i) the high stability provided by the chelating iminopyridine ligands and the carbosilane scaffold, ii) the water-solubility, iii) the structure perfection of the dendritic molecule, which enables an exceptional structure-to-property relationship, iv) the unique interaction with cell membranes, tunable through the dendrimer generation and the Cu(II) counter-ion.

In order to confirm in a real setting the previous results using cell-membrane models and gain insight into the complexes mode-of-action, in the present study, the interactions occurring between Cu(II) metallodendrimers and tumor and healthy cells were investigated over incubation time, by using a computer-aided analysis of electron paramagnetic resonance (EPR) spectra, as well as *in vitro* experiments. EPR analysis provided structural and dynamical information on the *in vitro* behavior of the metallodendrimers in healthy and tumor cells. This technique has been already used as a powerful tool to characterize Cu(II)–dendrimer complexes.[12, 22-25] Finally, the intracellular trafficking and mechanism of action of the Cu(II)-carbosilane dendrimers complexes to be used as anticancer drugs was evaluated by means of various biological tests, including cytotoxicity and alteration of mitochondria membrane potential as well as autophagy flux.

2. Methods

2.1 Cu(II) complexes and metallodendrimers

The selected metallodrugs comprised two families of copper (II) carbosilane complexes, with nitrate (1-3) and chloride (4-6) ligands (Figure 1). These complexes were selected in order to study the influence of the metal counter-ion and the generation on their antitumor activity. The Cu(II) mononuclear complexes and first and second-generation metallodendrimers were synthesized according to previously published protocols.[22, 23] Other reagents required for the sample preparations were purchased from Sigma-Aldrich (St Louis, MO, USA) and used without any further manipulation.

2.2 Cell lines and primary cultures

Human PBMCs (peripheral blood mononuclear cells) were isolated from buffy coats of anonymized donors obtained from the Transfusion Centre of Urbino Hospital. No specific approval

from an institutional review board was required for the use of buffy coats for the following reasons: (1) no personal patient information was made available; (2) buffy coats could not be used for treatment of patients and were waste products for the blood transfusion centre and (3) blood donors were verbally informed that parts of the donation that cannot be used for patient treatment may be used for scientific research. PBMCs were separated from buffy coats and obtained by density gradient separation using Lymphoprep solution (specific density, 1.077; Axis-Shield PoC AS, Oslo, Norway). Cells were washed twice in phosphate buffer saline (PBS) by centrifugation at 400 g and resuspended in RPMI- 1640 with 10% (v/v) heat inactivated fetal bovine serum (FBS), 100 μg/mL penicillin, 100 μg/mL streptomycin, and 2 mM L-glutamine.

U937 cell line was purchased from Sigma-Aldrich, USA, and was grown in RPMI-1640 culture medium supplemented with 10% (v/v) heat-inactivated FBS, 100 U/mL penicillin, 100 μg/mL streptomycin, and 2 mM L-glutamine, at 37 °C in humidified air with 5% CO_2.

2.3 Electronic Paramagnetic Resonance

Metallodendrimers solutions were prepared in RPMI buffer at a concentration of 1 mM in surface groups. The dendrimer solutions were analysed by EPR after addition to 12-well plates containing RPMI in the absence and presence of the cells (5×10^5 cells/mL; higher and lower cell amounts were also tested to verify the effect of cell concentration). The incubation times ranged from 0 to 72 h. The temperature was maintained at 37 °C.

EPR spectra were recorded by means of an EMX spectrometer (Bruker) operating at X band (9.5 GHz) and interfaced with a PC (software from Bruker for handling and analysis of the EPR spectra). The temperature was controlled with a Bruker ST3000 variable-temperature assembly.

Analysis of the EPR spectra of Cu(II)-metallodendrimers in RPMI in the absence and presence of the cells. The EPR spectra of Cu(II)-metallodendrimers were mainly constituted by two components. Each component was extracted and relatively quantified (in relative percentages, after double integration of the signals) by subtracting spectra containing these components in different relative amounts. The components were then computed by using the well-established procedure of Budil *et al*.,[26] which allowed us to extract the following main parameters: (a) the g_{ii} main components of the g tensor for the coupling between the unpaired electron spin and the magnetic field, and A_{ii} main components of the A tensor for the coupling between the electron spin and the **c**opper nuclear spin. For an axial symmetry, where g_{zz} and A_{zz} are the largest values, the z molecular axis corresponds to the main direction of the orbital containing the unpaired electron. The **magnetic** A_{ii} and g_{ii} components identified, by comparison with values found in previous literature:[12, 22-25, 27-33] i) the type of coordination, *e.g.*, the number of nitrogen and oxygen sites bonded to Cu(II), ii) the geometry of the complex, and iii) the strength of the coordination bonds. In detail, an increase in the A_{ii} values (mainly A_{zz}, but, for clarity, the average value $\langle A \rangle = (A_{xx}+A_{yy}+A_{zz})/3$ was calculated and compared between spectra) and a decrease in the g_{ii} values (mainly g_{xx} was clearly evaluable in all our spectra) usually correlate with an increase in the number of complexed nitrogen sites, and/or an increased strength of interaction; (b) the correlation time for the rotational motion (τ), which measures the mobility of the complex, in turn related to the dendrimer branches flexibility and the coordination strength; an increase in τ corresponds to an increase in microviscosity, and, consequently, to a decrease in mobility.

2.4 In vitro cytotoxicity assays

Cytotoxicity (absolute count and cell death) was evaluated through flow cytometry. U937 and PBMCs were seeded at a density of 10^6 cells/well in 12-well plates with 1 ml/well of medium to which 1 ml of metallodendrimer was added at a final concentration of 10^{-5} M and incubated for 24, 48 and 72 h at 37 °C in a 5% CO_2 humidified air. Therefore, the solutions for biological tests contained 100 times diluted metallodendrimer if compared to the solutions for EPR experiments. Despite the disadvantage created by the sensitivity limit of the EPR technique, which needs a relatively high concentration of paramagnetic species, this technique provides in situ information on the interactions occurring between the dendrimers and the cells. This information did not suffer of the concentration variation as demonstrated by the invariability of the EPR spectra in function of the cell concentration. Cell death features were evaluated using Propidium Iodide (PI, Sigma-Aldrich). The cells were incubated with 50 μg/mL for 30 min and then apoptotic and necrotic cells were detected as PI^{dim} and PI^{bright} clusters, respectively. Absolute cell counting was performed by using Dako CytoCountTM beads (Dako Denmark A/S). 100 μl of sample was carefully dispensed at the bottom of the tube and 50 μl beads were added. Samples were acquired by using a FACSCantoII cytometer (Becton Dickinson, BD, U.S.A) within 60 min. Approximately 20,000 cell events were collected. Set-up and calibration procedures were optimized for the absolute counting protocols.

2.5 Determination of mitochondrial potential ($\Delta\Psi_m$)

Mitochondrial features were investigated through staining with Tetramethylrhodamine ethyl ester perchlorate (TMRE, Sigma-Aldrich). TMRE is a $\Delta\Psi_m$-specific stain able to selectively enter into mitochondria depending on $\Delta\Psi_m$ producing red fluorescence. TMRE 40 nM was added to the sample 15 min before the acquisition time. Samples were analysed by flow cytometry using the appropriate fluorescence channel.

2.6 Detection of acidic organelles

To detect the acidification of the sub-cellular compartments, samples were labelled with 100 nM of LysoTracker Green dye (Molecular Probes) for 10 min at 37 °C. LysoTracker® probes are fluorescent acidotropic probes for labelling and tracking acidic organelles in live cells. The fluorescence intensity was measured by flow cytometry.

2.7 Autophagy detection

After dendrimer treatment, the cells were incubated with 50 μM Monodansylcadaverine (MDC, Sigma-Aldrich) at 37°C for 10 min and then analyzed by flow cytometry. MDC is an autofluorescent dye that accumulates in autophagic vacuoles (AVs) due to a combination of ion trapping and specific interactions with membrane lipids.

2.8 Cytometric analyses

Cytometric experiments were carried out with a FACSCanto II flow cytometer (BD, Biosciences) equipped with an argon laser (Blue, Ex 488 nm), a helium-neon laser (Red, Ex 633 nm) and a solid-state diode laser (Violet, Ex 405 nm). Analyses were performed with FACSDivaTM software (BD); approximately 10,000 cell events were acquired for each sample.

2.9 Statistical analyses

Data are shown as mean ± standard deviation (SD) of at least three independent experiments. Analyses of variance (ANOVA) approaches were used to compare values between more than two different experimental groups for data that met the normality assumption. Two-way ANOVA were followed by a Bonferroni post-hoc test. P values less than 0.05 were considered statistically significant. All statistical analyses were done using GraphPad Prism 5.0 (GraphPad software, U.S.A).

3. Results and discussion

In our previous studies,[22] copper(II)-carbosilane dendrimers (Figure 1) demonstrated an extraordinary interacting ability towards model cell membranes, i.e. CTAB micelles and Lecithin liposomes.

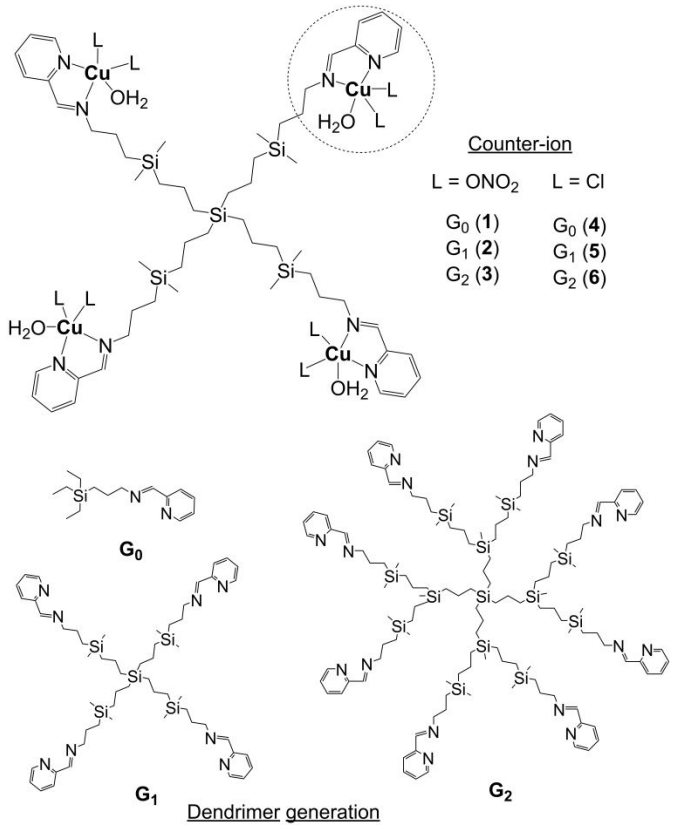

Figure 1. *Chemical representation of the tested Schiff base carbosilane metallodendrimers* ***1-6****, highlighting the structural parameters studied.*

EPR analysis indicated that the increase in generation and the change of Cu(II) counter-ion - from nitrate to chloride- produce an increased relative amount and strength of interaction of the Cu(II) ions with the dendrimer in presence of the model membranes. Interestingly, the stabilization of the Cu(II) complexes at the membrane level produced a lower toxicity towards cancer cells. Aiming to gain further insight into the mechanism of action of these metallodendrimers in viable cells, their interaction with healthy cell line PBMC and the tumour

cell line U937 was evaluated using computer aided EPR and a wide range of well validated tests for biological assays.

3.1 EPR evaluation of Cu(II) metallodendrimers in the absence and presence of cells

EPR enabled the evaluation of the dendrimers behavior in the absence and presence of selected cell lines, namely the healthy cell line PBMC and the tumor cell line U937, at different incubation times ranging from 0 to 72 h. Unlike former studies in model membranes using PBS,[22] this study was performed using RPMI medium. The spectra of the dendrimers alone in RPMI showed two components, which were termed "fast" and "slow" on the basis of the different resolution of the magnetic components for the g and A tensors. This is represented in Figure 2.A-top for G_1-(ONO_2) (2). Instead, three components have been found for the same dendrimers in PBS.[22] The change from PBS to RPMI media produced the disappearance of the component termed "component O" observed in PBS, arising from a Cu(II)-O_4 coordination (Cu(II) binding with 4 oxygen sites, which may be water or phosphate groups). This is probably due to the presence of amino groups in RPMI medium, which preferentially bind Cu(II) ions. Amino groups are present in several components of RPMI medium, like the vitamins (for instance vitamin B12), glutathione and biotin.

The magnetic parameters from computation (the computed line, in red, is also shown in **Figure 2.A**) of the fast component of dendrimer **2** in RPMI - <A>= 69 G and <g>= 2.123 – compared with literature ones,[12, 22-25, 27-33] indicate the formation of a square planar (orthorhombically distorted) Cu(II)-N_4 coordination. The nitrogen sites are the aminopyridine groups at the dendrimer surface and nitrogen sites present in RPMI medium and listed above. High mobility is supported by a correlation time for motion τ = 42 ps. The slow component is visible in **Figure 2.A** as a peak at relative low intensity and high magnetic field. Subtraction of the fast component allowed us to obtain the slow component and compute it. An example of computation of this component is shown in **Figure S1** (Electronic Supporting Information-**ESI**). For a better comparison, the **Table ST1,** also included in the Supporting Information, lists the g_{ii} and A_{ii} main magnetic parameters for selected examples of fast and slow components. The significant increase of τ from the fast to the slow component indicates that the ions are trapped at the dendrimer interface. The values <g> = 2.15 and <A> = 58 G used for computation (red line in **Figure S1**) also indicate a different coordination of these trapped ions with two nitrogen and two oxygen sites (Cu(II)-N_2O_2).The addition of PBMC to the Cu(II)-metallodendrimers produced negligible variations in the EPR spectra. Overall, EPR analysis indicated that PBMC barely interacted with the dendrimers and these results are not henceforth discussed. Conversely, a different situation was observed when U937 tumour cells were added to the dendrimers. After 24 h incubation with U937 cells, dendrimer G_1-Cu(ONO_2) (**2**) revealed a spectrum (**Figure 2.A-bottom**) where the fast component was computed using higher <A> (77 G) and τ (58 ps) values, and a lower <g> value (2.119) with respect to the absence of these cells. Furthermore, the relative percentage of slow component was higher in the presence (35%) than in the absence (27%) of U937 cells. Finally, the g_{xx} value of the slow component was lower in the presence (2.0305) than in the absence (2.0317) of U937 cells. Overall, these parameters indicate an interaction, mainly electrostatic through the Cu(II) complexes, between the dendrimer and the cancer cells.The fast components for all dendrimers in the absence and in the presence of U937 cells at different incubation times (2h, 4h, 24h, 48h) were computed and the calculated <A> values are shown in **Figure 2.C**. For all dendrimers, <A> increased by adding the U937 cells and by increasing the incubation time up to 24 h. This indicates a progressively increasing interaction between the dendrimers and U937 cells over time.

After 24 h, a decrease of <A> was observed, which may be provoked by cell degradation. The disruption at the membrane level well justifies a weakening of the Cu(II)-ligand binding strength, and an increased interaction with oxygen sites at the expenses of nitrogen sites. The results at the latest incubation time (72 h) were not reported because of poor reproducibility, but they were in any case in line with the trend shown from 24 to 48 h. The change of <A> over time was different among the evaluated dendrimers. In the absence of cells, chloride dendrimers showed slightly higher values than nitrate ones, indicating stronger interactions of the ions with the former than with the latter dendrimers. Furthermore, the interaction strength decreases with generation. This may be accounted by a perturbative effect of neighboring Cu(II) complexes. Indeed, the <A> values for G_2 dendrimers increased less than for the other generations at all incubation times. This means that the increased density of surface groups of G_2 dendrimers is perturbative for interactions at the dendrimer interface. Interestingly, G_1-$Cu(ONO_2)_2$ (**2**) showed the highest variation at 4 and 24 h, while G_1-$CuCl_2$ (**5**) showed a significant variation already at 2 h and then <A> barely changed until 24 h. This means that, for the fraction of complexes producing the fast component, **5** quickly interacted with the cells, while **2** required 24 h to produce stronger surface interactions with respect to the other dendrimers. Unexpectedly, G_0 dendrimers behaved quite oppositely: G_0-$CuCl_2$ (**4**) gave highest <A> values at 24-48 h, but G_0-$Cu(ONO_2)_2$ (**1**) interacted stronger at earlier times. The relatively strong and persistent interaction of G_0-$CuCl_2$ (**4**) is justified considering that this small, flexible and quite hydrophobic molecule was well adhering at and then entering the cell membrane. G_2-$Cu(ONO_2)_2$ (**3**) showed interactions at 2-4 h, then this effect decreased over time.

Further and complementary information was achieved from the analysis of the slow components. The relative percentage of the slow component changed for the different dendrimers from the absence to the presence of U937 cells as a function of the incubation time (**Figure 2.B**). These variations were accompanied by a variation in the binding ability, since the minimum of the high field peak for the slow component changed its position.

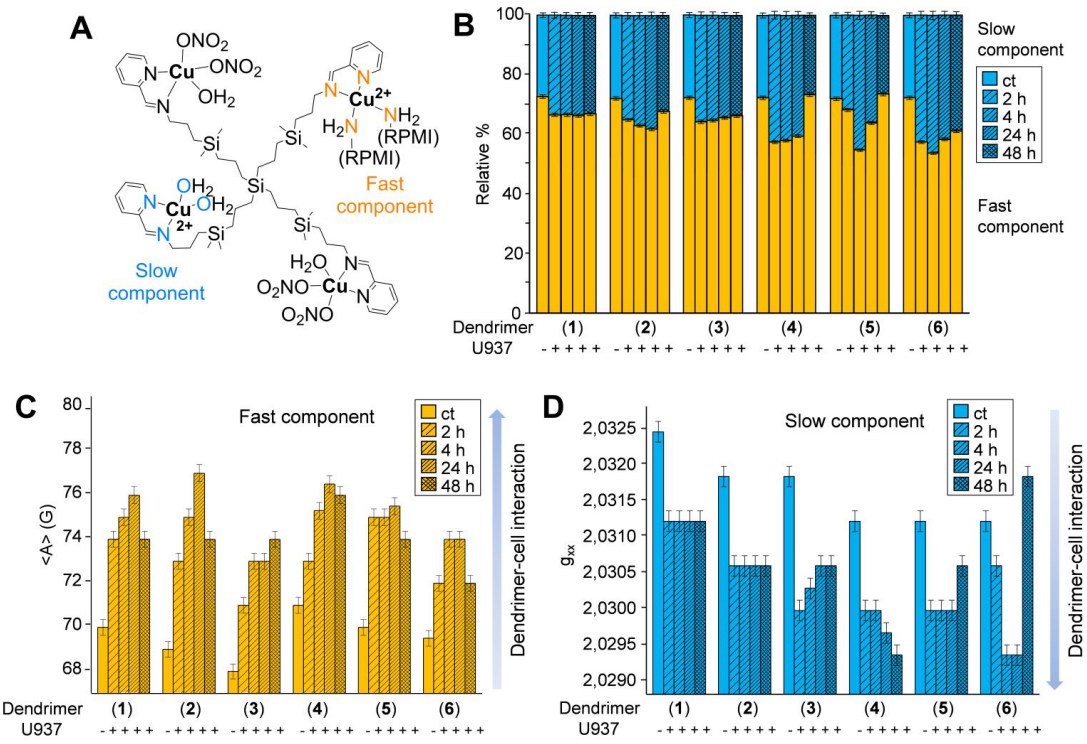

Figure 2. *Analysis of the EPR spectra of metallodendrimers **1**-**6** in the absence (ct) and presence of U937 tumor cells at different time points (2-48 h). A) Different Cu(II) environments leading to the Fast and Slow components in EPR spectra, using G1-Cu(ONO2)2 (**2**) in RPMI medium as example. B) Relative percentages of the spectral components. C) Comparison of <A> for the fast component. An increase in <A> indicates an increase in dendrimer-cell interaction. D) Comparison of gxx for the slow component. A decrease in gxx indicates an increase in dendrimer-cell interaction.*

This variation reflected the variation of the g_{xx} parameter (**Figure 2.D**), which therefore became the most reliable parameter in the computation of the slow component, together with its relative percentage, to describe the binding properties for the slow component. In detail, lower g_{xx}, stronger the interaction is. Comparing the results for the fast and the slow components in **Figure 2**, different dendrimer-cell interactions over time were observed, related to the increase of % and decrease of g_{xx} when U937 cells were present. In the absence of cells, the relative percentage of slow component remained invariant among the different dendrimers. However, the interaction strength measured by g_{xx} was stronger for chloride dendrimers than for nitrate ones, and an increased among the nitrate dendrimers, from G_0 to G_1 and G_2. These results confirm that $CuCl_2$ complexes are more stable than $Cu(ONO_2)_2$ complexes and the interactions with the cells perturb the complex stability mainly for the chloride counter-ion. Surprisingly, G_1-$CuCl_2$ (**5**), which showed a quick interaction for the fast component, at 2 h revealed the lower percentage of slow component among the various dendrimers, even if g_{xx} values indicated an increased interaction strength since 2 h. The relatively low % at 2 h is probably related to a barrier effect played by the fast-moving but better-interacting complexes. However, at 4 h, the % of slow component for **5** significantly increased, but at 24 h decreased again to be the minimum at 48 h. Therefore, this dendrimer quickly interacted, but slow and the fast cell-binding conditions competed with each other. The slow conditions (strong interactions) only won at 4 h. A completely different behaviour was found for G_2-$CuCl_2$ (**6**). This dendrimer showed low values of <A> for the fast component, while it showed the highest percentage of slow component in the presence of the cells at all incubation times. This means that dendrimer **6** well and persistently

interacted with the cell membrane, in agreement with the results on membrane models.[22] However, the interaction process was slower for dendrimer **6** than for dendrimer **5**, requiring more than 4 h to display a preferential interaction (lowest g_{xx} value). After 48 h, dendrimer **6** was still interacting, but cell degradation occurred, and the interaction strength significantly decreased (increase in g_{xx} values). The results from G_0-$CuCl_2$ (**4**) were also peculiar, since the interaction strength measured by g_{xx} increased progressively up to 48 h. At this time, complex **4** displayed the strongest interaction (lowest g_{xx}) but a small percentage of interacting component. In conclusion, dendrimer **4** showed a good and persistent interaction, as confirmed by the fast component results.

With regard to nitrate dendrimers, G_0-$Cu(ONO_2)_2$ (**1**) showed weaker interactions of the slow-moving ions than G_0-$CuCl_2$ (**4**), both in absence and in presence of U937 cells. These interactions remained invariant over the incubation time range. Therefore G_0-$Cu(ONO_2)_2$ (**1**) well interacted with U937 cells at the external surface. This most likely provoked a harmful and prolonged internalization into the cells, probably *via* phagocytosis, with a consequent invariance in the perturbation of the slow-moving ions over time. G_1-$Cu(ONO_2)_2$ (**2**) displayed stronger interactions than **1**, also invariant over time, but a small increase in percentage of slow component was observed until 24 h. This increase corresponded to the relatively high increase in interactions at the external surface, which indicates that this dendrimer may be active in partially degrading the U937 cells. Conversely, for G_2-$Cu(ONO_2)_2$ (**3**) the percentage of slow component poorly changed over time, while the interaction strength increased at 2 h and then progressively decreased. This held for both the fast and the slow component, indicating a perturbation played by neighboring Cu(II) complexes, probably due to the presence of a higher density of polar NO_3 groups. This probably stabilized the complex leading to a lower toxicity. In any case, the interactions were favored for G_2-$CuCl_2$ (**6**) with respect to G_2-$Cu(ONO_2)_2$ (**3**), due to the ability of **6** to enter the cell membrane, stabilize at the dendrimer/cell interface and potentially lead to an eventual phagocytosis.

These results are in agreement with previous results that demonstrate a unique interaction of dendrimers towards cell membranes by using both model membranes and real cells.[11, 12] Model membranes, such as liposomes and micelles, mimic the structural organization of cellular membranes and, making use of a range of characterization techniques, provide physical insights into the interactions between dendrimer and cell membranes.[34] In the present case, previous studies using CTAB micelles and lecithin liposomes have provided valuable insight in the interactions between Cu(II)-carbosilane metallodendrimers and model membranes.[22] It has been found that the increase in generation and the change of the Cu(II) counter-ion –from nitrate to chloride – produce an increased relative amount and strength of interaction of the dendrimer with the model membranes. The results found on U937 cells were perfectly in line with the previous ones on the model membranes, showing that they are good models for the cancer cell membrane. However, interestingly, former *in vitro* study also showed that the stabilization effect produced a lower toxicity towards cancer cells.[22]

Further conclusions can be obtained studying the interactions of different types of dendrimers with the cells. The presence of cationic groups in a dendrimer promotes the binding to the negatively charged cell surface, but also is responsible of potential toxicity, thus requiring a good compromise between effective internalization and toxicity. As an example, the interaction of cationic PAMAM dendrimers towards HeLa cells increased with generation, and thus the amount of positive charges.[14,15] Importantly, herein we demonstrated that close Cu(II) complexes at the surface of Cu(II)-carbosilane metallodendrimers exerted a perturbative effect on complex stability when increasing generation. This translated into a decreased interaction strength for G_2 dendrimers. The interaction is not only dependent on the number of positive charges, but also on

their distribution and interacting ability. The interactions and kinetics of dendrimer internalization are also modulated by the type of cells. G_4-PAMAM dendrimers underwent a fast endocytosis in HepG2 cells;[35] a very slow internalization and a high membrane affinity in PC-12 cells; and a complete uptake in 4 h in HeLa, astrocytes and lung fibroblasts.[14] According to the EPR study, our metallodendrimers showed a maximum interaction with U937 cells membrane at 24 h, thus confirming a stronger interaction with the cell membranes and a slower internalization mechanism, while ruling out the interactions with PBMC according to the absence of spectral variations. Overall, it can be concluded that cationic-carbosilane metallodendrimers cross cell membranes, but with different dynamics depending on the type of dendrimer, membrane chemical composition and cell-type recycling kinetics.

As previously mentioned, the dendrimer cell uptake depends on different parameters such as generation, functionalization, concentration, and surface charge of dendrimers, as well as the cell type. Within cells, the dendrimers fate depends on the mechanism of cell uptake. As an example, endocytosis has been reported to be the main cellular uptake mechanism of PAMAM dendrimers, but passive diffusion has also been reported. The cytotoxic response of PAMAM dendrimers is influenced by the cellular uptake pathway, which in turn is influenced by dendrimer-membrane interactions. In order to gain further insight into the intracellular fate of Cu(II)-carbosilane metallodendrimers, *in vitro* experiments were performed.

3.2 In vitro evaluation of PBMC and U937 myeloid cell line response to metallodendrimers administration

In order to translate the results obtained through EPR studies to a more strictly biological analysis, subsequent *in vitro* experiments were performed which evaluated the cytostatic and cytotoxic behaviour of the compounds in the tumour cell line U937, as well as in healthy peripheral blood lymphocytes (PBMC) from donors. Lower dendrimer concentrations (10^{-5} M) were used for the biological assays, in comparison to those used in the EPR analysis (10^{-3} M), aiming for a compromise between viability and biological effect (**Figure S2**). Additional sublethal effects regarding mitochondria function, lysosomal compartment and autophagic organelle involvement were studied and are herein presented.

3.2.1 Cytotoxic and cytostatic behaviour.

Cytotoxicity and cytostasis are desirable properties for antitumor drugs. Cytotoxic agents produce cell death and eventual tumour shrinkage, whereas cytostatic agents inhibit tumour growth through the alteration of their metabolism and blockage of cell division but without direct toxicity.[36] The cytostatic and cytotoxic properties of metallodendrimers 1-6 were evaluated through flow cytometry after 24, 48 and 72 h cell treatment. The results are shown in Figure 3, including absolute cell count (A, C) and dead cell count (B, D) by staining with fluorescent probe Propidium Iodide (PI). The experiments depict a different scenario for PBMC and U937 cells: in U937, a cytostatic and cytotoxic behaviour was observed already at 24 h, whereas in PBMCs a significant cytotoxic input occurs only at 72 h. These results match the conclusions from EPR analysis.

Both metallodendrimer families are antiproliferative (cytostatic) and moderate cytotoxic agents for U937 tumour cells (**Figure 3.A,B**). Control cells appear in exponential cell growth, unlike dendrimer-treated cells, confirming the cytostatic properties of these dendrimers. Supravital PI uptake measures the cytotoxicity of the compounds. Already after 24 h treatment, a significant cell

death is observed for first-generation dendrimers **2** and **5**, as well as for the G_0 complex **4** due to a mainly cytotoxic effect. These results are supported by EPR analysis, which suggests a probable harmful effect of compounds **2** and **5** against U937 cells, but the stabilization of the chloride complex **5** at the external cell surface seems to delay the internalization of the dendrimer into the cells. Also, the cytotoxicity of **4** is supported by the EPR results since this small, flexible and quite hydrophobic compound easily penetrates the cell membrane inducing a certain degree of cell death. Second-generation compounds **3** and **6** exhibit a similar mild effect on both viability and proliferation. EPR results also shows that the interacting ability between the complexes and U937 cells decreases from G_0 to G_2 probably due to the increase in surface-groups density that provokes perturbation between adjacent Cu(II) complexes.

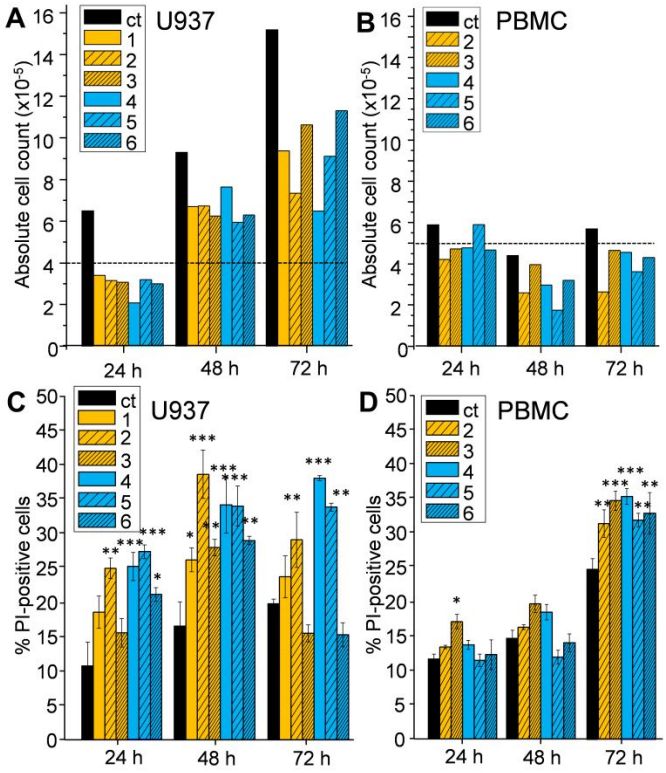

***Figure 3**. Evaluation of metallodendrimers toxicity on the tumour cell line U937 (A. Absolute cell count; B. % of PI-positive cells) and on healthy lymphocytes (C. Absolute cell count; D. % PI-positive cells). The dashed line indicates the absolute cell count at t = 0.*

The Cu(II) metallodendrimers barely affected the PBMC (**Figure 3.C**). The absolute cell number was only visibly reduced after 48 h treatment with first-generation dendrimers **2** and **5**, ascribed to a direct cytotoxic effect (the cytostatic effect is ruled out, due to the non-proliferating feature of normal lymphocytes). Nitrate metallodendrimer **2** showed a faster mechanism – probably necrosis and/or necroptosis- than the chloride counterpart **5** and the second-generation analogue **3**. Unfortunately, no reproducible results were obtained for complex **1**. The number of **2**-treated lymphocytes directly decreases, before the individuation of PI positivity, while **3**-treated cells suffer a lower decrease, although revealing a relevant and significant number of PI positive events. It was possible to distinguish early apoptotic and necrotic cells through the different PI fluorescent

intensity (**Figure S2**). This effect is especially remarkable for the nitrate-dendrimer **2**, with a significantly higher activity than the mononuclear and second-generation counterparts **1** and **3**. Again, the higher toxicity of dendrimer **2** was predicted by the EPR analysis. Such differences among the different generation analogues are diluted in the chloride-containing family.

Cu(II) carbosilane dendrimers are more cytotoxic towards U937 tumour cells than other cationic dendrimers. For example, treatment with second-generation dendrimer **6** at 10^{-5} M, bearing 8 iminopyridine Cu(II) complexes, produced 10% increased death compared to non-treated cells. A concentration 40 times higher of a G_2-polypropyleneimine dendrimer, comprising 8 $-NH_2$ peripheral groups, is necessary to reach a comparable cytotoxic response in U937 cells.[37] Unlike PPI and PAMAM dendrimers, which showed U937 toxicity in a time- and generation-dependent way,[37] our Cu(II) metallodendrimers follow the pattern previously observed with carbosilane analogues:[23] First-generation complexes **2** and **5** are the most effective among the different generation complexes.

Aiming for a deeper understanding on the mechanisms responsible for U937 cell death, we focused on analysing the sublethal effects on the residual cells from the previous experiments. The effect of the metallodendrimers on the mitochondria function, the lysosomal compartment and the involvement of autophagy was analysed. The results, which are shown below, indicate that the pathways involved in death processes involve the autophagic vacuole formation and the mitochondria-lysosome axis.

3.2.2 Effect on mitochondria transmembrane potential.

It has been reported that the mitochondrial transmembrane potential ($\Delta\Psi_m$) drives the production of ATP in the cell.[38] At high $\Delta\Psi_m$, the mitochondrial respiratory chain generates ROS in an exponential ratio to $\Delta\Psi_m$, being potentially harmful to mitochondria and ultimately to the cell. On the other hand, sustained low values of $\Delta\Psi_m$ lead to insufficient ability to produce ATP as well as "reductive stress", as detrimental to homeostasis as oxidative stress. Normal cell functioning requires stable levels of intracellular ATP and $\Delta\Psi_m$, and a prolonged perturbation of these factors may compromise the viability of the cells. In some pathological states such as cancer, the mitochondria exhibit significantly higher $\Delta\Psi_m$, compared to normal cells, and can be used as therapeutic antitumor target.[39] The changes in $\Delta\Psi_m$ after treatment with compounds **1**-**6** were evaluated through Tetramethylrhodamine ethyl ester (TMRE) labelling and the results are shown in **Figure 4**.

The treatment of U937 cells with Cu(II)-complexes **1**-**6** (**Figure 4.A**) produced an initial pro-oxidative effect, revealed by an increase in TMRE fluorescence at 24 h, especially remarkable for second generation metallodendrimer **6**. This result was expected on the basis of the peculiar interaction behaviour shown by this dendrimer based on the EPR analysis. However, such a strong and persistent interaction increases the mitochondria transmembrane potential but decreases the toxicity. An increase in membrane potential may related to a significant production of reactive oxygen species (ROS), exponentially dependent on $\Delta\Psi_m$, potentially harmful to the cell and detrimental to homeostasis. At 48 h the membrane potential collapsed, particularly for metallodendrimers **2**, **3** and **4**, and kept decreasing at 72 h for first-generation dendrimers **2** and **5**. Together with complex **6**, also complex **1** exhibited a prolonged pro-oxidative effect until 48 h, in agreement with the EPR results showing a quick interaction with the cell surface, which persists over time. These findings are in agreement with the data on viability and proliferation in **Figure 3**: **2**-treated U937 cells did not show any relevant partial recovery at 72 h, whereas compound **1** continues to increase the membrane potential, suggesting a delayed but prolonged effect. Also, this finding is supported by EPR results, since **1** showed an invariance in the perturbation of the slow-moving Cu(II) ions over time. A different situation is observed in PBMC. The metallodendrimers produced a stronger pro-oxidative effect at

24 h, if compared to U937, followed by a significant decrease at 48 h for all compounds, which is mildly recovered after 72 h.

Copper is an essential element with two fundamental intracellular functions, related to its redox ability as cofactor of either mitochondrial cytochrome c oxidase or the Cu/Zn superoxide dismutase, involved in detoxifying ROS. It has been reported that a surplus of copper within mitochondria can initiate oxidative damage and induce the destruction of this organelle.[40] In our case, the chelate coordination of the Cu(II) atoms through the iminopyridine moieties confirms the stability of the metal complex and rules out a potential release of Cu(II) ions. However, it is well-known that the nitrate ligands in Cu(II)-metallodendrimers **1**-**3** are more labile than the chloride ligands in compounds **4**-**6** and are prompt to be released after dissolution in water. The EPR results are in line with this finding. Accordingly, the higher overall positive charge in the nitrate-systems could explain their different effect on the mitochondria membrane potential. For example, first-generation nitrate complex **2** is more effective in decreasing $\Delta\Psi_m$ in U937 cells at 48 and 72 h than its chloride counterpart **5**.

Interestingly, the nature of the metal complex located at the periphery of the dendritic scaffold dictates the effect on the mitochondria membrane potential. Alternative metallodendrimers comprising the same carbosilane dendritic scaffold herein used and decorated with ruthenium (II) complexes have been evaluated for their antitumor activity towards acute promyelocytic leukaemia HL60 cells.[41]

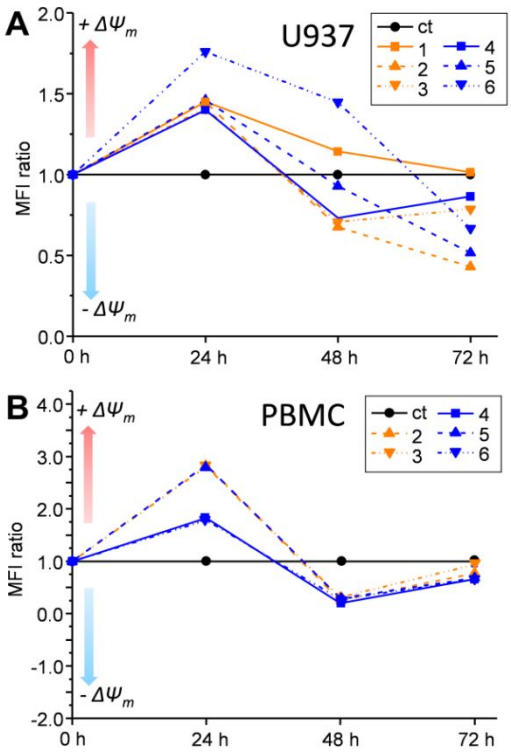

***Figure 4**. Changes on mitochondria membrane potential ($\Delta\Psi_m$) in U937 cells (A) and PBMC (B) after treatment with metallodendrimers **1**-**6**, measured through TMRE labelling.*

The study revealed a general mitochondrial hyperpolarization, where $\Delta\Psi_m$ increased when increasing metallodendrimer concentration (from 0.5 to 5.0 μM) and generation (from G_1 to G_2). A time-dependence was also observed, finding the maximum hyperpolarization at 3 h for G_1 and 72

h for G_2. The Cu(II) metallodendrimers, however, exhibited the highest hyperpolarization at 24 h and then a progressive decrease in $\Delta\Psi_m$, reaching values below the potential of non-treated cells.

3.2.3 Effect on lysosome and autophagosome routes.

The intracellular uptake of nanomaterials by both phagocytic and non-phagocytic mechanisms often culminates with internalization into lysosomes. The acidic pH and variety of hydrolytic enzymes (e.g. esterases, proteases, phosphatases, nucleases and lipases) found in the lysosome represent an extremely hostile environment which can degrade all but the most biopersistent of these nanomaterials. We evaluated the involvement of lysosomes after 24 h of dendrimer administration to U937 using LysoTracker®. The results indicated that the lysosome pathway was involved after 24 h treatment of the copper metallodendrimers with U937, especially for compounds **1** and **6**, the latter displaying a significant peak in lysosome number/acidity (**Figure 5.A**). In addition to the endo-lysosomal pathway, recent evidence suggests nanomaterials can also induce autophagy.[42] Autophagy is a catabolic strategy to degrade cellular components through lysosomes and thus mitigate cellular stress. In cancer therapy, it can act as cytoprotective or cytotoxic mechanism in a context-dependent fashion,[43] fostering a controlled cell death or supporting the survival of cancer cells by providing metabolic precursors. Furthermore, it plays many different roles in lymphocyte development and function.[44] It has been found that PAMAM dendrimers (G_5-NH_2) induce both reactive oxygen species and autophagy flux in neuronal cells.[45]

To elucidate lysosome-autophagosome routes after treatment with the Cu(II)-metallodendrimers, we performed a Monodansylcadaverine (MDC) labelling assay, a specific marker of Autophagic Vacuoles (AVs) (**Figure 5.B/C**). The increase in Mean Fluorescence Intensity (MFI) indicates an alteration of autophagy flux, with accumulation of autophagosomes, whereas the decrease represents an effective loss or disruption of the same organelles. In U937, cell treatment with nitrate-complexes **1**-**3** produced a mild increase at 24 h and a mild decrease at 48 h, with no clear dependence on dendrimer generation. The only remarkable increase was observed for monometallic complex **1** after 72 h. Chloride dendrimers **4**-**6** showed certain heterogeneity, especially second-generation dendrimer **6**. At 24 h, dendrimer **6** displayed the highest MFI value for MDC labelling, in agreement with data from Lysotracker green™ assay, and constantly decreased to MFI= 1 at 72 h. In this case too, the peculiar stability and interactions with the cell membrane for dendrimer **6**, as tested by EPR, support the occurrence of a phagocytosis process with the involvement of lysosomes.

Conversely, compounds **4** and **5** exhibited a decrease at 48 h and an increase at 72 h, quite remarkable for monometallic complex **4**. We already discussed the ability of dendrimer **4** to penetrate the cell membrane producing cell death. Overall, we can conclude that compounds **1** and **6** are the most efficient in autophagosome induction, followed by compound **4**. Regarding PBMC (**Figure 5.C**), autophagy seems more upregulated in nitrate-treated cells, compared to the chloride counterparts. In particular, first-generation metallodendrimer **2** induces an important formation of autophagic vacuoles after 24 h treatment, probably as a cytoprotective mechanism according to the absence of toxicity observed in **Figure 3.D**.

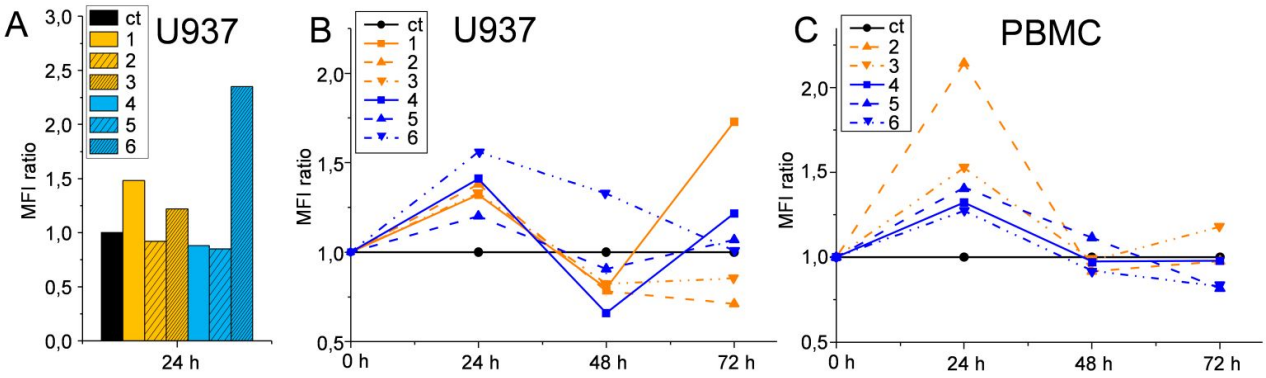

Figure 5. *A. Involvement of lysosome pathway in U937 cells after treatment with compounds* ***1****-****6****, measured using Lysotracker green®. B/C. Autophagy perturbation induced by treatment with the different compounds and measured using MDC labelling in U937 and PBMC.*

Altogether, these results suggest that treatment with carbosilane copper metallodendrimers induce death processes through mitochondria-lysosome axis as well as autophagic vacuole formation. The dendrimers seem to stabilize different subcellular compartments, playing an important role in the exerted toxicity. They may cause lysosomal overload with indigestible material, including copper, disrupting lysosomes fusion with other cell compartments and resulting in vacuole accumulation, as observed in our assays. Other cationic dendrimers, such as PAMAM dendrimers, induce the loss of mitochondrial membrane potential and lysosome membrane permeabilization, through a proton sponge mechanism.[46] Lysosome membrane permeabilization is a well-known cell death mechanism, which may result in mitochondrial outer membrane permeabilization or be contemporaneous, giving the subsequent induction of reactive oxygen species (ROS) generation and apoptosis, or even necrosis.

Nanomaterial-induced autophagy perturbation, both induction and blockade, has been widely reported,[47] with several plausible mechanisms including oxidative stress, mitochondrial damage, alteration of signalling pathways or a simple attempt to degrade a foreign entity. The dysfunction of autophagy and lysosomal pathways are a potential cytotoxicity mechanism but may also be a potential therapeutic mechanism.

4. Conclusions

In the search of efficient and selective antitumor therapies, copper(II) carbosilane dendrimers stand out due to the high stability, exceptional structure-to-property relationship and unique interaction with cell membranes, which can be fine-tuned altering the dendrimer generation and the metal counter-ion. This extraordinary interaction, which further explains the potent and selective cytotoxic behaviour, has been studied through EPR in model cell membranes and herein confirmed in myeloid cancer (U937) and healthy (PBMC) cells.

EPR spectral computation showed that the Cu(II)-N_2O_2 coordination observed when the ions are trapped in slow motion at the dendrimer interface was perturbed or stabilized during the electrostatic interaction with the membranes of U937 cancer cells. Importantly, these interactions were preferential with the cancer cells and weak or absent with healthy PBMCs. The interaction between the Cu(II) complexes and U937 cells progressively increased over the incubation time. Cell degradation started probably after dendrimer uptake, when the disruption at the membrane

level well justifies the weakening of the Cu(II)-ligand binding strength measured by EPR, and an increased interaction of Cu(II) with oxygen sites at the expenses of nitrogen sites. The biological *in vitro* assays confirmed that Cu(II) metallodendrimers are cytostatic and moderate cytotoxic agents for U937 tumor cells, while barely affecting healthy PBMCs. They altered the mitochondria transmembrane potential of U937 cancer cells, producing an initial pro-oxidative effect at 24 h and a subsequent collapse up to 72 h. These metallodrugs perturbed the lysosome pathway and the autophagy flux in U937 cells, increasing the formation of autophagic vacuoles at 24 h, which were progressively disrupted over time. A similar effect was observed in PBMC, but the initial pro-oxidative effect is buffered over time, recovering the control values at 72 h. The increased formation of autophagic vacuoles at 24 h and subsequent degradation may be related to a cytoprotective response, considering the absence of toxicity at 24 and 48 h. This effect is particularly remarkable for G_1-$Cu(ONO_2)_2$ (**2**), with an extremely high increase in autophagy after 24 h treatment.

The structural perfection of Cu(II) metallodendrimers provided valuable insight into the influence of dendritic generation and metal counter-ion on the interaction with cancer cells and the subsequent therapeutic effect. Overall, the following conclusions can be drawn:

1. Both in absence and in presence of the cells, the interactions of the ions were stronger (more stable Cu(II) complexes) for chloride dendrimers than for the nitrate ones and may lead to different uptake mechanism. For example, G_0-$CuCl_2$ (**4**) gives a strong and persistent interaction with U937 cells after 24 h, as this small, flexible and hydrophobic complex easily penetrates the cell membrane and leads to cell death. However, G_0-$Cu(ONO_2)_2$ (**1**) interacts stronger at the external surface and at shorter times, producing a harmful and prolonged internalization of **1** through phagocytosis, with a consequent invariance in the perturbation of the slow-moving ions over time.
2. The interaction strength decreased from G_0 to G_2 probably due to the increase in surface-groups density that provokes perturbation between adjacent Cu(II) complexes. Nevertheless, this does not exclude strong and persistent interactions with the cell membrane with second-generation metallodendrimers such as G_2-$CuCl_2$ (**6**), in agreement with the results on membrane models,[22] favoring phagocytosis and a persistent mitochondria hyperpolarization.
3. A strong and persistent interaction with the cell membrane, such as that observed for metallodendrimers **1** and **6**, favors phagocytosis, increases the mitochondria transmembrane potential and leads to a prolonged formation of autophagy vacuoles that degrade cellular components. Importantly, such persistent interaction decreased the metallodendrimer toxicity.
4. The structural features of first-generation metallodendrimers G_1-$Cu(ONO_2)_2$ (**2**) and G_1-$CuCl_2$ (**5**), such as the metal complexes distribution and the hydrophilic-hydrophobic balance, induced a remarkable cytotoxicity in U937 cells already at 24 h, coinciding with an initial pro-oxidative effect, and an outstanding collapse of mitochondria transmembrane potential up to 72 h, in agreement with their higher toxicity. A simple exchange of counter-ion modified the interaction speed: G_1-$CuCl_2$ (**5**) interacted quickly (2-4 h), but the interactions were not persistent, as shown by the EPR results; the biological data on **5** showed that the labile interactions at the external surface delayed the internalization in the cells. Conversely, G_1-$Cu(ONO_2)_2$ (**2**) required 24 h to produce strong and persistent interactions at the U937 cell surface (EPR results). These interactions favored for **2** a higher activity and faster cytotoxic mechanism (mainly at 24-48 h) – probably necrosis and/or necroptosis- than the chloride counterpart **5**. The fast and selective cytotoxic response of metallodendrimer **2** in myeloid cancer cells well justifies the selection as the most promising candidate for further anticancer evaluation, as previously reported in our study towards resistant prostate cancer.[22] Complex **2** inhibited the proliferation of PC3 cells, decreased their adhesion to collagen type-I and decreased the tumour size up to 37% in an *ex vivo* mice model.

The potency and selectivity of Cu(II) metallodendrimers in myeloid cancer cells open new avenues in the use of nanosized metallodrugs for the treatment of leukaemia, which cannot benefit from the well-known Enhanced Permeation and Retention effect that improves the anticancer effect of nanodrugs in solid tumors.

Conflicts of interest

"There are no conflicts to declare".

Acknowledgements

This research was funded by grants from CTQ2017-86224-P (MINECO), consortiums IMMUNOTHERCAN-CM B2017/BMD-3733, Project SBPLY/17/180501/000358 Junta de Comunidades de Castilla-la Mancha (JCCM) and the Comunidad de Madrid Research Talent Attraction Program 2017-T2/IND-5243. CIBER-BBN is an initiative funded by the VI National R&D&I Plan 2008–2011, Iniciativa Ingenio 2010, Consolider Program, CIBER Actions and financed by the Instituto de Salud Carlos III with assistance from the European Regional Development Fund. N.S.O. wishes to thank JCCM for a predoctoral fellowship. The authors thank DiSPeA and DiSB at the University of Urbino for the financial support for the EPR experiments and the cytometric experiments, and the Italian Ministry of University and Research for the financial support through PRIN 2017 project "FIBRES: a multidisciplinary mineralogical, crystal-chemical and biological project to amend the paradigm of toxicity and cancerogenicity of mineral fibres." This article is based upon work from COST Action CA17140 "Cancer Nanomedicine from the Bench to the Bedside" supported by COST (European Cooperation in Science and Technology). This work has been supported partially by a EUROPARTNER: Strengthening and spreading international partnership activities of the Faculty of Biology and Environmental Protection for interdisciplinary research and innovation of the University of Lodz Programme: NAWA International Academic Partnership Programme.

Supporting Information

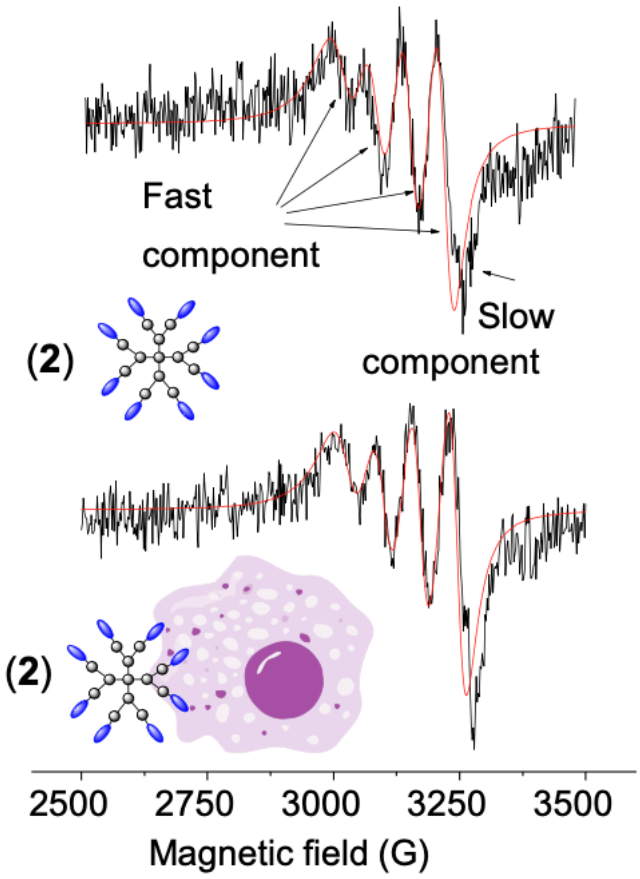

Figure S1: EPR spectra of G_1-$Cu(ONO_2)_2$ (**2**) in RPMI medium (top) and after incubation with U937 for 24 h (bottom). Red lines indicate computed spectra. Spectra are normalized in height.

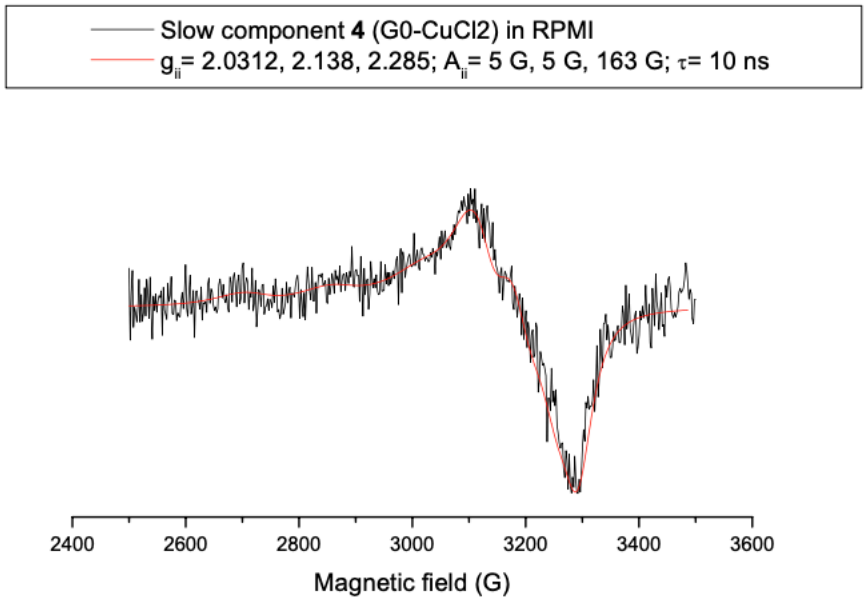

Figure S2: Example of computation of the slow component for **4** in RPMI.

Table ST1: Magnetic parameters for selected examples of EPR components (samples in RPMI), and proposed Cu(II) coordination

Sample	g_{xx}	g_{yy}	g_{zz}	A_{xx} (G)	A_{yy} (G)	A_{zz} (G)	Coordination
4 slow	2.0312	2.138	2.285	5	5	163	Cu-N_2O_2
2 slow	2.0318	2.140	2.288	5	5	158	Cu-N_2O_2
2+U937 24h slow	2.0306	2.137	2.283	5	5	168	Cu-N_2O_2
2 fast	2.010	2.110	2.249	10	10	187	Cu-N_4
2+U937 24h fast	2.007	2.110	2.240	15	15	201	Cu-N_4

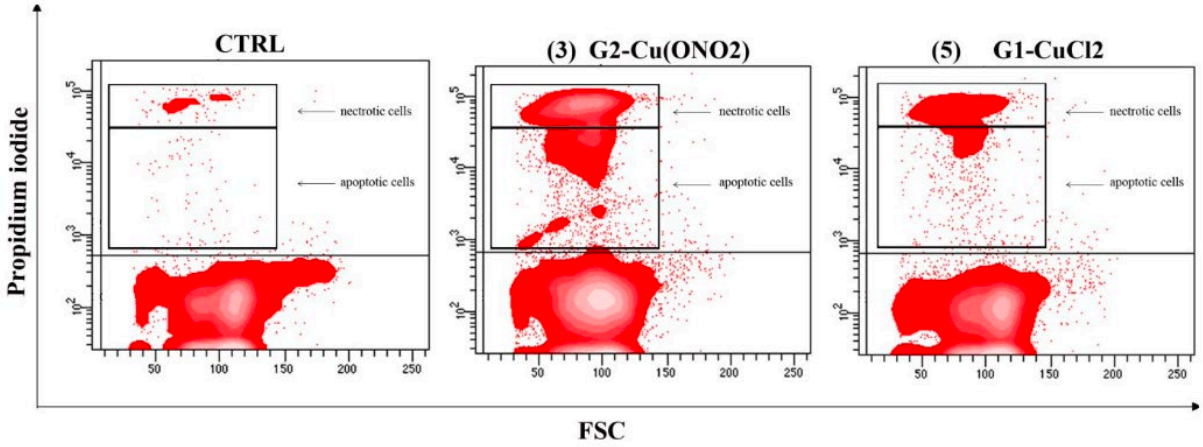

Figure S3: plots of a PI positivity in U937 cells, PI^{dim} and PI^{bright} necrotic events.

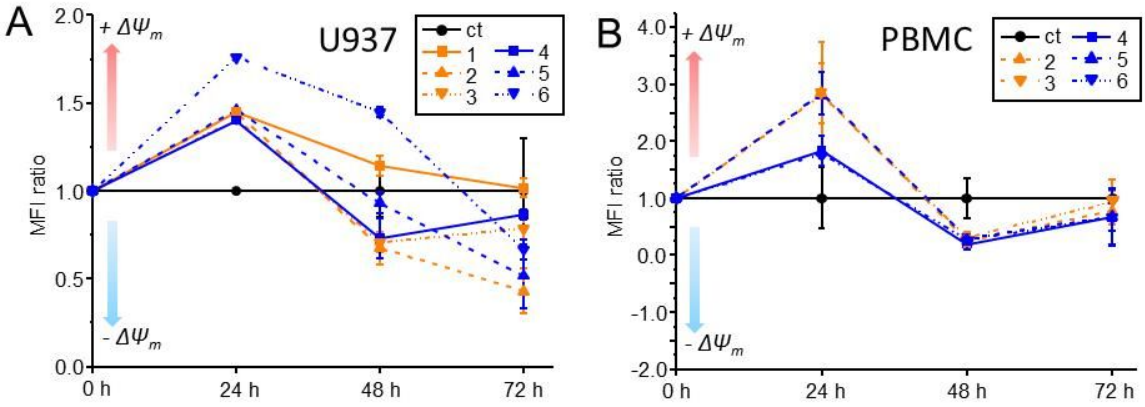

Figure S4: Changes on mitochondria membrane potential ($\Delta\Psi_m$) in U937 cells (A) and PBMC (B) after treatment with metallodendrimers **1-6**, were measured through TMRE labelling.

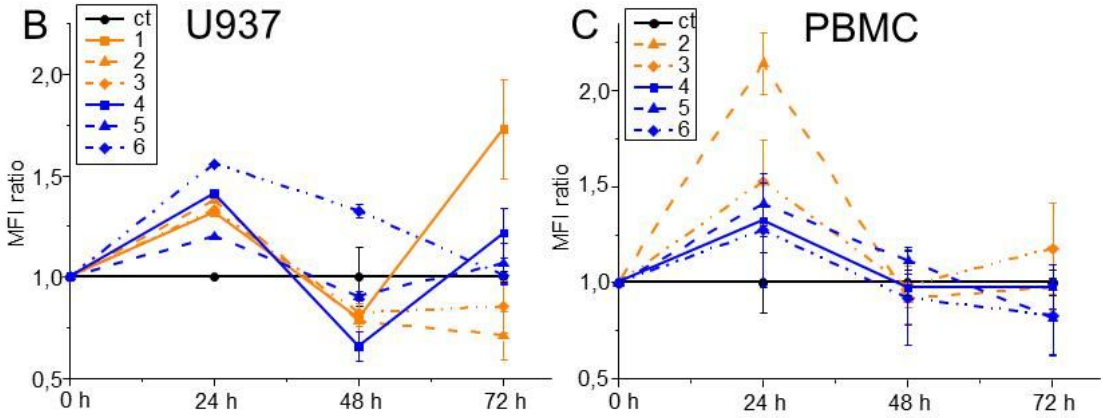

Figure S5: Authophagy perturbation induced by treatment with the different compounds and measured using MDC labelling in U937 (B) and PBMC (C).

Notes and references

1. F. Bray, J. Ferlay, I. Soerjomataram, R. L. Siegel, L. A. Torre and A. Jemal, CA Cancer J. Clin., 2018, 68, 394-424.
2. I. A. f. R. o. Cancer, eds. C. P. Wild, E. Weiderpass and B. W. Stewart, Lyon, France, 2019.
3. R. Misra, S. Acharya and S. K. Sahoo, Drug Discov. Today, 2010, 15, 842-850.
4. V. K. Chaturvedi, A. Singh, V. K. Singh and M. P. Singh, Curr. Drug Metab., 2019, 20, 416-429.
5. L. Shang, K. Nienhaus and G. U. Nienhaus, J. Nanobiotechnol., 2014, 12, 5.
6. Dendrimers in biomedical applications Royal Society of Chemistry, 2013, P001-204
7. I. J. Majoros, C. R. Williams and J. R. Baker, Jr., Curr. Top. Med. Chem., 2008, 8, 1165-1179.
8. A. K. Sharma, A. Gothwal, P. Kesharwani, H. Alsaab, A. K. Iyer and U. Gupta, Drug Discov. Today, 2017, 22, 314-326.
9. Y. Ma, Q. Mou, D. Wang, X. Zhu and D. Yan, Theranostics, 2016, 6, 930-947.
10. U. H. Sk and C. Kojima, Biomol. Concepts, 2015, 6, 205-217.
11. E. Andreozzi, A. Antonelli, M. Cangiotti, B. Canonico, C. Sfara, A. Pianetti, F. Bruscolini, K. Sahre, D. Appelhans, S. Papa and M. F. Ottaviani, Bioconjugate Chem., 2017, 28, 524-538.
12. M. F. Ottaviani, N. El Brahmi, M. Cangiotti, C. Coppola, F. Buccella, T. Cresteil, S. Mignani, A. M. Caminade, J. P. Costes and J. P. Majoral, RSC Adv., 2014, 4, 36573-36583.
13. A. Kaur, K. Jain, N. K. Mehra and N. K. Jain, J. Colloid Sci. Biotechnol., 2015, 4, 99-109.
14. L. Albertazzi, M. Serresi, A. Albanese and F. Beltram, Mol. Pharm., 2010, 7, 680-688.
15. L. Albertazzi, M. Fernández-Villamarin, R. Riguera and E. Fernández-Megia, Bioconjugate Chem., 2012, 23, 1059-1068.
16. S. P. Mukherjee, F. M. Lyng, A. García, M. Davoren and H. J. Byrne, Toxicol. Appl. Pharmacol., 2010, 248, 259-268.
17. X. Zeng, Y. Zhang and A. M. Nyström, Biomacromolecules, 2012, 13, 3814-3822.
18. J. H. Kuo, M. S. Jan and Y. L. Lin, J. Control. Release, 2007, 120, 51-59.
19. J. H. Lee, K. E. Cha, M. S. Kim, H. W. Hong, D. J. Chung, G. Ryu and H. Myung, Toxicol. Lett., 2009, 190, 202-207.
20. J. Lazniewska, K. Milowska, M. Zablocka, S. Mignani, A.-M. Caminade, J.-P. Majoral, M. Bryszewska and T. Gabryelak, Mol. Pharm., 2013, 10, 3484-3496.
21. D. Wrobel, K. Kolanowska, A. Gajek, R. Gomez-Ramirez, J. de la Mata, E. Pedziwiatr-Werbicka, B. Klajnert, I. Waczulikova and M. Bryszewska, Biochim. Biophys. Acta, Biomembr., 2014, 1838, 882-889.
22. N. Sanz del Olmo, R. Carloni, A. M. Bajo, P. Ortega, A. Fattori, R. Gómez, M. F. Ottaviani, S. García-Gallego, M. Cangiotti and F. J. de la Mata, Nanoscale, 2019, 11, 13330-13342.
23. N. Sanz del Olmo, M. Maroto-Díaz, R. Gómez, P. Ortega, M. Cangiotti, M. F. Ottaviani and F. J. de la Mata, J. Inorg. Biochem., 2017, 177, 211-218.
24. J.-C. Rossi, B. Maret, K. Vidot, J.-P. Francoia, M. Cangiotti, S. Lucchi, C. Coppola and M. F. Ottaviani, Macromol. Biosci., 2015, 15, 275-290.
25. M. F. Ottaviani, M. Cangiotti, A. Fattori, C. Coppola, S. Lucchi, M. Ficker, J. F. Petersen and J. B. Christensen, J. Phys. Chem. B, 2013, 117, 14163-14172.
26. D. E. Budil, S. Lee, S. Saxena and J. H. Freed, J Magn. Reson., 1996, 120, 155-189.
27. M. F. Ottaviani, S. Bossmann, N. J. Turro and D. A. Tomalia, J. Am. Chem. Soc. , 1994, 116, 661-671.
28. M. F. Ottaviani, F. Montalti, N. J. Turro and D. A. Tomalia, J. Phys. Chem. B, 1997, 101, 158-166.
29. M. F. Ottaviani, R. Valluzzi and L. Balogh, Macromolecules, 2002, 35, 5105-5115.
30. D. Appelhans, U. Oertel, R. Mazzeo, H. Komber, J. Hoffmann, S. Weidner, B. Brutschy, B. Voit and M. F. Ottaviani, Proc. R. Soc. A, 2010, 466, 1489-1513.
31. M. F. Ottaviani, M. Cangiotti, A. Fattori, C. Coppola, P. Posocco, E. Laurini, X. Liu, C. Liu, M. Fermeglia, L. Peng and S. Pricl, Phys. Chem. Chem. Phys., 2014, 16, 685-694.
32. S. García-Gallego, M. Cangiotti, L. Fiorani, A. Fattori, M. a. Á. Muñoz-Fernández, R. Gomez, M. F. Ottaviani and F. Javier de la Mata, Dalton Trans., 2013, 42, 5874-5889.
33. Y.-H. Tang, M. Cangiotti, C.-L. Kao and M. F. Ottaviani, J. Phys. Chem. B, 2017, 121, 10498-10507.

34. L. J. Fox, R. M. Richardson and W. H. Briscoe, Adv. Colloid Interface Sci, 2018, 257, 1-18.
35. F. P. Seib, A. T. Jones and R. Duncan, J. Control. Release, 2007, 117, 291-300.
36. S. Kummar, M. Gutierrez, J. H. Doroshow and A. J. Murgo, Br. J. Clin. Pharmacol., 2006, 62, 15-26.
37. A. Janaszewska, M. Gorzkiewicz, M. Ficker, J. F. Petersen, V. Paolucci, J. B. Christensen and B. Klajnert-Maculewicz, Mol. Pharm., 2018, 15, 12-20.
38. L. D. Zorova, V. A. Popkov, E. Y. Plotnikov, D. N. Silachev, I. B. Pevzner, S. S. Jankauskas, V. A. Babenko, S. D. Zorov, A. V. Balakireva, M. Juhaszova, S. J. Sollott and D. B. Zorov, Anal. Biochem., 2018, 552, 50-59.
39. G. Battogtokh, Y. S. Choi, D. S. Kang, S. J. Park, M. S. Shim, K. M. Huh, Y.-Y. Cho, J. Y. Lee, H. S. Lee and H. C. Kang, Acta Pharm. Sin. B, 2018.
40. H. Zischka and C. Einer, Int. J. Biochem. Cell Biol., 2018, 102, 71-75.
41. S. Michlewska, M. Ionov, D. Shcharbin, M. Maroto-Díaz, R. Gomez Ramirez, F. Javier de la Mata and M. Bryszewska, Eur. Polym. J., 2017, 87, 39-47.
42. Y. Li and D. Ju, Adv. Exp. Med. Biol., 2018, 1048, 71-84.
43. S. Fulda, Front. Oncol., 2017, 7, 128-128.
44. I. X. McLeod and Y. He, Cell Mol. Immunol., 2010, 7, 104-107.
45. Y. Li, H. Zhu, S. Wang, X. Qian, J. Fan, Z. Wang, P. Song, X. Zhang, W. Lu and D. Ju, Theranostics, 2015, 5, 1363-1377.
46. T. P. Thomas, I. Majoros, A. Kotlyar, D. Mullen, M. M. B. Holl and J. R. Baker, Jr., Biomacromolecules, 2009, 10, 3207-3214.
47. S. T. Stern, P. P. Adiseshaiah and R. M. Crist, Part. Fibre Toxicol., 2012, 9, 20-20.

PAPER 3

Insight into the antitumor activity of carbosilane Cu(II)-metallodendrimers through their interaction with biological membrane models

Natalia Sanz del Olmo, Riccardo Carloni, Ana M. Bajo, Paula Ortega, Alberto Fattori, Rafael Gomez, Maria Francesca Ottaviani, Sandra García-Gallego, Michela Cangiotti, F. Javier de la Mata

Nanoscale, 2019, 11, 13330
https://doi.org/10.1039/c9nr03313k

Insight into the antitumor activity of carbosilane Cu(II)-metallodendrimers through their interaction with biological membrane models

Natalia Sanz del Olmo, [†a] Riccardo Carloni, [†b] Ana M. Bajo,[a] Paula Ortega,[ade] Alberto Fattori,[b] Rafael Gómez,[ade] Maria Francesca Ottaviani,[b] Sandra García-Gallego,[*ade] Michela Cangiotti,[*b] and F. Javier de la Mata[*ade]

a. Department of Organic and Inorganic Chemistry, and Research Institute in
b. Chemistry "Andrés M. del Río" (IQAR), University of Alcalá, Madrid, Spain. b. Department of Pure and Applied Sciences, University of Urbino "Carlo Bo", Urbino, Italy.
c. Department of Biology of Systems, Biochemistry and Molecular Biology Unit, University of Alcalá, Madrid, Spain
d. Networking Research Center on Bioengineering, Biomaterials and Nanomedicine
e. (CIBER-BBN), Spain.
f. Institute Ramón y Cajal for Health Research (IRYCIS).
g. [†]Both authors contributed equally to the work.
h. Corresponding authors.

Table of Content Graphic

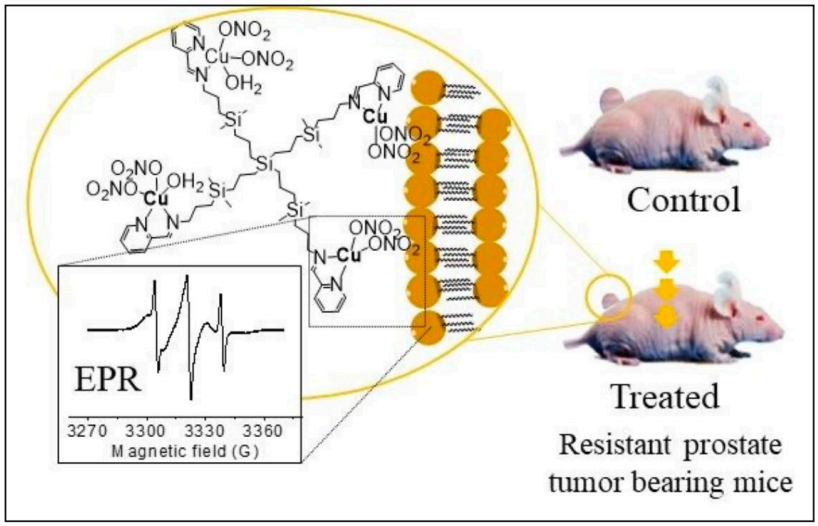

Abstract

Current cancer therapies present serious drawbacks including severe side-effects and development of drug resistance. Strategies based on nanosized metallodrugs combine the structural diversity and non-classical modes of action of metal complexes with the selectivity arising from the unique interaction of nanoparticles with biological membranes. A new family of water-soluble copper (II) carbosilane metallodendrimers was synthesized and characterized as a nanotechnological alternative to current therapies. The interactions occurring over time between

the dendrimers, at different generations (G_0 to G_2) and with different Cu(II) counter-ions (nitrate vs chloride), and cell-membranes models (cethyl-trimethylammonium bromide (CTAB) micelles and lecithin liposomes) were investigated using a computer-aided analysis of the electron paramagnetic resonance (EPR) spectra. The EPR analysis provided structural and dynamical information on the systems indicating that the increase in generation and the change of Cu(II) contra-ion -from nitrate to chloride- produces an increased relative amount and strength of interaction of the dendrimer with the model membranes. Interestingly, the stabilization effect produced a lower toxicity towards cancer cells. The cytotoxic effect of Cu(II) metallodendrimers was verified by an *in vitro* screening in a selection of tumor cell lines, revealing the impact of multivalency on the effectivity and selectivity of the metallodrugs. As proof-of-concept, first-generation dendrimer G_1-$Cu(ONO_2)_2$ was selected for in-depth *in vitro* and *in vivo* antitumor evaluation towards resistant prostate cancer. The Cu(II)-metallodendrimers produced a significant tumor size reduction with no signs of toxicity during the experiment, confirming their promising potential as anticancer metallodrugs.

1. Introduction

Cancer is the leading cause of death worldwide, accounting for 1 in 6 deaths globally.[1] This multifactorial disease arises from the transformation of normal cells into tumor cells as the result of the interaction of the patient´s genetic factors and a number of external agents, including physical, chemical and biological carcinogens. Consequently, each cancer displays its own fingerprint and a global antitumor therapy is still a difficult project to accomplish. Current cancer therapies, i.e. surgery, radiation and chemotherapy, often damage healthy tissues and display an incomplete eradication of the tumor cells. Until recently, cisplatin had been the most used anticancer drug in the world, administered alone or combined with other compounds. It presents extraordinary antitumor properties but also serious drawbacks such as the development of drug resistance and serious side-effects including anemia, neurotoxicity or nefrotoxicity.[2] Despite this duality, the prevalent success of cisplatin placed organometallic drugs on the forefront of anticancer therapy. The inclusion of metal atoms into a drug provides exceptional properties not achievable with organic compounds, such as an adjustable redox potential, photochemistry properties, variable kinetic rates, different geometries and stereochemical complexity. The design of anticancer metallodrugs nowadays focuses on new strategies and new formulations that explore non-classical modes of action, selective antitumor activity and immunogenic anticancer properties.[3] The broad structural diversity of metal complexes enables the development of new strategies with higher activity, selectivity and specificity. Cytotoxic metal-based compounds have been reported capable of light and electron-transfer triggered production of reactive oxygen species (ROS), release of NO or CO, and hypoxia- responsive agents.[4] Numerous metallodrugs based on other metals, besides platinum, have been reported with excellent therapeutic results, including palladium, gold, cobalt, ruthenium, gallium, tin and titanium.[3,5-7] In particular, copper-containing compounds are promising antitumor candidates due to:[8] i) the intrinsic biocompatibility, physiologically necessary to the organism, acting as a co-factor for many enzymes; ii) the ability to oscillate between Cu(II) and Cu(I) in biological medium, and the possibility to use this redox process as a targeting mechanism in cancer cells, with tumor hypoxia; iii) the ability of the reduced Cu(I) complexes to catalyze the formation of Reactive Oxygen and Nitrogen species (ROS and RNS) and induce pro-apoptotic oxidative stress; and iv) the possibility to modulate the affinity to ligands through the redox state of copper atoms. Several copper-based metallodrugs have showed their efficacy in animal models of cancer, including the two complexes in clinical trials Elesclomol (Cu(II)) and Casiopeína IIIia (Cu(I)).[8] Despite the successful application of cisplatin and its derivatives, the percentage of currently approved metallodrugs is still very low. Nevertheless,

metallodrugs present several limitations related to their low solubility, low bioavailability, low hydrolytic stability and serious side-effects, which can be overcome using nanotechnological tools. Nanotechnology appears as a revolutionary approach to improve cancer treatment, enabling new formulations for traditional antitumor drugs or establishing completely new strategies. As an example, several nanoparticle-based formulations of cisplatin have entered clinical trials, relying on polymers (AP5280), micelles (NC-6004) and liposomes (L-NDDP, SPI-077, Lipoplatin).[2] Nanotechnology provides the tools to selectively target chemotherapies to tumor cells, thus enhancing the efficacy and minimizing the toxicity and side-effects. On one side, the large surface area of the carriers enables the encapsulation or conjugation of the drug into the nanoparticles, increasing the drug´s therapeutic index. On the other side, the nanometric size of the nanoparticles provides a selective delivery and accumulation in the solid tumor through the enhanced permeability and retention effect.[9] This passive targeting mechanism relies on the defects in lymphatic drainage and the increased tumor vasculature permeability. Furthermore, the variability of nanoparticles supports personalized treatments and controlled drug release. The extraordinary biological properties of nanoparticles are directly related to their possibility of interacting with biological membranes.[10] Cell-nanoparticle interactions are modulated by both the physicochemical properties of the NPs – size, shape, surface charge, surface chemistry- and cell-specific parameters – cell type, cell cycle phase. Indeed, the size of NPs has a strong influence on the interactions with living cells, affecting uptake efficiency, internalization pathway selection, subcellular distribution and cytotoxicity. The thorough understanding of the NP/membrane interaction is an important feature in the design of effective antitumor agents with enhanced cellular uptake. Dendrimers, being the ultimate precision nanoparticles, have been reported to interact with membranes and cells.[11,12] Their monodisperse structure, highly branched nature and on-demand functionalization are valuable properties for their use as delivery vectors in nanomedicine. Unlike most of the commercially available dendritic macromolecules, carbosilane dendrimers present a hydrophobic scaffold. The multiple C-C and C-Si bonds provide high stability, extraordinary flexibility and enhance the interaction with biological membranes, thus enabling their applications as antiviral agents, antitumor drugs d non-viral vectors for nucleic acid delivery, among others.[13] Our group has recently described the use of carbosilane dendrimers as delivery agents of metallodrugs in cancer therapy. Ruthenium (II) η^6-p-cymene-based metallodendrimers displayed highly cytotoxic and selective activity towards a range of tumor cell lines, in comparison to non-tumor cells.[14,15] Exploring a different approach, more biocompatible than platinum and cheaper than ruthenium, we also described the synthesis of copper (II) metallodendrimers.[16] The dendritic precursors containing N,N- and N,O- donor ligands were efficient chelators of CuCl2, and the resultant metallodendrimers displayed in vitro cytotoxic activity towards human prostate (PC3) and human cervical (HeLa) cancer cell lines with IC50 values in the low micromolar range. However, these metallodendrimers were limited by their low solubility in water. Relying on a thorough multidisciplinary approach, we present water-soluble carbosilane Cu(II)-metallodendrimers, as a promising nanotechnological anticancer solution. The interactions occurring between the dendrimers and cell-membrane models were investigated over time by using a computer-aided analysis of electron paramagnetic resonance (EPR) spectra. The structural and dynamical information provided useful insight into the in vitro antitumor behavior in a selection of tumor cells. Finally, a mice model for resistant prostate cancer was used as in vivo proof-of-concept.

2. Methods

2.1 Synthesis and characterization of metallodendrimers

Compounds **1**-**3** were prepared from the iminopyridine ligand G_0-[NCPh(*o*-N)] (**I**) and dendrimers G_1-[NCPh(*o*-N)]$_4$ (**II**) and G_2-[NCPh(*o*-N)]$_8$ (**III**) previously reported,[17] according to the metal complexation reactions described below:

G_0-[NCPh(*o*-N)Cu(ONO$_2$)$_2$·H$_2$O] (1). A DMF solution of compound G_0-[NCPh(*o*-N)] **I** (96.4 mg, 0.37 mmol) was dropwise added to a solution of Cu(NO$_3$)$_2$·3H$_2$O (88.7 mg, 0.37 mmol) in DMF. After 12 h reaction at r.t. under stirring, solvent was evaporated to dryness and compound **1** was isolated as green solid (123.3 mg, 72%). $C_{15}H_{28}CuN_4O_7Si$ (468.0 g/mol). ESI-TOF: *m*/*z calc.* 325.12 uma; exp. 325.12 uma. E. A. (%): calc. C, 38.49; H, 6.03; N, 11.97. exp. C, 38.64; H, 5.44; N, 11.58. IR, *v*(C=N): 1646 cm^{-1}.

G_1-[NCPh(*o*-N)Cu(ONO$_2$)$_2$·H$_2$O]$_4$ (2). First generation metallodendrimer **2** was synthesized according to the same protocol described above, using the following reagents: G_1-[NCPh(*o*-N)]$_4$ **II** (69.2 mg, 0.068 mmol) and Cu(NO$_3$)$_2$·3H$_2$O (65.7 mg, 0.27 mmol). Compound **2** was isolated as green solid (102.5 mg, 82%). $C_{56}H_{100}Cu_4N_{16}O_{28}Si_5$ (1840.1 g/mol). E. A. (%): calc. C, 36.55; H, 5.48; N, 12.18. exp. C, 36.15; H, 5.17; N, 12.34. IR, *v*(C=N): 1646 cm^{-1}.

G_2-[NCPh(*o*-N)Cu(ONO$_2$)$_2$·H$_2$O]$_8$ (3). Second generation metallodendrimer **3** was synthesized according to the same protocol described above, using the following reagents: G_2-[NCPh(*o*-N)]$_8$ **III** (54.1 mg, 0.023 mmol) and Cu(NO$_3$)$_2$·3H$_2$O (44.5 mg, 0.18 mmol). Compound 3 was isolated as green solid (64.7 mg, 70%). $C_{128}H_{236}Cu_8N_{32}O_{56}Si_{13}$ (3992.9 g/mol). E.A.(%): calc. C, 38.50; H, 5.96; N, 11.23. exp. C, 38.91; H, 5.95; N, 11.97. IR, *v*(C=N): 1646 cm^{-1}.

2.2 Electronic Paramagnetic Resonance

The spectra were recorded immediately after the sample preparations (after 15 min stirring) and after an equilibration under stirring of 24 h. The concentrations used for model membranes were: Ligands and dendrimers: 0.5 mM in surface groups; CTAB or lecithin 25 mM; CAT12 0.125 mM. All solutions were prepared in PBS buffer (pH=7.2).

2.2.1 Analysis of the EPR spectra of the spin probe CAT12 inserted in model membranes in the absence and presence of Cu(II)- metallodendrimers.

The EPR spectra of the spin probe CAT12 were mainly constituted by two components. Each component was extracted and relatively quantified (in relative percentages, after double integration of the signals) by subtracting spectra containing these components in different relative amounts. The components were then computed by using the well-established procedure of Budil et al. to extract the following main parameters: (a) the Azz components of the A tensor for the coupling between the electron spin and the nuclear spin of the nitrogen nucleus of the nitroxide group. Axx=Ayy=6 G were assumed constant for simplicity. The increase in Azz reflects an increase in the polarity of the nitroxide environment. The accuracy is in the second decimal and is calculated by computation; (b) the correlation time for the rotational diffusion motion of the nitroxide group, τ, which measures the

microviscosity of the nitroxide environment, and, in turn, evaluates to strength of interaction occurring at the nitroxide site. The accuracy is ± 0.001 ns for the fast component and ± 0.01 ns for the slow component and is calculated by computation; (c) for the lecithin liposomes, it was necessary to include in the calculation also an order parameter S, due to the formation of a partially ordered phospholipid bilayer.

2.2.2 Analysis of the EPR spectra of Cu(II)-metallodendrimers in PBS.

In the case of the EPR spectra of Cu(II), similarly as CAT12, different components constitute the EPR spectra. To evaluate the relative percentages of these components and also obtain each component separately, a subtraction procedure was performed by subtracting one spectrum from another containing the different components at different extents. Then, each component was doubly integrated to obtain the effective intensity and evaluate the relative percentages. However, this procedure was successful in few cases because the line shape of the components changed from one to another sample. So, we started from these few cases to construct a rough calibration curve and, then, we used a simple parametrization based on the heights and widths of the peaks. Whenever it was possible, the components were extracted and computed using the same computation procedure used for computing CAT12 spectra (Budil et al.). In these cases, the main parameters for computation were: i) the gii and Aii components, which identify the type of coordination, e.g., the number of nitrogen and oxygen sites bonded to Cu(II), the geometry of the strength of the coordination bonds. In detail, an increase in the Aii values (mainly Azz) and a decrease in the gii values usually correlate with an increase in the number of complexed nitrogen sites, and/or an increased strength of interaction; ii) the correlation time for the rotational motion (τ), which measures the mobility of the complex, in turn related to the dendrimer branches flexibility and the coordination strength; an increase in τ corresponds to an increase in microviscosity, and, consequently, to a decrease in mobility; and iii) the line width, which increases if the local concentration of paramagnetic species increases.

2.3 Cell cultures

The metallodendrimers cytotoxicity was evaluated in a selection of cell lines, including a healthy cell line of human fibroblasts (142BR), and tumor cell lines from cervix (HeLa), normal and resistant breast cancer cells (MCF7 and HCC1806), advanced prostate cancer (PC3), and colorectal tumor (HT29). Further details about cell cultures are included in the Supporting Information.

2.4 In vitro cytotoxicity assays

Cells were seeded in 96-well plates (Nunclon Delta Surface, Thermo Fischer Scientific; 1.5x105 cells/ml) and grown for 24 h in complete medium (90 μl). Solutions of compounds were prepared by diluting a freshly prepared stock solution in water (compounds **1-3**) or DMSO (compounds **4-6**) of the corresponding compound in aqueous medium. Afterward, the intermediate dilutions of the compounds were serially diluted to the appropriate concentration (ranging from 0 to 100 μM) and the cells were incubated for another 24 h (0.6% (v/v) is the maximum final content of DMSO). DMSO at comparable concentrations did not show any effects on cell cytotoxicity. Cytotoxicity was determined using an MTT assay (MTT, 3-(4,5-dimethyl 2-thiazolyl)-2,5-diphenyl-2H-tetrazolium bromide). MTT (0.1 mg/ml solution) was added to the cells and the plates were further incubated for 1.5 h. Then the culture medium was removed and the purple formazan crystals

formed by the mitochondrial dehydrogenase and reductase activity of vital cells were dissolved in DMSO. The optical density, directly proportional to the number of surviving cells, was quantified at 570 nm (background correction at 620 nm) using a multiwell plate reader Multiskan FC and the fraction of surviving cells was calculated from the absorbance of untreated control cells. The Inhibitory Concentration 50 (IC_{50}) value indicates the concentration needed to inhibit the biological function of the cells by half and is presented as the mean (± standard error) of three independent experiments, each comprising three microcultures per concentration level.

2.5 Cell proliferation assays

PC3 cells ($2x10^5$ cells/cm^2) were grown in 6-well plates. After 24 h, the culture medium was removed and replaced with RPMI-1640 medium containing 0% FBS and 1% penicillin/streptomycin/amphotericin B for 16 h. Then, cells were subjected to different treatments for 24 h. During the last 30 min of incubation, cells were labeled with 10 μM bromodeoxyuridine (BrdU). Thereafter, cells were washed with PBS, fixed with ice-cold absolute ethanol, and stored at 20°C for 30 min. The fixative was removed by centrifugation and pellets were washed with PBS. DNA was partially denatured by incubation with 1 M HCl for 30 min at room temperature and then cells were washed three times with PBS containing 0.05% Tween-20 (pH 7.4) and 0.1% Bovine Serum Albumin (BSA). Cells were incubated with 20 ml of anti-BrdU monoclonal antibody linked to fluorescein isothiocyanate (FITC, BD Bioscience, San Agustin de Guadalix, Spain) for 30 min in the dark. For flow cytometry analysis, cells were stained with propidium iodide (PI) staining solution (50 mg/ml PI and 10 mg/ml RNase). The number of BrdU-positive cells was counted using flow cytometry.

2.6 Cell cycle evaluation

PC3 cells ($2x10^5$ cells/cm^2) were grown in 6-well plates. After 24 h, the culture medium was removed and replaced with RPMI-1640 medium containing 0% FBS and 1% penicillin/streptomycin/ amphotericin B for 16 h. After that, cells were subjected to various treatments for 8 h and subsequently washed with PBS and detached with 0.25% trypsin/0.2% EDTA. The cells were centrifuged at 500 g for 5 min at 4°C and the pellets were mixed with ice-cold 70% ethanol and then kept at 20°C for 30 min. After removing the ethanol by centrifugation, the pellets were washed with PBS and centrifuged again. The supernatants were discarded and the pellets were suspended in PBS, 0.2 mg/ml RNase A and 20 mg/ml PI before flow cytometry analysis.

2.7 Cell adhesion assays

Concentrated type-I collagen solution was diluted in 10 mM glacial acetic acid and coated onto 96-well plates for 1 h at 37 °C. Plates were washed twice with PBS (pH 7.4). Cells were harvested with 0.25% trypsin/0.2% EDTA and collected by centrifugation. They were resuspended in RPMI medium/0.1% (w/v) containing BSA (pH=7.4). Then, cells were cultured at a density of $2.5x10^4$ cells/100 ml. The assay was terminated at indicated time intervals by aspiration of the wells. Cell adhesion was quantified by adding 1 mg/ml MTT followed by 1 h incubation. Isopropanol (50 μl) was added to each well to dissolve the formazan precipitate and absorbance at 540 nm with a reference wavelength at 630 nm was measured.

2.8 Animals, xenografts and ex vivo assays

The Ethics Committee of Research and Animal Experimentation as Animal Welfare Body of the University of Alcalá (Madrid, Spain) in compliance with the article 33.1 of the Royal Decree 53/2013 of Spain and the European Directive 2010/63/EU on animal experimentation, has evaluated the present animal research project (code PROEX 194/16). The project has been performed at the Animal Research Center of the University of Alcalá (Legal registration code ES280050001165). After examining the application for evaluation, the Ethics Committee has considered that the research project and their procedures on animals are technically, ethically and methodologically suitable and therefore give this adequacy report, having regard to its possible effect on the animals used and having determined and evaluated the elements that best contribute to the replacement, reduction and refinement. In the same way, the Committee had been in charge of monitoring the project, in accordance to the article 38 of the mentioned Royal Decree. Athymic male nude mice (nu/nu) 5–6 weeks old were obtained from Harlan (Oxon, UK) and maintained in microisolator units on a standard sterilizable diet. Mice were housed under humidity- and temperature-controlled conditions and the light/dark cycle was set at 12 h intervals. For preparation of xenografts, PC3 cells were washed with PBS, detached with 0.25% trypsin/0.2% EDTA, centrifuged at 1,500 rpm and resuspended in fresh medium at 5×10^7 cells/ml. The cell suspension was mixed with Matrigel synthetic basement membrane (1:1, v/v, Becton Dickinson, Madrid, Spain) and then injected subcutaneously (s.c.) into the right flank of nude mice (5×10^6 cells/mouse). Xenografts were developed according to two different treatment groups: group I (ten mice), injection of non-treated PC3 cells; group II (ten mice), injection of PC3 cells treated with metallodendrimer **2** (3.4 μM, IC_{50}) for 24 h. None of the animals died during the experiment. The experiment was finished after 55 days. Animals were sacrificed through euthanasia by inhalation of CO_2. During the assay, the mice health was visually examined, their weight was controlled twice a week as well as any behavioral anomaly. The animals' condition was evaluated according to established tests on severity for the efficiency of new antitumor drugs, which were set as end point criteria. Tumor volume was measured with a microcaliper and calculated with formula (I):[18]

$$Volume = high \times wide \times deep \times 0.5236 \quad (1)$$

Statistical analyses

Results were expressed as the mean ± standard deviation or standard error of the mean (S.E.M.). Statistical significance was assessed through Bonferroni´s test for multiple comparisons after one or two-way analysis of variance (ANOVA). Differences were considered statistically significant *$p < 0.05$; **$p < 0.01$; ***$p < 0.001$.

3. Results and discussion

3.1 Synthesis and characterization of water-soluble Cu(II)- metallodendrimers and complexes

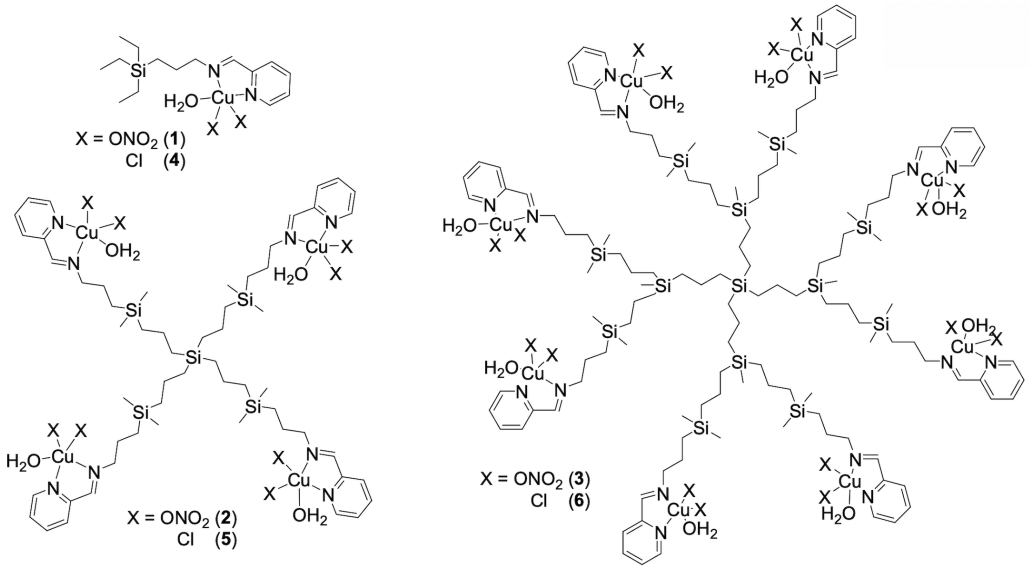

*Figure 1. Chemical structure of carbosilane Cu(II)-complexes and metallodendrimers comprising nitrate (**1-3**) or chloride (**4-6**) ligands.*

With the aim of accomplishing water-soluble Cu(II)- metallodendrimers with high cytotoxic activity, we closely examined those previously reported by our group.[16] We found out that the chloride ligands bound to the copper atoms hindered the adequate dissolution of the compounds in water. Consequently, we designed the alternative Cu(II)-complexes and metallodendrimers 1-3 (Figure 1), displaying nitrate ligands bound to the copper atoms. The NO_3 groups are known to be more labile than the Cl ligands, and are prompt to be released after dissolution in water creating an overall positive charge in the metallodendrimer. Compounds 1-3 were synthesized by a simple metal coordination reaction of $Cu(NO_3)_2{\cdot}3H_2O$ to the dendritic precursors Gn-[NCPh(*o*-N)]m (I-III),[14] using a molar ratio 1:1 between branch and Cu(II). The reactions proceeded at r.t. for 12 h, and the complex and metallodendrimers were isolated as dark green solids with high yields (>72%) using simple evaporation procedures. As expected, compounds 1-3 showcased enhanced solubility in water and high stability due to the chelate coordination of the Cu(II) atoms through the iminopyridine moieties. In solid state, the copper atom probably adopts a square- pyramidal geometry, completing the coordination sphere with three oxygen atoms from the two NO_3 ligands and one molecule of water (Figure 1). This geometry is in agreement with the experimental values obtained through elemental analysis and high resolution mass spectrum, and has been previously described for the similar compound $Cu(ppma)(NO_3)_2(CH_3OH)$ (pmma = *N*-(2- pyridylmethylene)aniline), which also displays a dark green color.[19] The same authors also demonstrated the influence of the ligands on the complex structure. The monomeric nature of $Cu(ppma)(NO_3)_2(CH_3OH)$ and $Cu(ppmma)Br_2$ (ppmma = phenyl-*N*- [(pyridine-2-yl)methylene]methaneamide) is transformed into μ-chloro bridged dimeric complexes in $[Cu(ppmma)Cl_2]_2$, due to the smaller nature of the chloride ligands.[20] The formation of dimeric complexes was also found after the reaction of $CuCl_2$ with the dendrimers Gn-[NCPh(*o*-OH)]m, leading to intermolecular (G_0) or intramolecular (G_1) species.[16] However, no signs of dimerization were observed in the present case for Gn-[NCPh(*p*-N)]m dendrimers. In solution, the

coordination of the metal atom to the dendritic ligands was confirmed by the shift of the intense FT-IR band at 1650 cm^{-1}, assigned to the stretching of the C=N bond, to values around 1645 cm^{-1} after coordination of the copper atom. Furthermore, the UV-Vis spectra in methanol or water of Cu(II)-complexes 1-3 displayed a charge transfer band LMCT at λmax = 300-400 nm. The band assigned to the d-d transitions could not be observed.

3.2 EPR evaluation of Cu(II)-metallodendrimers in the absence and presence of model biological membranes

Herein, we present the most relevant results accomplished from the EPR analysis of Cu(II)-metallodendrimers in the absence and presence of model biological membranes. We evaluated nitrate- containing complex and metallodendrimers Gn-Cu(ONO_2)$_2$ **1**-**3**, in comparison to the chloride analogues Gn-$CuCl_2$ **4**-**6**. The EPR technique has already demonstrated to be a powerful tool to provide structural and dynamical information on the dendrimers interactions with biological membrane models using spin probes and spin labels, including dendrimer/model membrane complexes,[21-24] as such as dendrimer/cells interactions.[11] Furthermore, the EPR analysis has allowed to differentiate the internal/external interacting sites of the dendrimers in respect to their availability for Cu(II) complexation, also characterizing interactions with cells.[12, 16, 25-31] Based on the previous EPR studies, a spin-probe was selected to provide specific information about the structure, the types and strengths of interactions in Cu(II)-metallodendrimers. The EPR study was carried out by analyzing the spectra of (a) Cu(II), which change as a function of Cu(II) concentration, monitoring the formation of different complexes in the absence and presence of the model membrane; (b) the selected spin probe, 4-(N,N-dimethyl-N-dodecyl)- ammonium-2,2,6,6-tetramethylpiperidine-1-oxyl bromide (CAT12), able to enter the model cell membrane with the C12 chain, while the positively charged CAT group stays at the membrane surface, monitoring the interactions. This probe was selected after an accurate screening since it demonstrated to well monitor the membrane structural variations in the absence and presence of the dendrimers. It is important to underline that this probe well mimics the surfactants constituting the model membranes. The CTAB micelles and egg lecithin (LEC) liposomes were selected because they represent the simplest membrane models useful to investigate the interacting ability of the dendrimers with cell membranes. The results obtained from Cu(II) and CAT12 are separately presented, but the conclusive discussion compares and integrates the information from both the points of view.

3.2.1. Analysis of the EPR spectra of the spin probe CAT12.

As schematically represented in Figure 2A, the CAT12 probe is entering the model cell membrane with the C12 chain, while the positively charged CAT group stays at the membrane surface, monitoring the interactions with the dendrimers. Figures 2B and 2C show the EPR spectra of CAT12 in two selected samples, respectively: G_0-Cu(ONO_2)$_2$ (**1**) in the presence of lecithin liposomes after 15 min of equilibration (Figure 2.B); and G2-Cu(ONO_2)$_2$ (**3**) in the presence of CTAB micelles after 24 h of equilibration (Figure 2.C). The spectra are constituted by two components. Arrows in the figures indicate the main features of these two components. The first component (termed "fast") is constituted by three narrow lines, which are characteristic of fast moving nitroxide radicals. Only fast moving nitroxide radicals are present in the dendrimer solution, in the absence of model membranes. Therefore, the fast component arises from a weak interaction of the radical groups, at the dendrimer external interface. The second component

(termed "slow") shows a partial resolution of the anisotropic components of the magnetic tensor g, for the coupling between the electron spin and the static magnetic field, and of the hyperfine coupling tensor A, for the coupling between the electron spin and the nuclear spin of the nitrogen of the nitroxide group. The resolution of the anisotropies occurs in case of slow motion of the nitroxide group, due to an increase of the local microviscosity, which, in turn, is related to interactions occurring at the nitroxide environment. In the case of LEC, the slow component was well distinguishable from the fast component due to a significant slowing down of motion. Conversely, for CTAB, the slow component barely differed from the fast component and only in the third line the two components became well distinguishable.

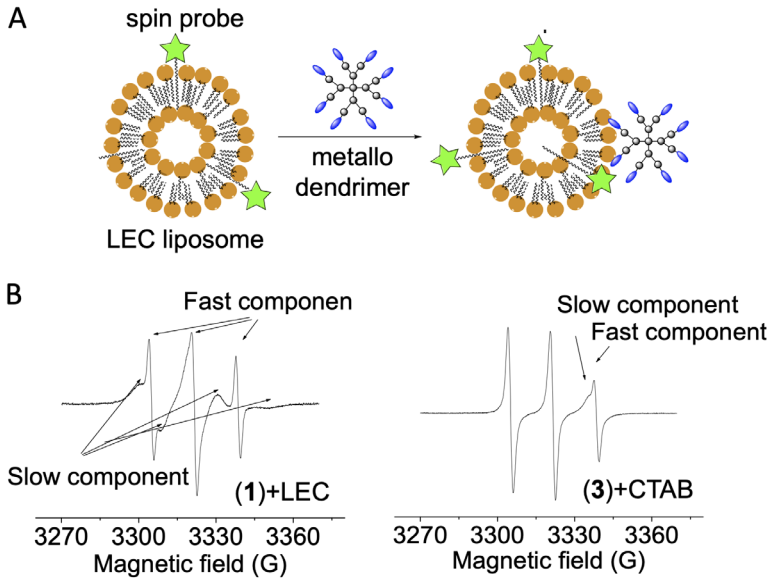

Figure 2. A) Cartoon showing the spin probe differently inserted into LEC liposomes before and after interaction with metallodendrimers. B) EPR spectrum of CAT12 in lecithin liposomes in the presence of G_0-$Cu(ONO_2)_2$ (1) after 15 min of equilibration; (c) EPR spectrum of CAT12 in CTAB micelles in the presence of G_2-$Cu(ONO_2)_2$ (3) after 24 h of equilibration. The arrows in the figures indicate the main features of the two components constituting the spectra. The spectra are normalized in height.

Table 1. *Main parameters of computation for selected samples. [a]Line width: 2.3 G. [b]Order parameter (S): 0.248*

Entry / Sample	Components	A_{zz} (G)	τ (ns)
1 / PBS	Fast (single)	38.58 / -	0.021 / -
2 / G_0-Cu$(ONO_2)_2$ (**1**)	Fast (single)	38.35 / -	0.039 / -
3 / G_2-$CuCl_2$ (**6**)	Fast + Slow[a]	38.34/36.76	0.040/1
4 / LEC	Fast + Slow[b]	38.56/37.1	0.027/2.86
5 / G_0-Cu$(ONO_2)_2$ (**1**) + LEC 15 min	Fast + Slow[b]	38.58/37.1	0.041/2.81
6 / G_2-$CuCl_2$ (**6**) + LEC 15 min	Fast + Slow	38.65/37.1	0.072/2.56
7 / CTAB	Fast + Slow	38.32/36.8	0.042/0.78
8 / G_0-Cu$(ONO_2)_2$ (**1**) + CTAB 15 min	Fast + Slow	38.35/36.4	0.042/0.76
9 / G_2-$CuCl_2$ (**6**) + CTAB 15 min	Fast + Slow	38.36/36.45	0.04/0.95

The slow components were extracted, relatively quantified from the overall EPR spectra and computed to extract the main parameters, *i.e*. the Azz component of the **A** tensor, whose increase reflects an increase in the polarity of the nitroxide environment; the correlation time for the rotational motion of the nitroxide group (τ), which measures the microviscosity of the nitroxide environment and enables the evaluation of the strength of interaction occurring at the nitroxide site. For the lecithin liposomes, it was necessary to include in the calculation the order parameter S, which indicates the formation of a partially ordered lipid bilayer. Figure S1 in the Supporting Information (SI) shows selected examples of experimental and computed fast and slow components, and Table 1 presents the main parameters of computation for selected samples. The EPR spectrum of the spin probe in buffer (PBS, pH=7.2) solution is constituted by a single fast component (Table 1, Entry 1). Interestingly, in the presence of compound G_0-Cu$(ONO_2)_2$ (**1**, Entry 2), the polarity (Azz) decreases and the microviscosity (τ) increases with respect to Entry 1, due to the interactions of the CAT12 probe with the dendrimer external surface. All dendrimers reveal spectra only constituted by a fast component, with the exception of G_2-$CuCl_2$ (**6**, Entry 3). In this case, a fraction of probes originates a fast component equivalent to the other dendrimers, but another fraction develops a slow component (τ = 1 ns) with a lower Azz value. Therefore, it can be concluded that compound **6** is able to host a fraction of spin probes inside the dendrimer in vicinity of low-polar sites. Liposomes (LEC, Entry 4 in Table 1) also show a fast component, but this component was computed using only slightly different Azz and τ parameters if compared to the PBS solution. This means that the fast-moving CAT group is located out of the external liposome interphase. The addition of liposomes to the dendrimer solution changes the fast component, which shows an increase in both polarity and microviscosity (Entries 5 and 6 in Table 1). The variation of τ of the fast component for the various dendrimer solutions containing LEC is better

visualized in Figure 3A. From this evaluation it can be concluded that the microviscosity: *i)* increases by adding the dendrimer to the liposomes, thus demonstrating the ability of the probe to monitor even a weak liposome-dendrimer interaction; *ii)* increases from G_0 to G_2, indicating that the increased density of surface groups provokes an increased strength of interaction between the liposomes and the dendrimers; *iii)* decreases from 15 min to 24 h of equilibration, indicating that, after 24 h, a structural modification occurs, which redistributes the probes in less viscous regions; *iv)* increases from Gn-Cu$(ONO_2)_2$ to Gn-$CuCl_2$, mainly for G_2 (compound **6** presents the highest decrease in mobility), indicating that the Cu(II) contra-ion plays a significant role in the dendrimer- liposome interaction. These results may be explained considering that, for the dendrimers in the absence of LEC, the probe partially enters the dendrimer structure feeling a lower polarity than in the buffer. Then, in the presence of both dendrimer and LEC, due to LEC-dendrimer interactions, the probe goes to the dendrimer/LEC interphase, in buffer pools squeezed between the two surfaces. The highest increase of the Azz and τ values was found for G_2-$CuCl_2$ – LEC (entry 6 in Table 1), due to a stronger bonding between this dendrimer and LEC.

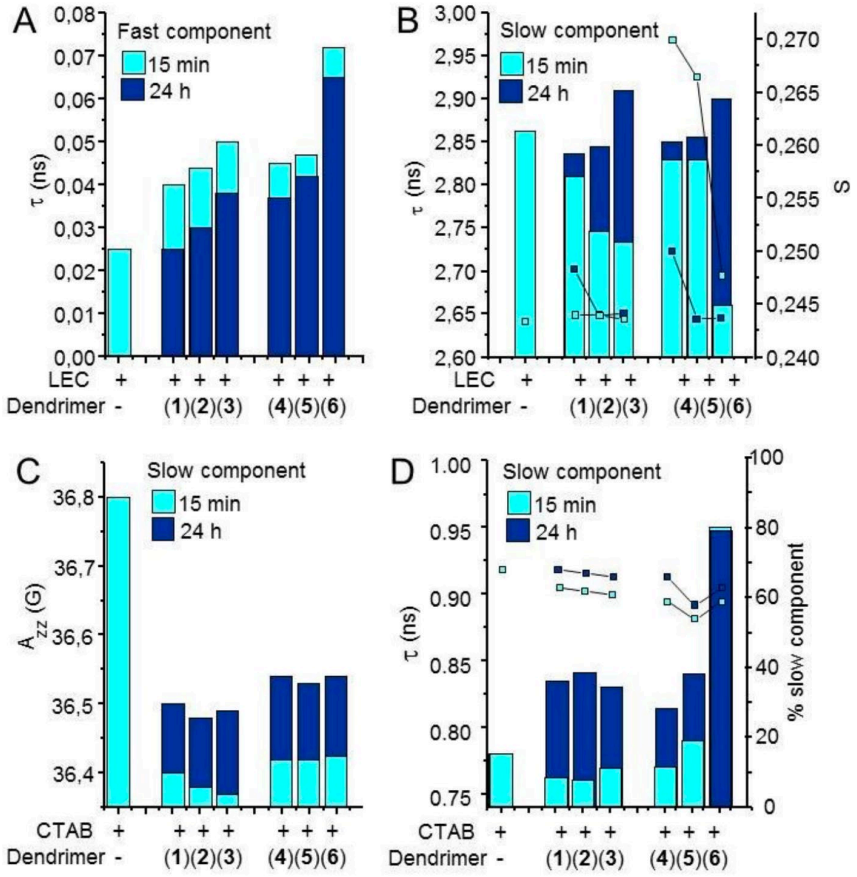

Figure 3. Change of EPR computation parameters for CAT12 in the presence of model membranes and the different metallodendrimers. A) Parameter measuring microviscosity (τ) for the fast component of the EPR spectra of liposomes in the absence and presence of the different dendrimers. B) Parameters measuring microviscosity (τ, bars) and order (S, dots) for the slow component of liposomes in the absence and presence of the various dendrimers. C) Variation of polarity (Azz) for the slow component of micelles in the absence and presence of the different dendrimers. D) Variation of microviscosity (τ, bars) and the relative percentage of the slow component (dots), for the slow component of CTAB micelles in the absence and presence of the

dendrimers. The accuracy of the parameters is 1%, as obtained from computation and by repeating the EPR measurements in the same experimental conditions.

For the fast component of CTAB sample (Table 1, Entry 7 vs 1)), the polarity slightly decreases while the microviscosity increases with respect to the PBS solution. The micelle structure is less packed than the liposome structure and the fast-moving CAT12 probes are partially trapped at the micelle surface. For the dendrimers solution containing CTAB, the fast component poorly changed when changing dendrimer generation or Cu(II) ligands (chloride or nitrate). Therefore, these results were not shown in Figure 3. For the slow components, compared to the fast ones in Table 1, it can be observed that, in all cases, the microviscosity significantly increases, the polarity decreases and for LEC samples it is necessary to include in the calculation also an order parameter S. Therefore, this slow component arises from probes inserted into the model membranes. A better insight into the changes in the liposome structure when interacting with the different dendrimers is obtained by comparing the microviscosity and the order parameters for CAT12 in the liposomes (slow component) in the absence and in the presence of the various dendrimers (Figure 3.B). Interestingly, the addition of any dendrimer, after 15 min, provokes a small but significant decrease in microviscosity and an increase in order. Such effects may be justified considering a variation of liposome structure, due to the interactions with the dendrimers, towards a flatter bilayer-like organization. This effect has been previously found for similar systems.[15-17] In the absence of the dendrimers, the positively charged CAT group electrostatically interacts with the negatively charged phosphate groups at the liposome surface; when the liposome-dendrimer interaction occurs, a perturbation of this interaction provokes a weakening of the interaction strength measured by τ. This perturbation is accompanied by the formation of a more flattened, bilayer-like, structuration of the phospholipids which is responsible of the increase in the order parameter. Interestingly, the ordering effect is more effective for chloride dendrimers than for nitrate ones and decreases from G_0 to G_2 and from 15 min to 24 h of equilibration. Conversely, for the freshly prepared samples (15 min), τ decreases (increase in mobility, decrease of microviscosity) with the increase in generation. This is well explained by an increased dendrimer-liposome interaction strength with generation, because this interaction perturbs the probe interactions with the liposome surface. After 24 h, the situation is inverted and G_2 dendrimers show an increased τ and almost no variation of order. This indicates a different mode of interaction between these dendrimers and liposomes: after 24 h, the probes heads better approach the interacting sites of the G2- dendrimers. It is useful to remember that the CAT12 probe mimics the surfactant components of the model membranes, and, therefore, we hypothesize that the interactions between the phospholipid heads are perturbed by the dendrimers, and preferential interactions, mainly electrostatic, but also ion-dipole, prevail between the phospholipid heads and the dendrimer surface. When CTAB micelles are used as model membranes, the addition of the dendrimer produces a decrease in polarity and an increase in microviscosity (Table 1, Entries 8 and 9 vs 7 for the slow component), as expected for a better insertion of the probe into the CTAB micelles due to the micelle-dendrimer interactions. However, to provide information about the interactions of the different dendrimers with CTAB micelles, it is useful to analyze, for the slow component, the variations of (a) the polarity parameter Azz (Figure 3C); (b) the microviscosity parameter τ (Figure 3D, left axis); and (c) the relative percentage of the slow component (Figure 3D, right axis). The highest decrease in polarity is produced after 15 min addition of nitrate dendrimers, but, interestingly, also the microviscosity slightly decreases. This is due to the insertion of the probe into the fluid micellar core provoked by the interaction of the micelle with

the dendrimer. This insertion also induces a decrease in the relative percentage of slow component since the solubility of the probe into the micelles decreases due to charge-repulsion effects at the level of the positively charged CAT groups. After 24 h of equilibration, all values increase in agreement with structural modifications over time as found for the liposomes. In the case of chloride dendrimers, the polarity and microviscosity are higher than for nitrate ones. Furthermore, as found with the liposomes, also in the presence of micelles the microviscosity significantly increases in the presence of the dendrimer G_2-$CuCl_2$ (**6**), which shows peculiar interacting properties. Also, the relative percentage of the slow component shows an inversion of the trend, since it decreases from **4** to **5**, but then it increases from **5** to **6**. This is probably because there is a balance among different competing forces and interactions, as such as the repulsion between the Cu^{2+} ions at the surface, increasing with generation, competing with the increased density of interacting sites at the dendrimer surface, also increasing with generation. In this balance of forces, it is expected that the G_1 dendrimers provides less selectivity for the interaction with the cell membrane, but this turns out to a higher selectivity and cytotoxicity towards cancer cells with respect to normal cells, due to the high concentration (proliferation) of cancer cells and cell membrane degradation. Indeed, it was already found that a stronger interaction with the cell membrane surface, both external and internal, prevents the dendrimer from moving into the cell causing damage.[19]

3.2.2 Analysis of the EPR spectra of Cu(II)-dendrimer complexes.

The analysis of the spectra at 298K of the paramagnetic Cu(II) contained in the dendrimers, in the absence and presence of model membranes and in the absence of other EPR probes, revealed interesting features characteristic of a distribution of Cu(II) ions at different coordination states and in different environments. As example, Figure 4A displays the spectrum of complex G_0-$Cu(ONO_2)_2$ (**1**) in the presence of CTAB micelles, resulting from the superposition of three different components: *(i)* a fast component, constituted by 4 hyperfine lines due to the coupling of the electron spin with the Cu nuclear spin. The separation between the lines corresponds to the hyperfine coupling constant (<A>= (Axx+Ayy+Azz)/3). By comparing the Aii components with those found in the literature for similar systems,[11, 12, 16, 21-31] it is possible to get information on the type of coordination, mainly referred to the number of nitrogen and oxygen sites bonded to Cu(II), the geometry of the complex and the strength of the coordination bonds. Another parameter informative of the coordination type is the central magnetic field of the 4 lines which changes accordingly to a variation of the <g> = (gxx+gyy+gzz)/3 value, where gii are the main components of the **g** tensor for the coupling between the electron spin and the magnetic field; *(ii)* a Slow component, whose presence is evidenced by the high field peak, corresponding to the perpendicular component (X and Y) after resolution of the anisotropies due to slow rotational motion of the Cu(II) complex. In other simple words, when the rotational motion is slowed down, the gii and Aii components resolved in the spectrum, giving rise to differently separated (Axx, Ayy, Azz) and differently positioned (different magnetic fields corresponding to gxx, gyy, gzz) peaks; *(iii)* an EPR signal constituted by a single unresolved broad peak, centered at a lower magnetic field and indicated as component O. This signal arises from a preferential binding of Cu (II) with oxygenated sites and appears in PBS solutions, probably due to the binding of Cu(II) with phosphate groups and water molecules. A cartoon summarizing these three interactions is depicted in Figure 4B.

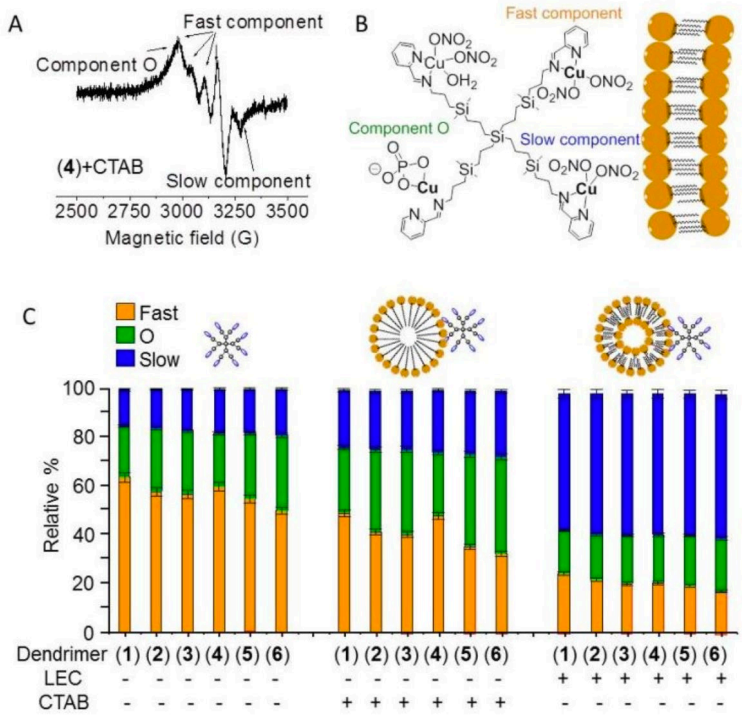

Figure 4. A) Experimental EPR spectrum of metal complex 4 in the presence of CTAB micelles (normalized height), selected as example. B) Cartoon showing the different Cu(II) environments found in the presence of liposomes. C) Relative percentages of the spectral components of the dendrimers in the absence and presence of the model membranes.

Interestingly, the relative percentages of the three components (fast, slow and O) changed among the different dendrimers and in respect to the absence and presence of CTAB micelles and LEC liposomes (Figure 4C). In the absence of model membranes: *i)* the fast component prevailed, and the slow component was present at a low extent; *ii)* by increasing generation, the slow component and component O increased in relative percentage at the expenses of the fast component. The increase in slow component is well accounted by the increase in dendrimer-branches density, while the increase in component O indicates that the ions approach each other and need the "protection" of the solvent to avoid repulsions; *iii)* from nitrate to chloride dendrimers, the fast component decreases in favor of the slow one and component O. This indicates a higher stability of the $CuCl_2$ complex in the dendrimers if compared to the $Cu(ONO_2)_2$ one. The addition of the model membranes produces an alteration of the components distribution. In the presence of CTAB, the slow component and component O relatively increase at the expenses of the fast component, indicating an interaction between the dendrimers and the micelles. However, the Cu (II) ions, being positively charged, do not directly interact with the positively charged micelle surface and solvent and contra-ion protection remains, mainly at the higher generations. Nevertheless, the trends as a function of generation and Cu(II) contra-ions are similar as in the absence of micelles. In the presence of lecithin liposomes, the relative increase in percentage of slow component was really significant, indicating that the dendrimers and the liposomes interact well with each other. The variation as a function of the Cu(II) contra-ions was still present, as in the absence of liposomes, indicating that the contra-ions are playing a role in the dendrimer-liposome interactions. The components were extracted and computed (Figure S2 in the SI), using the following parameters: *i)* the gii and Aii components, which identify the type and

strength of Cu(II) coordination; *ii)* the correlation time for the rotational motion (τ), which measures the mobility of the complex, in turn related to the branches flexibility and the coordination strength; and *iii)* the line width, which increases if the local concentration of paramagnetic species increases. The analysis of the main parameters of computation, compared to those found in the literature for similar systems,[11, 12, 16, 21-31] provides the following information: The fast component arises from a rhombically-distorted square planar Cu-N2O2 geometry in solution, where the 2 nitrogen sites are from the Py group.[12, 31] In the presence of CTAB, the signal barely changed with the increase in generation or from nitrate to chloride, as the fast mobility did not allow the contra-ions to remain in vicinity of the Cu(II). However, a small increase of <A> was observed in the few cases in which <A> was measurable for the blanks (from 55-56 G in the blank to 58.5 G), accounting for a weak interaction between the fast-moving dendrimer-complexed ions and the micelles. Interestingly, in the presence of LEC, in spite of the low relative percentage of the fast components, their computations indicate a different behavior for G_0-$CuCl_2$ (**4**) with respect to G_0-$Cu(ONO_2)$ (**1**) (Fig S2). The Cl complexed ions show, on the basis of the parameters (higher <A>, lower <g>, and higher τ and line width), a stronger interaction than the NO_3 derivative. This fact indicates that the contra-ions are partially retained at the dendrimer-liposome interface when interaction occurs, as depicted in Figure 4B. The fraction of dendrimer-complexed ions trapped in slow mobility at the model membrane surface generates the slow component. The low resolution of the magnetic components in the spectra decreased the accuracy in the calculations, but the parameters still indicate the presence of a Cu-N_2O_2 coordination, even if the increased differentiation among the gii values with respect to the fast component suggests an increased orthorhombic distortion of the complex. Overall, EPR analysis concludes that the change in generation and Cu(II) contra-ion produces a variation in the interactions of the dendrimer with the model membrane. While G_0-$CuCl_2$ (**4**) shows the strongest interactions, G_2-$CuCl_2$ (**6**) shows a preferential complexation and a higher stability of the formed complex.

3.3 In vitro and ex vivo antitumor behavior of Cu(II)- metallodendrimers

3.3.1. Cytotoxicity screening in a selection of tumor cells.

An effective cancer therapy should display cytotoxic activity towards tumor cells, without affecting healthy tissues, and it would be desirable that it has a broad antitumor behavior against several types of cancer.

Table 2. In vitro antitumor results of Cu(II)-complexes and metallodendrimers 1-6 in a selection of healthy and tumor cells.

Compound	*Cu(II) atoms*	*Cytotoxicity* [IC_{50} (μM) ± SD]					
		HeLa	MCF7	PC3	HCC1806	HT29	142BR
1	1	47.3 ± 3.8	30.2 ± 5.1	21.8 ± 2.0	17.3 ± 2.5	32.7 ± 0.9	60.9 ± 0.3
2	4	1.7 ± 0.5	2.1 ± 0.2	3.4 ± 0.2	1.9 ± 0.1	9.3 ± 0.5	7.7 ± 0.4
3	8	5.2 ± 0.3	9.6 ± 1.4	2.5 ± 0.3	0.69 ± 0.03	12.3 ± 0.2	6.1 ± 0.1
4	1	7.6 ± 0.3[a]	44.9 ± 5.1	9.7 ± 3.1[a]	13.9 ± 1.2	44.9 ± 1.8	>100
5	4	10.5 ± 0.3[a]	5.4 ± 0.1	4.5 ± 0.9[a]	2.2 ± 0.1	0.5 ± 0.1	73.4
6	8	10.0 ± 2.6[a]	7.7 ± 0.4	12.5 ± 0.3[a]	7.3 ± 0.1	1.8 ± 0.9	83.6

[a]Previously published results.[16]

In order to evaluate the selectivity and versatility of the Cu(II)- complexes and metallodendrimers **1**-**6**, we performed MTT assays in a selection of cell lines, including a healthy cell line of human fibroblasts (142BR), and tumor cell lines from cervix (HeLa), normal and resistant breast cancer cells (MCF7 and HCC1806), advanced prostate cancer (PC3), and colorectal tumor (HT29). Table 2 summarizes the experimental IC_{50} values, after 24 h treatment with compounds **1**-**6**.

The monometallic G_0-Cu(ONO_2) (**1**) displayed a selective cytotoxic action towards all tumor cell lines in comparison to 142BR fibroblasts, with IC_{50} values ranging 17.3-47.3 μM. Significantly lower IC_{50} values (<12.3 μM) were obtained with first- and second-generation nitrate metallodendrimers **2** and **3**, revealing the impact of multivalency on the cytotoxic behavior. As an example, the cytotoxicity towards HeLa cell line exerted by the tetrametallic dendrimer G_1-Cu(ONO_2) (**2**) was 28 times higher than that shown by monometallic **1**. Importantly, resistant tumor cells were effectively killed by Cu(II)-metallodendrimers, with IC_{50} values below 3.4 μM in prostate PC3 and below 1.9 μM in breast HCC1806. The exchange of the nitrate ligands for chloride ones in Gn-$CuCl_2$ (**4**-**6**) decreased not only the water-solubility but also the general cytotoxic activity, probably explained by the higher stability at the cell membrane as EPR assays showed. Nitrate moieties are more labile ligands than chlorides, providing the overall metallodendrimer with cationic properties that induce a more effective destabilization of the cell membrane. Consequently, the selectivity towards tumor cells also increased, when compared to non-tumor cells. Interestingly, chloride metallodendrimers **5** and **6** appeared as promising antitumor agents towards colorectal cancer HT29 cells. They were highly cytotoxic – 90 times more effective than the monometallic compound **4** – as well as highly selective - 150 times more effective in HT29 compared to control fibroblasts. The selectivity was not observed with the nitrate counterparts **2** and **3**. The promising antitumor activity of pyridine-containing Schiff- base copper(II) complexes has been previously reported. As an example, the complex [Cu(5-Cl-pap)(OAc)(H_2O)]·2H_2O bearing the ligand *N*-2-pyridiylmethylidene-2-hydroxy-5-chloro-phenylamine induced growth inhibition and apoptosis in MCF-7 cell line, with IC_{50} = 20.7 μM after 24 h treatment, similar to cisplatin (IC_{50} = 25.0 μM).[32] This compound rapidly increased intracellular copper levels and induced an antitumor effect via the mitochondrial pathway. Under similar conditions, monometallic complex **1** displayed comparable cytotoxicity to cisplatin while first-generation metallodendrimer **2** revealed a 12-fold decrease in IC_{50} values compared to this well- known metallodrug. Our results confirm the impact of the additional ligands (nitrate, chloride) on the cytotoxicity of the iminopyridine Cu(II) complex, as previously showed by Roy *et al*.[33] In this case, the higher cytotoxic effect was found with the chloride-bearing [Cu(Pyimpy)Cl2], which exhibited IC_{50} values around 5 μM in MCF-7, PC3 and HEK 293 cells, again significantly lower values than cisplatin (64.13, 80.00 and 78.3 μM, respectively). This compound inhibited the tumor growth on a breast tumor rat model and inhibited some antioxidant enzymes responsible for drug resistant condition in tumor tissues. The results shown in Table 2 again confirm the crucial role of both the carbosilane dendritic scaffold and the metal complex multivalency in the antitumor behavior. The lipophilic skeleton favors the interaction with cell membranes and low-generation dendrimers (mainly G_1) are enough to exert a potent antitumor action, unlike similar phosphorous dendrimers which need higher generations.[34] The IC_{50} values obtained for Cu(II) metallodendrimers in PC3 cell line are lower to those reported for the analogous Ru(II) metallodendrimers, with IC50 7.8 μM for first-generation dendrimer.[15] Considering the easier synthetic protocol towards Cu(II) metallodendrimers, as well as the cheaper and less toxic properties of copper compared to ruthenium, these compounds appeared as promising agents in cancer therapy. In particular, the potent activity and selectivity

of compound **2** in the different cell lines evaluated, as well as its water-solubility, encouraged us to pursue further evaluation of its antitumor behavior. While developing effective antitumor treatments is extremely important, it is particularly mandatory for resistant prostate cancer patients – currently only treated with palliative therapy. In consequence, we selected PC3 cell line as proof-of-concept to analyze the effect of compound **2** on tumor cell proliferation, adhesion and cell cycle.

3.3.2 Effect on PC3 cell proliferation, adhesion to Collagen type- I and cell cycle.

In tumor cells, the proliferation deregulation and the suppression of cell apoptosis may lead to an uncontrolled tumor invasion and metastasis. The effect of metallodendrimer **2** on these crucial events was evaluated through flow cytometry. PC3 cells were exposed to compound **2** (3.4 μM, IC50) for 24 and 48 h and subsequently their proliferation was evaluated through bromodeoxyuridine (BrdU) assay, in comparison to non-treated cells (Figure 5.A). After 24 h treatment, compound **2** produced a significant inhibition of cell proliferation (5.8 %), which was further increased to 16.3 % after 48 h treatment. These results were further explained through the analysis of PC3 cell cycle, using flow cytometry and propidium iodide staining. After 24 h treatment, small signs of apoptosis (2.6% cells in SubG0) and no appreciable change in cell cycle were observed. However, a longer exposure time increased apoptosis level to 8.9% (48 h) and 17% (72 h). Interestingly, metallodendrimer **2** reduced PC3 cell adhesion - 48% decrease- to type I collagen (Figure 5B). This type of collagen is the major component of bones, an organ in which 80% of cases of metastasis occur. In this assay, compound **2** was used at concentration 20% below the IC50. In conclusion, treatment with compound **2** could make it difficult to adhere to this secondary tissue and thus reduce metastatic behavior of prostate cancer. It can be observed that, compared to its Ru(II) counterpart,[15] compound **2** needs a longer cell exposure to achieve comparable inhibition of proliferation and cell cycle deregulation. This could indicate a different mechanism of action depending on the metal complex bound to dendritic scaffold.

3.3.3 Ex vivo antitumor behavior towards resistant prostate cancer.

The antitumor behavior of metallodendrimer 2 was assayed in an experimental *ex vivo* mice model of human prostate cancer. Besides its promising *in vitro* cytotoxicity, compound 2 inhibited proliferation of PC3 cells and decreased their adhesion to collagen type-I. PC3 cells treated with compound 2 at 3.4 μM (IC_{50}) for 24 h, and untreated cells as control, were subcutaneously inoculated into two groups of immune depressed mice. Tumor growth was measured once a week for 55 days (Figure 5 D-E). During half the span of the experiment, no significant differences were observed between control and treated mice.

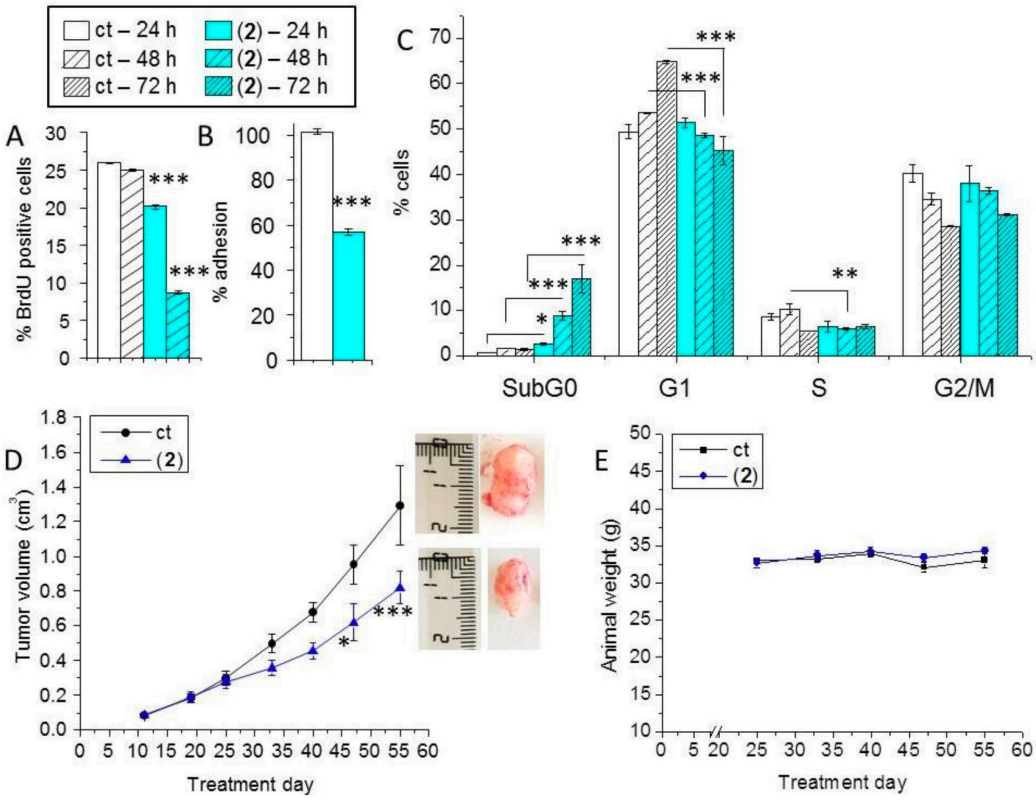

*Figure 5. In vitro and ex vivo evaluation of G_1-$Cu(ONO_2)_2$ (**2**) effect over (A) PC3 cell proliferation; (B) adhesion to collagen type-I; and (C) distribution (% PC3 cells) in each phase of cell cycle after 24, 48 and 72 h treatment with metallodendrimer **2** (3.4 μM). Results are the mean ± SEM of 3 independent assays. (D) Tumor growth on athymic mice generated by PC3 cells pretreated with metallodendrimer **2** (3.4 μM, blue), in comparison to non-treated cells (control, black). Insert picture shows final tumor size for mice injected with pretreated and non-treated PC3 cells. (E) Changes on the animals' body weight during treatment (same color code as in D). Data represents mean ± SEM. ***p < 0.001, **p < 0.01, *p < 0.1 vs control (10 mice).*

Nevertheless, the inhibition of tumor growth started to be apparent from day 25, reaching up to 37% smaller tumor size in comparison to non-treated group at the end of the experiment. No significant changes were found in the animals' weight after treatment, in comparison to the non-treated group, and observed mild growth inhibition in our mice model is quite promising and further studies will be pursued to improve the inhibition levels.

4. Conclusions

Nanosized metallodrugs are an alternative strategy that can overcome current limitations of antitumor therapies. The copper(II) carbosilane dendrimers presented here revealed promising features, including *i)* high stability, arising from the strong carbosilane scaffold and the chelating effect of iminopyridine ligands; *ii)* high solubility in water, due to the labile character of nitrate ligands; *iii)* batch-to- batch consistency and exceptional structure-to-property relationship, according to their monodisperse dendritic structure achieved through a controlled synthetic process; *iv)* and a unique interaction with cell membranes, arising from the nanometric size and the multivalency, which depends on the dendrimer generation as well as the Cu(II) counterion.

This extraordinary interacting ability of the dendrimers towards cell membranes, which can further explain their potent and selective cytotoxic behavior, was thoroughly studied by analyzing the EPR spectra of both the Cu(II) complexes and the CAT12 spin probe, able to insert into the membrane of the models – namely CTAB micelles and lecithin liposomes-, mimicking the behavior of the membrane lipidic components. Indeed, valuable structural and dynamical information on the systems was extracted from EPR spectra computations. For the CAT12 spin probe, the spectra were constituted by a fast component, where the CAT group was at the external interface, and a slow component, with the CAT groups inserted in the head groups interface. Both components were affected by the model membranes added to the dendrimers, mainly by the liposomes, showing an increase in the parameters measuring the microviscosity, the order and the percentage of interacting probes. Mainly electrostatic and ion-dipole interactions were hypothesized and the results indicated that the increase in generation and the chloride Cu(II) contra-ion, if compared to nitrate, increased the relative amount and the strength of interaction of the dendrimer with the model membranes. Stable complexes were formed preferentially with the G_2-$CuCl_2$ dendrimer. The liposomes changed structure towards a bilayer-like conformation upon interacting with the dendrimers. The spectra of Cu(II) were constituted by three components: a fast and a slow component for a Cu-N_2O_2 coordination (two nitrogen sites and two oxygen sites) and a further component for a Cu-O_4 coordination (interactions with oxygenated molecules or ions in solution). The Cu-N_2O_2 coordination strongly prevailed in the presence of liposomes. G_0-$CuCl_2$ complex shows the strongest interactions, but, again, G_2-$CuCl_2$ shows a preferential complexation and a higher stability of the formed complex. Surprisingly, this stabilization effect led to a lower *in vitro* cytotoxicity but also a higher selectivity towards cancer cells. Prioritizing the water-solubility as well as the high cytotoxicity towards tumor cells including resistant cell lines, we demonstrated that nitrate-containing copper(II) carbosilane metallodendrimers decreased resistant prostate tumor growth in a xenograft mice model, with long-term survival of the animals and no signs of toxicity. Further studies to gain a deeper understanding of the mechanism of action of copper(II) metallodendrimers are currently being performed.

Conflicts of interest

"There are no conflicts to declare".

Acknowledgements

This work was supported by grants from CTQ2017-86224-P (MINECO), Consortium IMMUNOTHERCAN-CM B2017/BMD-3733 (CAM) and project SBPLY/17/180501/000358 JCCM. CIBER-BBN is an initiative funded by the VI National R&D&i Plan 2008–2011, Iniciativa Ingenio 2010, Consolider Program, CIBER Actions and financed by the Instituto de Salud Carlos III with assistance from the European Regional Development Fund. N. S.O. wishes to thank JCCM for a predoctoral fellowship. This article is based upon work from COST Action CA 17140 "Cancer Nanomedicine from the Bench to the Bedside" supported by COST (European Cooperation in Science and Technology).

Supporting Information

Materials

Cell lines. All cell lines were obtained from the American Type Culture Collection (Manassas, VA). The selection included a healthy cell line of human fibroblasts (142BR), and tumor cell lines from cervix (HeLa), normal and resistant breast cancer cells (MCF7 and HCC1806), advanced prostate cancer (PC3), and colorectal tumor (HT29). General culture protocol: cells were grown routinely in a

corresponding media, containing 10% fetal bovine serum (FBS) and 1% penicillin/streptomycin/amphotericin B (Life Technologies, Barcelona, Spain) at 37 °C and 5% CO2. After the cells reached 70–80% confluence, they were washed with phosphate buffered saline (PBS), detached with 0.25% trypsin/0.2% ethylenediaminetetraacetic acid (EDTA) and seeded at 3-4 x 104 cells/cm2. The culture medium was changed every 3 days. RPMI-1640 (PC3, HCC1806), DMEM (MCF7, HeLa), Mccoy´s 5 Medium (HT29) were the media used. For 142BR fibroblasts used as control, MEM Eagle with 15% FBS, glutamine, non-essential aminoacids and antibiotics.

Methods

Elemental analysis. C, H and N elemental analysis assays were performed on a Leco elemental analyzer CHNSO-932.

Mass Spectrometry. The exact mass measurements of the molecular ion were made in an Agilent 6210 TOF LC/MS mass spectrometer.

Infrared Spectroscopy. The infrared spectra have been performed in a PerkinElmer Frontier spectrometer.

UV-Vis Spectroscopy. The ultraviolet-visible spectra have been performed on a PerkinElmer Lambda 35 spectrometer.

Electronic Paramagnetic Resonance. EPR spectra were recorded by means of an EMX- Bruker Spectrometer operating at X band (9.5 GHz) and interfaced with a PC (software from Bruker). The temperature was controlled with a Bruker ST3000 variable- temperature assembly cooled with liquid nitrogen.

Flow cytometry. Flow cytometry experiments were performed using FACSCalibur cytometer (BD Bioscience). The results were analyzed using Cyflogic v1.2.1 program.

Figures

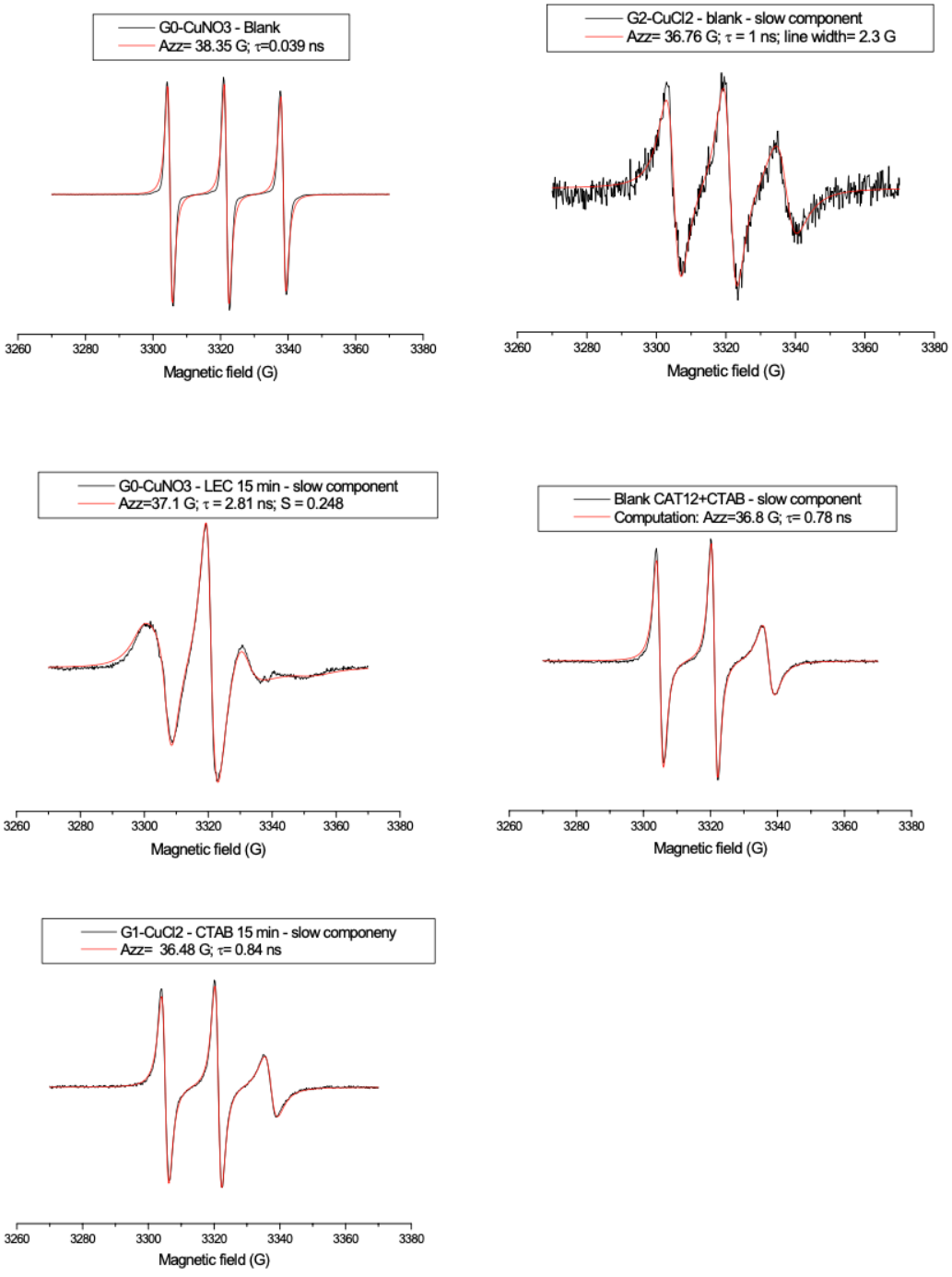

Figure S1: Selected examples of experimental and computed fast and slow components extracted by subtraction of spectra. In the legend, the main parameters of computation are reported. The spectra are normalized in height.

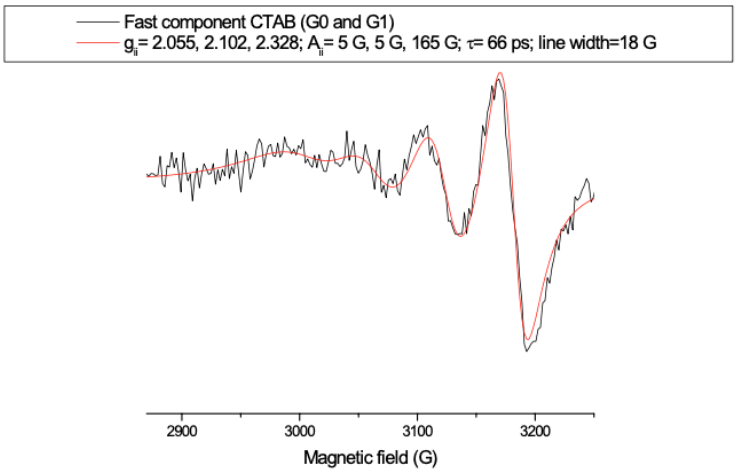
Fast component CTAB (G0 and G1)
g_{ii}= 2.055, 2.102, 2.328; A_{ii}= 5 G, 5 G, 165 G; τ= 66 ps; line width=18 G
2900
3000
3100
3200
Magnetic field (G)

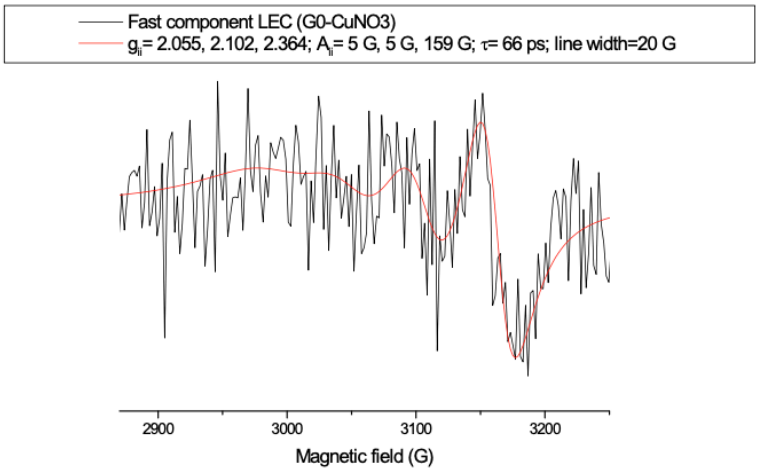
Fast component LEC (G0-CuNO3)
g_{ii}= 2.055, 2.102, 2.364; A_{ii}= 5 G, 5 G, 159 G; τ= 66 ps; line width=20 G
2900
3000
3100
3200
Magnetic field (G)

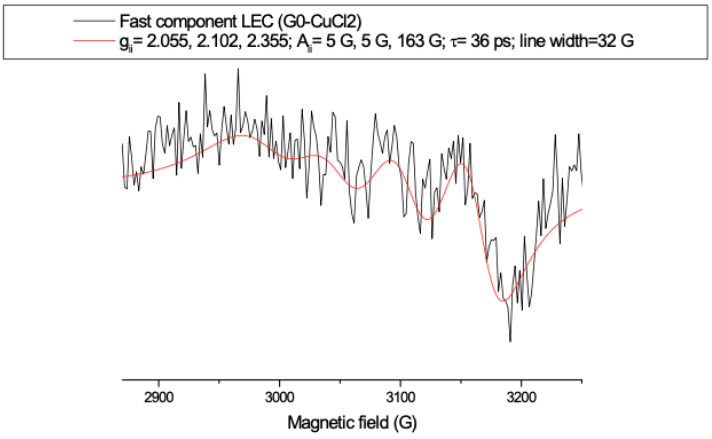
Fast component LEC (G0-CuCl2)
g_{ii}= 2.055, 2.102, 2.355; A_{ii}= 5 G, 5 G, 163 G; τ= 36 ps; line width=32 G
2900
3000
3100
3200
Magnetic field (G)

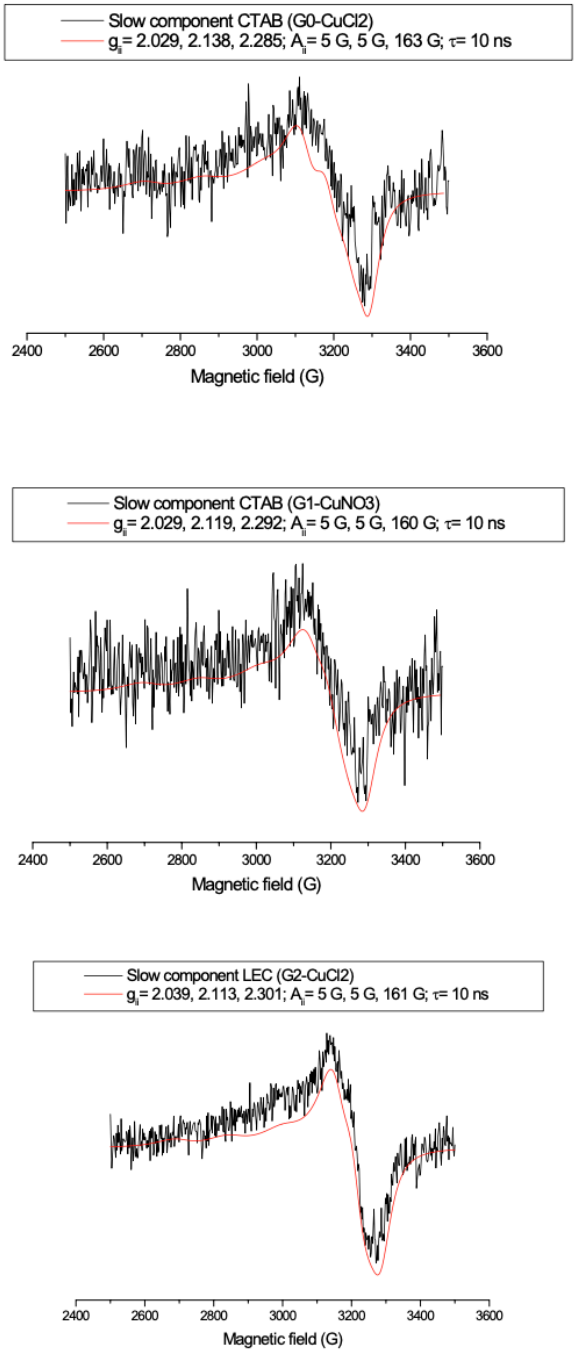

Figure S2. Best computations of fast and slow components of Cu(II) in the studied systems using the subtraction procedure. Figure legends report the main parameters of computation. The spectra were normalized in height.

References

1. www.who.int, (accessed 2018-11-26, 2018).
2. X. Duan, C. He, S. J. Kron and W. Lin, Wiley interdisciplinary reviews. Nanomedicine and nanobiotechnology, 2016, **8**, 776-791.
3. K. Seiji and C. Angela, *Current Topics in Medicinal Chemistry*, 2012, **12**, 219-235.
4. P. Zhang and P. J. Sadler, *European Journal of Inorganic Chemistry*, 2017, **2017**, 1541-1548.
5. Y. Ellahioui, S. Prashar and S. Gómez-Ruiz, *Inorganics*, 2017, **5**, 4.
6. L. Ignacio Esteban, C.-V. Juan Fernando, V. Ana Laura Di and E. Susana Beatriz, *Current Medicinal Chemistry*, 2017, **24**, 112-148.
7. S.J.Tan,Y.K.Yan,P.P.F.LeeandK.H.Lim,*Future Medicinal Chemistry*, 2010, **2**, 1591-1608.
8. R. Tabti, N. Tounsi, C. Gaiddon, E. Bentouhami and L. Désaubry, *Med. Chem. (Los Angeles)*, 2017, **7**, 875-879.
9. H. Maeda, *Journal of Controlled Release*, 2012, **164**, 138- 144.
10. L. Shang, K. Nienhaus and G. U. Nienhaus, *Journal of nanobiotechnology*, 2014, **12**, 5.
11. E. Andreozzi, A. Antonelli, M. Cangiotti, B. Canonico, C. Sfara, A. Pianetti, F. Bruscolini, K. Sahre, D. Appelhans, S. Papa and M. F. Ottaviani, *Bioconjugate Chemistry*, 2017, **28**, 524-538.
12. M. F. Ottaviani, N. El Brahmi, M. Cangiotti, C. Coppola, F. Buccella, T. Cresteil, S. Mignani, A. M. Caminade, J. P. Costes and J. P. Majoral, *RSC Advances*, 2014, **4**, 36573- 36583.
13. J. Sánchez-Nieves, P. Ortega, J. Cano, R. Gómez and F. J. d. l. Mata, in *Dendrimer Chemistry: Synthetic approaches towards complex architectures*, eds. M. Malkoch and S. García-Gallego, Royal Society of Chemistry, 2019.
14. M. Maroto-Díaz, B. T. Elie, P. Gómez-Sal, J. Pérez-Serrano, R. Gómez, M. Contel and F. Javier de la Mata, *Dalton Transactions*, 2016, **45**, 7049-7066.
15. M. Maroto-Díaz, N. Sanz del Olmo, L. Muñoz-Moreno, A. M. Bajo, M. J. Carmena, R. Gómez, S. García-Gallego and F. J. de la Mata, *Eur. Polym. J.* , 2019, **113**, 229-235.
16. N. Sanz del Olmo, M. Maroto-Díaz, R. Gómez, P. Ortega, M. Cangiotti, M. F. Ottaviani and F. J. de la Mata, *Journal of Inorganic Biochemistry*, 2017, **177**, 211-218.
17. M. Maroto-Díaz, B. T. Elie, P. Gomez-Sal, J. Perez-Serrano, R. Gomez, M. Contel and F. J. de la Mata, *Dalton Trans.*, 2016, **45**, 7049-7066.
18. M. M. Tomayko and C. P. Reynolds, *Cancer Chemotherapy and Pharmacology*, 1989, **24**, 148-154.
19. Y.-I. Kim, H. W. Lee, J.-H. Kim, S. Y. Park and S. K. Kang, *Acta Crystallographica Section E*, 2009, **65**, m1362.
20. H. W. Lee, N. Sengottuvelan, H.-J. Seo, J.-S. Choi, S.-K. Kang and Y.-I. Kim, *Bulletin of the Korean Chemical Society*, 2008, **29**, 1711-1716.
21. M. F. Ottaviani, P. Matteini, M. Brustolon, N. J. Turro, S. Jockusch and D. A. Tomalia, *The Journal of Physical Chemistry B*, 1998, **102**, 6029-6039.
22. M. F. Ottaviani, R. Daddi, M. Brustolon, N. J. Turro and D. A. Tomalia, *Langmuir*, 1999, **15**, 1973-1980.
23. M. F. Ottaviani, P. Favuzza, B. Sacchi, N. J. Turro, S. Jockusch and D. A. Tomalia, *Langmuir*, 2002, **18**, 2347-2357.
24. K. N. Kontogiannopoulos, A. Dasargyri, M. F. Ottaviani, M. Cangiotti, D. Fessas, V. P. Papageorgiou and A. N. Assimopoulou, *Langmuir*, 2018, **34**, 9424-9434.
25. M. F. Ottaviani, M. Cangiotti, A. Fattori, C. Coppola, P. Posocco, E. Laurini, X. Liu, C. Liu, M. Fermeglia, L. Peng and S. Pricl, *Physical Chemistry Chemical Physics*, 2014, **16**, 685- 694.
26. M. F. Ottaviani, M. Cangiotti, A. Fattori, C. Coppola, S. Lucchi, M. Ficker, J. F. Petersen and J. B. Christensen, *The Journal of Physical Chemistry B*, 2013, **117**, 14163-14172.
27. M. F. Ottaviani, S. Bossmann, N. J. Turro and D. A. Tomalia, *Journal of the American Chemical Society*, 1994, **116**, 661- 671.
28. M. F. Ottaviani, F. Montalti, N. J. Turro and D. A. Tomalia, *The Journal of Physical Chemistry B*, 1997, **101**, 158-166.
29. M. Galan, J. Sanchez-Rodriguez, M. Cangiotti, S. García- Gallego, J. L. Jimenez, R. Gomez, M. F. Ottaviani, M. A. Muñoz-Fernández and F. J. d. l. Mata, *Current Medicinal Chemistry*, 2012, **19**, 4984-4994.

30. S. García-Gallego, M. Cangiotti, L. Fiorani, A. Fattori, M. a. Á. Muñoz-Fernández, R. Gomez, M. F. Ottaviani and F. Javier de la Mata, *Dalton Transactions*, 2013, **42**, 5874- 5889.
31. Y.-H. Tang, M. Cangiotti, C.-L. Kao and M. F. Ottaviani, *The Journal of Physical Chemistry B*, 2017, **121**, 10498-10507.
32. Z.-Y. Ma, X. Qiao, C.-Z. Xie, J. Shao, J.-Y. Xu, Z.-Y. Qiang and J.-S. Lou, *Journal of Inorganic Biochemistry*, 2012, **117**, 1-9. Chakraborty, P. Kumar, K. Ghosh and P. Roy, *European Journal of Pharmacology*, 2010, **647**, 1-12.
33. N. El Brahmi, S. El Kazzouli, S. M. Mignani, E. M. Essassi, G. Aubert, R. Laurent, A.-M. Caminade, M. M. Bousmina, T. Cresteil and J.-P. Majoral, *Molecular Pharmaceutics*, 2013, **10**, 1459-1464.

CHAPTER 2

A potential Wilson's Disease treatment

1 - INTRODUCTION AND GOALS

1.1 Introduction

1.1.1 History of Wilson's Disease

"There is a most unusual thing
Known as the Kayser Fleischer ring.
In fact, it is so very rare
Few doctors know when it is there.
So, whether brown or whether green
It's very, very seldom seen.
Had it been red, or even pink,
Why then I really dare to think
That most physicians would perchance
See it with a perfunctory glance.
So, let us deem it right and proper
To seek this little ring of copper. "

The Lancet, 1969, II, 740.

The first evidence of the disease dates back to 1912, when Dr. Samuel Alexander Kinnier Wilson, after whom the pathology is named, described in the magazine "*Brain*" four cases of patients who presented liver cirrhosis accompanied by a peculiar retinal degeneration.

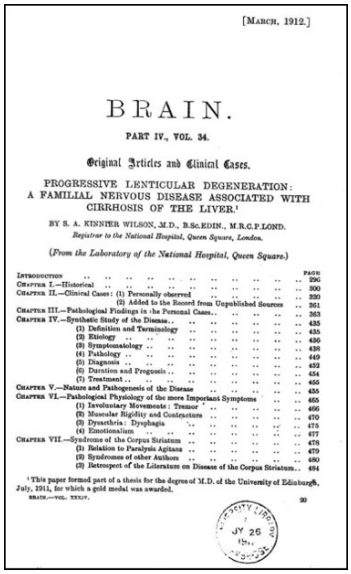

[MARCH, 1912.]

BRAIN.

PART IV., VOL. 34.

Original Articles and Clinical Cases.

PROGRESSIVE LENTICULAR DEGENERATION: A FAMILIAL NERVOUS DISEASE ASSOCIATED WITH CIRRHOSIS OF THE LIVER.[1]

BY S. A. KINNIER WILSON, M.D., B.Sc.EDIN., M.R.C.P.LOND.

Registrar to the National Hospital, Queen Square, London.

(From the Laboratory of the National Hospital, Queen Square.)

[1] This paper formed part of a thesis for the degree of M.D. of the University of Edinburgh, July, 1911, for which a gold medal was awarded.

Figure 1.1 Original frontispiece of the article in Brain magazine, https://doi.org/10.1093/brain/34.4.295

Wilson's studies allowed the identification of the pathological process of cerebral-tissue degeneration. However, the details of the disease remained unnoticed for 40 years, until Cumings published his work "*The copper and iron content of brain and liver in the normal and in hepatolenticular*

degeneration", [13] inextricably linking the progress of the pathology with the systemic accumulation of copper. Cumings proposed the first hypothesis of drug treatment: this involved taking BAL (dimercaprol), a chelating agent that would improve patients' prognosis. It wasn't until 1960, however, that penicillamine was introduced as a detoxifying agent for excessive copper. This avoided the painful injections that BAL entailed, being taken orally.

To date, the genetics and biochemistry of Wilson's disease are clear, but drug therapy remains unsatisfactory: the numerous side effects of penicillamine and BAL, still in use, leave the field open to research. [1]

1.1.2 Symptoms

Wilson's disease is a rare autosomal recessive genetic disorder of copper metabolism, which affects one in 30,000 people. [2] Its symptoms, caused by the accumulation of copper in tissues, tend to appear in patients from 10 to 30 years old, leading, if not treated, to the patient's death.

Clinical manifestations of the disease include liver disorders, hemolysis, neurological, and psychiatric problems. Hepatic involvement can range from being asymptomatic to presenting in the form of hepatomegaly, hepatitis, liver failure, jaundice, and cirrhosis. The Kayser-Fleischer ring, the typical copper deposit in the cornea, is visible in 50/60% of patients. [3]

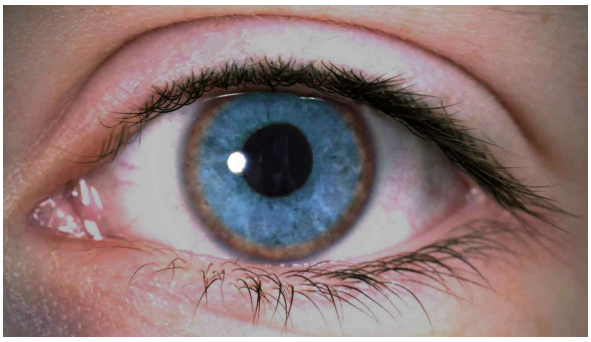

Figure 1.2 Kayser Fleischer ring

Neurological manifestations occur typically during adolescence or in the third decade of life. The neurological presentation frameworks have been classified into three subgroups:

1. **Akinetic-rigid syndrome,** similar to Parkinson's disease, characterized by bradykinesia, cognitive alterations, mood disorders.
2. **Pseudo-sclerosis,** characterized by ataxia and tremors with focal thalamic lesions.
3. **Dystonia,** present in patients with dyskinesia, dysarthria, and personality disorders which correlates with focal lesions of the putamen and pale globe.

In pediatric patients, early neurological and/or psychiatric manifestations are usually subtle: personality changes, mood changes (depression, psychosis), poor school performance, inability to perform activities that require good hand-eye coordination, and alterations in writing. [4]

1.1.3 Pathogenesis and diagnosis

The gene responsible for Wilson's disease was detected almost simultaneously in three different laboratories. The gene, ATP7B, is highly expressed in the liver, kidneys, and placenta. This encodes

a transmembrane transport protein called ATP7B-transporter, also named Wilson disease protein. [5]

Such protein has a dual function:

- **Synthetic**: promotes the transport of copper in the trans-Golgi compartment for its subsequent incorporation into ceruloplasmin.
- **Excretory**: expels copper through the bile ducts when it is in excess.

Copper is absorbed through the diet in the stomach and duodenum, and transported via portal vein to the liver, which represents the most important organ for its homeostasis. [6] [7]

The expression of malfunctioning Wilson proteins results in an accumulation of copper in the liver, leading to the hepatic and neurological symptoms described above. The diagnosis of Wilson's disease is based on a series of clinical and laboratory tests, and can be carried out at any age and regardless of gender. A prompt diagnosis of Wilson's disease is of fundamental importance: in fact, an early started treatment prevents the onset of serious and irreversible lesions related to the accumulation of copper. Tests investigate the urinary excretion of copper over 24 hours, its liver concentration, the free copper concentration in serum, and the levels of ceruloplasmin. Genetic screening tests for the Wilson protein gene mutation are available, and in case of positive result, the disease can be confirmed through copper concentration tests. In the event of a negative outcome, however, its presence cannot be excluded.

The detection of the Kayser-Fleisher ring significantly helps to direct the suspects to Wilson's disease. As already mentioned, however, this cannot be considered a gold standard. In fact, as for today there is no real gold standard for diagnosis. [8]

1.1.4 Treatment

Treatment of Wilson's disease consists in increasing urinary copper excretion or reducing intestinal absorption. The success rate of therapy increases the sooner it is diagnosed.

Table 1: *Currently Available Treatments for Wilson´s Disease*

Drug	Description
D-Penicillamine	**D-Penicillamine, a metabolite of Penicillin, chelates copper, forming stable complexes excreted in the urine. Most treated patients show improvement in 6/8 months, although it can take up to 12 months to see a tangible effect. To increase drug tolerability, it is necessary to start with low doses, and then gradually increase. About 30% of treated patients are affected by hypersensitivity reactions such as fever, rash, lymphadenopathy. These symptoms are usually transient, but discontinuation of therapy and treatment with corticosteroids may occasionally be necessary. The main side effects of penicillamine include skin grazes, joint problems, and Lupus-like immune-mediated responses. Myasthenia gravis and Goodpasture syndrome often occur during the treatment. Despite**

	being the chosen therapy to date, 50% of patients report aggravation of neurological symptoms. [9]
Trientine	Trientine is a copper chelator, which increases urinary excretion. It is used as an alternative to penicillamine, when it fails due to established tolerance. It is less toxic than penicillamine and the worsening of neurological symptoms following administration settles around 26%.
Zinc	Zinc increases intestinal levels of metallothionein, a protein with a high affinity for copper. This is captured before the absorption and excreted via feces. It's the best therapy for patients who have not yet developed symptoms, for maintenance therapy, and for patients with severe neurological symptoms, since the aggravation of these is just 10%, compared to 50% and 26% of the above described therapies. Zinc is generally well tolerated, the most frequent problem is gastric irritation, which can be overcome by replacing zinc sulfate with zinc acetate or by taking the drug after breakfast. [10]
Tetrathiomolybdate	Tetrathiomolybdate has two mechanisms of action: It complexes copper in the intestinal lumen, preventing its absorption; it promotes the complexion of copper with serum albumin. The use of Tetrathiomolibdate is recommended in patients with neurological symptoms, but given the poor clinical experience, it is still little used and not available in Europe or United States. The side effects observed so far are few and far between: these include anemia, thrombocytopenia, and neutropenia. [8]
Combined Therapies	The combined therapy of zinc and penicillamine is not recommended. It is a contradiction to administer a metal and a similar metal chelator together. Such treatment does not lead to an advantage, as clinically proven. An experimental combined treatment recently put into practice consists of administering trientine and zinc for 8 weeks, then moving on to zinc maintenance therapy alone. In patients with hepatic decompensation, it has been shown to be an effective treatment, with a significant reduction in liver fibrosis.
Liver transplantation	Transplantation in Wilson's disease patients is problematic yet necessary in cases of liver failure. The greatest risk is linked to the high probability of hemorrhage in patients affected by the disease: the damage to the bone marrow prevents the correct synthesis of

	blood clotting factors. Furthermore, most of the anesthetics used in surgery are metabolized by cytochrome p450, which, being located in areas of the liver already damaged, may not adequately perform its duty, leading to systemic toxicity. [11]
Diet	**Foods rich in copper such as chocolate, offal, nuts, mushrooms, etc. should be avoided, especially during the first few years after diagnosis. Domestic water should be kept under control as it may contain high levels of heavy metals including copper.**

1.2 Goals

A side-effects free treatment for Wilson's disease is currently not available. Our goal is to synthetize a fully biocompatible selective chelator for Cu(II), to remove the excessive copper from the body. Such molecule is aimed to selectively bind copper, forming a water-soluble complex, and then being excreted from the organism via urines or stool. In particular, the real improvement would come from a chelating agent which, unlike the currently available options, avoids the recontribution of copper from the liver to the brain, worsening the psychiatric symptoms of the disease. [12]

1.3 Methodology

The synthesis of the following compound was performed at the Leibniz Institute for polymer research, Dresden, under the guidance of Prof. Dietmar Appelhans.

PPI dendrimers present complexing properties for bivalent metals, naturally acting like a Schiff-base donor in the inner shell. Such skeleton was therefore selected as a promising starting point for the development of a chelating agent.

To maximize the effectiveness of the skeleton itself, generation 4 was selected. Such dimension shows the best compromise between flexibility of the structure, internal room of the dendrimer and steric hinderance of the superficial groups.

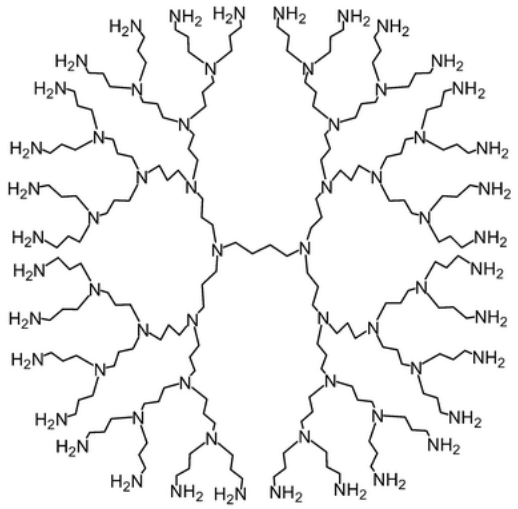

PPI-G4

Figure 1.3 Generation 4 Polypropilenimine Dendrimer Skeleton

A further step for the efficiency of the new drug, was taken by decorating the external layer of the dendrimer with DOTA groups, forming an amide bond between terminal dendrimer -NH_2 and one of the carboxylic groups of the DOTA itself. Such a molecule was chosen due to its ability to selectively chelate Cu(II), out of all the metal ions present in the human body fluids.

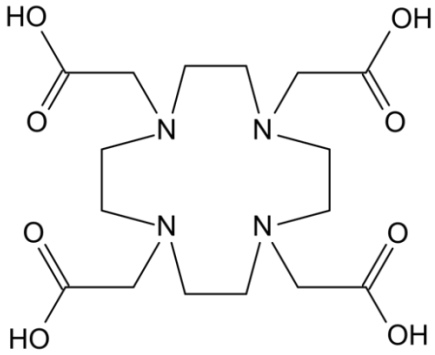

Figure 1.4 DOTA group.

Six units of DOTA were bound on each dendrimer, to reach the desired balance between stoichiometry of chelation and toxicity of the molecule. Indeed, the hydrogens of the remaining -NH_2 groups of the dendrimer skeleton were substituted by maltose groups, in order to reduce the toxicity of the positively charged amines, turning the dendrimer into a glycodendrimer.

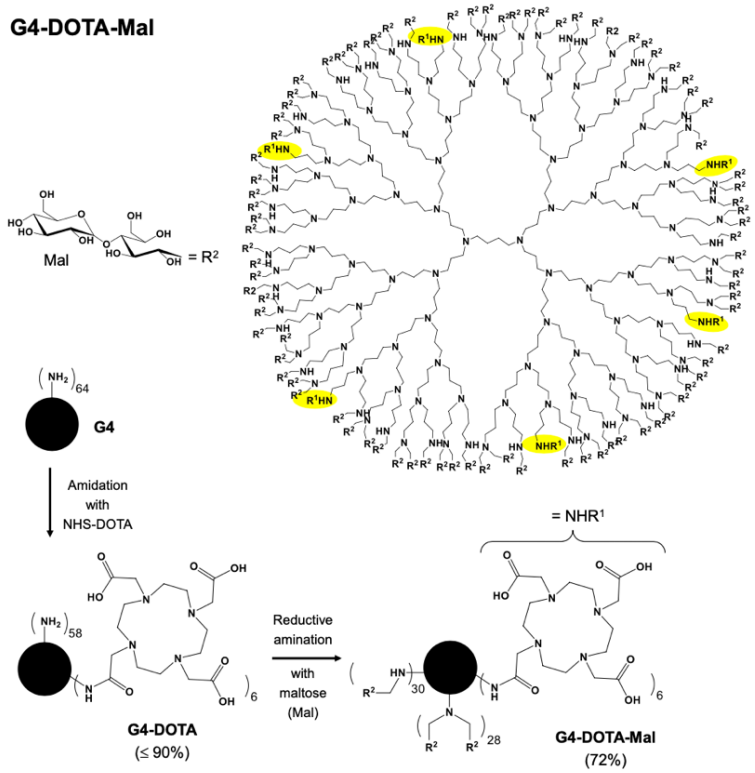

Figure 1.5 Synthetic pathway for the PPI-G4-DOTA-DS-mal (figure 1, article 4)

The synthesis is described in details in paper 4.

1.4 Results

Our work originated a paper, published on Langmuir, which can be found in the following pages. The results of the study are going to be briefly summarized in the next section.

2 - RESULTS AND DISCUSSION

An EPR study was conducted to study the interaction of the previously described dendrimer with model membranes. The preliminary knowledge of the mode of interaction of such dendrimers with cells was essential to move on to *invitro* studies. Furthermore, EPR technique allowed to characterize the complexation mechanism of Cu(II), being this paramagnetic.

G4-DOTA-Mal glycodendrimer was therefore analyzed in the absence and in the presence of both Cu(II) ions at various concentrations and different types of liposomes.

The chosen liposomes, prepared from 1,2-dimyristoyl-sn-glycero-3-phospho-rac-(1-glycerol) sodium salt (DMPG), 1,2-dimyristoyl-sn- glycero-3-phosphocholine (DMPC) and 1,2-Diacyl-sn-glycero-3-phosphocholine 3-sn-Phosphatidylcholine (egg lecithin), had previously been analyzed by DLS, ZP and cryo-TEM, proving unilamellar and non-aggregating.

2.1 Spin Probe Studies

With the help of the CAT12 spin probe, it was possible to characterize the non-covalent, surface drive interactions between dendrimers and liposomes in the absence of Cu(II), as shown in figure 2.1

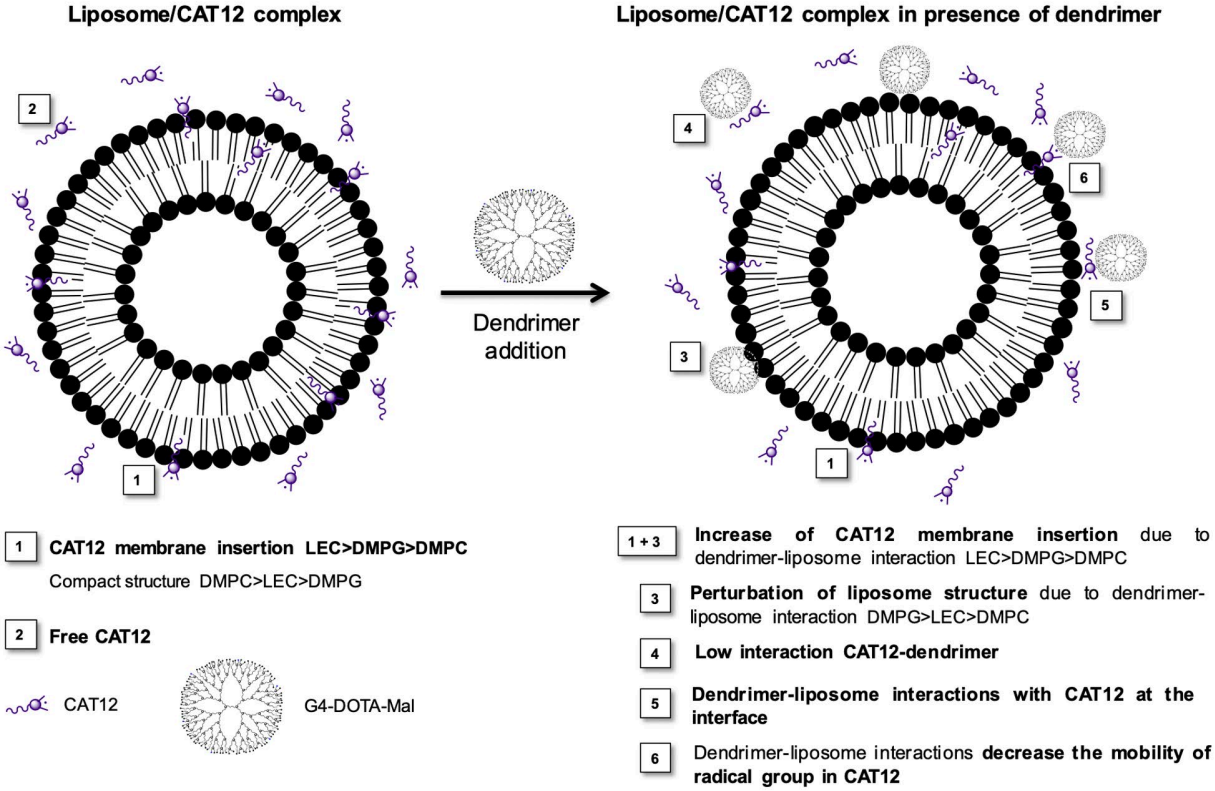

Figure 2.1 Dendrimers-liposomes interaction in the presence of CAT12 (article 4, scheme 1)

Electrostatic, H-bond and ion-dipoles interaction were present with every type of liposome. In particular, ionic interaction with the anionic DMPG surface were very evident. Due to the heterogeneous nature of LEC liposomes surface, stable adducts were formed with the dendrimer, despite being these poorly interacting.

2.2 Cu(II) Studies

EPR spectra in the presence of Cu(II) show how the newly synthetized glycodendrimer is an excellent chelator of copper. Two coordination mechanisms are highlighted by such study:

a. A highly distorted square planar Cu-N_2O_2 coordination, with two nitrogens belonging either to the DOTA structure or to the inner nitrogens of the dendritic scaffold;
b. A Cu-O_4 component, with copper surrounded by water molecules only.

Cu-N_2O_2 coordination prevailed in all cases, even in the case of a Cu(II) amount as high as 28 mM, as shown in Figure 2.2. Cu-O_4 coordination only arises in the presence of very high amount of copper. The system has therefore a high chelation potential before saturation.

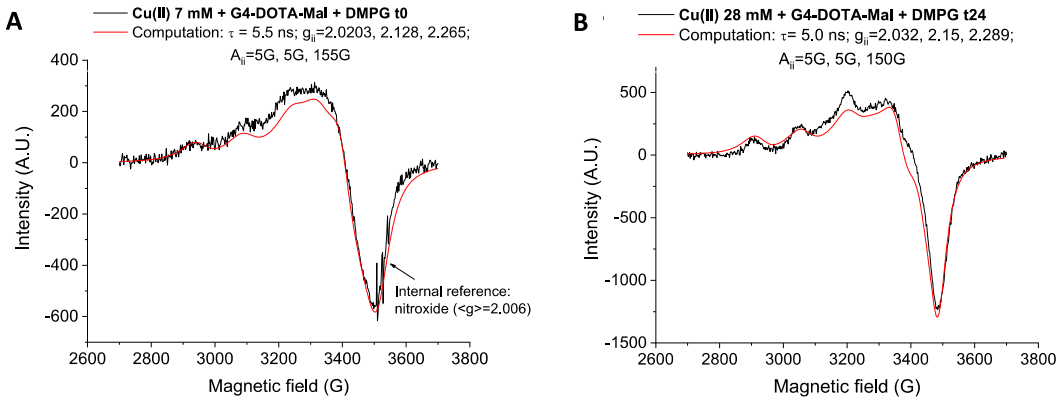

Figure 2.2 Computed (red) and experimental (black) EPR spectra of G4-DOTA-Mal in the presence of DMPG and 7mM (A) or 28mM (B) Cu(II) (article 4, figure 5)

Liposomes actively perturb the Cu(II) chelation if compared to the dendrimer-Cu(II) system only, due to the previously described superficial interactions. LEC proved to be the most perturbative in this sense. Such LEC-dendrimer interaction was later studied in detail by fluorescence anisotropy. Despite this weakening in the coordination, the overall chelation potency is not jeopardized, as EPR values suggest.

Figure 2.3 shows all scenarios arising from EPR findings.

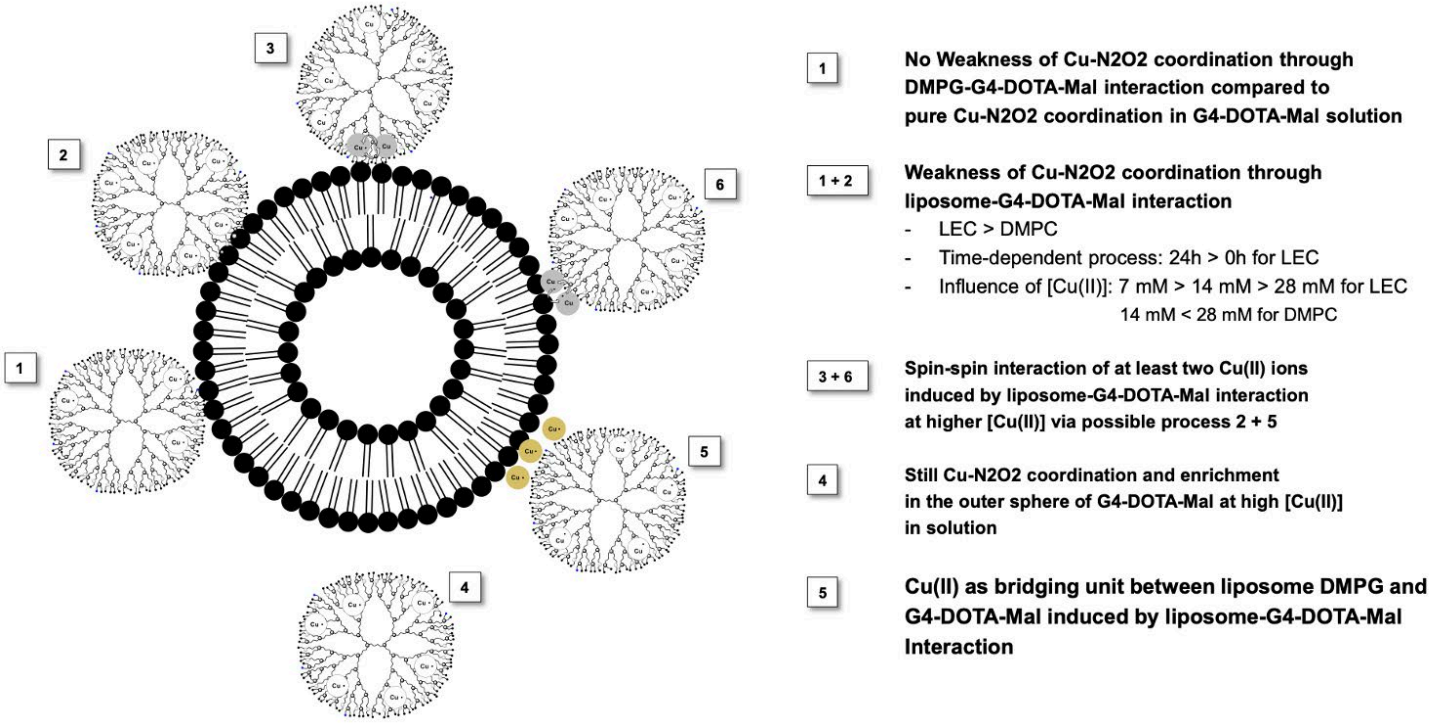

Figure 2.3 Cu(II) complexation in the presence of liposomes. (article 4, scheme 3)

In conclusion, G4-DOTA-Mal is a promising copper chelator, due to its strong coordination properties.

The Cu(II)-Glycodendrimer complex is stable in the presence of different types of model membranes. This is very important to prevent the worsening of neurological symptoms of Wilson disease, an effect induced by most drugs currently used like penicillamine.

Moreover, G4-DOTA-Mal and its Cu(II) complexes are not internalized by the membrane models. This desirable behavior will likely lower glycodendrimer toxicity in the future *in-vivo* studies.

3 - BIBLIOGRAPHY

1. Walshe J.M., "*History of Wilson's Disease: 1912 to 2000*", Movement Disorders, 2006, 21, 2, 142–147
2. Bull P.C., Thomas G.R., Rommens J.M., Forbes J.R., Cox D.W., "*The Wilson disease gene is a putative copper transporting P–type ATPase similar to the Menkes gene*", Nature Genetics, 1993, 5, 327-337
3. Ala A., Walker A.P., Ashkan K., Dooley J.S., Schilsky M.L., "*Wilson's disease*", The Lancet, 2007, 369, 397-408
4. Ranucci G., Zappu A., Lepori M.B., Lorio R., Loudianos G., "*La Malattia di Wilson*", Prospettive in Pediatria, 2012, 42, 165, 12-20
5. Di Donato M., Sarkar B., "*Copper transport and its alterations in Menkes and Wilson diseases*", Biochimica Et Biophysica Acta-Molecular Basis of Disease, 1997, 1360, 1, 3-16
6. Strausak D., Mercer J.F.B., Dieter H.H., Stremmel W., Multhaup G., "*Copper in disorders with neurological symptoms: Alzheimer's, Menkes, and Wilson diseases*", Brain Research Bulletin, 2001, 55, 2, 175–185
7. Kaler S.G., "*Microbial peptide de-coppers mitochondria: implications for Wilson disease*", J. Clin. Invest., 2016, 126, 7, 2412–2414
8. Medici V., Rossaro L., Sturniolo G.C., "*Wilson disease—A practical approach to diagnosis, treatment and follow-up*", Digestive and Liver Disease, 2007, 39, 601–609
9. Teive H.A.G, Barbosa E.R., Lees A.J., "*Wilson's disease: the 60th anniversary of Walshe's article on treatment with penicillamine*", Arq. Neuropsiquiatr. 2017, 75, 1, 69-71
10. Roberts E.A., Schilsky M.L., "*Diagnosis and treatment of Wilson disease: An update*", Hepatology, 2008, 47, 2089-2111
11. Cholakova R., Drangov M., Markova K., Zidarova V., Avramova M., "*Surgical Treatment in Patients with Wilson's Disease*", Journal of IMAB., 2017, 23, 1, 1447-1450
12. Li W.,Chen C., You Z., Yang R., Wang X., "*Current Drug Managements of Wilson's Disease: From West to East*", Curr Neuropharmacol., 2016, 14(4): 322–325.
13. Cumings J.N., "*The copper and iron content of brain and liver in the normal and in hepatolenticular degeneration*", Brain, 1948, 71-4

PAPER 4

DOTA-Glycodendrimers as Cu(II) complexing agents and their dynamic interaction characteristics towards liposomes

Marianna Carone, Silvia Moreno, Michela Cangiotti, Maria Francesca Ottaviani, Peng Wang, Riccardo Carloni, Dietmar Appelhans

Langmuir, 2020
https://doi.org/10.1021/acs.langmuir.0c01776

DOTA-Glycodendrimers as Cu(II) complexing agents and their dynamic interaction characteristics towards liposomes

Marianna Carone, Silvia Moreno, Michela Cangiotti, Maria Francesca Ottaviani, Peng Wang, Riccardo Carloni*, Dietmar Appelhans*

Table of content Graphics

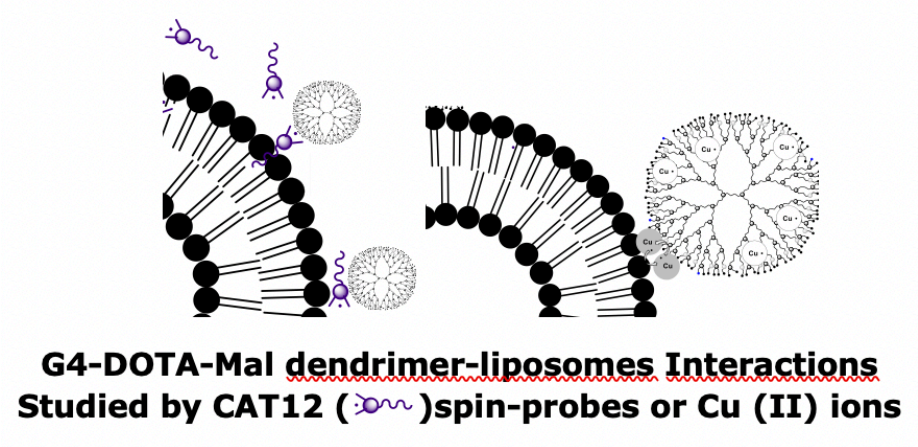

Abstract

Copper (Cu) (II) ions, mainly an excess amount, play a negative role in the course of several diseases, like cancer, neurodegenerative diseases and the so-called Wilson disease. In opposite Cu(II) ions are also capable of improving anticancer-drug efficiency. For this reason, it is of great interest to study the interacting ability of Cu(II)-nanodrug and Cu(II)-nanocarrier complexes with cell membranes for the potential use as nano-therapeutics. In this study, the complex interaction between of DOTA-functionalized poly(propyleneimine) (PPI) glycodendrimers and Cu(II) ions and/or neutral and anionic lipid membrane models, using different liposomes, is described. These interactions were investigated via dynamic light scattering (DLS), zeta-potential (ZP), electron paramagnetic resonance (EPR), fluorescence anisotropy and cryo-TEM. Structural and dynamic information about PPI glycodendrimer and its Cu(II) complexes towards liposomes were obtained via EPR. At the binding site Cu-N_2O_2 coordination prevails, while at the external interface this coordination partially weakens due to competitive dendrimer-liposome interactions, with only small liposome structural perturbation. Fluorescence spectroscopy was used to evaluate the membrane fluidity of both the hydrophobic and hydrophilic parts of the lipid bilayer, while DLS and ZP allowed us to determine the distribution profile of the nanoparticles (PPI glycodendrimer and liposomes) size and surface charge, respectively. From this multitechnique approach, it is deduced that DOTA-PPI glycodendrimers selectively extract Cu(II) ions from the bio-environment, while these complexes interact with the liposome surface, preferentially with even more negatively charged liposomes. However, these complexes are not able to cross the cell-membrane model and poorly perturb the membrane structure showing their potential for the biomedical use.

Keywords: electron paramagnetic resonance; glycodendrimers; liposomes; copper; fluorescence anisotropy; dynamic light scattering; cryo-TEM; Z-Potential

Introduction

Copper is an essential microelement for the body whose intake comes from diet.[1] A very sophisticated system ensures safe transportation to the sites of interest and safe elimination through the biliary secretion.[2] However, Cu (II) ions may play a toxic role in several diseases, like Alzheimer, cancer, and, more specifically, the so-called Wilson disease (WD). WD is a rare disease, which compromises the copper transportation provoking the accumulation of copper ions in the liver.[3-11] Not only this increasing copper deposition eventually compromises hepatic function, but also, when the hepatic storage capacity is exceeded, the unbound copper ions are poured from the liver to the bloodstream and are deposited in other organs and tissues, leading, among the others, to neurological and psychiatric complications.

Medical treatments for avoiding the toxic effects of an excess of Cu(II) ions are mainly limited to the use of low-molecular-weight chelating agents, such as D-penicillamine and Trientine,[7,12] which are associated with numerous side effects, including neurological deterioration, sideroblastic anemia and hypersensitive reactions.[7] Under this shadow, nanotechnology offers an unprecedented opportunity of tailoring drugs with a view to find a new class of chelators for copper ions, as an alternative to Penicillamine. Several efforts have been made in the direction of creating highly biocompatible nano-sized macromolecules, which can be used as nanocarrier and per se as polymeric therapeutics.[13,14] Very promising nanoparticles in this field are dendrimers. Dendrimers are perfectly branched, nanometer-sized and monodisperse structures with a strictly tailored architecture consisting of a central core surrounded by repeating layers (termed generations) of chemical units. The external end-groups can be functionalized for optimizing their pharmacokinetics or biological properties.[15] Despite the many advantages of these nanoparticles, previous researches have demonstrated unmodified amino-terminated dendrimers are not ideal candidates for medical applications due to their high cytotoxicity.[16] Specifically, the toxicity comes from the strong electrostatic interaction which is established between the positively charged dendrimer and negatively charged cell membranes, leading to cell lysis. This behavior is the main reason why cationic dendrimers are rapidly cleared from plasma.[17] Therefore, modification of the periphery may be used for adapting cellular interactions and biodistribution of dendrimers. Additionally, the trigger or inhibition of biological events is usually determined by carbohydrate-protein interactions such as immune response[18,19] or bacterial adhesion.[20] Under this shadow, the combination of carbohydrate and dendrimers not only reduces the toxicity, but also improves the biocompatibility, thus allowing glycodendrimers to be used as polymeric therapeutics and diagnostics for in-vitro and in-vivo studies.[13,21-29] For example, poly(propylenimine) (PPI) glycodendrimers are suited materials with promising potential as anti-amyloidogenic agents for treating and hampering undesired peptide/protein aggregation in neurodegenerative diseases (Alzheimer, prion disease and sporadic Jakob-Creutzfeld disease). They also show general neuroprotective properties for improving memory and synapses function by crossing the blood-brain-barrier.[21,22,23]

The aim of this study was to find new dendrimeric structures, able to complex the excess of copper. This includes the characterization of their resulting Cu(II) complexes as well as their interactions with biostructures, starting from simplified cell-membrane models. Motivated by our previous studies,[13,21-23,26] a 4th generation PPI glycodendrimer, constituted by a dense maltose (Mal) shell, was enriched with 6 groups of dodecane tetraacetic acid (DOTA), presenting specific chelating properties for copper ions and few other rare metals, including gadolinium.[27] For simplicity, this PPI glycodendrimer (Figure 1) was termed G4-DOTA-Mal.

On the basis of previous studies dealing with the interactions of dendrimers with biological membranes,[28-32] liposomes were used as simplified cell-membrane models to investigate their interactions with G4-DOTA-Mal dendrimer and its copper complexes. Thus, it was possible to imitate the impact of G4-DOTA-Mal and its Cu(II) complexes on cell-membrane fluidity, permeability and fusion. The use of membrane models like liposomes was justified since (i) the physico-chemical interaction study is not affected by the influence of membrane or plasma proteins; (ii) the liposomes are characterized by a high reproducibility and a long-term stability; (iii) we used phospholipids which are naturally present in biological membranes. To simulate dendrimer-cell interactions, different membrane models were used, specifically liposomes constituted by egg lecithin (termed LEC), 1,2-dimyristoyl-sn-glycero-3-phosphocholine (termed DMPC) and a binary mixture of DMPC and 1,2-dimyristoyl-sn-glycero-3-phospho-rac-(1- glycerol) sodium salt (DMPG) 3%. In the last case the liposomes were simply termed DMPG.

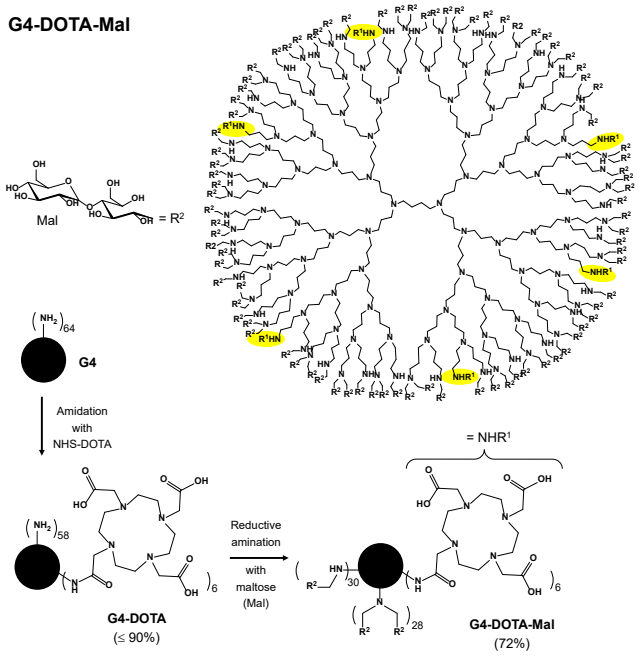

Figure 1. Simplified structure of G4-DOTA-Mal attributed by total functionalization of terminal NH_2 groups with maltose and 6 DOTA groups. The synthetic route is also shown.

We selected lecithin since we recently verified its suitability as model membranes to analyze interactions with dendrimers.[32] On the other side, DMPC has been found to satisfactorily work as model membrane interacting with dendrimers.[28-29] The addition of 3 % DMPG is enough to change the interacting ability of the liposome surface and the structural properties as tested by the variations of the parameters extracted by means of the different techniques used in the present study. Indeed, the interacting ability of the G4-DOTA-Mal dendrimer with the above-mentioned membrane models was investigated through different experimental techniques: dynamic light scattering (DLS) and Zeta-potential (ZP) that allowed us to determine the distribution profile of the nanoparticle size and surface charge, respectively; fluorescence anisotropy, used to evaluate the membrane fluidity of both the hydrophobic and hydrophilic parts of the lipid bilayer; [33] cryo-TEM and electron paramagnetic resonance (EPR), which provided structural and dynamic information about the dendrimer-liposome systems and characterized their interacting behavior. Based on previous studies, two different

approaches were followed in the EPR investigation: i) analyzing selected surfactant radicals, inserted in the membrane models, [28-31] and ii) focusing on Cu(II) ions as complexing agent,[32,34-42] measuring the interacting strength between the coordinated dendrimers and the membrane models. This multitechnique study allowed us to verify that the G4-DOTA-Mal glycodendrimer is a good and selective copper complexing agent and how these G4-DOTA-Mal glycodendrimer-Cu(II) complexes interact with lipid bilayers predicting the phenomena that may happen in presence of biological membranes.

Experimental Section

Materials

The phospholipids - 1,2-Diacyl-sn-glycero-3-phosphocholine (Egg Lecithin); 1,2-dimyristoyl-sn-glycero-3-phosphocholine (DMPC); 1,2-dimyristoyl-sn-glycero-3-phospho-rac-(1-glycerol) sodium salt (DMPG) -, phosphate-buffered saline (PBS), copper (II) nitrate hydrate and fluorescent probes - 1,6-diphenyl-1,3,5-hexatriene (DPH); N,N,N-trimethyl-4-(6-phenyl-1,3,5-hexatrien-1-yl) phenylammonium p-toluenesulfonate (TMA-DPH) were purchased from Merck (Germany). PPI dendrimer was supplied by SyMoChem (Eindhoven, The Netherlands). The synthesis and characterization of G4-DOTA-Mal is described in the Supporting Information (SI), following a previously published procedure. 43 The nomenclature of PPI dendrimers is based on Tomalia et al. 44 CAT12 surfactant nitroxide radical (4-(dodecyl dimethyl ammonium)-1-oxyl-2,2,6,6-tetramethyl piperidine bromide) was supplied by Chemical Laboratories of Columbia University (New York, USA).

Liposomes preparation in the absence and presence of G4-DOTA-Mal

Three different liposomes were prepared: (i) Lecithin liposomes (simply termed LEC), (ii) DMPC liposomes (simply termed DMPC), (iii) DMPC/DMPG 3% liposomes (simply termed DMPG). In all cases the following preparation protocol was followed. Phospholipids were dissolved under stirring in chloroform/ methanol 2:1 to obtain a 0.65 mM solution for the DLS, Cryo-TEM, ZP and fluorescence measurements, and a 25 mM solution for the EPR measurements. Then, the organic solvents were evaporated under vacuum at 40°C using a rotary evaporator (Rotavapor). The obtained lipid thin film was placed under vacuum for 24 hours and then hydrated with a PBS (10 mM, pH 7.4) solution in the absence and in the presence of G4-DOTA-Mal at a concentration of 0.05 mM for the DLS, Cryo-TEM, ZP and fluorescence measurements, and 1.56 mM for the EPR measurements (corresponding to 0.2 M in external surface groups). The higher concentrations for EPR measurements were needed due to the technique sensitivity. However, the same molar ratio between the phospholipid and the dendrimer (16) was used for all techniques. PBS solution was selected as solvent for two reasons: i) to maintain pH in neutral conditions in order to better compare experimental results from various samples with the various techniques; ii) to use a salt solution as used with cell cultures. However, the presence of PBS affects the ZP, as such as the interacting ability of liposomes and dendrimers, but we are interested to investigate the interacting behavior mimicking the biological conditions. The hydration was carried out under mechanical stirring for 1 h at 40°C.45 The sample thus obtained was divided into two parts and each part was subjected to sonication or extrusion treatment as described in the following: (i) Sonication method: 10 Cycles (30 seconds interspersed + 30 seconds pause). The resulting suspension containing liposomes was incubated at 40 °C overnight (CF = 25 mM); (ii)

Extrusion method: the suspension was extruded through a polycarbonate filter (100 nm pore size filter, 11 times) with two 1000 μL Hamilton gastight syringes at 40°C by using an Avant Mini extruder (CF = 25 mM); the suspension thus obtained was incubated at 40 °C overnight. (CF = 25 mM).

A study was first performed to verify the stability of liposomes obtained by means of the two methods. On the basis of these results, for the characterization of the interactions with the dendrimer, only the extrusion method was used, since the liposomes demonstrated a long-time structural stability.

EPR, DLS, ZP, cryo-TEM and fluorescence experiments

Experimental descriptions of these methods are presented in the SI as well as the concentrations of liposomes, G4-DOTA-Mal, CAT12 and Cu(II).

Results and Discussion

Characterization of liposomes, G4-DOTA-Mal and their mixtures, in the absence and presence of Cu(II) by using DLS, ZP and cryo-TEM

Prerequisites for the validation of interaction characteristics of G4-DOTA-Mal/Cu(II) complexes in presence of liposome models by EPR study were to first study the properties (size and charge) and the stability of liposomes (LEC, DMPC and DMPG) in presence of G4-DOTA-Mal, followed by the addition of increasing Cu(II) concentrations at 0, 1 and 24h, using DLS and ZP. This also includes the use of cryo-TEM for visualizing and comparing liposomes in absence and presence of G4-DOTA-Mal. Stable and well characterized vesicles are needed for performing EPR and fluorescence anisotropy experiments. The dynamics of liposomes (e.g. fusion and fission) per se need to be measured to get the right conclusions for the G4-DOTA-Mal-liposomes interactions in presence and absence of Cu(II).

Table S1 (SI) summarizes the hydrodynamic diameter (Dh, Z-average) and surface charge (ζ) of G4-DOTA-Mal (0.05 M) in absence and presence of Cu(II) (7, 14 and 28 mM) at 25 and 37 °C, respectively. In comparison to non-aggregated G4-DOTA-Mal macromolecules in aqueous solution (Figure S3), G4-DOTA-Mal macromolecules immediately aggregate in PBS solution (10 mM) (337 nm at 25 °C and 670 nm at 37°C, Table S1 in SI). This indicates the action of phosphate ions as glueing agent in PBS-containing dendrimer solutions at which uncontrolled aggregation of G4-DOTA-Mal occurs, justified by high polydispersity (PDI) values (Table S1) at both applied temperatures. The same situation occurs when Cu(II) is added, still showing high PDI values (from 0.7 for 7 mM Cu(II) to 0.4 for 28 mM Cu(II)) due to aggregated Cu(II)/G4-DOTA-Mal complexes with higher and lower z-average data. This demonstrates that the glueing properties of phosphate ions between G4-DOTA-Mal macromolecules are partially diminished by the highest Cu(II) concentration. The addition of Cu(II) also provokes an increase in the cationic surface charge (ζ) of G4-DOTA-Mal aggregates (from 16.5 to 32 mV at 25 °C). The EPR study (see below) demonstrates that this kind of glycodendrimer is able to complex Cu(II). Overall, G4-DOTA-Mal PBS solution are highly polydisperse due to the presence of dendrimer aggregates in the absence and presence of Cu(II) tailored by non-covalent interactions.

Table S2 (SI) depicts the hydrodynamic diameters (Dh, Z-average) and surface charge (ζ) of liposomes (LEC, DMPC, and DMPG) in absence and presence of G4-DOTA-Mal and their adducts with Cu(II) at three concentrations (7 mM, 14 mM and 28 mM), determined at 0, 1 and 24 h. The almost invariance of the size over time of the two and three component systems - liposome/G4-DOTA-Mal and (liposome/G4-DOTA-Mal/Cu(II) - is proved by DLS experiments, which show the stability of each liposome system at different compositions after 24 h. However, the PDI values change from 0.43 to 0.15 with still partly high values after 24 h. On the basis of the variations of Dh

(z-average data) and ζ in Table S2 for liposomes in presence of G4-DOTA-Mal and various Cu(II) concentrations extracted from DLS and ZP results after 24 h at 25 °C, we note that (i) all liposomes show similar Dh values (∅ 120-130 nm); (ii) the addition of G4-DOTA-Mal to all liposomes provides a slight increase or decrease of Dh (± ≤ 10 nm). This implies that each liposome is stable in presence of G4-DOTA-Mal; (iii) by further adding Cu(II) at increasing concentrations, the liposome diameter, after an evident instability at 0 time, already after 1 h and, more, at 24 h, only slightly changes, underlining the desired stability of liposomes (± ≤ 10 nm compared to pure liposomes with ∅ 120-130 nm). Two exceptions are given by DMPC and DMPG with G4-DOTA-Mal and 28 mM of Cu(II), showing a Dh of about 170 nm and 96 nm, respectively. The size increase may be related to the formation of adducts driven by the excess amount of Cu(II). Further details on the interacting behavior within the two and three component systems will be shown in the EPR part below.

In any case, the small variations of the structural parameters in Table S2 for the liposomes from the absence to the presence of the dendrimers or dendrimer-Cu(II) complexes indicate that non-covalent interactions (electrostatic, dipole-dipole, H-bonding) in the two and three component systems exist to destroy or break down the undesired dendrimer and dendrimer/Cu(II) aggregates. This undoubtedly indicates interfering properties of liposomes towards G4-DOTA-Mal macromolecules in PBS (10 mM) solutions (Table S2). Furthermore, isolated G4-DOTA-Mal and few aggregated liposome/G4-DOTA-Mal hybrid structures in the absence and presence of Cu(II) are also assumed, when considering the still high PDI values for two and three component systems with DMPC and DMPG. In this context LEC systems slightly look more homogeneous than DMPC and DMPG systems. This further implies that the glueing properties of phosphate ions do not play any deciding role as in the case of one and two component systems of G4-DOTA-Mal and G4-DOTA-Mal/Cu(II) (Table S1).

Beside the achievement of z-average data by DLS (Table S2), a deeper analysis of the volume plots for liposomes in presence of G4-DOTA-Mal and one selected Cu(II) concentration of 14 mM (Figures S5 in SI) further underlines the high stability of liposomes, outlining peak maxima for Dh around 100 nm for DMPC and DMPG liposomes, and a little bit higher (about 120 nm) for LEC liposomes. We observe a similar solution behavior of G4-DOTA-Mal macromolecules (Figure S5A) in the presence and absence of liposomes and Cu(II) as discussed above. This thoroughly means that G4-DOTA-Mal macromolecules preferentially interact with the liposomes surface due to the absence of any other particles in the volume plots (presenting three repeating measurements of each solution). Moreover, the Cu(II) complexation and/or interaction must occur in the environment of liposome/G4-DOTA-Mal hybrid structures.

The high stability of liposomes was further confirmed through long-term analysis over 30 days, storage at 4°C and 25 ºC and use of different pure liposome concentrations (Figures S7-8 in SI). In all time ranges and different experimental conditions, the particle size and volume remain almost the same at 100 nm. Moreover, we expected that the surface charge of liposomes might be affected, when pure G4-DOTA-Mal or the combination of G4-DOTA-Mal/Cu(II) is added to the liposome solutions. DMPC surface is almost neutral, while, as expected, DMPG surface is negatively charged. Conversely, the negative surface charge of the zwitterionic LEC liposome surface is not expected, since LEC and DMPC have similar charges in the headgroups. However, the different packing of PC and PE lipids in LEC modulates the surface charge at the interface. By adding the cationic dendrimer macromolecules, first, and then different cationic Cu(II) concentrations, the surface charge differently increases, but at a low extent (ZP in Table S2, SI). Surprisingly, there is no real change of the surface charge of liposome DMPC, when adding G4-DOTA-Mal. This behavior may suggest weak interactions between the components. In case of LEC and DMPG a

conversion from anionic to slightly positive surface charge is observed, leading to a compensation at the highest Cu(II) concentration (28 mM). This may imply a stronger physical interaction at the interface of liposome and dendrimer macromolecule in absence and presence of Cu(II) compared to DMPC samples. The interactions within the two and three component systems (liposome/G4-DOTA-Mal and liposome/G4-DOTA-Mal/Cu(II)) are better characterized by the EPR and fluorescence analyses and are described below.

Finally, originally observed aggregates for G4-DOTA-Mal with/without Cu(II) (Table S1) are immediately destroyed or cannot be formed in the presence of liposomes. This event is confirmed by the observation, by means of DLS, of much more disperse and heterogeneous solutions (Table S2).

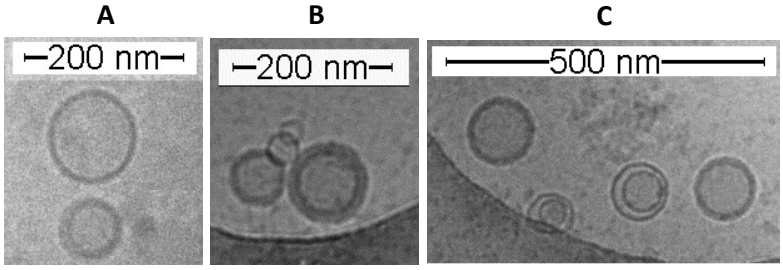

D

Samples	Z-average	Cryo-TEM	
	Diameter (nm)	Diameter (nm)	Membrane thickness (nm)
Empty-LEC liposome	141	96.0 ± 19.7	14.7 ± 2.7
post G4-DOTA-Mal loaded LEC	138	91.0 ± 21.9	15.3 ± 3.0
Empty-DMPC liposome	126	83.9 ± 20.5	15.3 ± 1.8
post G4-DOTA-Mal loaded DMPC	126	83.8 ± 17.5	15.5 ± 1.4
Empty-DMPG liposome	125	90.8 ± 24.2	15.6 ± 2.0
post G4-DOTA-Mal loaded DMPG	121	90.9 ± 24.5	15.5 ± 2.0

Figure 2. Cryo-TEM images of post-loaded G4-DOTA-Mal with liposomes (A) LEC, (B) DMPC, (C) DMPG; (D) comparison of the data evaluated by DLS and cryo-TEM study; used concentrations are reported in the Experimental details in SI.

To further underline the presence of stable liposomes with unilamellar lipid bilayer structure, fabricated by the extrusion method, cryo-TEM investigation was used to obtain additional information about real diameter and membrane thickness, since DLS did not provide desired characteristics regarding the morphology and shape of liposomes. Figure 2 highlights the comparison of pure and G4-DOTA-Mal loaded liposome solutions (LEC, DMPC and DMPG) determined by DLS and cryo-TEM at which defined concentrations of the components have been used. As known, Dh from DLS results is always larger compared to diameters obtained from analyzed cryo-TEM images.46,47 It is important to underline that membrane thickness usually ranges between 6 and 4 nm, depending on the temperature. In our case, the thickness is much higher. However, it is reported in the literature that the effect of a soluble salt is a "threefold increased size as compared to single lipids", due to ions and water coordination at the charged lipid heads.[48] First, the cryo-TEM study shows that the extrusion method is suited to fabricate unilamellar liposomes. This is a further prerequisite for the EPR study. Second, the post-loading of G4-DOTA-Mal to liposome solutions does not show any effect on the diameter and membrane thickness of each liposome. Therefore, the model membrane does not integrate G4-DOTA-Mal after post-loading. This certainly occurs for DMPC and

DMPG, which do not show any structural variations after addition of the dendrimer. Conversely, a small change in liposome diameter is detected in LEC liposomes from the absence to the presence of G4-DOTA-Mal. The diameter slightly decreases (from 96 to 91 nm), while the membrane thickness keeps nearly constant. This open issue of the type and strength of interaction of G4-DOTA-Mal with liposome structures will be clarified hereafter by EPR and fluorescence anisotropy study. DLS, ZP, and cryo-TEM studies show that the presence of G4-DOTA-Mal does not affect the main structural characteristics of liposomes.

EPR Study of the interactions between DOTA Glycodendrimers complexed by Cu(II) and membrane models (LEC, DMPC, and DMPG)

Two requirements are considered for the EPR analysis to emphasize the desired interaction characteristics between the G4-DOTA-Mal dendrimer and the liposomes (LEC, DMPC and DMPG). The first requirement is achieved by adding a surfactant nitroxide radical (CAT12) at a concentration of 1 mM, which is lower than CAT12 cmc value (7.1 mM at 295 K).[41] We already found CAT12 suitable for analyzing liposome structures in previous studies, where the interactions between dendrimers and liposomes are studied in the absence and presence of Cu(II).[32] The presence of an interacting component indicates that the probe enters the liposome and we hypothesize that it mimics lipids in the liposome structure. A limited impact of CAT12 on liposome structure was demonstrated by the invariance of the EPR spectra line-shape by changing CAT12 concentration up to 1 mM. The second requirement is to understand the complexation characteristics of G4-DOTA-Mal (1.56 mM) towards Cu(II) in the absence of liposomes by analyzing the EPR spectra of Cu(II) at different molar ratios with respect to the DOTA groups at the dendrimer surface (1:0.75/1:1.5/1:3 of DOTA: Cu).

Characterization of liposomes and their interactions with G4-DOTA-Mal using a surfactant nitroxide radical

CAT12 is selected for this study since it has already proved to be a very informative spin probe for monitoring and validating structural modifications of liposomes and their membrane interactions with various dendrimers.[26] Furthermore, CAT12 mimics the behavior of the phospholipids constituting the membrane and is able to insert into the lipid aggregates with the hydrophobic chain, while the paramagnetic CAT group remains at the liposome / water interface.

Figure 3 shows a selected example for the experimental spectrum of CAT12 (1 mM) in presence of LEC (25 mM in phospholipids) + G4-DOTA-Mal (1.56 mM) system (A). The spectra were recorded at 25 °C. Experiments at 37 °C were also performed and the results showed the same trends for the different samples, but lower differences among the samples with respect to the experiments at 25 °C. Since we are mainly interested in the interacting behavior also differentiating the various samples, here only the results at 25 °C are described. Two spectral components are identified, whose first peaks are indicated by arrows in Figure 3A. These components are termed "free component" and "interacting component" on the basis of the line-shape features. These two components are present also for the liposomes/CAT12 systems in the absence of the dendrimers (see, for example Figure S9 in the SI). Indeed, the free component consists of three narrow lines. This is characteristic of radical groups that are free to rotate in solution. The free component of CAT12 is present in all cases and it is the only component present for the dendrimer in the absence of liposomes (Figure S10 in the SI). Figure 3A shows the computation of this free component for the case of LEC + G4-DOTA-Mal. Here, the well-known calculation method of Budil et al. (NLSL

program), [49] is used to obtain structural and dynamic parameters of CAT12 in presence of G4-DOTA-Mal, Cu(II) and/or liposomes. The resulting main parameters, <A> and τ, are useful for the present study, and are generally shown in figure legends: <A> is the hyperfine coupling constant between the electron spin and the nitrogen nuclear spin, expressed by <A> = (Axx + Ayy + Azz)/3. <A> measures the micropolarity at CAT12 environment. τ is the correlation time for the rotational motion of CAT12, which measures the microviscosity and, consequently, the interaction strength of the CAT12 probe in the liposome membranes in absence and presence of dendrimers. The values of <A> = 16.25 G and τ = 116 ps, obtained by simulating the free component in Figure 3A, indicate a fast moving CAT12 radical group in presence of liposomes LEC and G4-DOTA-Mal at the external interface. Considering the aqueous solubility of CAT12, a fraction of it remains partitioned in water even in the presence of liposomes, but we found that its mobility is differently affected by different compounds in solution, thus suggesting a location at the liposome external interface (Scheme 1). In these conditions, a competitive interaction of the liposome between the dendrimer and the cationic EPR probe occurs, which modulates the partitioning (relative percentage) of the probe between the external solution (free component) and the internalization of the CAT12 chain into the liposomes (interacting component).

By subtracting the computed free component in Figure 3A from the total spectrum in the same figure, the interacting component is obtained (Figure 3B). The interacting component shows the resolution of the anisotropies of the magnetic parameters. This indicates a slowing of the motion, consequently showing the interactions of the spin probe embedded into the liposome membrane. In detail, the CAT12 chain is inserted into the membrane, while the positively charged CAT groups electrostatically interact with the phosphate groups at the liposome surface. This interacting component is simulated as shown in Figure 3B. The τ value (4 ns, in the legend of Figure 3B) is significantly higher, if compared to the free component (Figure 3A), and indicates quite strong electrostatic interactions occurring at the liposome surface.[30-32] On the other side, the parameter <A> (15.8 G, legend of Figure 3B) indicates a lower micropolarity with respect to the free component (Figure 3A). The polarity reduction further supports the occurrence of electrostatic interactions, where the charges neutralize.

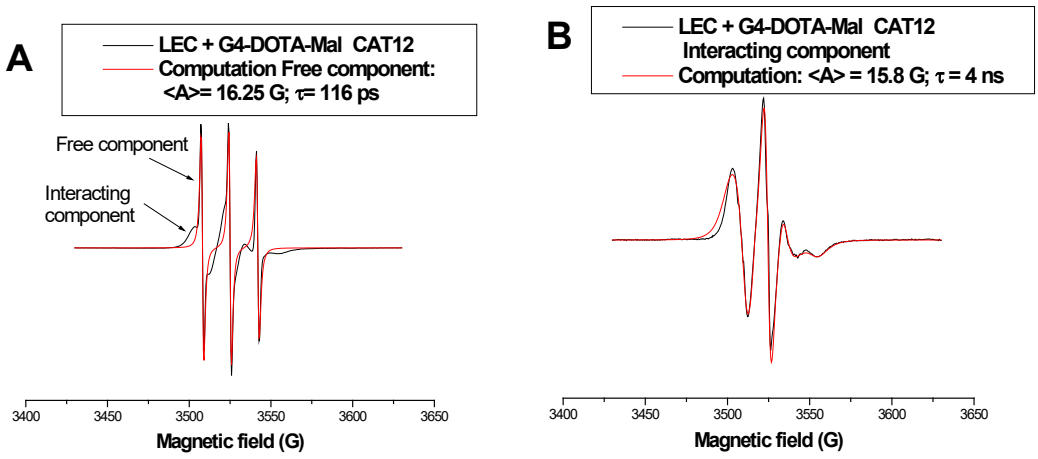

Figure 3. (A) EPR experimental spectra of CAT12 in the systems LEC + G4-DOTA-Mal, which also shows the computation of the free component; (B) computation of the interacting component obtained after subtraction of the free component. The legends show the main parameters of computations.

In addition to τ and <A>, other parameters are useful for clarifying the interaction characteristics of dendrimer-liposome systems, as follows:

a) The total intensity (obtained by double integration of the spectra), which measures the solubility of CAT12 (mimicking lipids) in the systems (in arbitrary units = A.U.). An increased "solubility" corresponds to an increased concentration in the systems.

b) The relative percentage of the interacting component.

c) The order parameter S for the interacting component. This parameter, also obtained from computation, measures the order of lipid aggregates and changes from 0 (no order) to 1 (maximum order). In several cases, the fitting between the experimental and the computed line shape improves if both τ and S are included in the calculation. However, the simultaneous variations of τ and S significantly increase the error in the values. Therefore, it is usually preferred to change only one of the two parameters maintaining constant the other, mainly to follow the structural variations in a series of spectra from similar systems, as such as in the present case.

With this in mind, Figure 4 shows the variations of the spectral intensity (A), the relative % of the interacting component (B), τ of the free component (C), S of the interacting component for a constant τ = 5 ns value (D), <A> of the Interacting (E) and Free (F) components, for CAT12 in solution with the three different liposomes, and in the absence and presence of G4-DOTA-Mal. Further comments on the results in Figure 4 are presented in section 5.4 of the SI. The main characteristics of the various systems deduced from the data in Figure 4 are sketched in Scheme 1, and described/discussed in the following:

For the system "liposome + CAT12" in the absence of G4-DOTA-Mal, the results show that CAT12 is able to insert in the bilayer structure of liposomes (Scheme 1), where the intensity reports about an increased solubility (concentration) of CAT12 into the liposomes in the series LEC < DMPC < DMPG (Figure 4A). Here it is interesting to note that phospholipids are used at a concentration of 25 mM. Therefore, assuming that all lipids are solubilized, the theoretical CAT12/phospholipid ratio is 1:25. But, the interacting component involves only 30-40 % of the probes, therefore the theoretical ratio becomes about 1:75. The heterogeneity of LEC ingredients may be responsible for a lower concentration of free CAT12 in LEC-liposomes solutions. Thus, the free component is mainly reduced, since the relative percentage of interacting component (Figure 4B) is the highest with LEC with respect to the other liposomes. This last result indicates that the surface heterogeneity of LEC liposomes favors electrostatic interactions between the positively charged CAT and phosphate groups at the LEC-liposome surface. On the other side, the negative charge of DMPG surface also enhances the electrostatic interactions with the positive CAT group. This provokes a slight increase of membrane integration (Figure 4A) and percentage of the interacting component (Figure 4B) for DMPG if compared to DMPC. The enhanced interactions (insertion into the bilayer and electrostatic interaction at the liposome interface) of CAT12 embedded into DMPG liposomes are finally proved by the higher order parameter (Figure 4D) and the lower polarity (measured by <A> in Figure 4E) if compared to the other liposomes.

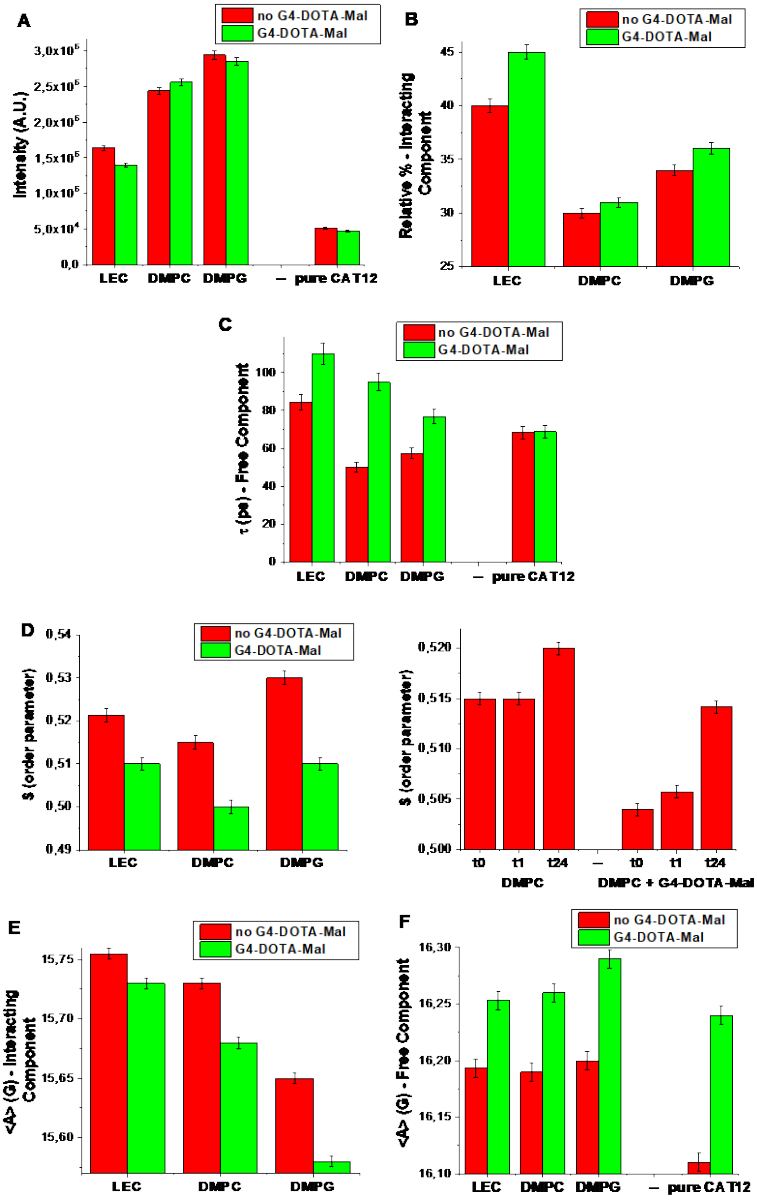

Figure 4. Variations of the EPR spectra intensity (A), relative % of the interacting component (B), τ for the Free component (C), S of the interacting component (D), <A> for the Interacting (E) and Free (F) components, for the three different liposomes in the absence and presence of G4-DOTA-Mal.

For the systems "liposome + G4-DOTA-Mal + CAT12" the addition of G4-DOTA-Mal to the liposomes provides the following effects: (i) an increase in the percentage of the interacting component (Figure 4B); (ii) an increase of τ (measuring the interaction strength, Figure 4C) and <A> (measuring the polarity, Figure 4F) for the free component; and (iii) a decrease of the order parameter S (Figure 4D) and <A> (Figure 4E) for the interacting component. The increase in percentage of interacting component is unexpected, since the presence of a positively charged dendrimer, that prefers to bind to the liposome surface, should impede the insertion of CAT12, which is also positively charged. But, CAT12 needs to escape from the solution due to both electrostatic repulsion with the dendrimer approaching the liposome surface, and increased instability of the hydrophobic chain caused by an increased ionic strength in solution. This provokes an increased CAT12

solubilization into the liposomes. The variations of the parameters in Figure 4 are indeed quite small, but support the occurrence of weak dendrimer-liposomes interactions (Scheme 1). These interactions slightly perturb the liposome structure, as tested by the decrease in the lipid order (order parameter) and the increase of the polarity (<A>) of the interacting component. These variations are larger for DMPG and smaller for LEC. Conversely, the increase in the percentage of the slow component is larger for LEC. This is accompanied by a decrease in the spectral intensity for LEC (Figure 4A), while this behavior is not found for the other liposomes. Therefore, G4-DOTA-Mal interactions with LEC perturb the solubilization (= membrane integration) of free CAT12 probes in LEC-liposomes solutions, thus decreasing the intensity and increasing the percentage of interacting probes. As shown in Scheme 1, the EPR results indicate a stronger structural perturbation tailored by cationic G4-DOTA-Mal on anionic DMPG liposomes. Contrary, more stable dendrimer-liposomes adducts are formed by LEC. The postulated surface interactions between G4-DOTA-Mal and LEC are probably related to the heterogeneity of lecithin ingredients at liposome interface, which enhances surface interactions. Indeed, lecithin contains the zwitterionic PC and PE lipids: more unsaturated lipids will result in packing defects that facilitate dendrimer attachment and/or adsorption at the interface, where the phosphate group is located, without perturbing the lipid order. The interactions of cationic CAT12 at the interface between G4-DOTA-Mal and liposomes (Scheme 1) is also measured by the increase of τ (Figure 4C) and <A> (Figure 4F) for the free component in liposomes solution from the absence to the presence of G4-DOTA-Mal. Surface interactions of G4-DOTA-Mal with LEC are additionally proven by fluorescence anisotropy experiments (further details in SI, Figure S9). The results in Figure S12 using TMA-DPH fluorescent probe clearly indicate a more decisive hydrophilic interaction with the dendrimer for LEC. Using DPH, the lower starting r/r0 values for LEC indicate a more fluidic membrane with respect to DMPC and DMPG. DMPG shows a progressive negative slope, which may be related to an increased fluidity at the higher dendrimer concentrations.

Both Fluorescence and EPR results show that DMPC possesses a more compact bilayer structure if compared to the other liposomes. Thus, DMPC outlines the lowest interactions at the interface.

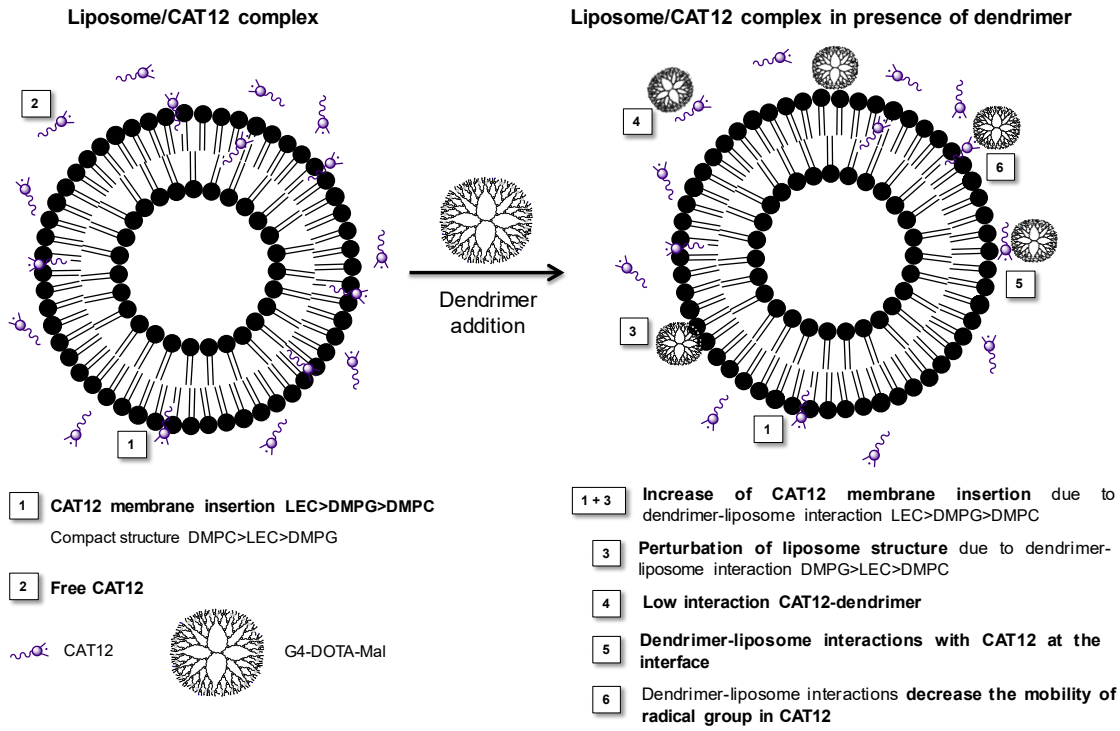

Scheme 1. Different distributions and interactions of the surfactant radical, CAT12, mimicking the lipid surfactants in the liposome membrane, in the absence and presence of the G4-DOTA-Mal dendrimer.

The EPR results are in agreement with ZP data (Table S2), thus confirming the compensation of the negative surface charge in the cases of LEC and DMPG liposomes for turning them to nearly neutral surface charge. Conversely, nearly neutral DMPC liposomes do not undergo charge neutralization through the addition of cationic G4-DOTA-Mal (Table S2). Indeed, electrostatic interactions between anionic DMPG and LEC and cationic G4-DOTA-Mal are expected. Therefore, without doubt electrostatic interactions are the driving forces between liposome and dendrimer surfaces. Moreover, the interactions between the DMPC liposome and G4-DOTA-Mal dendrimers are mainly driven by dipole-ionic bonds and hydrogen bonds. The multiple H-bond interactions of G4-DOTA-Mal on the neutral surface can cause perturbations of the membrane fluidity, [50-52] which also happen in case of LEC and DMPC. In respect to EPR results, H-bonds are less significant for DMPC probably related to the neat and compact structure. In conclusion, the radical surfactant, CAT12, mimicking the phospholipid behavior, reveals to be a good probe to characterize the interactions between liposomes and G4-DOTA-Mal. This probe differently distributes in the different liposome solutions in absence and presence of G4-DOTA-Mal, thus monitoring the liposome-dendrimer interactions.

Analysis of the EPR spectra of G4-DOTA-Mal - Cu(II) complexes interacting with liposomes

The complexation of G4-DOTA-Mal (1.56 mM, corresponding to 9.36 mM in DOTA groups) with Cu(II) ions is analyzed at three different concentrations of Cu(II), 7 mM, 14 mM and 28 mM (corresponding to 0.75, 1.5, and 3 molar ratios between Cu(II) and DOTA), in absence and presence of the three different liposomes (LEC, DMPC and DMPG) and at different equilibration times up to 24 h. Longer equilibration times (up to 15 days) showed poor spectral variations, indicating the stability of the liposomes solutions, despite the high phospholipid concentration. Liposome solutions

are added to solutions of preformed glycodendrimer-Cu(II) complexes. For comparison, also the binary Cu(II)-liposomes and Cu(II)-G4-DOTA-Mal solutions are analyzed by EPR.

The computation of Cu(II) spectra is performed using the same procedure used for computing the EPR spectra of the nitroxide radicals,41 but in this case the parameters and information extracted from computations are different. First of all, the Aii components of the A tensor for the coupling between the electron spin and the nuclear spin (Cu, I=3/2) characterize the type and geometry of the Cu(II) complex, together with the gii components of the g tensor for the coupling between the electron spin and the magnetic field. The attribution to a certain Cu(II) coordination and geometry is based on comparison with the Aii and gii values reported in the literature for similar systems.[32-42] This computation procedure has the advantage to also provide the correlation time for motion, τ, which measures the mobility of the Cu(II) complex.

Samples "Cu(II)-Liposomes" outlined an abundant "Free component" for the Cu(II) coordination with 4 oxygen sites in a square planar geometry and fast mobility, exemplified for LEC in Figure S11 of the SI, bottom spectrum. This free Cu-O4 component is most probably characterized through the coordination of Cu(II) with 4 water molecules. In opposite, only the Cu(II)-LEC sample, due to the heterogeneity of the lecithin components, additionally depicts the presence of a so-called "weakly interacting" component (Figure S11 of the SI, bottom spectrum; on the basis of the partial resolution of the g and A anisotropies, this component is attributed to ions weakly interacting with the LEC surface in slow mobility conditions (trapped in the interface). The heterogeneity of the LEC interface due to the PE and PC lipids well accounts for this behavior.

The intensity of the weakly interacting component in case of LEC-Cu(II) system decreases, relatively to the free component, as the Cu(II) concentration increases from 7 mM to 14 and 28 mM, due to saturation of the weakly interacting sites at the surface of LEC liposomes. Therefore, only the Cu(II)-O_4 coordination is visible at the highest Cu(II) concentration for LEC liposomes, and at all concentrations for DMPC and DMPG liposomes.

The other binary system, constituted by Cu(II) and G4-DOTA-Mal, shows completely different spectra if compared to the Cu(II) – liposomes binary systems: the spectra of Cu(II) – G4-DOTA-Mal at all concentrations (7-28 mM), both in absence and presence of the liposomes, are only constituted by a so-called interacting component, as shown in the examples in Figures 7A and 7B. The interacting behavior is accounted by the τ value (5.5 and 5 ns; Figure 7A and 7B respectively), obtained from the computations (red lines in Figs. 7A and7B). These τ values indicate a slow-moving complex, due to Cu(II) ions binding within G_4-DOTA-Mal scaffold. The magnetic parameters gii and Aii (also reported in the legends of Figures 7A and 7B) indicate a square planar Cu-N2O2 coordination, but with strong orthorhombic distortion. This distortion is caused by a stronger coordination with two nitrogen sites, probably those present in the DOTA group. The two oxygen sites, which coordinate the ions, are probably water molecules. Alternatively, it is also reasonable to think that two nitrogen atoms of the dendritic scaffold of G_4-DOTA-Mal may be involved in Cu-N_2O_2 coordination, especially at the highest Cu(II) concentration (28 mM), as shown in Scheme 2. Indeed, DOTA ligands are saturated by Cu(II) ions, when considering the Cu(II) complexation by G4-DOTA-Mal at the highest DOTA/Cu(II) molar ratio (1:3).

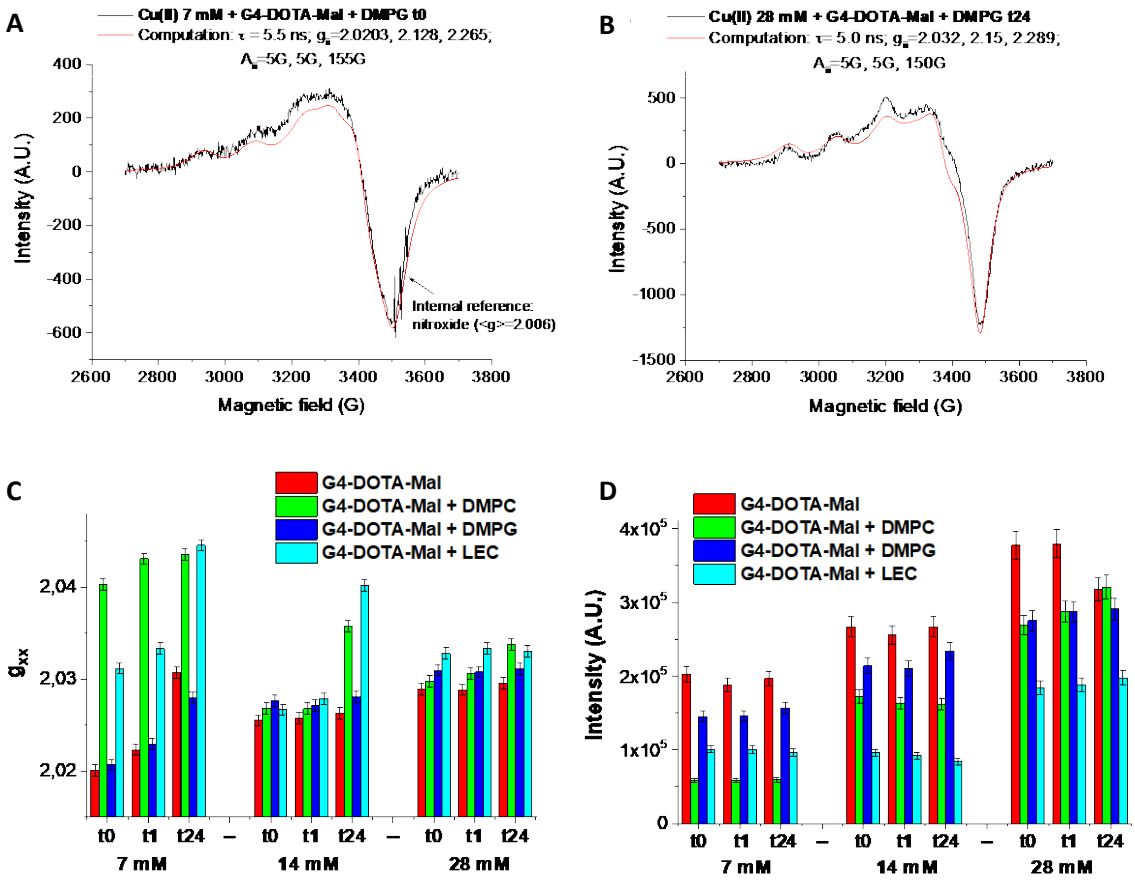

Figure 5. Experimental and computed EPR spectra of G4-DOTA-Mal -Cu(II) 7mM+DMPG at t0 (A), and G4-DOTA-Mal - Cu(II) 28 mM+ DMPG at t24 (B); gxx values (C), and intensity values (D) for the various systems.

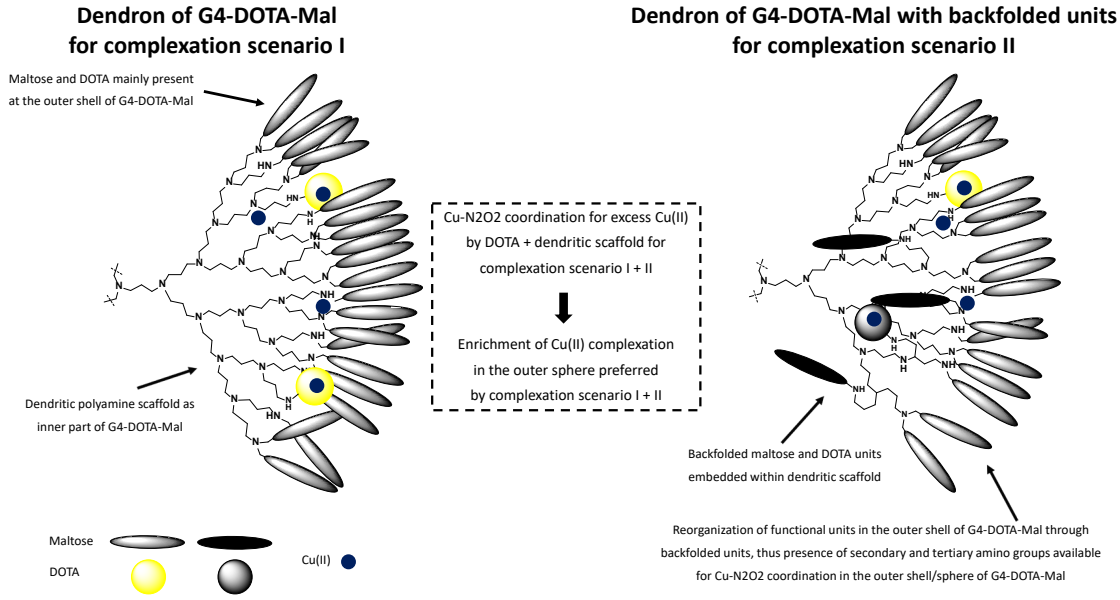

Scheme 2. Complexation of Cu(II) by G4-DOTA-Mal and molecular rearrangement of G4-DOTA-Mal by back-folded functional groups. Core-shell model suggested for G4-DOTA-Mal (left).[52] Backfolded maltose

units in G4-DOTA-Mal, inducing the presence of amino groups for Cu(II) coordination in the outer sphere. No core-shell structure, resembling "fluffy model" of open-shell architecture of maltose-modified hyperbranched poly(ethyleneimine) (right).[53] Part structure (dendron) of G4-DOTA-Mal for exemplifying Cu(II) coordination. Excess Cu(II) may only be complexed by amino groups of G4-DOTA-Mal scaffold, as shown in scenario I and II.

The use of an internal reference system (a nitroxide radical with <g> = (gxx + gyy + gzz)/3=2.006, indicated with an arrow in Figure 5A) allows us an accurate measurement of the gii values (error in the third decimal). In this Cu(II)-dendrimer binary case, the line shape modifies by increasing Cu(II) concentration. This modification in line shapes is described and discussed together with those obtained for the ternary liposome – Cu(II) - dendrimer systems in the following.

Indeed, liposome solutions (LEC, DMPC and DMPG) are added to Cu(II)/G4-DOTA-complex solution to clarify the complex interaction characteristics between the three components on the basis of the mobility parameter, τ, and the magnetic parameters, gii and Aii (identifying Cu(II) complex coordination) obtained from the computation process.

Figure 5B shows an example of experimental (black line) EPR spectrum (in red the computation) obtained after the addition of the liposome DMPG to Cu(II)/G4-DOTA-Mal complex solution, recorded at an equilibration time of 24h and at a Cu(II) concentration of 28 mM. The spectrum in Figure 5B is constituted by a single interacting component, similarly to the spectrum in the absence of the liposomes in Figure 5A. However, the main parameters used for computations and listed in the legends of the two figures (5A and 5B) differ between the two computations. We found that gxx and spectral intensity parameters (Figures 5C and 5D, respectively) are the most informative to describe the structural variations of the Cu/G4-DOTA-Mal complex from the absence to the presence of the different liposomes, at different equilibration times and Cu(II) concentrations.

To analyze the gxx data, it must be taken into account that an increase of gxx corresponds to a weaker interaction and/or a lower number of nitrogen sites coordinated to Cu(II). On the other side, a decrease in intensity (Figure 5D) may arise from a decrease of ions concentration in the systems and/or strong spin-spin interactions, which provoke a significant line broadening. Consequently to this broadening, the corresponding EPR signal almost "disappears" in the magnetic-field range of analysis. Thus, the following Cu(II)/dendrimer interaction characteristics with the liposomes can be deduced and are sketched in Scheme 3.

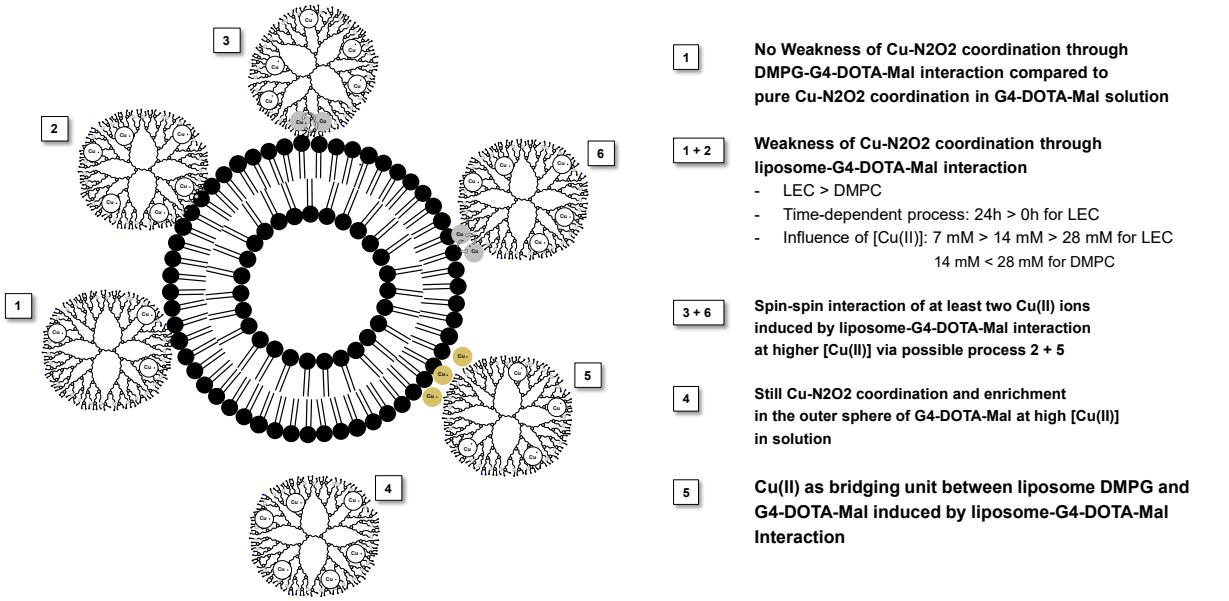

Scheme 3. Different complexation behavior of Cu(II) with the dendrimer in the absence and presence of the liposomes.

First, as depicted in Scheme 2, there is a higher probability of back-folded maltose and DOTA inside of the dendritic scaffold of G_4-DOTA-Mal, also described as a lower probability to form a dense-shell PPI glycodendrimer.[52] Thus, with this molecular rearrangement of maltose and DOTA units, nitrogen atoms of dendritic scaffold are available at the outer surface of G_4-DOTA-Mal, ready to complex the excess Cu(II) with a Cu-N_2O_2 coordination. Potential oxygen ligands can be water molecules and/or oxygen-containing surface groups of liposomes (Complexation scenario II in Scheme 2). On the other hand, the Cu-N_2O_2 coordination of the excess Cu(II) may also occur in the inner and outer sphere of dendritic scaffold of G_4-DOTA-Mal besides Cu(II) complexation by DOTA ligand (Complexation scenario I in Scheme 2).

The first consideration (Scheme 3: case 1 + 2) is that the addition of LEC and DMPC liposomes to Cu(II)/G_4-DOTA-Mal complex decreases the interaction strength (increase of gxx in Figure 5C) between Cu(II) and the nitrogen ligands of the dendrimer. This mainly happens at the lowest Cu(II) concentration and is necessarily ascribed to the interactions between the Cu(II)-dendrimer complexes and liposomes. This perturbation effect is almost immediate (at t0 and t = 1 h) for DMPC, while it needs time (up to 24 h) for LEC. Conversely, in the presence of DMPG the interaction strength between Cu(II) and the nitrogen ligands remains almost unchanged with respect to the complex in the absence of liposomes (Scheme 3: case 1). In this case, Cu(II) ions, maintaining the Cu-N_2O_2 coordination, are probably directly interacting with the negative groups (phosphate) at the DMPG interface (the two oxygen ligands) and probably work as a bridge between the liposomes and the two nitrogen sites of the dendrimers (Scheme 3: cases 4 + 5). Here, it is postulated the complexation scenario II (Scheme 2).

The interaction strength measured by gxx (Figure 5C) decreases for all systems by increasing the Cu(II) concentration (from 7 mM to 14 and 28 mM) and the equilibration time (from 0 to 24 h). Thus Cu-N_2O_2 coordination in Cu(II) - G_4-DOTA-Mal complexes is weakened both over time and by increasing Cu(II) concentration from 7 to 14 mM, both in absence and in presence of all liposomes. The increase in Cu(II) ions at the dendrimer or dendrimer/liposome interface provokes charge repulsions, which are also disturbing the Cu(II)-N bonds. At the highest Cu(II) concentration (28 mM), the complex-weakening effect played by the various liposomes becomes quite small. The excess

ions localize in a Cu-N_2O_2 coordination more internally to the dendrimer (Scenario II, Scheme 2), and, consequently, the perturbations due to liposome-dendrimer interactions are less effective.

Moreover, the increase in gxx parameter by adding LEC and DMPC to the Cu(II)-dendrimer complex at the Cu(II) concentration of 7 mM (Figure 5C) is accompanied by a decrease in intensity (Figure 5D). The decrease in intensity is mainly ascribable to spin-spin interactions occurring between Cu(II) ions, which concentrate at the dendrimer-liposome interface (Scheme 3: cases 3 and 5). Again, both complexation variants I and II (Scheme 2) can be involved to initiate such spin-spin interactions due to next to next complexation locations within the dendritic scaffold of G_4-DOTA-Mal at the dendrimer-liposome interface, but not really between two G4-DOTA-Mal macromolecules on the liposome surface.

It is noteworthy that the intensity increases with the increase in concentration of Cu(II) but far from a logic of proportionality. This further demonstrates that the Cu(II) ions concentrate (spin-spin interactions) at the G_4-DOTA-Mal surface/interface, both in absence and presence of liposomes. The Cu-N_2O_2 coordination with a weakening of the Cu(II)-N bonds is the only one visible in the EPR spectra at all Cu(II) concentrations, supporting the hypothesis of Cu(II) coordinating nitrogen sites into the dendrimer scaffold, and concentrating at the interface. Such Cu(II) enrichment in the outer sphere of dendrimers is already described in a previous study on similar systems, using dense shell PPI glycodendrimers.[51] The lowest variation in intensity by increasing the Cu(II) concentration is found in the presence of LEC. In this case, the heterogeneous liposome surface favors the aggregation of ion/dendrimer complexes at the LEC surface itself.

All these considerations show that the EPR analysis provides useful interaction properties of G_4-DOTA-Mal in respect to its ability to selectively complex Cu(II) ions and then interact with the external liposome surface. These interactions are modulated by the type of liposome, the copper concentration and the equilibration time.

Conclusions

The aim of this study is to deeply characterize the Cu(II)-complexing ability of a DOTA-functionalized 4th generation PPI glycodendrimer with a dense maltose shell (G_4-DOTA-Mal), and its surface/interface interactions with various liposomes (LEC, DMPC and DMPC/DMPG 3 %, simply termed DMPG), without being internalized or destroying/disrupting the liposome-membrane structure. For such basic study, it is preferable to use stable liposomes instead of heterogeneous and poorly stable cell cultures. Surface-driven interactions of potential polymeric therapeutics is desirable to develop supramolecular Cu(II)-complexing drugs for treating various pathologies where Cu(II) has revealed a harmful role.

Therefore, this multitechniques study analyzes liposomes in absence and presence of G4-DOTA-Mal, and in absence and presence of different molar ratios of Cu(II). The combination of DLS, ZP and cryo-TEM shows that unilamellar, long-term stable and non-aggregating liposomes are obtained, whose structure characteristics are retained also in presence of G_4-DOTA-Mal. The dendrimers in the absence of liposomes form aggregates, which break down when dendrimer-liposome interactions occur.

EPR, supported by fluorescence anisotropy, helps to clarify the interaction characteristics of G_4-DOTA-Mal in absence and presence of Cu(II) combined with the presence of the liposomes.

The use of the specific spin probe CAT12 clarifies that non-covalent surface-driven interactions (electrostatic, H-bonds, ion-dipoles) of G_4-DOTA-Mal with all liposomes are present, proving the presence of different interaction adducts (Scheme 1). Especially, ionic interactions mainly occur between cationic G_4-DOTA-Mal and anionic DMPG surface. Weak interactions arise between G_4-

DOTA-Mal with nearly neutral DMPC liposomes, attributed to a compact liposome structure. This liposome surface poorly adapts to the dendrimer surface. Conversely, competitive interactions are evident at the anionic LEC interface, assuming ionic and H-bond interactions with G_4-DOTA-Mal. This is mainly ascribed to the heterogeneous LEC surface. The main characteristic, which creates structural defects that favor the dendrimer-liposome interactions at the LEC interface, is the mixture of saturated and unsaturated alkyl chains of the two zwitterionic PC and PE lipids, characterized by a smaller ethanolamine group with potential for H-bonding and a larger choline group. Therefore, stable adducts are formed between LEC and G_4-DOTA-Mal, but the weak interactions favor fast exchange with the bulk solution.

The EPR spectra of the Cu(II)/G_4-DOTA-Mal solutions indicate that cationic G_4-DOTA-Mal is an excellent copper complexing agent. A Cu-N_2O_2 coordination with an orthorhombic distortion of a square planar geometry takes place by coordinating two nitrogen sites of the DOTA group and two water molecules. However, we cannot exclude that also dendrimer-internal nitrogen sites and the phosphate ions of PBS buffer are involved in the coordination.

By adding DMPC and LEC liposomes to Cu(II)/G4-DOTA-Mal complexes (Cu-N_2O_2 coordination), a weakening of the Cu(II)-nitrogen ligands binding strength occurs, due to competitive liposome – dendrimer and Cu(II) – dendrimer binding and influenced by the liposome characteristics (e.g. composition, surface charge and surface heterogeneity) and the dendrimer concentration. The weakness of Cu-N_2O_2 coordination is still available at the lowest Cu(II) concentration in presence of DMPC since the earliest incubation times (Scheme 3). At later incubation times and higher dendrimer concentration, LEC liposomes become more perturbative of the Cu(II)-dendrimer complexes, due to LEC-dendrimer interactions. Fluorescence anisotropy results, performed using a lipid concentration of 500 μM and increased dendrimer concentration (from 0 to 100 μM) also supported the finding of LEC-dendrimer interactions. In Figure S12 the maximum interaction with the TMA-DPH probe was found at the same dendrimer/lipid molar ratio used for EPR. A different interacting mode is hypothesized for DMPG, for which perturbation of the complex stability is smaller. We hypothesize that this negatively-charged liposome interacts with the whole complex at the interface without weakening the postulated Cu-N2O2 coordination (Scheme 3).

At high Cu(II) concentrations, spin-spin interactions between close ions prevail at the dendrimer/liposome interface, mainly in cases of LEC and DMPC (Scheme 3). In summary, G4-DOTA-Mal PPI glycodendrimer forms stable Cu(II) complexes, and outlines the desired surface-driven interactions with the membrane surfaces of the different tested liposomes. The binding strength of G_4-DOTA-Mal towards liposome systems is tailored by the membrane composition, Cu(II) concentration and interaction time.

Moreover, the results suggest that G_4-DOTA-Mal and its Cu(II) complexes do not undergo internalization by any liposome, and that G_4-DOTA-Mal is usable as Cu(II) complexation agent in presence of bilayer structures, needed for future in-vitro study. This is smoothly attributed to dynamic and over-time stable glycodendrimer-liposome interactions without destroying the bilayer. Further studies are in progress to deepen the cell-membrane interaction of G_4-DOTA-Mal with more sensitive labels and the understanding of the biological action of G_4-DOTA-Mal for capturing Cu(II).

Associated content

Supporting Information.

The Supporting Information (SI) is available free of charge on the ACS Publications website at DOI: 10.1021/acs.langmuir.0c01776. SI contains additional experimental details (Materials, Devices, Synthesis of G4-DOTA-Mal, Experimental procedures) and data on DLS (also dealing on the stability

of liposomes obtained by means of the extrusion method), ZP and Fluorescence Anisotropy experiments: comments and associated figures (S1-S12) and tables (S1-S2). Further comments on Figure 4 about the intensity of the EPR spectra.

Author information

Corresponding Authors:

- *Dietmar Appelhans, Leibniz Institute for Polymer Research Dresden, Hohe Strasse 6, D-01069 Dresden, Germany (ORCID 0000-0003-4611-8963): applhans@ipfdd.de
- *Riccardo Carloni, Department of Pure and Applied Sciences, Università degli studi di Urbino "Carlo Bo", Urbino, Italy (ORCID 0000-0001-8052-213X): riccardocarloni93@gmail.com

Other Authors:

- Marianna Carone, Department of chemistry and biochemistry, University of Bern, Bern, Switzerland
- Silvia Moreno, Leibniz Institute for Polymer Research Dresden, Hohe Strasse 6, D-01069 Dresden, Germany
- Michela Cangiotti, Department of Pure and Applied Sciences, Università degli studi di Urbino "Carlo Bo", Urbino, Italy
- Maria Francesca Ottaviani, Department of Pure and Applied Sciences, Università degli studi di Urbino "Carlo Bo", Urbino, Italy
- Peng Wang, Leibniz Institute for Polymer Research Dresden, Hohe Strasse 6, D-01069 Dresden, Germany

Notes

The authors declare no competing financial interest.

Acknoledgements

The authors thank DiSPeA, University of Urbino, for funding and Dr. Xuegong Lei, from Columbia University, NY, USA, for the paramagnetic probe CAT12. This article is based upon work from COST Action CA 17140 "Cancer Nanomedicine from the Bench to the Bedside" supported by COST (European Cooperation in Science and Technology).

Supporting Information

Table of Contents

Experimental details:

materials; devices; details on the synthesis of the dendrimer; experimental procedures.

Additional information for the Results and Discussion:

DLS and ZP study providing size and charge of dendrimers and/or liposomes in the absence and presence of Cu(II); long-term stability of liposomes at different temperatures by DLS; further

examples of CAT12 EPR spectra, details about Figure 4 in the manuscript; fluorescence anisotropy study.

1. Materials

PPI dendrimers of DAB-Am64 were supplied by SyMO-Chem (Eindhoven, Netherland). D(+)-Maltose monohydrate, sodium borate, borane–pyridine complex (BH_3*Py, 8 M solution in THF) and anhydrous dimethylsulfoxide were used as purchased from Fluka (Darmstadt, Germany). 1,4,7,10-Tetraazacyclododecane-1,4,7,10-tetraacetic acid mono(N- hydroxysuccinimide ester) (DOTA-NHS-ester) was purchased from Macrocyclis (Dallas, TX). Nomenclature of PPI dendrimers was from the suggestion of the literature [Tomalia, D. A.; Rookmaker, M. In Polymer Data Handbook, 2nd ed.; Mark, J. E., Eds.; Oxford University Press: Oxford, New York, 2009, 979-982]. Regenerated cellulose dialysis membranes with a molecular weight cut-off (M_{WCO}) of 1000 and 2000 were acquired from Fisher (Pittsburgh, PA).

Phospholipids:

Egg lecithin:

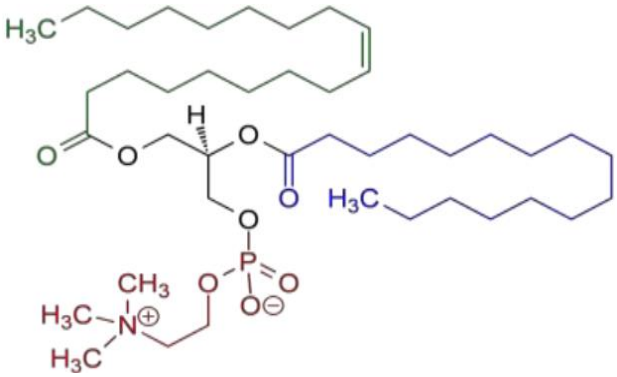

Dimyristoylphosphatidylcholine (DMPC):

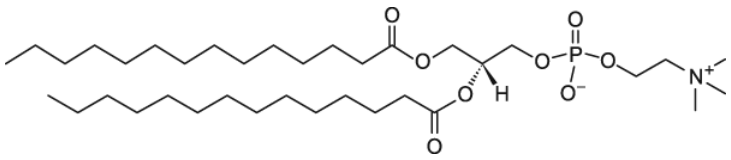

1,2-Dimyristoyl-sn-glycero-3-phospho-rac-(1-glycerol) sodium salt (DMPG):

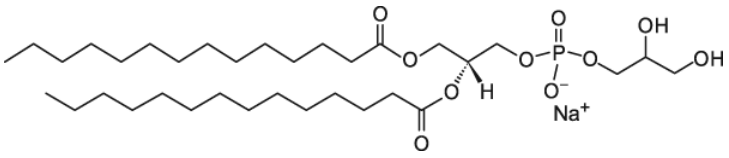

2. Devices

NMR measurements were carried out on a Bruker DRX 500 NMR spectrometer operating at 500.13 MHz for ^1H NMR using D_2O or DMSO-d_6 as a solvent. Sodium 3-(trimethylsilyl)- 3,3,2,2-tetradeuteropropionate was added for internal calibration (δ (^1H) = 0 ppm). The signal assignments were performed by a combination of 1D and 2D NMR experiments using the standard pulse sequences provided by Bruker.

Time of Flight Mass Spectrometry (MALDI-TOF MS) investigations were performed on a Bruker Autoflex Speed TOF/TOF in reflector or linear modes, respectively, and positive polarity by pulsed smart beam laser (modified Nd:YAG laser). The ion acceleration voltage was set to 20 k. For the sample preparation, the substances were mixed with 2,5-dihydroxy benzoic acid as matrix, both dissolved in millipore water.

Zeta-potential (ZP) and dynamic light scattering (DLS) measurements were performed using a Malvern Zetasizer Nano ZS system (model ZEN3600, Worcestershire, UK) equipped with a standard 633 nm laser. Perkin Elmer Optima 7000 DV with a spectral range of 160-900 nm and a resolution < 9 pm were used for carrying out ICP-OES. 2% nitric acid solution was used as solvent.

Cryo-TEM images were acquired using Libra 120 microscope (Carl Zeiss Microscopy GmbH, Oberkochen, Germany) at an acceleration voltage of 120 kV.

EPR experiments were performed by using an EMX-Bruker spectrometer working at X-band (9.5 GHz).

3. Synthesis of DOTA- and maltose modified 4th generation poly(propyleneimine)dendrimer (G4-DOTA-Mal)

DOTA-modified 4th generation poly(propyleneimine)dendrimer (G4-DOTA). DAB-Am64 (0.1 g, 0.0139 mmol) and DOTA-NHS-ester (0.124 g, 0.125 mmol) were reacted in anhydrous DMSO (20 mL) under a N_2 atmosphere. The reaction mixture was stirred overnight followed by dialysis against water (6 times, 2 L) for 2 days using a dialysis membrane with an MWCO of 1000. After freeze drying, a viscous liquid of the product G4- DOTA was quantitatively obtained. 1H NMR spectrum is presented in Figure S1.

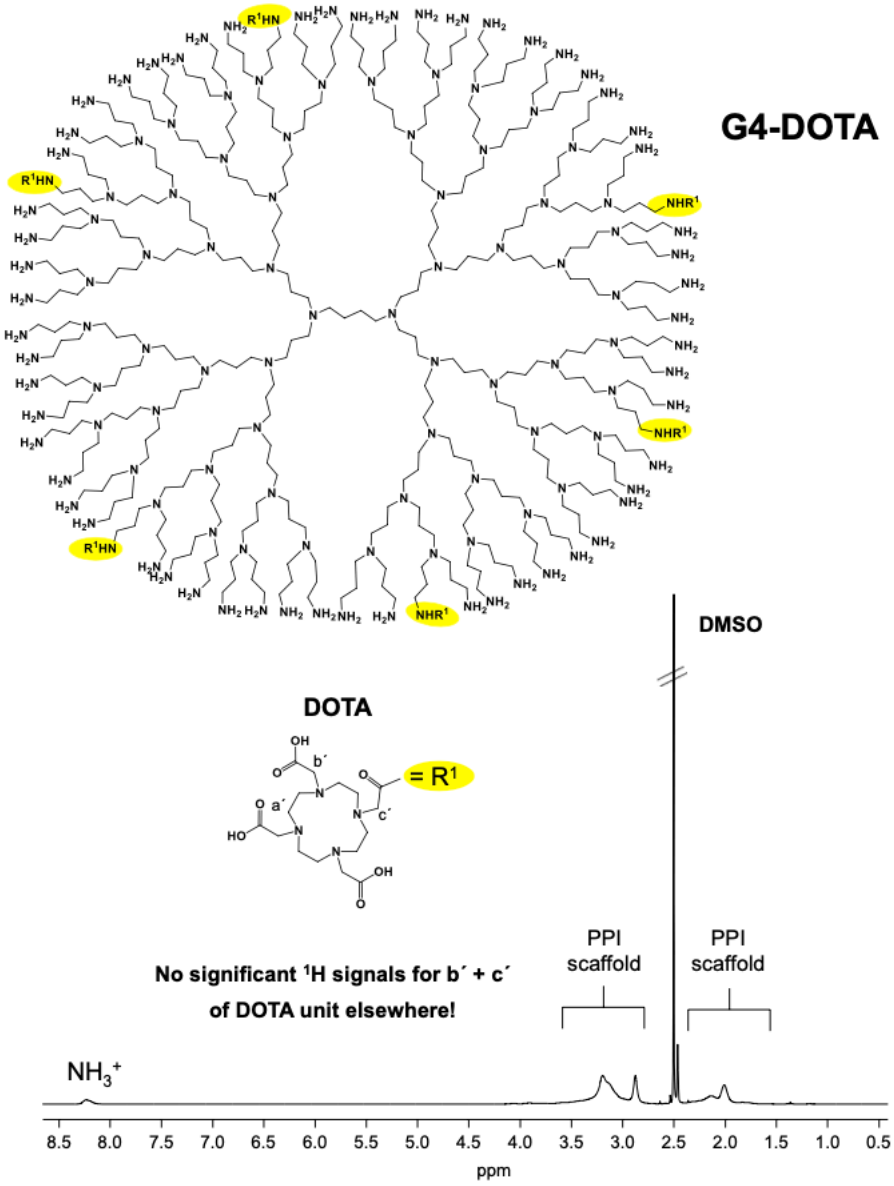

Figure S1. 1H NMR spectrum of DOTA-modified 4th generation poly(propyleneimine) (PPI) dendrimer (G4-DOTA) in DMSO-d_6. 1H NMR spectrum of G4-DOTA is similar to previously published 1H NMR spectrum of DOTA-modified 4th generation poly(propyleneimine) dendrimer [Xiong Z. et al., Biomaterials Science 2016, 4, 1622-1629].

DOTA- and maltose modified 4th generation poly(propyleneimine)dendrimer (G4-DOTA- Mal). The G4-DOTA dendrimer (0.10 g, 0.014 mmol), maltose monohydrate (14.74 g, 41 mmol), and borane–pyridine complex (5 mL, 40 mmol, 8 M solution) were mixed in a sodium borate buffer (30 mL, 0.1 M). The reaction solution was stirred at 50 °C for 7 days, thereafter the crude product was purified by dialysis against water (6 times, 2 L) for 4 days. Further lyophilization gave rise to the formation of the G4-DOTA-Mal dendrimer with a yield of 0.400 g (95%). 1H NMR signals of the DOTA unit attached on the G4-DOTA-Mal are suppressed by the dendritic PPI scaffold and maltose units. All other typical 1H NMR signals of the G4-DOTA-Mal glycodendrimer with dense maltose shell are the same as previously published [Xiong Z. et al., Biomaterials Science 2016, 4, 1622-1629]: 1H NMR

(D_2O): δ = 1.4–2.3 (a, d, g, j, m and p); 2.3–3.35 (1′, b, c, e, f, h, i, k, l, n, o and q); 3.35–4.55 (2–6 and 2′-6′); 4.95–5.35 ppm (1). In Figure S2, 1H NMR signals are only determinable for PPI-scaffold and maltose units in G4-DOTA-Mal, while degree of DOTA units attached to PPI scaffold was determined by ICP-OES. The degree of chemically coupled DOTA units on G4-DOTA-Mal was determined by inductively coupled plasma-optical emission spectroscopy (ICP-OES) through complexation of Gd(III) ions. About 6 DOTA are attached to the scaffold of dendritic poly(propyleneimine). Molecular weight of G4-DOTA-Mal is 37,500 g/mol determined by MALDI-TOF MS. Thus about 86 maltose units are attached on the dendritic PPI scaffold (Figure S2).

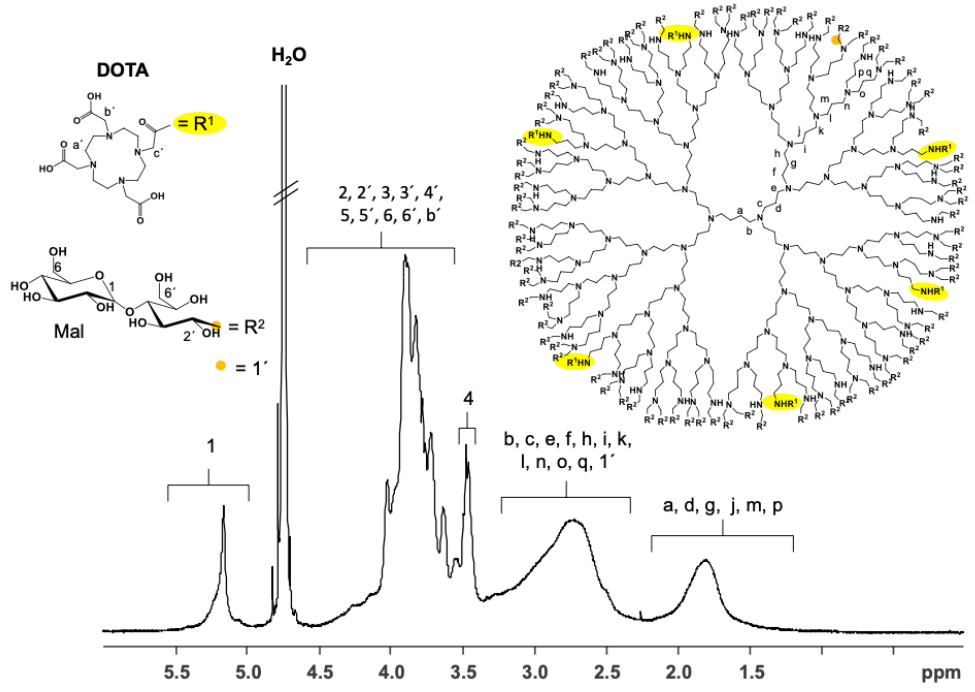

Figure S2. ^{1}H NMR spectrum of DOTA-modified 4th generation poly(propyleneimine) dendrimer with dense maltose shell (G4-DOTA-Mal) in D_2O.

4. Experimental procedures

4.1 DLS and ZP experiments

The size of particles and the polydispersity index (PDI) were measured using the DLS technique. The equilibration time was 60 sec., while the measurement angle was 173° and the number of measurements was 3 per 25 runs (run duration 5 sec). The peak size gives the z- average. All the experiments were performed at 25°C, and at different equilibration times, t = 0, 1h, and 24 h. The surface charge was determined by using the Zetasizer Nano-ZS with a combination of electrophoresis and laser Doppler velocimetry. Electrophoretic mobility of particles was measured by using capillary plastic cells with a copper electrode, covered with gold, in order to apply an electric field. The data evaluation was carried out by using Malvern Software from the Helmholtz–Smoluchowski equation. First, liposomes (in the absence of dendrimers) were tested to monitor their thermal stability over time; each liposome (LEC, DMPC and DMPG) solution were divided into two aliquots and incubated at 4°C and 37°C, respectively. The liposome stability was performed after 3, 10, 20 and 30 days since the day of preparation, and at 25°C, 30°C, 37°C, and 40°C. Liposome solutions were prepared in 10 mM PBS at a concentration of 0.50 mg/mL for LEC, and 0.30 mg/mL for DMPC

and DMPG.
To study the interactions of G4-DOTA-Mal - Cu(II) complex with the liposomes, the compounds were added following a specific order: firstly, G4-DOTA-Mal and Cu(II) nitrate solutions were equilibrated for 10 minutes, then the complex was added to liposomes solutions. The following samples were tested: a) 0.65 mM of lecithin + 0.728 mM/0.364 mM/0.182 mM Cu(II) + 0.04 mM of G4-DOTA-Mal; and b) 0.83 mM of DMPC or DMPC/DMPG 3% + 0.929 mM/ 0.464 mM/ 0.230 mM Cu(II) + 0.05 mM (G4-DOTA-Mal). LEC was used at a different concentration with respect to DMPC and DMPC/DMPG 3% since the lipid concentrations were initially selected in order to optimize the structural characteristics of liposomes for performing DLS measurements. However, the molar ratios between lipids, dendrimers and Cu(II) ions were maintained constant in all experiments.
The volume vs. size plots of dendrimer alone, liposomes alone, and the samples obtained by adding dendrimers to liposomes in the absence and presence of Cu(II) at the different concentrations allowed us to evaluate the particle sizes to structurally characterize the systems, together with PDI and ZP. As a reference, the dendrimer alone was also investigated in aqueous solution (Figure S3).

4.2 EPR experiments

The suspension was placed in EPR tubes (1 mm internal diameter) and subjected to different equilibration times (t = 0, 1 and 24 h). All experiments were performed at 25 °C. Data were analyzed via Budil at al. calculation program.[Budil, D. E.et al. J. Magn. Reson., 1996, 120, 155-189].
For the analysis of Cu(II) spectra, according to the sensitivity of the instrument, the used experimental concentrations were 25 mM for the phospholipids, 28 mM/ 14 mM/ 7 mM for Cu(II), and 1.56 mM for G4-DOTA-Mal. First, G4-DOTA-Mal and Cu(II) nitrate solutions were mixed under stirring for 10 minutes, then liposome solutions were added.
For the analysis of the spectra of the spin probe CAT12, CAT12 (1 mM) was added to the liposome solutions (25 mM in phospholipids), and the final liposomal suspension was stirred overnight. For both the EPR studies using Cu(II) and CAT12, the EPR spectra of samples consisting of the ternary system constituted by the paramagnetic species + dendrimer + liposome were compared to the simple binary systems constituted by the paramagnetic species + liposome or dendrimer.
4.3 Fluorescence anisotropy experiments
Fluorescence spectra were measured by means of a Fluorolog 3 (Horiba JobinYvon, USA) fluorescence spectrophotometer. The polarization values (r) were calculated using FluorEssence software with the following equation:

$$\text{Anisotropy, r} = \frac{I_{VV} - GI_{VH}}{I_{VV} + 2GI_{VH}}$$

Where I_{VV} stands for vertical excitation and vertical emission; I_{VH} stands for vertical excitation and horizontal emission; G is the grating factor which is I_{HV}/I_{HH}. For the three different liposomes (LEC, DMPC and DMPG) the phospholipids (500 μM) were dissolved in chloroform/ methanol 2:1 in presence of the fluorescent probe, 1,6-diphenylhexatriene (DPH) or 1-(4-(trimethylamino)phenyl)-6-phenylhexa-1,3,5-triene (TMA-DPH), at a lipid/ fluorescent probe molar ratio of 500:1. The liposome preparation was performed as described above. Then, a sample of liposomes (1 ml) was placed in the semi-cuvette and 10 μL of G4- DOTA-Mal (C_{Stock} = 0.001M in MilliQ) was added to each measurement. The concentration of G4-DOTA-Mal was increased from 0 μM to 100 μM during

measurements. The wavelength at which the analysis was carried out were 380 nm as excitation, 426 nm as emission for DPH and 430 nm for TMA-DPH. All the experiments were performed at room temperature.

Fluorescence anisotropy provides information on the main localization of molecules by means of specific fluorescent probes. In our case we evaluated the membrane fluidity and glycodendrimer localization in presence of the three liposomes: LEC, DMPC and DMPG, using the following two fluorescent probes [Do Canto, A. M. T. M.et al. BBA Biomembranes, 2016, 1858(11), 2647–2661]: 1) DPH is a popular probe of membrane interiors, useful for evaluating the possible interaction between glycodendrimer and liposomes in the hydrophobic membrane region. It provides info on mobility not on localization. In fact, DPH can be between the chains but also flat in the core of the bilayer, with a not defined localization; (2) TMA-DPH is well-known to act as an anchor on membrane surface; the molar moiety limits the insertion but the DPH part is still in the upper part of the hydrophobic section. In the present study, DPH was used to detect surface interactions between glycodendrimer and liposomes surface.

4.4 Cryo-TEM images

Samples for acquiring Cryo-TEM images were prepared by dropping 2 μL of liposome solution (1.3 mM LEC + 0.08 mM DOTA in PBS 10 mM; 1.5 mM DMPC or DMPG + 0.09 mM DOTA in PBS 10 mM) on copper grids coated with holey carbon foil (so-called Lacey type). A piece of filter paper was used to remove the excess water; the sample was then rapidly frozen in liquid ethane at -178°C. The blotting with the filter paper and plunging into liquid ethane was done in a Leica GP device (Leica Microsystems GmbH, Wetzlar, Germany). All images were recorded in bright field at -172°C. The diameter (60-80 particles) and membrane thickness (10-20 particles) of the empty and loaded-liposome were determined from cryo-TEM images by using TEM Image Processing Software.

5. Additional information for the Results and Discussion

5.1 DLS and ZP study providing size and charge of dendrimers and/or liposomes in the absence and presence of Cu(II)

Figure S3 shows the volume plot of G4-DOTA-Mal (0.05 mM) in aqueous solution evaluated by dynamic light scattering experiments. D_h = hydrodynamic diameter.

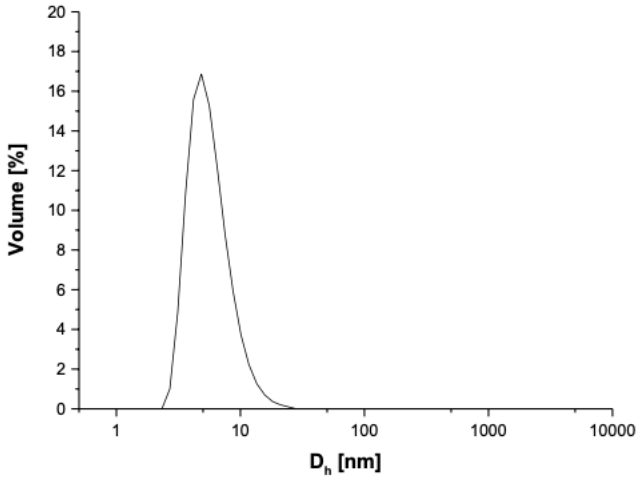

Figure S3. Volume as a function of size distribution for G4-DOTA-Mal (0.05 mM) in aqueous solution evaluated by dynamic light scattering experiments. D_h = hydrodynamic diameter.

Figure S4 shows the pH-dependence of the zeta potential of G4-DOTA-Mal.

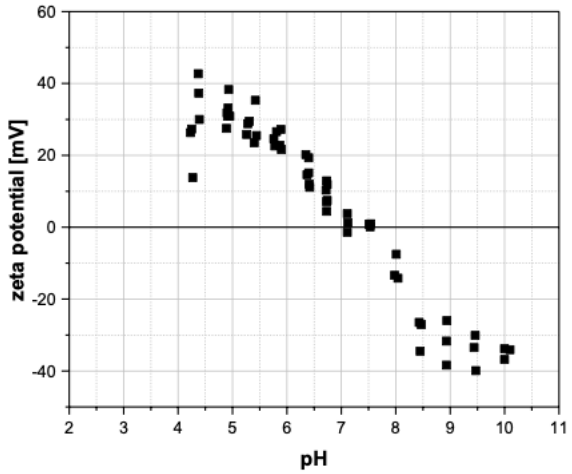

Figure S4. pH-dependent zeta potential of G4-DOTA-Mal

Table S1 summarizes the D_h, Z-average values, and surface charge (ζ) of aggregated G4- DOTA-Mal macromolecules (0.04 M) in absence and presence of Cu(II) (7, 14 and 28 mM) at 25 and 37 °C, respectively.

Table S1. Z-average (diameter, D_h), PDI and ZP (ζ) of G4-DOTA-Mal (0.05 mM) in absence and presence of Cu(II) in PBS (10 mM) at 25 and 37°C.

Samples	25°C		37°C		25°C	37°C
	D_h nm	PDI	D_h nm	PDI	ζ mV	ζ mV
G4-DOTA-Mal	337	0.500	670	0.564	16.5	21.5
G4-DOTA-Mal + 7 mM Cu(II)	583	0.622	1072	0.737	25.0	26.1
G4-DOTA-Mal + 14 mM Cu(II)	338	0.412	632	0.534	28.3	26.0
G4-DOTA-Mal + 28 mM Cu(II)	186	0.477	436	0.403	32.0	28.3

Z-average are shown, but the samples are highly polydisperse, the D_h data is not reliable.

Table S2 depicts the hydrodynamic diameters (D_h, Z-average) and surface charge (ζ) of liposomes (LEC, DMPC, and DMPG) in absence and presence of G4-DOTA-Mal and their adducts with Cu(II) at three concentrations (7 mM, 14 mM and 28 mM), determined at 0, 1 and 24h.

Table S2. Z-average (diameter, D_h), PDI and ZP (ζ) of the different liposomes (LEC, DMPC, DMPG) in absence and presence of G4-DOTA-Mal (0.05 mM) and Cu(II) in PBS (10 mM) at 25°C. On the basis of DLS results, ZP was only measured after the equilibration of the sample (24 h).

Sample	0 h		1 h		24 h		
LEC	**D_h nm**	**PDI**	**D_h nm**	**PDI**	**Dh nm**	**PDI**	**ζ mV**
Pure liposome	130	0.037	130	0.037	130	0.037	-6.37
0 mM Cu(II) + G4-DOTA-Mal	130	0.154	132	0.154	135	0.154	-1.39
7 mM Cu(II)+ G4-DOTA-Mal	255	0.430	190	0.258	130	0.190	3.80
14 mM Cu(II) + G4-DOTA-Mal	186	0.420	130	0.235	131	0.193	0.09
28 mM Cu(II) + G4-DOTA-Mal	136	0.129	169	0.347	127	0.156	2.03
	0 h		**1 h**		**24 h**		
DMPC	**D_h nm**	**PDI**	**D_h nm**	**PDI**	**D_h Nm**	**PDI**	**ζ mV**
Pure liposome	129	0.040	129	0.040	129	0.040	-0.32
0 mM Cu(II) + G4-DOTA-Mal	156	0.363	122	0.340	116	0.198	-0.65
7 mM Cu(II)+ G4-DOTA-Mal	191	0.403	142	0.310	132	0.313	1.21
14 mM Cu(II) + G4-DOTA-Mal	150	0.368	119	0.327	119	0.214	1.75
28 mM Cu(II) + G4-DOTA-Mal	143	0.381	121	0.375	170	0.326	2.54

	0 h		1 h		24 h		
DMPG	**D_h nm**	**PDI**	**D_h nm**	**PDI**	**D_h Nm**	**PDI**	**ζ mV**
Pure liposome	119	0.038	119	0.038	119	0.038	-7.20
0 mM Cu(II) + G4-DOTA-Mal	140	0.365	144	0.260	129	0.430	-1.47
7 mM Cu(II)+ G4-DOTA-Mal	137	0.284	167	0.283	113	0.319	-0.12
14 mM Cu(II) + G4-DOTA-Mal	158	0.305	124	0.277	122	0.369	0.02
28 mM Cu(II) + G4-DOTA-Mal	173	0.267	127	0.301	96	0.226	0.69

Concerning the lecithin liposomes, the post-loading addition of G4-DOTA-Mal had no effect on the liposome size. The addition of glycodendrimers is reflected in immediate increase in PDI followed by restoration of initial conditions after 24 hours (PDI lower than 0.2, resulting in homogenous systems). Additionally, the interaction of the G4-DOTA-Mal - Cu(II) complex and LEC resulted in a further increase in the positively charged surface and the system appeared homogenous at t=0h, t=1h and t=24h.

The interaction between the G4-DOTA-Mal - Cu(II) complex and DMPC liposomes makes the surface charge positive. Unlike what was observed for lecithin liposomes, for DMPC systems the Cu(II) concentration was less affecting the polydispersity of the particles.

For DMPG (DMPC/DMPG 3 %) liposomes, as shown in Table S2, the addition of G4- DOTA-Mal and the further addition of Cu(II) to the dendrimer increases the positive charge of the DMPG surface. Concerning the polydispersity, the presence of G4-DOTA-Mal and the complex is reflected in the increase of PDI also after 24 h.

The volume in function of the size distribution in Figure S5 shows a peak around 100 nm highlighting that no aggregation processes occurred. The hydrodynamic diameter obtained from DLS refers to particles diffusion within a fluid; surface structure, concentration as well as the type of ions in the medium affect the diffusion speed of particles and, consequently, the hydrodynamic diameter.

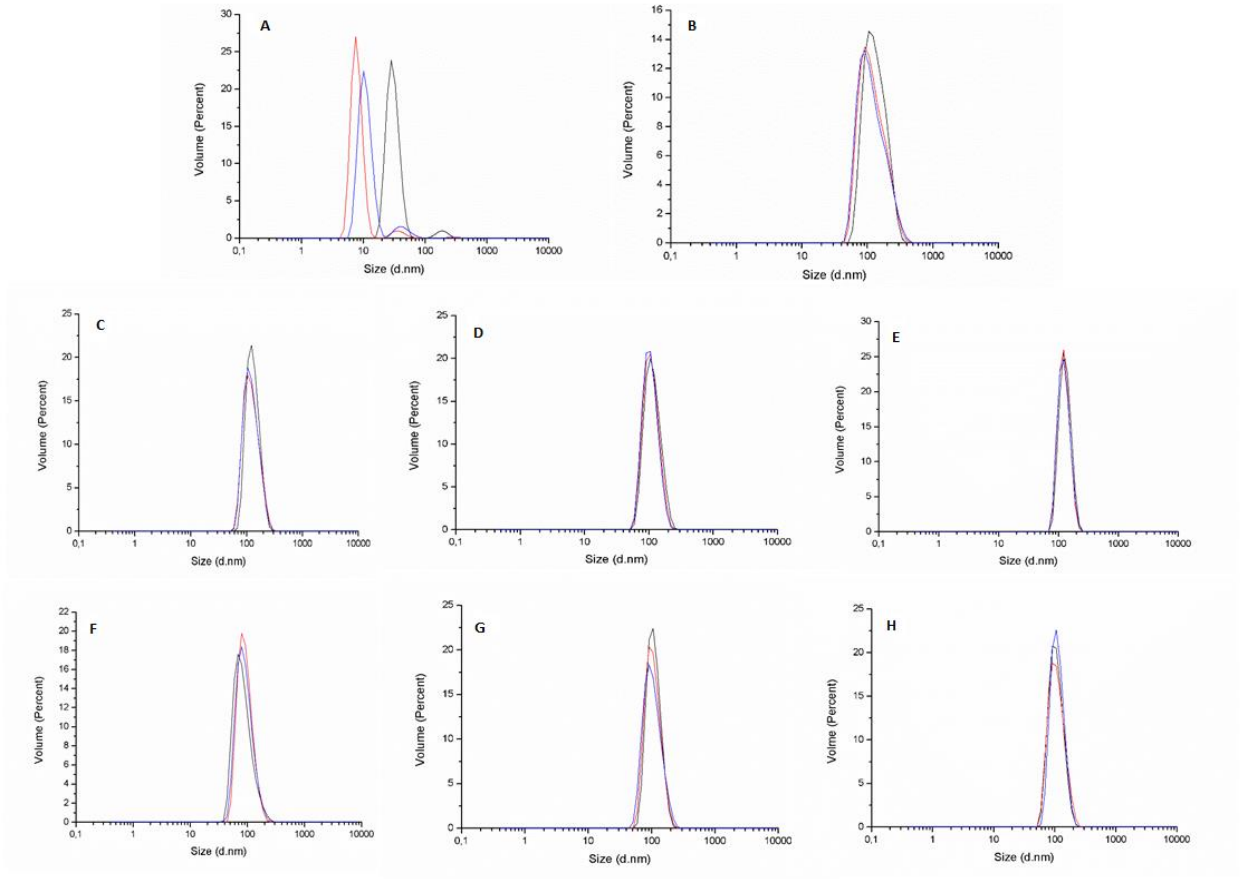

Figure S5. DLS volume plot of G4-DOTA-Mal (A) showing 3 measurements of the same batch in PBS (10 mM). DLS volume plots for LEC liposomes + G4-DOTA-Mal (B); DMPC liposomes (C); DMPC liposomes and G4-DOTA-Mal (D); DMPC liposomes, G4-DOTA-Mal and Cu(II) (E); DMPG liposomes (F); DMPG liposomes and G4-DOTA-Mal (G); DMPG liposomes, G4-DOTA-Mal and Cu(II) (H). All compounds were dissolved in PBS (10 mM, pH 7.4) at 25°C; compounds concentrations reported in the experimental section. 3 measurements of the same batch in PBS (10 mM) for B to H. Therefore, a well-defined liposome structure forms both in the absence and in the presence of the glycodendrimer and Cu(II).

5.2 Long-term stability of liposomes at different temperatures by DLS

Further DLS measurements over time were performed to verify the stability of the liposomes (Figures S6-S8). Figure S6 shows the difference between LEC liposomes obtained using sonication or extrusion treatments. The sonication treatment (Figure S6) leads to unstable and non-homogenous liposomes; the system is indeed characterized by a high polydispersity index (PDI greater than 0.2; results not shown). Conversely, the extrusion treatment produces homogeneous, monolamellar and long-term stable liposomes.

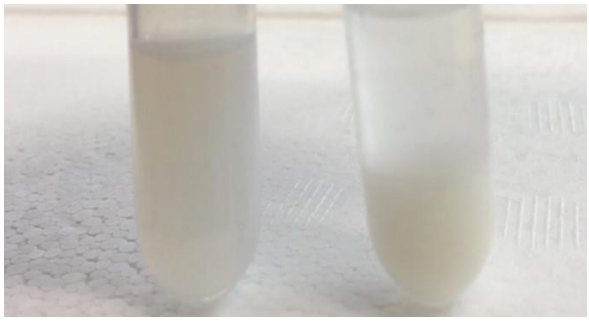

Figure S6. Lecithin suspension after the overnight incubation: on the left, the sample obtained by extrusion treatment, on the right, the sonication one.

Figures S7 and S8 show that the variation of the average size of liposomes obtained by means of the extrusion method at 25 °C and 37 °C, respectively, was almost constant throughout one month; in particular, there was a good similarity between the liposomes stored at room temperature and those at 4 °C.

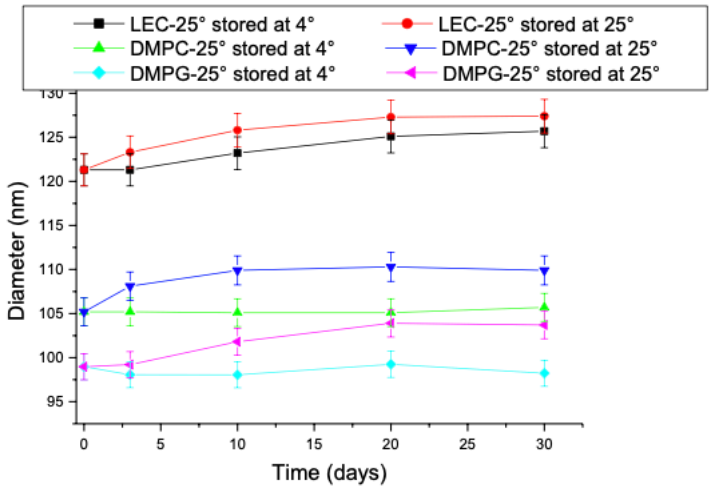

Figure S7. Variation of the liposome diameter (mean z-average diameter) over equilibration time at 25 °C, proving the long-term stability of the liposomes obtained by the extrusion method at different temperatures (4 and 25 °C). The liposomes were stored at 4oC or 25oC for different periods (3, 10, 20 and 30 days). The DLS was carried out at 25oC. C_{LEC} = 0.5 mg/mL; C_{DMPC} = 0.3 mg/mL; C_{DMPG} = 0.3 mg/mL. Data are expressed as mean ± SD.

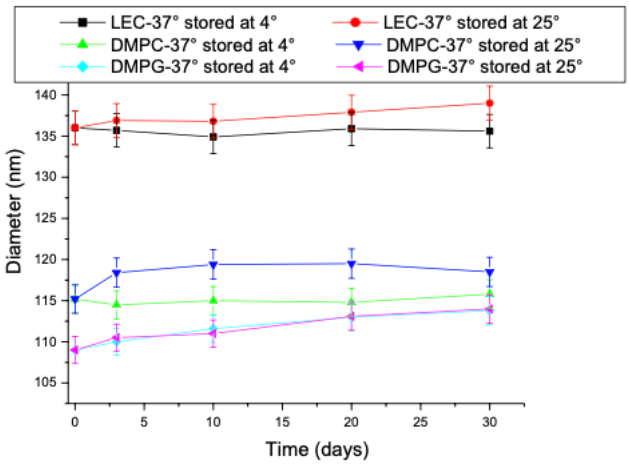

Figure S8. Variation of the liposome diameter (mean z-average diameter) over equilibration time at 37 °C, proving the long-term stability of the liposomes obtained by the extrusion method at different temperatures (4 and 25 °C). The liposomes were stored at 4oC or 25oC for different periods (3, 10, 20 and 30 days). The DLS was carried out at 37 oC. C_{LEC} = 0.5 mg/mL; C_{DMPC} = 0.3 mg/mL; C_{DMPG} = 0.3 mg/mL. Data are expressed as mean ± SD.

Furthermore, passing from 25 °C to 37 °C the average size progressively increased for liposomes stored at room temperature as well as 4°C, due to the faster dynamics at the higher temperature. However, the size of the liposomes was completely maintained after 30 days from samples preparation. An important conclusion is that the used protocol, associated with the extrusion treatment, leads to the production of unilamellar liposomes that are stable and uniform over time, showing PDI values lower than 0.2 and having reproducible diameters. In addition to this, the liposomes show to be resistant to temperature changes.

Furthermore, the observations confirm that the size of the vesicles are not concentration and temperature dependent for the different types of lipids.

5.3 Further examples of CAT12 EPR spectra

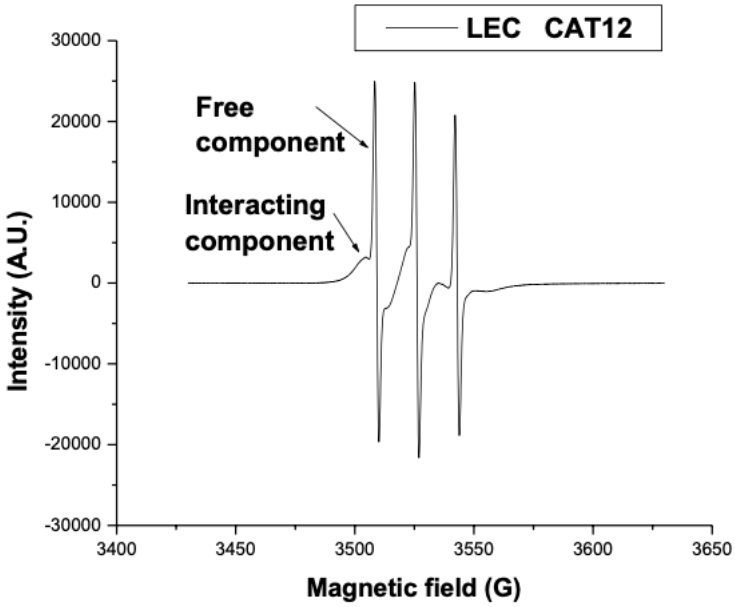

Figure S9. EPR experimental spectrum of CAT 12 in the two component system LEC/CAT12.

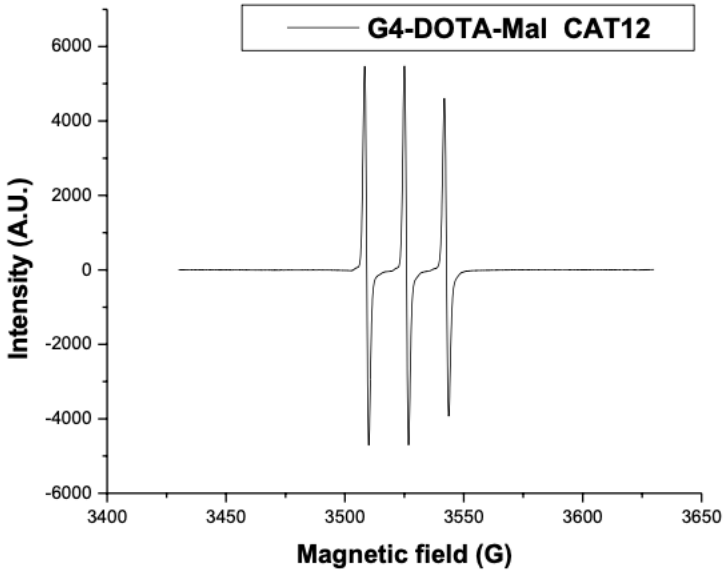

Figure S10. EPR experimental spectrum of CAT 12 in the two component system G4- DOTA-Mal/CAT12.

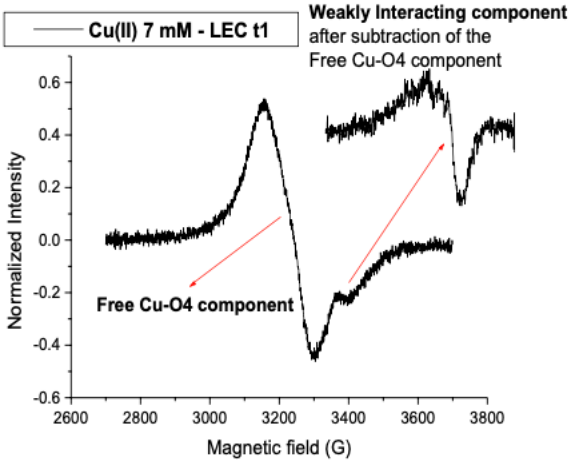

Figure S11. EPR spectrum of the two component system LEC/Cu(II) with a Cu(II) concentration of 7 mM at 1 h.

5.4 Further comments on the variations of the EPR spectra intensity, relative % of the interacting component, τ for the Free component, S of the interacting component, <A> for the Interacting and Free components, for the three different liposomes in the absence and presence of G4-DOTA-Mal (shown in Figure 4 of the manuscript):

The intensity increases in the presence of liposomes compared to pure CAT12 solutions, confirming that CAT12 inserts into the liposomes (LEC < DMPC < DMPG) increasing its solubility. The lower solubility found for LEC compared to other liposomes was accompanied by a higher relative percentage of interacting component. By adding G4-DOTA-Mal, the interacting percentage increased (DMPC<DMPG<LEC).

The microviscosity measured by τ for the free component followed the series (DMPC<DMPG<LEC) in the absence of the dendrimer, which become (pureCAT12<DMPG<DMPC<LEC) in presence of the dendrimer. This behavior reflects the interactions occurring at the dendrimer/liposome surface, connected to the presence of the hydrocarbon chain in CAT12, which, in the free component, stays at the interface and not inside the liposome. Therefore, by adding G4-DOTA-Mal, the microviscosity of the free component increases, because the dendrimer interacts with the liposome surface and blocks CAT12. This increase is more significant for DMPC with respect to the other liposomes as a consequence of the more compact DMPC structure. For DMPG the presence of the charge makes this increase less significant.

A minor internalization of CAT12 in compact DMPC liposomes was proved by the lower value of the order parameter S (DMPC<LEC<DMPG). S decreased by adding G4-DOTA- Mal to all liposomes, in line with a perturbative effect due to liposome-dendrimer interactions. This decrease was more significant for DMPG, which reached the value of LEC. Therefore, the DMPG liposome structure was partially deformed due to the interaction with the dendrimer.

The variation of the polarity parameter, <A> for the interacting probes follows the trend DMPG<DMPC<LEC. The lower micropolarity for DMPG is probably due to neutralization of the positive charge of the CAT group with the negative charge of the liposome surface

The micropolarity <A> of the free component (DMPC ~ LEC<DMPG) varied in an opposite way if compared to the interacting component: in fact <A> was the higher for DMPG (due to the negative

charge) and increased from the absence to the presence of G4- DOTA-Mal in agreement with a location of the radical group at the external surface of the
liposomes where the charged groups of the phospholipids are located. G4-DOTA-Mal created a more polar environment for CAT12 surfactants at the liposome/dendrimer interface.

5.5 Fluorescence anisotropy study

Fluorescence anisotropy provides information on the main localization of molecules by means of specific fluorescent probes. In our case we evaluated the membrane fluidity and glycodendrimer localization in presence of the three liposomes: LEC, DMPC and DMPG, using two fluorescent probes: (1) DPH is a popular probe of membrane interiors, useful for evaluating the possible interaction between glycodendrimer and liposomes in the hydrophobic membrane region; (2) TMA-DPH is well-known to act as an anchor on membrane surface; in the present study, it was used to detect surface interactions between glycodendrimer and liposomes. The change in the fluorescence anisotropy is shown in Figure S9 as a function of the dendrimer concentration towards the three liposomes, LEC, DMPC and DMPG.

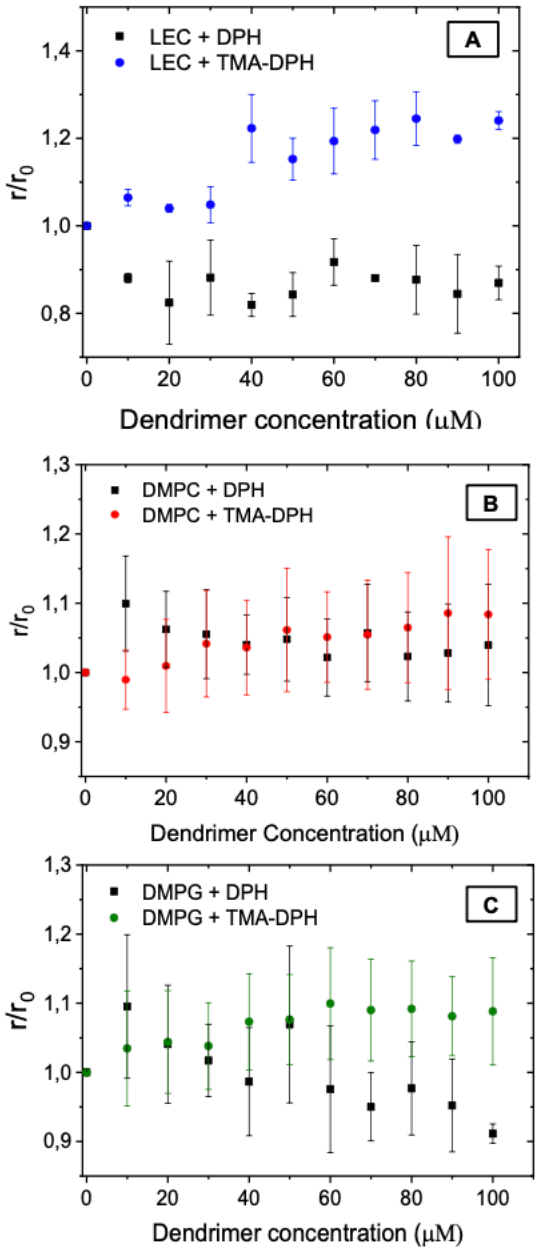

Figure S12. Fluorescence anisotropy of DPH and TMA-DPH probes in LEC (A), DMPC (B) and DMPG(C) liposome/G4-DOTA-Mal mixtures. r, fluorescence anisotropy value; r0 control fluorescence anisotropy value in the absence of G4-DOTA-Mal. Data are expressed as mean ± SD.

A more decisive hydrophilic interaction of TMA-DPH with the glycodendrimer is shown by LEC (Figure S9, top), if compared to the other liposomes, DMPC and DMPG (Figure S9, middle + bottom). This implies a surface interaction of G4-DOTA-Mal with LEC, which is in line with the EPR results. Weaker interactions are present in case of liposomes, DMPC and DMPG, with nearly differences. The hydrophilic surface interactions of TMA-DPH- integrated liposomes with G4-DOTA-Mal are only visible at higher dendrimer concentration. This is partially explainable, when considering the surface charge (Table S2) and perturbation properties of liposomses, induced by G4-DOTA-Mal (EPR study), only a combination of both parameters may induce hydrophilic interaction of less extent with G4-DOTA-Mal.

Using the hydrophobic probe DPH, negligible interactions are observed in all samples (Figure S9). In the case of DMPG at low dendrimer concentration, a small interaction occurs with the hydrophobic part of the membrane probably related to the structural deformation hypothesized on the basis of the EPR results. As the concentration increases, hydrophilic interactions prevail.

References

1. Bost, M.; Houdart, S.; Oberli, M.; Kalonji, E.; Huneau, JF.; Margaritis, I. Dietary Copper and Human Health: Current Evidence and Unresolved Issues, J Trace Elem Med Biol, 2016, 35, 107–15.
2. Cater, M.A.; La Fontaine, S.; Shield, K.; Deal, Y.; Mercer, J.F. ATP7B Mediates Vesicular Sequestration of Copper: Insight Into Biliary Copper Excretion, Gastroenterology, 2006, 130(2), 493–506.
3. Chang, I.J.; Hahn, S.H. The Genetics of Wilson Disease, Hand b. Clin. Neurol., 2017, 142, 19–34.
4. Ranucci, G.; Polishchuck, R.; Iorio, R. Wilson's Disease: Prospective Developments towards New Therapies, World J. Gastroenterol., 2017, 23(30), 5451.
5. Liu, J.; Luan, J.; Zhou, X.; Cui, Y.; Han, J. Epidemiology, Diagnosis, and Treatment of Wilson's Disease, Intractable & rare diseases research, 2017, 6(4), 249–55.
6. European Association for the Study of the Liver, EASL Clinical Practice Guidelines: Wilson's Disease, Journal of Hepatology, 2012, 56, 671–85.
7. Aggarwal, A.; Bhatt, M. Advances in Treatment of Wilson Disease, Tremor and other hyperkinetic movements, 2018, 8, 525.
8. Kozlowski, H.; Janicka-Klos, A.; Brasun, J.; Gaggelli, E.; Valesin, D.; Valesin, G. Copper, Iron, and Zinc Ions Homeostasis and Their Role in Neurodegenerative Disorders (Metal Uptake, Transport, Distribution and Regulation), Coord. Chem. Rev. 2009, 253(21–22), 2665–85.
9. Gerosa, C.; Fanni, D.; Congiu, T.; Piras, M.; Cau, F.; Moi, M.; Faa, G. Liver Pathology in Wilson's Disease: From Copper Overload to Cirrhosis, J. Inorg. Biochem., 2019, 193, 106–11.
10. Harris Z.L. Ceruloplasmin, Clinical and Translational Perspectives on Wilson Disease, 2019, 77–84.
11. Wu, F.; Wang, J.; Pu, C.; Qiao, L.; Jiang, C. Wilson's Disease: A Comprehensive Review of the Molecular Mechanisms, Int. J. Mol. Sci., 2015, 16(3), 6419–31.
12. Schilsky, M.L. Wilson Disease: Diagnosis, Treatment, and Follow-Up, Clin Liver Dis, 2017, 21(4), 755–67.
13. Appelhans, D.; Klajnert-Maculewicz, B.; Janaszewska, A.; Lazniewska, J.; Voit, B. Dendritic Glycopolymers Based on Dendritic Polyamine Scaffolds: View on Their Synthetic Approaches, Characteristics and Potential for Biomedical Applications, Chem. Soc. Rev., 2015, 44(12), 3968–96.
14. Sherje, A.; Jadhav, M.; Dravyakar, B.R.; Kadam, D. Dendrimers: A Versatile Nanocarrier for Drug Delivery and Targeting, Int. J. Pharm., 2018, 548(1), 707–20.
15. Abbasi, E.; Aval, S.F.; Akbarzadeh, A.; Milani, M.; Nasrabadi, H.T.; Hanifehpour, Y,; Nejati-Koshki, K.; Joo, S.W.; Pashaei-Asl, R. Dendrimers: Synthesis, Applications, and Properties, Nanoscale Res. Lett, 2014, 9(1), 247.
16. Janaszewska, A.; Lazniewska, J.; Trzepiński, P.; Marcinkowska, M.; Klajnert-Maculewicz, B. Cytotoxicity of Dendrimers, Biomolecules, 2019, 9(8), 1–23.
17. Jones, C.F.; Campbell, R.A.; Brooks, A.E.; Assemi, S.; Tadjiki, S.; Thiagarajan, G.; Mulcock, C.; Weyrich, A.S.; Brooks, B.D.; Ghandehari, H.; Grainger, D.W. Cationic PAMAM Dendrimers Aggressively Initiate Blood Clot Formation, ACS Nano, 2012, 6(11), 9900–9910.
18. 18. Yu, S.; Bond, M.R.; Whitman, C.M.; Kohler, J.J.; Metabolic Labeling of Glycoconjugates with Photocrosslinking Sugars, Method Enzymol, 2010, 478, 541–62.
19. 19. Sun, L.; Middleton, D.R.; Wantuch, P.L.; Ozdilek, A.; Avci, F.Y. Carbohydrates as T-Cell Antigens with Implications in Health and Disease, Glycobiology, 2016, 26(10), 1029–40.
20. Pieters, R.J. Carbohydrate mediated bacterial adhesion, Adv Exp Med Biol, 2011,715, 227–240.
21. Appelhans, D. ; Cladera, J. ; Rogers, M. ; Voit, B.: Dendritic glyco architectures - from H-bond-driven molecular interactions to their potential use in brain disease therapy. In Glycopolymer Code: Synthesis of Glycopolymers and Their Applications, ed. Royal Society of Chemistry (2015) Chapter 5, 149-177
22. Aso, E.; Marinsson, I.; Appelhans, D.; Benseny-Cases, N.; Effenberg, C.; Cladera, J.; Gouras, G.; Ferrer, I.; Klementieva, O. Poly(propylene imine) dendrimers with histidine-maltose shell as novel type of nanoparticles for synapse and memory protection. Nanomedicine: Nanotechnology, Medicine and Biology, 2019, 17, 198-209.
23. Schmitz, M.; Candelise, N.; Kanata, E.; Llorens, F.; Thüne, K.; Villar-Piqué, A.; da Silva Correia, S. M.; Dafou, D.; Sklaviadis, T.; Appelhans, D.; Zerr, I. Screening and testing of anti-prion glycodendrimers towards

scrapie-infected cells and sporadic Creutzfeldt-Jakob disease patients prions. Molecular Neurobiology, 2020, 57,1863–1874.
24. Ziemba, B.; Sikorska, H.; Jander, M.; Kuncman, W.; Danilewicz, M.; Appelhans, D.; Bryszewska, M.; Borowiec, M.; Franiak-Pietryga, I. Anti-tumour activity of glycodendrimer nanoparticles in a subcutaneous MEC-1 xenograft model of human chronic lymphocytic leukemia. Anti-Cancer Agents in Medicinal Chemistry, 2020, 20, 325-334.
25. Gorzkiewicz, M.; Deriu, M. A.; Studizan, M.; Janaszewska, A.; Grasso, G.; Pulaski, L.; Appelhans, D.; Danani, A.; Klajnert-Maculewicz, B. Fludarabine-specific molecular interactions with maltose-modified poly(propyleneimine) dendrimer enable effective cell entry of active drug form: comparison with clofarabine, Biomacromolecules, 2019, 20, 1429-1442.
26. Andreozzi, E.; Antonelli, A.; Cangiotti, M.; Canonico, B.; Sfara, C.; Pianetti, A.; Bruscolini, F.; Appelhans, D.; Papa, S. Ottaviani, M.F. Interactions of Nitroxide-Conjugated and non-Conjugated Glycodendrimers with Normal and Cancer Cells and Biocompatibility Studies. Bioconjugate Chemistry, 2017, 28 (2), 524–538.
27. Chengjie, S.; Hongyu, L.; Xuanqing, G.; Zhao-xuan, Y.; Yan, M.; Xiaoyuan, C.; Jinhao, G. DOTA-Branched Organic Frameworks as Giant and Potent Metal Chelators, J. Am. Chem. Soc., 2020, 142(1), 198–206.
28. Ottaviani, M. F.; Matteini, P.; Brustolon, M.; Turro, N. J.; Jockusch, S.; Tomalia, D. A. Characterization of Starburst Dendrimers and Vesicle Solutions and Their Interactions by CW- and Pulsed-EPR, TEM, and Dynamic Light Scattering. J, Phys. Chem. B, 1998, 102 (31), 6029-6039.
29. Ottaviani, M. F.; Daddi, R.; Brustolon, M.; Turro, N. J.; Tomalia, D. A. Structural Modifications of DMPC Vesicles upon Interaction with Poly(amidoamine) Dendrimers Studied by CW-Electron Paramagnetic Resonance and Electron Spin−Echo Techniques. Langmuir, 1999, 15 (6), 1973-1980.
30. Ottaviani, M. F.; Favuzza, P., Sacchi, B.; Turro, N. J.; Jockusch, S.; Tomalia, D. A. Interactions between Starburst Dendrimers and Mixed DMPC/DMPA-Na Vesicles Studied by the Spin Label and the Spin Probe Techniques, Supported by Transmission Electron Microscopy. Langmuir, 2002, 18 (6), 2347-2357.
31. Kontogiannopoulos, K. N.; Dasargyri, A.; Ottaviani, M. F.; Cangiotti, M.; Fessas, D.; Papageorgiou, V. P.; Assimopoulou, A. N. Advanced Drug Delivery Nanosystems for Shikonin: A Calorimetric and Electron Paramagnetic Resonance Study. Langmuir, 2018, 34 (32), 9424-9434.
32. Del Olmo, N.S.; Carloni, R.; Bajo, A.M.; Ortega, P.; Fattori, A.; Gómez, R.; Ottaviani, M.F.; García-Gallego, S.; Cangiotti, M.; Mata, F.J. d.l. Insight into the antitumor activity of carbosilane Cu(II)-metallodendrimers through their interaction with biological membrane models, Nanoscale, 2019, 11(28), 13330-13342.
33. Do Canto, A. M. T. M.; Robalo, J. R.; Santos, P.D.; Carvalho, A.J.P.; Ramalho, J.P.P.; Loura, L.M.S. Diphenylhexatriene membrane probes DPH and TMA-DPH: A comparative molecular dynamics simulation study, BBA Biomembranes, 2016, 1858(11), 2647–2661.
34. Ottaviani, M. F.; Cangiotti, M.; Fattori, A.; Coppola, C.; Posocco, P.; Laurini, E.; Liu, X.; Liu, C.; Fermeglia, M.; Peng, L.; Pricl, S. Copper (II) binding to flexible triethanolamine-core PAMAM dendrimers: a combined experimental/in silico approach. Phys. Chem. Chem. Phys., 2014, 16 (2), 685-694.
35. Ottaviani, M. F.; Cangiotti, M.; Fattori, A.; Coppola, C.; Lucchi, S.; Ficker, M.; Petersen, J. F.; Christensen, J. B. Copper(II) Complexes with 4-Carbomethoxypyrrolidone Functionalized PAMAM-Dendrimers: An EPR Study. J. Phys. Chem. B, 2013, 117 (45), 14163-14172.
36. Ottaviani, M. F.; Bossmann, S.; Turro, N. J.; Tomalia, D. A. Characterization of starburst dendrimers by the EPR technique. 1. Copper complexes in water solution. J.A.C.S. 1994, 116 (2), 661-671.
37. Ottaviani, M. F.; Montalti, F.; Turro, N. J.; Tomalia, D. A Characterization of Starburst Dendrimers by the EPR Technique. Copper(II) Ions Binding Full-Generation Dendrimers. J. Phys. Chem. B ,1997, 101 (2), 158-166.
38. Galan, M.; Sanchez-Rodriguez, J.; Cangiotti, M.; García-Gallego, S.; Jimenez, J. L.; Gomez, R.; Ottaviani, M. F.; Muñoz-Fernández, M. A.; Mata, F. J. d. l. Antiviral Properties Against HIV of Water Soluble Copper Carbosilane Dendrimers and their EPR Characterization. Curr. Med. Chem., 2012, 19 (29), 4984-4994.
39. García-Gallego, S.; Cangiotti, M.; Fiorani, L.; Fattori, A.; Muñoz-Fernández, M. a. Á.; Gomez, R.; Ottaviani, M. F.; Mata, F.J. d.l. Anionic sulfonated and carboxylated PPI dendrimers with the EDA core: synthesis and characterization of selective metal complexing agents. Dalton Trans., 2013, 42 (16), 5874-5889.

40. Tang, Y.-H.; Cangiotti, M.; Kao, C.L.; Ottaviani, M. F. EPR Characterization of Copper(II) Complexes of PAMAM-Py Dendrimers for Biocatalysis in the Absence and Presence of Reducing Agents and a Spin Trap. J. Phys. Chem. B, 2017, 121 (46), 10498-10507.
41. Valko, M.; Pelikan, P.; Biskupic, S.; Mazur, M. ESR spectra of copper (II) complexes in the solids, Chem Pap, 1990, 44(6), 805- 813.
42. Garribba, E.; Micera, G. The Determination of the Geometry of Cu (II) Complexes, An EPR Spectroscopy Experiment, J. Chem. Educ., 2006, 83(8), 1229-1232.
43. Xiong, Z.; Wang, Y.; Zhu, J.; He, Y.; Qu, J.; Xia, J.; Appelhans, D.; Shi, X. Gd-chelated poly(propylene imine) dendrimers with densely organized maltose shells for enhanced MR imaging applications. Biomaterials Science, 2016, 4, 1622-1629.
44. Tomalia, D. A.; Rookmaker, M. In Polymer Data Handbook, 2nd ed.; Mark, J. E., Eds.; Oxford University Press: Oxford, New York, 2009, 979-982.
45. Bangham, A.D.; Horne, R.W. Negative staining of phospholipids and their structural modification by surface-active agents as observed in the electron microscope, J. Mol. Biol., 1964, 8, 660-668.
46. Ennen, F; Fenner, P.; Stoychev, G.; Boye, S.; Lederer, A.; Voit, B.; Appelhans, D.: Coil-like Enzymatic Biohybrid Sructures Fabricated by Avidin-biotin Conjugations: Controlling Sizes and Enzyme Activity over Sequential Conjugations and Filtration Steps. ACS Applied Materials & Interfaces ,2016, 8, 6261-6268.
47. Gaitzsch, J.; Appelhans, D.; Wang, L.; Battaglia, G.; Voit, B.: Synthetic bio-nanoreactor: Mechanical and chemical control of polymersome membrane permeability. Angew. Chem. Int. Ed., 2012, 51, 4448-4451.
48. Böckmann, R. A.; Hac, A.; Heimburg, T.; Grubmüller, H. Effect of sodium chloride on a lipid bilayer, Biophys J. 2003, 85(3), 1647–1655
49. Budil, D. E.; Lee, S.; Saxena, S.; Freed, J.H. Nonlinear-Least-Squares Analysis of Slow-Motion EPR Spectra in One and Two Dimensions Using a Modified Levenberg–Marquardt Algorithm, J. Magn. Reson., 1996, 120, 155-189.
50. Wrobel, D.; Appelhans, D.; Signorelli, M.; Wiesner, B.; Fessas, D.; Scheler, U.; Voit, B.; Maly, J. Interaction study between maltose-modified PPI dendrimers and lipidic model membranes, Biochim Biophys Acta,2015, 1848, 1490-1501.
51. Furlan, S.; La Penna, G.; Appelhans, D.; Cangiotti, M.; Ottaviani, M. F.; Danani, A. Combined EPR and Molecular Modeling Study of PPI Dendrimers Interacting with Copper Ions: Effect of Generation and Maltose Decoration.The Journal of Physical Chemistry B, 2014, 118 (42),12098–12111.
52. McCarthy, J. M.; Rasines Moreno, B.; Filippini, D.; Komber, H.; Maly, M.; Cernescu, M.; Brutschy, B.; Appelhans, D.; Rogers, M. S.: Influence of Surface Groups on Poly(propylene imine) Dendrimers Anti-prion Activity. Biomacromolecules 2013, 14, 27-37
53. Bekhradnia, S.; Naz, I.; Lund, R.; Effenberg, C.; Appelhans, D.; Sande, S. A.; Nyström, B.: Characterization of oligosaccharide-functionalized hyperbranched poly(ethylene imine) and their complexes with retinol in aqueous solution. Journal of Colloid & Interface Science, 2015, 458, 178-186.

CHAPTER 3

An environmental pollution case

1 - INTRODUCTION AND GOALS

1.1 Introduction

Plastic usage has vertically grown ever since its industrial production started, in the early 1900. Nowadays, plastics are the most abundant marine debris [1,2] with severe and unpredictable effects on the whole marine biosystem.

Most of the plastic sink out to the bottom of the seas, making their way through the water column. [3,4,5] Some of them though feature a specific density lower than water and may float, significantly growing their spread potential. This is the case of polyethylene (PE), which alone constitutes more than one third of world's plastic production. [6]

Plastic debris can be divided into three main categories, up to their size:

- Macroplastics (>5mm)
- Microplastics (0.1 μm to 5 mm)
- Nanoplastics (<0.1 μm)

The natural degradation process brings to the disassemble of most plastics into nanoplastics, in a process that may last for decades.

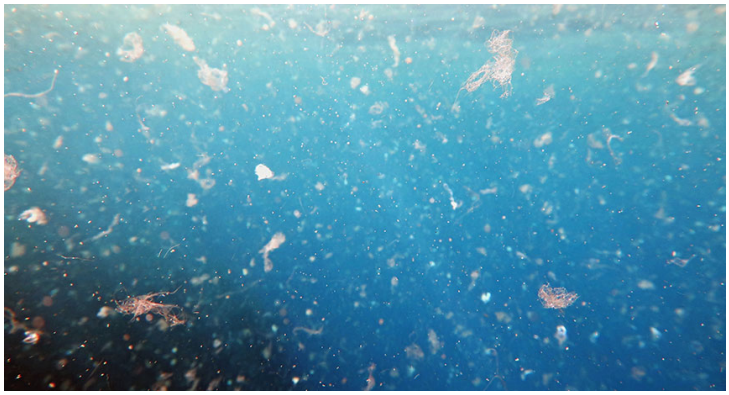

Figure 1.1 Marine Macroplastics and Microplastics

Microplastic debris are ubiquitous, and capable of interacting with nearly every living specie, from algae to mammals, [7,8,9] giving birth to processes of biofouling and bioaccumulation.

It is documented how such debris can be unnatural vectors for bacteria, which spread to new areas while being carried by microplastics. [10,11] The wide superficial area of such debris offers a favorable growing environment for bacteria, which are stimulated by plastic hydrophobicity [7] and produce biofilm, anchoring themselves on the debris.

Despite this issue is lately rising more and more attention by the international community, the interaction of microplastics and eucaryotic (especially micro-eukaryotic) organisms is still poorly understood.

1.2 Goals

Our goal was therefore to characterize the physical interaction between polyethylene terephthalate (PET) fragments and microalgal cells in synthetic seawater. Marine diatom *Skeletonema marinoi* and *Lingulodinium polyedrum* were selected for this purpose, after a wide screening, since they showed different adhesion and growing capability in presence of the microplastics.

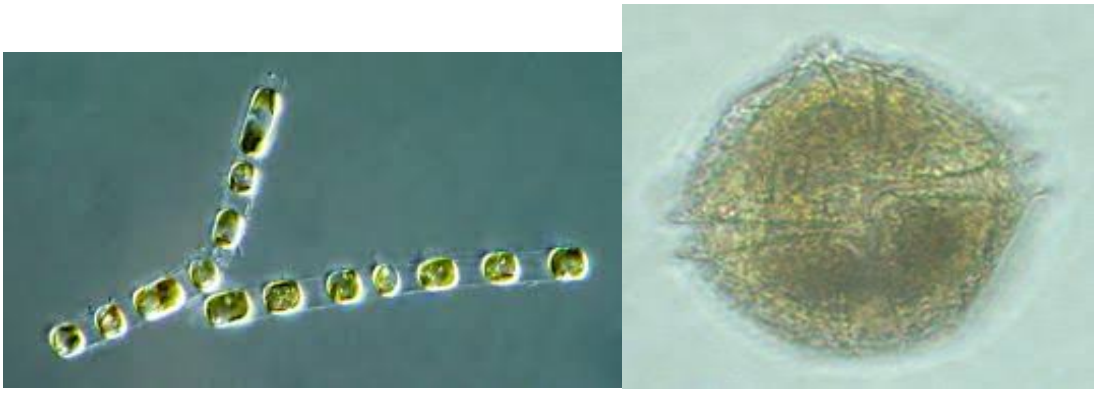

Figure 1.2 S. marinoi (on the left), and L. polyedrum (on the right).

1.3 Methodology

EPR technique had already proved able to characterize *in-situ* interaction in seawater. [12,13,14,15,16,17,18] To be able to visualize the interaction (or the non-interaction) between the abovementioned items, a paramagnetic spin probe was added in solution. 4-dodecyldimethylammonium-2,2,6,6-tetramethyl-piperidine-N-oxide bromide (CAT12), was selected among other candidates due to its surfactant nature and previous studies in which it already demonstrated to well monitor interactions occurring between biocomponents. This probe is indeed able to insert into cell membranes, as well as to adapt to the hydrophobic plastic surface.

These combined properties allow such probe to monitor the approach and adhesion of the microalgae to the plastic surface.

2 - RESULTS AND DISCUSSION

The chosen candidates for this experiment, *L. polyedrum* and *S. marinoi*, were incubated in F/2-L/1 enriched artificial seawater ASPM (Artificial Seawater Provasoli-McLachlan), together with sterilized PET sheets obtained from PET bottles, to mimic the marine environment pollution.

Light microscopy counting and EPR experiments were conducted in parallel to monitor the adhesion of the phytoplankton into the PET sheets.

The counting results show a significantly different outcome for the two specimens:

- *S. marinoi* grows almost at the same rate both in solution and on plastic sheets. In particular, the maximum free-living cell amount of *S. marinoi* was $1.6x10^6$ (± $1.6x10^5$) cells/mL, while it was $8.5x10^3 \pm 2.1x10^3$ cells/mm^2 on the plastic sheets. The calculated adhesion rate was 0.15 d^{-1}.
- *L. polyedrum* showed no correlation between the abundance in culture and on plastics, with just 2 ± 1 cells/mm^2 on PET sheets. The calculated adhesion rate was 0.06 d^{-1}.

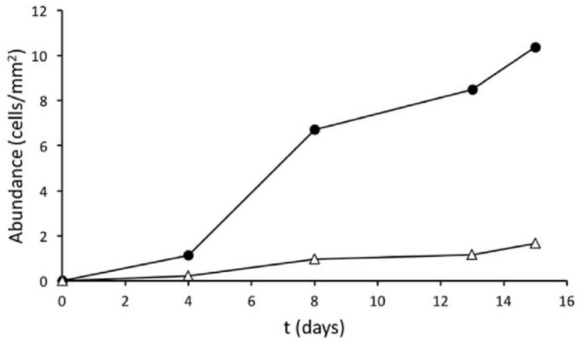

Figure 2.1 Cell adhesion onto the plastic sheets, expressed in x103 for S. marinoi (black dots) and x10^0 for L. polyedrum (white triangles) cells/mm (article 5, figure 1)

EPR results perfectly match these findings. In fact, a much larger portion of CAT12 is adsorbed onto the plastic in the case of *S. marinoi*, led by the microalgal adhesion on the PET sheet, as shown by the various parameters extracted from the computer-aided EPR analysis and reported in Table 1.

Table 1 Extracted values from EPR analysis

Maximum Values Recorded	*S. Marinoi*	*L. Polyedrum*
Adsorbed % onto the plastic	21 (± 1)	13 (± 1)
Interacting Component %	95 (± 3)	75 (± 3)
Interacting Component τ_c *(ns)*	40 (± 1)	32 (± 1)
Free Component τ_c *(ns)*	1 (± 0.1)	0.6 (± 0.1)

The cell growth in Figure 3 is directly linked to the relative percentage of interacting probes, which for *S. marinoi* is close to 100%, meaning that almost all CAT12 probes are trapped between plastic and phytoplankton. The percentage in the case of *L. polyedrum* is much lower.

A direct consequence of the increased interaction is the increase in the correlation time for the rotational motion of CAT12, which measures the interaction strength. For *S. marinoi*, CAT12 rotational mobility is slower by 8 ns, a very significant value, mirroring the interaction of the probe with both the cell membrane and the plastic.

Nevertheless, the most significant parameter is the correlation time of the less interacting probes. These probes give rise to a so-called "weakly interacting component" that is important in the evaluation of the strength of interaction, due to its sensitiveness to the slightest change of the system. In the case of *S. marinoi*, this value is almost twice as much as in *L. polyedrum*, highlighting a significant interaction of *S. marinoi* with the plastic.

A complete analysis and visual representation of each parameter is presented in Paper 5, figures 5 and 7.

Our analysis proved successful:

- It is possible to monitor the physical interaction between plastics and phytoplankton *via* EPR, with the help of CAT12 probes.
- *S. marinoi* is a highly interacting specimen, with a high adhesion potential, giving birth to a possible process of biofouling and long-range biological pollution.
- *L. polyedrum* doesn't show a particular affinity for PET microplastics, featuring low adhesion rate. The EPR data show how this specimen "rolls" on the plastic surface, with no risk of biofouling.

3 - BIBLIOGRAPHY

1. Dafne Eerkes-Medrano, Richard C Thompson, David C Aldridge "*Microplastics in freshwater systems: a review of the emerging threats, identification of knowledge gaps and prioritisation of research needs*", Water Res. 2015 May 15;75:63-82. Epub 2015 Feb 17. 2015;
2. Law K.L.,"*Plastics in the Marine Environment*", Annual Review of Marine Science Vol. 9:205-229, 2017
3. Cozar, A., Echevarría, F., Gonzalez-Gordillo, I.J., Irigoien, X., Úbeda, B., Hernandez- Leond, S., Palmae, A.T., Navarrof, S., García-de-Lomas, J., Ruizg, A., Fernández- de- Puellesh, M.L., Duartei, C.M., "Plastic debris in the open ocean". 2014 Proc. Natl. Acad. Sci. U.S.A. 111, 10239e10244.
4. Cauwenberghe L.V., Vanreusel A., Mees J., Janssen C.R., "*Microplastic pollution in deep-sea sediments*" Environmental Pollution 182, 2013, 495e499 2013,
5. Woodall L., Sanchez-Vidal A., Canals M., Paterson G.L.J., Coppock R., Sleightm V.A., Calafat A., David A., Rogers Bhavani, E Narayanaswamy, Richard C Thompson. "*The deep sea is a major sink for microplastic debris*" Royal Society Open Science Woodall, 2014
6. Andrady, A.L., 2011. "*Microplastics in the marine environment*". Mar. Pollut. Bull. 62, 1596e1605. 2011
7. Zettler E.R., Mincer T.J., Amaral-Zettler L.A., 2013. "*Life in the 'plastisphere': microbial communities on plastic marine debris*". Environ. Sci. Technol. 47, 7137e7146. 2013;
8. Gall, S. C., and Thompson, R. C. (2015). "*The impact of debris on marine life*". Mar. Pollut. Bull. 92, 170–179. Gall and Thompson, 2015;
9. Clark, J. R., Cole, M., Lindeque, P. K., Fileman, E., Blackford, J., Lewis, C., et al. "*Marine microplastic debris: a targeted plan for understanding and quantifying interactions with marine life*". Front. Ecol. Environ. 14:317–324. 2016
10. Hoellein T, Rojas M, Pink A, Gasior J, Kelly J (2014) "*Anthropogenic Litter in Urban Freshwater Ecosystems: Distribution and Microbial Interactions*". PLoS ONE 9(6): e98485. 2014,
11. Amanda R. McCormick Timothy J. Hoellein Maxwell G. London Joshua Hittie John W. Scott John J. Kelly "*Microplastic in surface waters of urban rivers: concentration, sources, and associated bacterial assemblages*". 2016,
12. Casabianca, S., Penna, A., Capellacci, S., Cangiotti, M., Ottaviani, M.F., 2018. "*Silicification process in diatom algae using different silicon chemical sources: colloidal silicic acid interactions at cell surface*". Colloids Surfaces B Biointerfaces 161, 620e627. 2018;
13. Deriu, M.A., Cangiotti, M., Grasso, G., Licandro, G., Lavasanifar, A., Tuszynski, J.A., Ottaviani, M.F., Danani, A.,"*Self-assembled ligands targeting TLR7: a molecular level investigation*". Langmuir 33 (50), 14460e144712017;
14. Nguyen, H., Chen, Q., Paletta, J., Harvey, P., Jiang, Y., Zhang, H., Boska, M., Ottaviani, M.F., Jasanoff, A., Rajca, A., Johnson, J., 2017. "*Nitroxide-based macro- molecular contrast agents with unprecedented transverse relaxivity and stability for magnetic resonance imaging of tumo*rs". ACS Cent. Sci. 3 (7), 800e811. 2017;
15. Andreozzi, E., Antonelli, A., Cangiotti, M., Canonico, B., Sfara, C., Pianetti, A., Bruscolini, F.A., Sahre, K., Appelhans, D., Papa, S., Ottaviani, M.F., 2017. "*In-teractions of nitroxide-conjugated and non-conjugated glycodendrimers with normal and cancer cells and biocompatibility studies*". Bioconjug. Chem. 28, 524e538. 2017;
16. Ottaviani, M.F., El Brahmi, N., Cangiotti, M., Coppola, C., Buccella, F., Cresteil, T., Mignani, S., Caminade, A.M., Costes, J.P., Majoral, J.P., 2014. "*Comparative EPR studies of Cu(II)-conjugated phosphorous-dendrimers in the absence and presence of normal and cancer cells*". RSC Adv. 4, 36573e36583. 2014;
17. Ottaviani, M.F., Pregnolato, M., Cangiotti, M., Fiorani, L., Fattori, A., Danani, A., 2012. "*Spin probe analysis of microtubules structure and formation*". Arch. Biochem. Biophys. 522, 1e8. 2012;
18. Mishraki, T., Ottaviani, M.F., Shames, A.I., Aserin, A., Garti, N., 2011. "*Structural effects of insulin-loading into HII mesophases monitored by EPR, SAXS, and ATR-FTIR*." J. Phys. Chem. B 115 (25), 8054e8062. 2011

PAPER 5

Physical interactions between marine phytoplankton and PET plastics in seawater

Silvia Casabianca, Samuela Capellacci, Antonella Penna, Michela Cangiotti, Alberto Fattori, Ilaria Corsi, Maria Francesca Ottaviani, Riccardo Carloni

Chemosphere 238 (2020) 124560
https://doi.org/10.1016/j.chemosphere.2019.124560

Physical interactions between marine phytoplankton and PET plastics in seawater

Silvia Casabianca [1,2], Samuela Capellacci [1,2], Antonella Penna [1,2], Michela Cangiotti [3], Alberto Fattori [3], Ilaria Corsi [4], Maria Francesca Ottaviani [3], Riccardo Carloni [3]

1. Department of Biomolecular Sciences, Campus E. Mattei, Via Cà le Suore 2/4, 61029 Urbino (PU), Italy
2. Conisma, Consorzio di Scienze Interuniversitario sul Mare, Piazzale Flaminio 6, 00136 Rome, Italy
3. Department of Pure and Applied Sciences, Campus E. Mattei, Via Cà le Suore 2/4, 61029 Urbino (PU), Italy
4. Department of Physical, Earth and Environmental Sciences, University of Siena, Italy

Corresponding Authors: Riccardo Carloni, r.carloni1@campus.uniurb.it Silvia Casabianca, silvia.casabianca@uniurb.it

Graphical Abstract

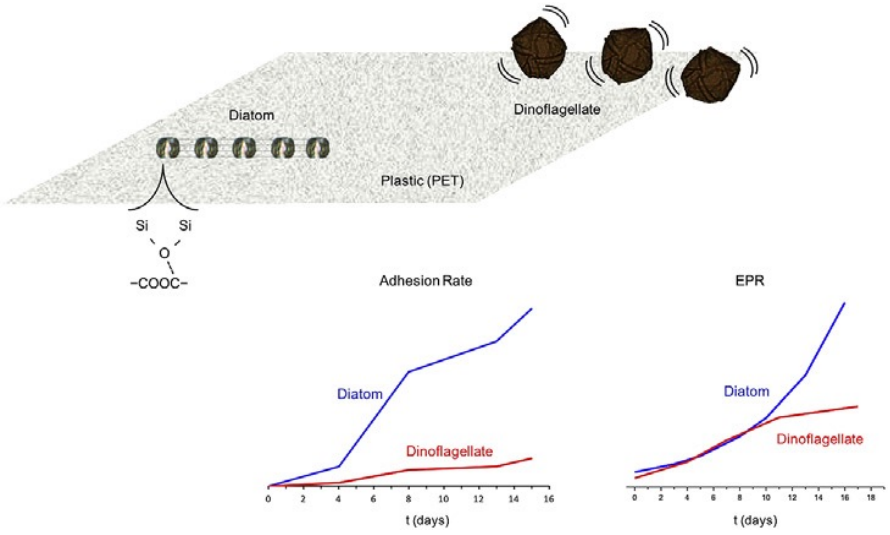

Abstract

Plastics are the most abundant marine debris globally dispersed in the oceans and its production is rising with documented negative impacts in marine ecosystems. However, the chemical-physical and biological interactions occurring between plastic and planktonic communities of different types of microorganisms are poorly understood. In these respects, it is of paramount importance to understand, on a molecular level on the surface, what happens to plastic fragments when dispersed in the ocean and directly interacting with phytoplankton assemblages. This study presents a computer-aided analysis of electron paramagnetic resonance (EPR) spectra of selected spin probes able to enter the phyoplanktonic cell interface and interact with the plastic surface. Two different marine phytoplankton species were analyzed, such as the diatom

Skeletonema marinoi and dinoflagellate Lingulodinium polyedrum, in absence and presence of polyethylene terephthalate (PET) fragments in synthetic seawater (ASPM), in order to in-situ characterize the interactions occurring between the microalgal cells and plastic surfaces. The analysis was performed at increasing incubation times. The cellular growth and adhesion rates of microalgae in batch culture medium and on the plastic fragments were also evaluated. The data agreed with the EPR results, which showed a significant difference in terms of surface properties between the diatom and dinoflagellate species. Low-polar interactions of lipid aggregates with the plastic surface sites were mainly responsible for the cell-plastic adhesion by S. marinoi, which is exponentially growing on the plastic surface over the incubation time.

Keywords: Adhesion rate; electron paramagnetic resonance; Lingulodinium polyedrum phytoplankton; Skeletonema marinoi

Introduction

Every year, millions of tons of plastic material flow into the oceans. Over the past few months, there has been an increasing public and political concern about marine pollution, not only for the highly negative impact on the marine organisms, but also for the cascade onto environmental issues related to climate changes (Derraik, 2002; Obbard et al., 2014; Windsor et al., 2019; Fang et al., 2017; Horton and Dixon, 2017). The ubiquitous nature of plastics and microplastics led to their accumulation along the water column and on the bottom of the oceans over the last decades. It is generally assumed that much of this plastic debris persists on the ocean surface for years or even decades (Van Sebille et al., 2012; Cozar et al., 2014) due to the robustness of plastics and the fact that more than 50% of polymers have a density lower than that of seawater (Andrady, 2011), allowing durable and persistent substratum for the bio-adhesion of marine organisms. In fact, plastics can represent the carrying way of many organisms, including not allochthonous species, to new habitats altering the endemic communities. Floating plastics can transport disease vectors through the sea or absorb biotoxins, chemical, and organic pollutants. (Zettler et al., 2013; Reisser et al., 2014; Fazey and Ryan, 2016; Casabianca et al., 2019). But it is also known that plastics are subjected to sinking especially due to the microorganism colonization which favors the formation of hetero-aggregates or general aggregates (Long et al., 2015; Moriceau et al., 2017). The biofouling or bio-adhesion can modify the density of particles and buoyant particles may, in the end, sink to the bottom. Microalgal and microbial adhesion, and subsequent colonization on plastic fragments occur quickly (Bakker et al., 2003; Zettler et al., 2013; Oberbeckmann et al., 2015). The sticking ability is mediated by the phytoplankton polysaccharide excretion that may coagulate due to turbulence to form sticky particles or TEPs (transparent exopolymer particles) allowing the microalgal cell aggregation to TEP (Passow, 2002; Bhattacharya et al., 2010). These aggregates transport the phytoplanktonic cell and marine detritus to the sea bottom along the water column. Microplastics can be incorporated in these aggregates and transported as well to the sea floor (Long et al., 2015). Furthermore, the marine aggregates incorporating microplastics are food for grazers, gaining access to the higher levels of the trophic web (Carson, 2013; Farrell and Nelson, 2013). Therefore, both sinking and ingestion of microplastics through adhesion/aggregation to microbiota have a significant impact on marine ecosystems (Cole et al., 2013; Kiessling et al., 2015). It is also known that the biological adhesion to plastics is mediated by the hydrophobic surface that seems to stimulate the colonization of microorganisms by biofilm formation and the rapid succession of microbial communities (Zettler et

al., 2013). In this study, the computer-aided analysis of electron paramagnetic resonance (EPR) spectra was carried out as a first attempt to provide a suitable method for investigating the interactions occurring between the microalgal cells and plastic surfaces. Marine diatom Skeletonema marinoi and Lingulodinium polyedrum have been grown in the presence and absence of polyethylene terephthalate (PET) fragments in synthetic seawater to *in-situ* characterize the interactions occurring between the microalgal cells and plastic surfaces. For this purpose, a selected spin probe was added in solution. Previous studies of similar systems have already demonstrated the ability of the spin-probe EPR technique to obtain *in-situ* structural and dynamical information on interactions occurring in the medium (Casabianca et al., 2018; Deriu et al., 2017; Nguyen et al., 2017; Andreozzi et al., 2017; Ottaviani et al., 2014; Ottaviani et al., 2012; Mishraki et al., 2011). After an accurate screening, we selected the surfactant spin probe 4-dodecyldimethylammonium-2,2,6,6-tetramethyl-piperidine-N-oxide bromide (CAT12), which has a double advantage: (a) to monitor the cell-plastic interactions; its surfactant nature favors the insertion into the cell membrane, but also well adapt at the hydrophobic plastic surface in contact with salted water, due to the presence of both an hydrophobic chain and a charged polar head; (b) as a surfactant, CAT12 works as a water pollutant and it becomes an important ingredient of the system, also reporting about the interacting properties of surfactants and lipids with plastic and algal cells in the seawater. With the aim to investigate interactions on a time-scale basis, the analysis was performed at increasing incubation times, up to 16 days. We will discuss separately, in a comparative way, the results obtained from the two different phytoplanktonic species.

2. Materials and methods

2.1 Microalgal culture conditions

The diatom Skeletonema marinoi CBA4 and dinoflagellate Ligulodinium polyedrum VGO1024 were maintained in F/2 and L/1 medium (Guillard, 1975) respectively. Culture conditions were 16 ± 1 °C and 23 ± 1 °C for the diatom and dinoflagellate species, respectively, under a standard 12:12 h light-dark cycle. Light was provided by cool-white fluorescent bulbs (photon flux of 100 mE m^2s^1).

2.2 Adhesion rate of microalgal species to the plastic substrate

All experiments were performed in sterile polycarbonate flasks. The artificial seawater ASPM (Artificial Seawater Provasoli-McLachlan) base (Guillard, 1975), enriched with F/2 and L/1 medium components, was used as medium in each condition to have comparable results, not affected by natural seawater usually used in media preparation. S. marinoi CBA4 (initial concentration of 1.0 x 10^5 cells/mL) and L. polyedrum VGO1024 (initial concentration of 1.0 x 10^4 cells/mL) were grown in 50 mL flasks containing 40 mL of sterilized medium together with PET (polyethylene terephthalate) sheets (4mm20mm) obtained from sterilized PET bottles. Similar PET fragments can be found in seawater as a product of degradation of water bottles. Culture conditions were those described above. A single plastic sheet was harvested every four days since the inoculum, and gently scraped in 2 mL of sterile seawater. Cell amount was evaluated using Sedwhich-Rafter chamber under an inverted microscope (ZEISS Axiovert 40CFL) at 400X magnification. Cell abundance was expressed as cells/mL for cultures and cells/mm^2 for cells attached to the plastic surface. The growth and the adhesion rates, defined respectively as the rate of increased abundance in culture and on the plastic sheets, were calculated on the basis of the

longest possible period of exponential growth using the equation: $\mu = \ln (Nt/N0)/Dt$, where N is the number of cells/mL (for growth rate) or the number of the plastic adherent cells expressed as cells/mm^2 (for adhesion rate) and Dt the time interval expressed in days.

2.3 EPR analysis

2.3.1 Samples preparation

Together with light microscopy counting, EPR analyses were performed. Experimental conditions were the same described for adhesion rate determination. Samples for EPR analysis were obtained using a final concentration of 1 mM of CAT12 probes in ASPM medium. This solution (2 mL) in absence and in presence of the microalgae (0.45 cells/mL) was analyzed by EPR in absence and presence of the plastic sheet. The solutions were left equilibrating for 2 h before starting the analysis. The plastic sheets after equilibration were gently dried on a filter paper, while the supernatant was collected and inserted into an EPR tube. The EPR spectra were recorded for the solutions and for the plastic strips. The latest were assembled making them adhere on a glass rod using parafilm before the insertion into the EPR cavity. The following samples were analyzed as control references: (i) the culture media (ASPM F/2 and ASPM L/1), (ii) S. marinoi and L. polyedrum cell cultures without plastic sheets and (iii) plastic sheets maintained in ASPM F/2 and ASPM L/1 without cultured cells.

2.3.2 Instrumentation

EPR spectra were recorded by means of an EMX-Bruker Spectrometer operating at X band (9.5 GHz) and interfaced with a PC (software from Bruker). The temperature was controlled with a Bruker ST3000 variable-temperature assembly cooled with liquid nitrogen.

2.3.3 EPR spectra computation

Simulation of the EPR line shape was performed by using Budil et al. program (Budil et al., 1996). The main parameters extracted from computation were: (a) the g_{ii} values measuring the coupling between the electron spin and the magnetic field. These values were assumed constant that is g_{ii} = 2.009, 2.006, 2.003, on the basis of previous studies on similar systems (Kontogiannopoulos et al., 2018; Deriu et al.). (b) the A_{ii} values measuring the coupling between the electron spin and the nitrogen nuclear spin. We assumed $A_{XX} = A_{yy}$ = 6 G in all cases to limit the number of variables as already done in previous studies (Kontogiannopoulos et al., 2018; Deriu et al.). Therefore, only A_{ZZ} was changed. When the spectrum lines are narrow (Free component), the error of the A_{ZZ} parameter is ±0.01 G. This error increases for the spectra constituted by broader lines, up to ±0.1 G; (c) the correlation time for the diffusion rotational motion of the probe, t, which measures the microviscosity and therefore reports on the interactions occurring between the probe and the environmental molecules or interacting sites (error ± 0.01 ns, one order of magnitude lower for the Free component); and (d) the line width, which measures the spin-spin interactions between probes in close positions, measuring the proximity of interacting sites (error ± 0.1 G). The total intensities, calculated by double integration of the overall EPR spectra, provide a measure of the concentration of paramagnetic species in the samples. Finally, since two signal components, due to probes sitting in two different environments, constitute the spectra, the subtraction of spectra from one another allowed us to extract each signal and then compute it. The double integration of each signal referred to the double integral

of the spectra gives the relative percentage of the probes in each environmental condition (error ± 0.5%).

2.4 Statistical Analyses

Data analyses were performed using nonparametric Mann-Whitney and Spearman correlation tests using PAST ver. 2.17 (Hammer et al., 2001) with a p-value < 0.05 determining significance.

3. Results and Discussion

3.1 Growth and adhesion rate on the plastic surface of microalgal species

In the same batch culture, during the exponential growth phase, a significant positive correlation (Spearman's rs = 0.61, p = 0.01) between S. marinoi free-living abundance and S. marinoi abundance attached to plastic sheets was found. Thus, a higher abundance in the culture was directly linked to an increased abundance of cells attached to plastics. In particular, the maximum free-living cell amount of S. marinoi was $1.6 \times 10^6 \pm 1.6 \times 10^5$ cells/mL, while cell abundance attached to plastics was $3.4 \times 10^5 \pm 8.5 \times 10^4$ (corresponding to $8.5 \times 10^3 \pm 2.1 \times 10^3$ cells/mm^2). The adhesion rate of S. marinoi cells attached to the plastics was calculated during the 1 exponential growth phase with a value of 0.15 d . No correlation between L. polyedrum abundance in culture and L. polyedrum attached to plastic sheets was found (Spearman's rs = 0.31, p = 0.32). During the growth phase, L. polyedrum reached the abundance of $2.1 \times 10^4 \pm 5.9 \times 10^3$ cells/mL while cell abundance attached to plastics was 62 ± 22 (corresponding to 2 ± 1 cells/mm^2). The adhesion rate of L. polyedrum cells attached to 1 plastic was 0.06 d . The growth curves of cells attached to the plastic surface of the two-species showed that L. polyedrum retained much lower abundance to the plastic sheets of two orders of magnitude smaller than S. marinoi (Figure 1).

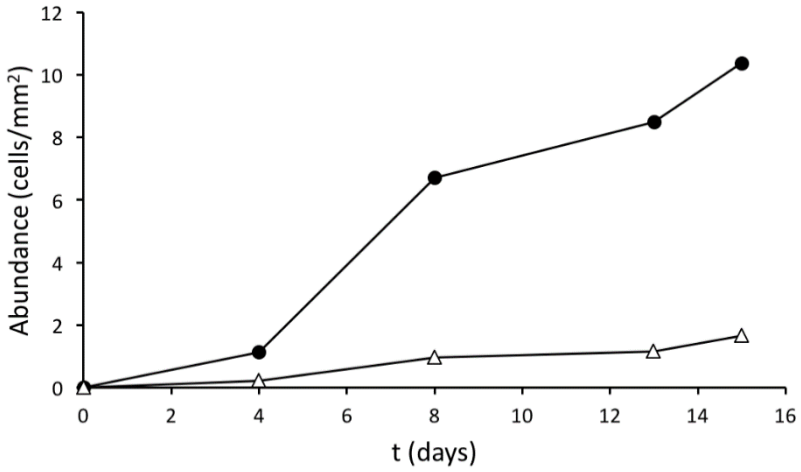

Figure 1. Amount adhesion of marine diatom Skeletonema marinoi CBA4 (balck dots) and dinoflagellate Lingulodinium polyedrum VGO1024 (white triangulum) to plastic sheets in cultured conditions over the studied period. Abundance is reported as S. marinoi (x 10^3) and L. polyedrum (x 10^0) cells/mm^2 .

3.2 EPR study

3.2.1 Diatom Skeletonema marinoi interactions with plastic surface

Figure 2A shows an example of an experimental EPR spectrum obtained from a plastic fragment extracted after 16-days incubation in the S. marinoi batch grown in ASPM medium enriched with nutrients and CAT12. As indicated in Figure 2A with arrows, two components constitute the spectra: (a) a three-narrow lines component, which is characteristic of free-moving CAT12 probes. However, as we will describe hereafter, the mobility of these probes was significantly lower than those in the medium incubated with S. marinoi, indicating that these "free" probes were located at the polar (solvent) interphase; (b) an anisotropic signal (the lines split into X, Y, and Z components) with broader lines. The anisotropy arises from the slowing down of the probe rotational motion after interaction with environmental molecules or interacting sites, like those at the plastic and/or the cell surface. For this reason, this component was called "interacting" component.

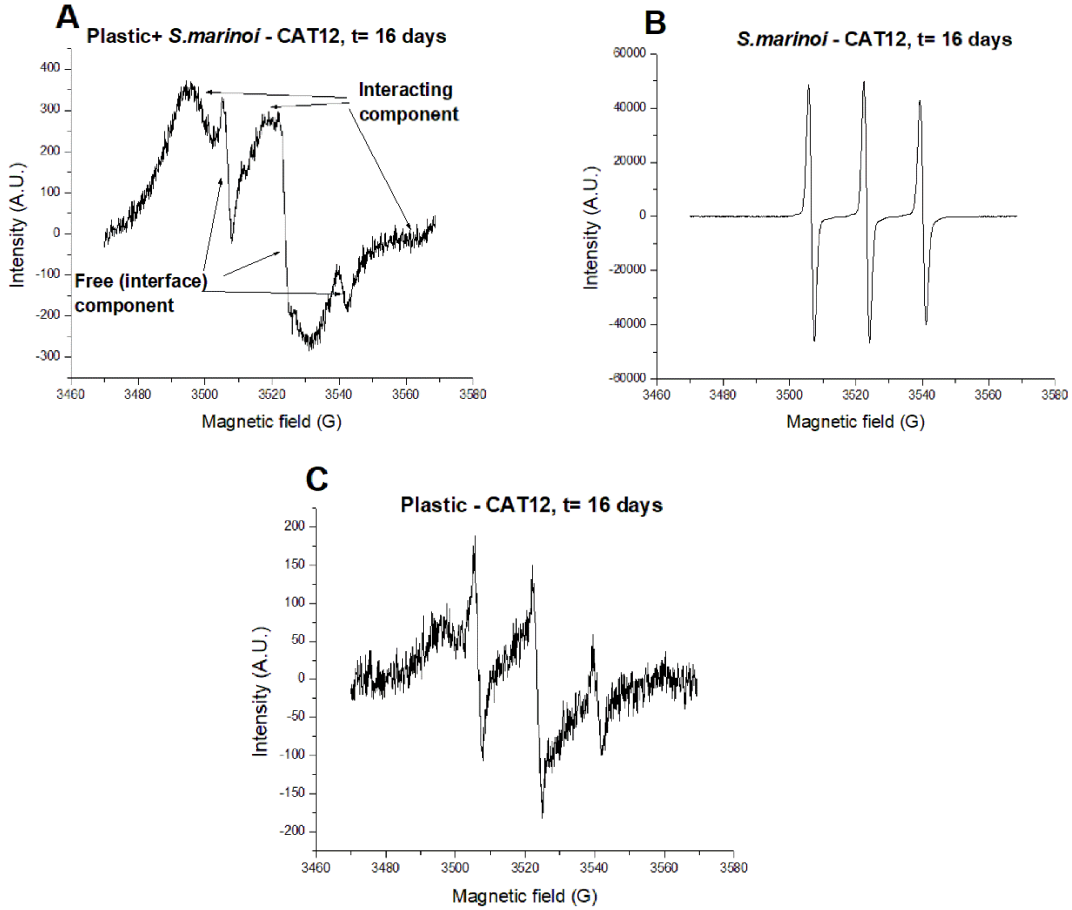

Figure 2. Experimental EPR spectra obtained from: A) a plastic fragment (simply termed "plastic") extracted after 16-days incubation in the S. marinoi batch grown in ASPM medium enriched with nutrients and CAT12; B) CAT12 in the S. marinoi batch culture; C) plastic extracted from the medium in the absence of S. marinoi after 16 days of incubation.

The spectrum of CAT12 in the S. marinoi batch culture, shown in Figure 2B, was only constituted by the Free component and differed from the spectra obtained in the supernatant solutions after

adsorption in the intensities (in arbitrary units = A.U.) and in the rotational motion, as described hereinafter. Conversely, as shown in Figure 2C, the spectrum of the plastic extracted from the medium in the absence of S. marinoi after 16 days of incubation also shows the two components as in the presence of the algal cells, but we visually note that there are significant differences, like: i) the intensity, higher in presence than in absence of S. marinoi; ii) the relative amounts of the two spectral components, being the interacting one in higher relative amount in presence of S. marinoi; and iii) the line shape of the interacting component, being the lines more resolved in presence than in absence of the S. marinoi. First, by double integration of the spectra, the total intensities were calculated. The variations in absolute intensities as a function of the equilibration time for all the liquid media - the supernatants with and without the cells after adsorption on plastic, and the S. marinoi culture in the absence of plastics - are reported in Figure 3A in the form of percentages, referring to the spectrum with the maximum intensity as a 100% intensity.

First, we note that the adsorption of CAT12 on plastic is already happening since t = 0, enhanced in the presence of S. marinoi. Indeed, S. marinoi increased the solubility of CAT12 due to the insertion of the C12 chain into the cell membrane. When S. marinoi cells are present, the intensity in the supernatant solutions significantly decreased over time due to the adhesion of the cells to the plastic surface. In any case, also in the S. marinoi medium in absence of plastic, the intensity decreased over time. This mainly happened in the first 3 days and then, from 3 to 8 days, the intensity poorly changed. After 8 days the decrease was very slow. We may ascribe this effect to the presence of antioxidants into the cells (Andreozzi et al., 2017). In the absence of plastics, the probe was free to partially cross the cell membrane and got slightly exposed to the antioxidants in the cytosol. The intensity ratios between the solutions before adsorption and the supernatants after adsorption allowed us to obtain the adsorption percentages of CAT12 onto the plastic, in the absence and presence of S. marinoi, as a function of the incubation time, shown in Figure 3B.

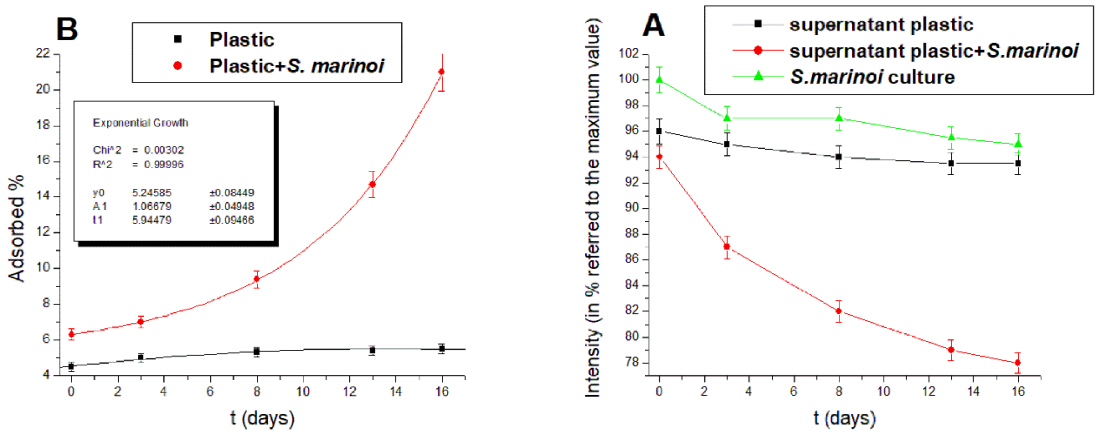

Figure 3. A) Variations in absolute intensities of the EPR spectra as a function of the equilibration time for all the liquid media: the supernatants with and without the cells after adsorption on plastic, and the S. marinoi culture in the absence of plastics Intensity values are reported in form of percentages, referring to the spectrum with the maximum intensity as a 100% in intensity; B) adsorption percentages of CAT12 onto the plastic, in the absence and presence of S. marinoi, as a function of the incubation time. The variation in the presence of S. marinoi was fitted as exponential growth.

Interestingly, the adsorbed percentage in the presence of S. marinoi increased over time, perfectly fitting an exponential growth, demonstrating the good choice of the probe, able to follow the fate of S. marinoi cells in the adhesion process with the plastic. In the absence of S. marinoi, the adsorbed percentage was low and poorly changed over time. The increase in the adsorbed percentage obtained from the supernatant medium strictly resembles the increase in the absolute intensity of the spectra of the plastic. The two spectral components obtained from the plastic samples were extracted from each other by using a subtraction procedure, that is, subtracting one from another spectrum recorded for the same sample in slightly different experimental conditions, thus containing the two identical components but in different relative amounts. This procedure allowed us to evaluate the relative percentages of the two components by double integration of each of them. Figure 4 shows the variation of the relative percentage of Interacting component for the plastic in the absence and presence of S. marinoi as a function of the equilibration time. In the absence of S. marinoi, the relative amount of Interacting component was about 43% and almost did not change over time. Conversely, in the presence of S. marinoi, the relative number of interacting probes was about 68% at t = 0, and a progressive increase occurred during the 17 days of incubation. This means that the increased adsorption evidenced in Figure 3 from the absence to the presence of S. marinoi and increasing over time is now confirmed as due to increased availability of interacting sites created by S. marinoi, which promotes its adhesion to the plastic. We know that S. marinoi cells are characterized by an amorphous silica coating and a parallelepiped shape connected to form strings. Both the shape and the amorphous silica coating may be considered as responsible for the cell adhesion to the hydrophobic plastic. Indeed, amorphous silica contains both polar and low polar sites, namely the SiOH and Si-O-Si groups. Mainly the latter sites may interact with the hydrophobic plastic surface. However, PET also contains -COO- groups which may generate dipole-dipole interactions with the SiOH groups of the silica surface. Further precious information came from a deep analysis of the spectral line shape. The above-described subtraction procedure led to extract the Free and the Interacting components from each spectrum of plastic samples. As described in the experimental section, these components were computed by using the well-established computation procedure of Budil et al., (1996) Figure 4

shows some selected examples of computations of the Free and Interacting components. The main parameters used for computation (Aii, t, and line width) are listed in the legends. The spectra are normalized in heights (intensity in the y-axis =1). Other examples of computation are shown in the Supplementary Information (Figs. S1 and SI).

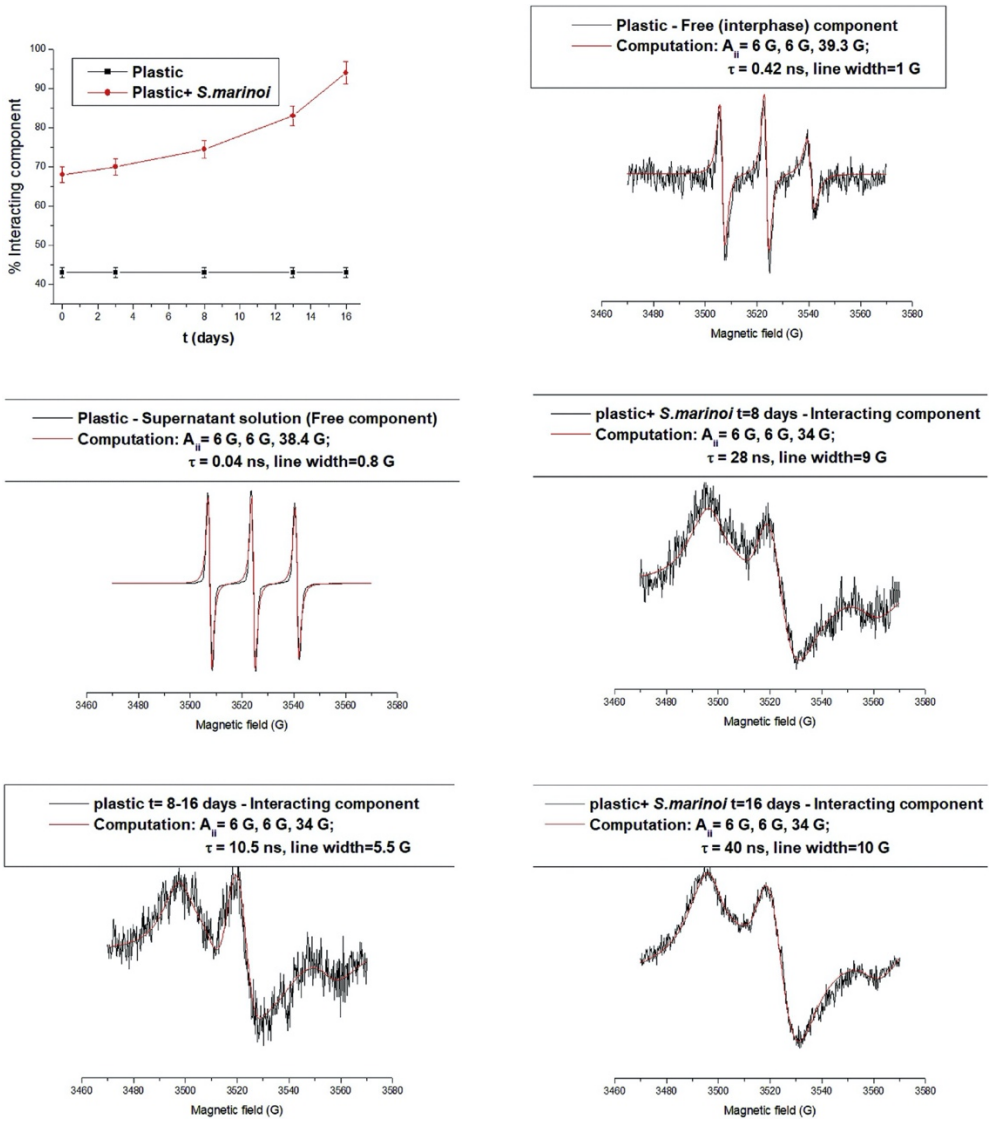

Figure 4. Variation of the relative percentage of Interacting component in the absence and presence of S. marinoi as a function of the equilibration time and selected examples of experimental (black lines) and computed (red lines) Free and Interacting components. The main parameters used for computation (Aii, t, and line width) are listed in the legends. The spectra are normalized in heights (intensity in the y-axis =1). (For interpretation of the references to color in this figure legend, the reader is referred to the Web version of this article.)

As a matter of comparison, Figure 4 shows the computations of both the spectrum of the supernatant solutions and the Free component of the plastic samples, which did not change over time. The two computations provided very different values of Azz (the micropolarity parameter) and t (the microviscosity parameter, measuring the interaction strength). The Free component at the plastic interface shows higher micropolarity and microviscosity with respect to that of the probes which remain free in the medium. This means that the salted medium concentrated in small

drops at the plastic surface. The reproducibility of this effect, also over time, confirms this interpretation. However, in the presence of S. marinoi, the microviscosity parameter of the Free component showed to change over time, even if the micropolarity remained almost unaffected. Figure 5 shows the variation of t as a function of the equilibration time for the Free (interface) component in the absence and presence of S. marinoi. Interestingly, in this case too, the variation of the parameter is well fitted by using an exponential growth model. This means that S. marinoi cells, interacting in increasing amounts at the plastic surface over time, are progressively compressing the medium drops at the cell/plastic interface.

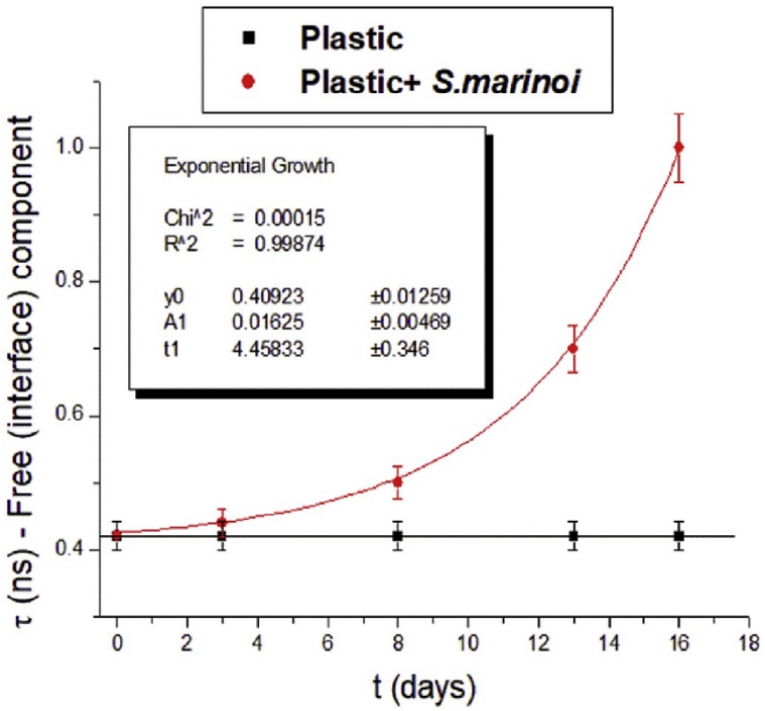

Figure 5. Variation of the microviscosity parameter, t, as a function of the equilibration time for the Free (interface) component of plastic samples in the absence and presence of S. marinoi.

Going back to Figure 4, the computations of the interacting components also show interesting trends. First, the micropolarity parameter, A_{ZZ}, significantly decreases for the CAT12 probes from the solution (38.4 G) to the plastic-interacting conditions (34 G). This means that these probes are approaching the hydrophobic plastic surface, in spite of the charged heads containing the nitroxide radical groups, promoted by the presence of the hydrophobic C12 chain. Therefore, surfactants and lipids like CAT12 well interact with the plastic surface in the seawater. The occurrence of strong interaction is proved by the high value of the microviscosity parameter, t. This strong interaction cannot match with a weak hydrophobic interaction, but the increase in line width provides another piece of information: the occurrence of cooperative interaction, that is, the formation of CAT12 aggregates at the plastic surface. So, the surfactants and lipids well interact with the plastic surface by forming aggregates. However, the situation is different in the absence and presence of the S. marinoi, as better demonstrated by analyzing Figure 6, which shows the variations of the microviscosity parameter, t (Figure 6A), and the line width (Figure 6B) as a function of the equilibration time for the Interacting component in the absence and presence of S. marinoi.

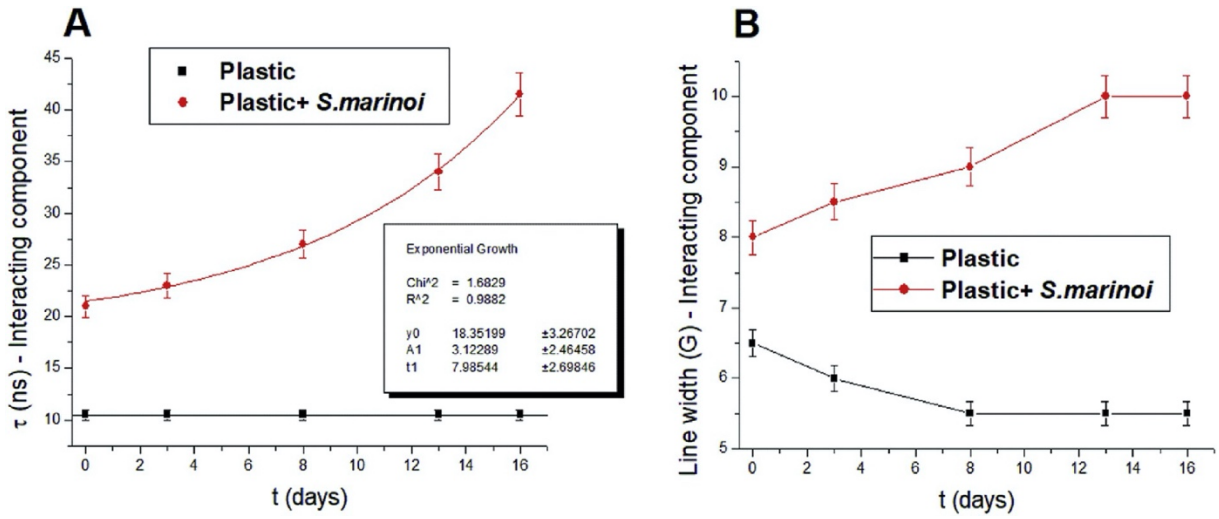

Figure 6. Variation of the microviscosity parameter, t (A), and the line width (B) obtained from EPR spectra computations as a function of the equilibration time for the Interacting component in the absence and presence of S. marinoi.

Again, the increase of the microviscosity parameter as a function of the incubation time in the presence of S. marinoi is fitted by an exponential growth model, indicating that S. marinoi cells are exponentially increasing their adhesion to the plastic, by means of low-polar interactions of the lipid aggregates, arising from the cell membrane. The line width also increases, even if this increase does not follow an exponential pattern, but an almost linear increase from 0 to 13 days and then it remains nearly unchanged from 13 to 17 days. However, we must take into consideration that this increase is lower than expected since it probably compensates the decrease in line width found between 0 and 8 days in the absence of S. marinoi. This decrease indicates that the CAT12 surfactants redistributed at the plastic surface in the 0-8 days range of time. Conversely, in the presence of S. marinoi, CAT12 surfactants cooperated with S. marinoi cell membrane lipids to form more packed aggregates, progressively (exponentially) crammed on the plastic surface over time. The exponential growth tested by EPR for S. marinoi at the plastic surface is in good agreement with the results described in Figure 1.

3.2.2 Dinoflagellate Lingulodinium polyedrum interactions with plastic surface

L. polyedrum cultured samples show different results with respect to S. marinoi. However, the EPR spectra and components of L. polyedrum samples and their computations look similar to those shown for S. marinoi in Figs. 2 and 4 and Figure S1 in the SI. Some examples of the interacting components and their computations for L. polyedrum samples are shown in the Supplementary Information (Figure S1). Figure 7 reports the variations over the equilibration time of the following parameters: the adsorbed percentage (A); the intensities (in form of percentage) of the supernatant of plastic, in the absence and presence of L. polyedrum, and for the L. polyedrum culture (B); the relative percentage of interacting component (C); the correlation time for the rotational diffusion motion of the probe, t, for the interacting (D) and the free (E) components, measuring the microviscosity, and, in turn, the strengths of interaction. For a better comparison with the results from S. marinoi samples, the same parameters variation range is considered in the Y-axis for the two cells samples. It is interesting to note that all the parameters are lower and/or undergo to a lower increase over time for L. polyedrum if compared to S. marinoi in the presence of plastic, in

agreement with lower adsorption and interaction with the plastic surface for the former with respect to the latter cell culture. This is also in agreement with the adhesion rates shown for the two algae species in Figure 1. Further information is obtained by analyzing in detail the shape of the parameter variation, as follows:

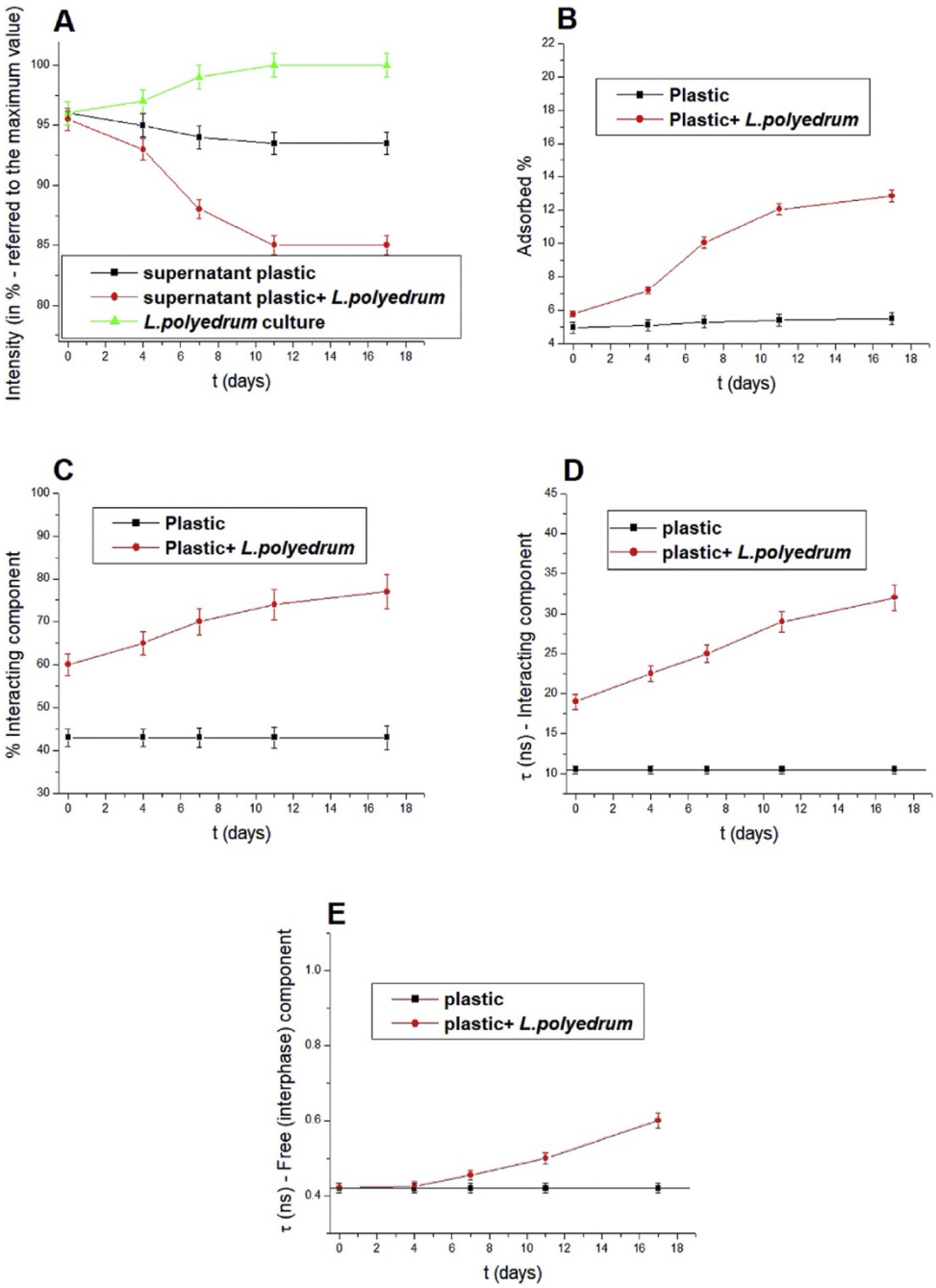

Figure 7. Variations over the incubation time of the following parameters obtained from the analysis of the EPR spectra of L. polyedrum samples: the intensities (in form of percentage) of the supernatant of plastic, in the absence and presence of L. polyedrum, and for the L. polyedrum culture (A); the adsorbed percentage (B); the relative percentage of interacting component (C); the correlation time for the rotational diffusion motion of the probe, t, for the interacting (D) and the free (E) components, measuring the microviscosity, and, in turn, the strengths of interaction.

The variations in the intensity of the EPR spectra of the super- natant solutions over time of L. polyedrum (Figure 7A) and S. marinoi (Figure 3A) in the presence of the plastic are in line with the variations of the adsorbed percentage in Figs. 7B and 3B. In the presence of plastic, in the first hours (mainly between 4 and 7 h) the adsorbed amount is higher for L. polyedrum (Figure 7A and B) with respect to S. marinoi (Figure 3A and B). The cellulose external frustule of the large (30 mm) L. polyedrum cells well adsorbs the CAT12 probes in the plastic interface when the cells precipitate on the surface. However, the L. polyedrum cells poorly adhere to the plastic surface and "roll" on the surface impeding further probe adsorption. Conversely, the silica external frustule of the smaller (10 mm) S. marinoi cells interacts with the plastic surface. Therefore, the CAT12 probes adsorbed at the cell surface follow the cell/plastic adhesion process, which is exponentially increasing over time. It is worth to note the difference in intensity variation between the two cell cultures in the absence of plastic (Figure 7A versus Figure 3A). In detail, for L. polyedrum the CAT12 intensity increases over time, mainly between 4 and 7 h. This indicates that the cellulose casing of these cells well entraps the CAT12 probes with a kinetics of 7 h, also justifying the increased adsorbed percentage of probes in this time range in Figure 7B, but it poorly interacts with the plastic surface. Conversely, the decrease in intensity for CAT12 adsorbed by S. marinoi cells culture (Figure 3A) is ascribed to a partial internalization of the probes into the cells, getting in touch with antioxidants in the cytosol. Therefore, the exponential increase of the adsorbed percentage for S. marinoi in the presence of the plastic (Figure 3B) is purely due to the increased adsorption/adhesion of the cells with the plastic surface, related to the interaction of the amorphous-silica cell surface with the plastic surface. Further information comes from the evaluation of the percentage of the interacting component, shown in Figure 7C for L. polyedrum, to be compared with the graph in Figure 4 for S. marinoi. For this latter cell culture, in the presence of plastic, the percentage of interacting component is already higher at t = 0 with respect to L. polyedrum. However, the percentage of interacting component for S. marinoi slowly increases in the first hours, boosting after 8 h. This boost, as discussed above, is related to the exponentially-increasing adhesion of S. marinoi onto the plastic. However, unlike S. marinoi, L. polyedrum shows an increase in the percentage of the interacting component since the first hours while the increase is very poor in the latest hours. This different behavior may be nicely related to different interactions of the two different cell cultures with the probe and the plastic surface, as already discussed for the intensity and adsorbed percentage variations (Figs. 3A-B and 7A-B). The probes adsorbed on the S. marinoi silica surface partially enter the cells and "disappear" in the cytosol, from the EPR point of view, due to the antioxidants. The remaining probes are able to monitor the cell adhesion on the plastic surface by means of low-polar interactions of lipid aggregates. Conversely, the probes are adsorbed at the external L. polyedrum surface when the cells precipitate on the plastic surface in the drying process, but then the cells roll on the plastic surface without adhering to it, and the percentage of interacting probes cannot increase anymore. The process of rolling on the plastic surface modifies the interacting strength of the probe at the L. polyedrum cell interface, which increases over time (Figure 7D). Here we have to remember that the interacting probes are those already inserted into the cell membrane, since the C12 chain of the probes enter the lipidic area of the membrane, while the CAT group is embedded in the phospholipid heads layer. However, this interacting-probes fraction is almost absent for the cell cultures in the absence of the plastic, because the CAT group containing the nitroxide radical is free to move at the cell surface. Only plastic adhesion creates this interacting fraction, and, therefore, it reports about the interacting mode and strength. We see that, for both S. marinoi and L. polyedrum, the probes are compressed in the cell/plastic interface thus increasing the per-

centage of the interacting component. We suppose that the cell/ plastic interaction forces the probes to deeper enter the cell membrane interface decreasing their mobility. For S. marinoi the exponential increase accounts for the progressive increase in the strength of interaction because the probes are able to penetrate in the cell interface and measure the adhesion strength of the cells that grow on the plastic. For L. polyedrum the interaction strength is much lower, mainly at the earlier times, due to the poor adhesion of these cells with the plastic. Final confirmation of the different interacting behavior of the two cells cultures with the plastic is obtained by comparing the interacting strength parameter, t, for the free (interface) component, in Figure 5 for S. marinoi and in Figure 7E for L. polyedrum: the latter only reach 0.6 ns after 17 h (Figure 7E), while S. marinoi shows a value of 1 ns at 17 h of incubation. The weakly interacting probes better report about the cell-plastic interactions than the strongly interacting probes, being well exposed at the external surface of the cells and directly feeling the plastic adhesion. The plastic adhesion is therefore quite poor for L. polyedrum if compared to S. marinoi. The line width variation is not reported in Figure 7 for L. polyedrum, because its variation is almost absent over time. Conversely, the increase of line width over time is quite significant for S. marinoi (Figure 6B). The line broadening indicates that, in the S. marinoi case, the binding occurs at sites quite close to each other. This accounts for the interaction of lipid aggregates at the S. marinoi/plastic interface, while the lipids are poorly aggregated when L. polyedrum precipitates on the plastic surface and then rolls over the surface.

4. Conclusions

The analysis of the EPR spectra of CAT12 probes adsorbed on the plastic surface in absence and presence of two different species of marine phytoplankton, diatom S. marinoi and dinoflagellate L. polyedrum, provides useful information about the mechanism of adhesion of the microalgae on the plastic surface floating on seawater. The CAT12 probes, mimicking the cell membrane components, show that packed cell-components aggregates stabilize at the plastic surface in presence of S. marinoi, with an exponentially increasing adsorption as a function of the incubation time. Conversely, L. polyedrum shows lower adsorption than S. marinoi, and a different mechanism of interaction with the plastic surface. Both the amount of probe adsorbed onto the plastic, and their interaction strength increase exponentially in the presence of S. marinoi, following its adhesion rate. Also, the drops of seawater, with a concentrated saline content, are compressed on the plastic surface by S. marinoi at the cell/plastic interface. After 17 days, an about 4-times lower amount of probe is adsorbed onto the plastic in absence S. marinoi, compared to the sample where this microalga is present. Similarly, the interaction strength is also about 4 times lower. Conversely, L. polyedrum shows a reduced interaction strength with the plastic surface, mainly at the earlier times. The probes are initially adsorbed by L. polyedrum cells when they precipitate on the plastic surface; but, then, we suppose that these cells start rolling on the plastic surface, due to their poor adhesion to the plastic, favored by their almost cellular spherical shape. Therefore, the probe binding to the plastic is largely prevented and only those adsorbed into the porous cellulose casing of L. polyedrum cells remain trapped. The silica frustule of S. marinoi cells is more permeable to the probes, mimicking the surfactants/lipids behavior, and the probes, which remain at the external cell surface, well monitor the exponential growth of S. marinoi cells at the plastic surface. The siloxane groups of the silica frustule are involved in the binding with the hydrophobic plastic surface and the C12 chain of the spin probes. This study demonstrates that the use of selected paramagnetic probes and an accurate computer-aided analysis of the EPR spectra, combined with biological tests, help to in-situ clarify the

interactions occurring between biological structures and pollutants, or, more importantly, the plastic debris, which are more and more invading the oceans.

Acknowledgements

This article is based on work from COST Action CA 17140 "Cancer Nanomedicine from the Bench to the Bedside" supported by COST (European Cooperation in Science and Technology).

Supplementary Information

Figure S1: Computations of Interacting components. The main parameters used for computation (τ, and line width) are listed in the legends. The spectra are normalized in heights (intensity in the y-axis =1).

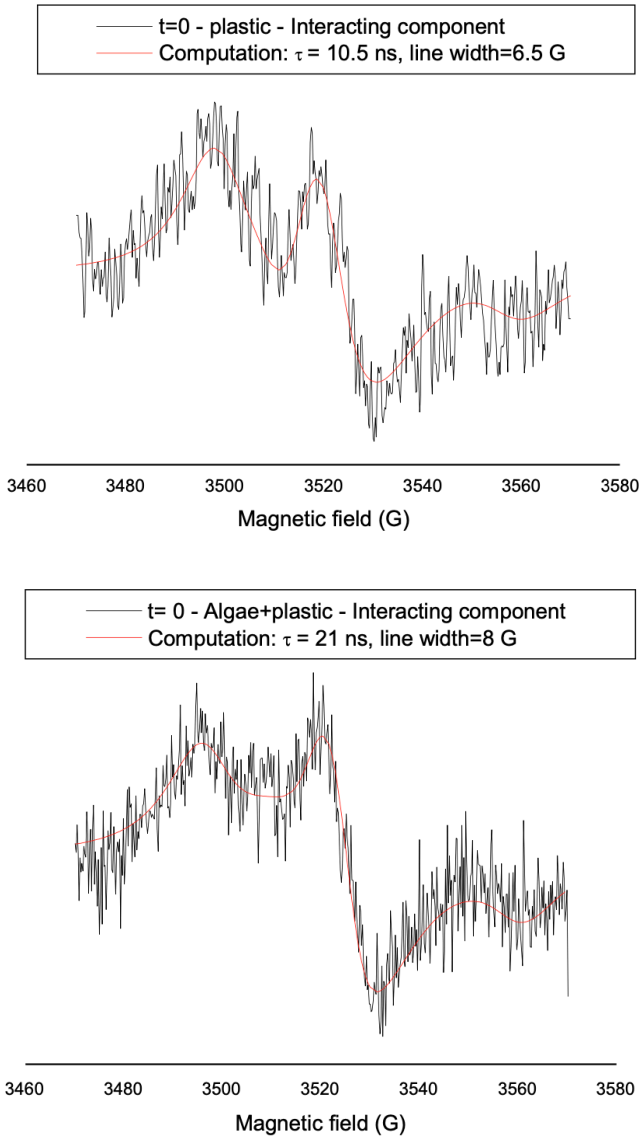

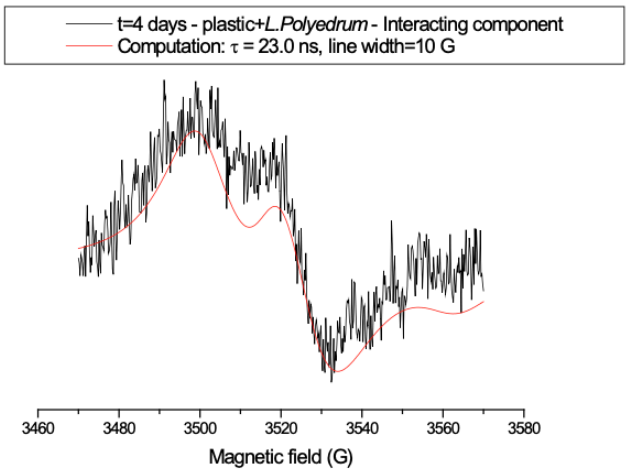
t=4 days - plastic+L.Polyedrum - Interacting component
Computation: τ = 23.0 ns, line width=10 G
3460
3480
3500
3520
3540
3560
3580
Magnetic field (G)

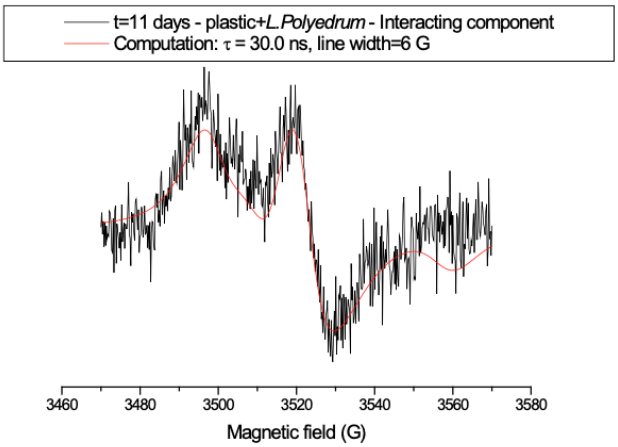
t=11 days - plastic+L.Polyedrum - Interacting component
Computation: τ = 30.0 ns, line width=6 G
3460
3480
3500
3520
3540
3560
3580
Magnetic field (G)

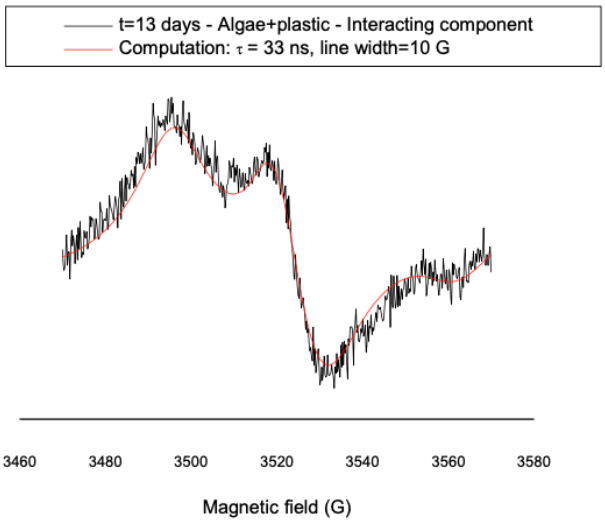
t=13 days - Algae+plastic - Interacting component
Computation: τ = 33 ns, line width=10 G
3460
3480
3500
3520
3540
3560
3580
Magnetic field (G)

References

1. Andrady, A.L., 2011. Microplastics in the marine environment. Mar. Pollut. Bull. 62, 1596e1605.
2. Andreozzi, E., Antonelli, A., Cangiotti, M., Canonico, B., Sfara, C., Pianetti, A., Bruscolini, F.A., Sahre, K., Appelhans, D., Papa, S., Ottaviani, M.F., 2017. Interactions of nitroxide-conjugated and non-conjugated glycodendrimers with normal and cancer cells and biocompatibility studies. Bioconjug. Chem. 28, 524e538.
3. Bakker, D.P., Klijnstra, J.W., Busscher, H.J., Van der Mei, H.C., 2003. The effect of dissolved organic carbon on bacterial adhesion to conditioning films adsorbed on glass from natural seawater collected during different seasons. Biofouling 19, 391.
4. Bhattacharya, P., Lin, S.J., Turner, J.P., Ke, P.C., 2010. Physical Adsorption of Charged Plastic nanoparticles affects algal photosynthesis. J. Phys. Chem. C 114 (39), 16556e16561.
5. Budil, D.E., Lee, S., Saxena, S., Freed, J.H., 1996. Nonlinear-least-squares analysis of slow-motion EPR spectra in one and two dimensions using a modified Levenberg-Marquardt algorithm. J. Magn. Reson. Ser. A 120, 155e189.
6. Carson, H.S., 2013. The incidence of plastic ingestion by fishes: from the prey's perspective. Mar. Pollut. Bull. 74 (1), 170e174.
7. Casabianca, S., Capellacci, S., Grazia, M., Dell, C., Tartaglione, L., Varriale, F., Penna, A., 2019. Plastic-associated harmful microalgal assemblages in marine. Environ. Pollut. 244, 617e626.
8. Casabianca, S., Penna, A., Capellacci, S., Cangiotti, M., Ottaviani, M.F., 2018. Silicification process in diatom algae using different silicon chemical sources: colloidal silicic acid interactions at cell surface. Colloids Surfaces B Biointerfaces 161, 620e627.
9. Cole, M., Lindeque, P., Fileman, E., Halsband, C., Goodhead, R., Moger, J., Galloway, T.S., 2013. Microplastic ingestion by zooplankton. Environ. Sci. Technol. 47 (12), 6646e6655.
10. Cozar, A., Echevarría, F., Gonzalez-Gordillo, I.J., Irigoien, X., Úbeda, B., Hernandez-Leond, S., Palmae, A.T., Navarrof, S., García-de-Lomas, J., Ruizg, A., Fernández-de-Puellesh, M.L., Duartei, C.M., 2014. Plastic debris in the open ocean. Proc. Natl. Acad. Sci. U.S.A. 111, 10239e10244.
11. Deriu, M.A., Cangiotti, M., Grasso, G., Licandro, G., Lavasanifar, A., Tuszynski, J.A., Ottaviani, M.F., Danani, A., 2017. Self-assembled ligands targeting TLR7: a molecular level investigation. Langmuir 33 (50), 14460e14471.
12. Derraik, J.G.B., 2002. The pollution of the marine environment by plastic debris: a review. Mar. Pollut. Bull. 44, 842e852.
13. Fang, X., Hou, X., Li, X., Hou, W., Nakaoka, M., Yu, X., 2017. Ecological connectivity between land and sea: a review. Ecol. Res. 33 (1), 51e61.
14. Farrell, P., Nelson, K., 2013. Trophic level transfer of microplastic: Mytilus edulis (L.) to Carcinus maenas (L.). Environ. Pollut. 177, 1e3.
15. Fazey, F.M., Ryan, P.G., 2016. Biofouling on buoyant marine plastics: an experimental study into the effect of size on surface longevity. Environ. Pollut. 210, 354e360.
16. Guillard, R.R.L., 1975. In: Smith, W.L., Chanley, M.H. (Eds.), Culture of Phytoplankton for Feeding Marine Invertebrates, Culture of Marine Invertebrate Animals. Plenum Press, New York, pp. 26e60.
17. Hammer, Ø., Harper, D.A.T., Ryan, P.D., 2001. PAST: paleontological statistics software package for education and data analysis. Palaeontol. Electron. 4, 1e9.
18. Horton, A.A., Dixon, S.J., 2017. Microplastics: an introduction to environmental transport processes. WIREs Water 5, e1268.
19. Kiessling, T., Gutow, L., Thiel, M., 2015. Marine litter as habitat and dispersal vector.In: Bergmann, M., Gutow, L., Klages, M. (Eds.), Marine Anthropogenic Litter. Springer International Publishing, pp. 141e181.
20. Kontogiannopoulos, K.N., Dasargyri, A., Ottaviani, M.F., Cangiotti, M., Fessas, D., Papageorgiou, V.P., Assimopoulou, A.N., 2018. Advanced drug delivery nanosystems for Shikonin: a calorimetric and electron paramagnetic resonance study. Langmuir 34 (32), 9424e9434.

21. Long, M., Moriceau, B., Gallinari, M., Lambert, C., Huvet, A., Raffray, J., Soudant, P., 2015. Interactions between microplastics and phytoplankton aggregates: impact on their respective fates. Mar. Chem. 175, 39e46.
22. Mishraki, T., Ottaviani, M.F., Shames, A.I., Aserin, A., Garti, N., 2011. Structural effects of insulin-loading into HII mesophases monitored by EPR, SAXS, and ATR-FTIR. J. Phys. Chem. B 115 (25), 8054e8062.
23. Moriceau, B., Long, M., Paul-pont, I., Lambert, C., Huvet, A., Soudant, P., 2017. Interactions between polystyrene microplastics and marine phytoplankton lead to species-specific hetero-aggregation. Environ. Pollut. 228, 454e463.
24. Nguyen, H., Chen, Q., Paletta, J., Harvey, P., Jiang, Y., Zhang, H., Boska, M., Ottaviani, M.F., Jasanoff, A., Rajca, A., Johnson, J., 2017. Nitroxide-based macromolecular contrast agents with unprecedented transverse relaxivity and stability for magnetic resonance imaging of tumors. ACS Cent. Sci. 3 (7), 800e811.
25. Obbard, R.W., Sadri, S., Wong, Y.Q., Khitun, A.A., Baker, I., Thompson, R.C., 2014. Global warming releases microplastic legacy frozen in Arctic Sea ice. Earth's future 2, 315e320.
26. Oberbeckmann, S., Martin, A.C., Lo€der, M.G.J., Labrenz, M., 2015. Marine microplastic-associated biofilms - a review. Environ. Chem. 12, 551e562.
27. Ottaviani, M.F., El Brahmi, N., Cangiotti, M., Coppola, C., Buccella, F., Cresteil, T., Mignani, S., Caminade, A.M., Costes, J.P., Majoral, J.P., 2014. Comparative EPR studies of Cu(II)-conjugated phosphorous-dendrimers in the absence and presence of normal and cancer cells. RSC Adv. 4, 36573e36583.
28. Ottaviani, M.F., Pregnolato, M., Cangiotti, M., Fiorani, L., Fattori, A., Danani, A., 2012. Spin probe analysis of microtubules structure and formation. Arch. Biochem. Biophys. 522, 1e8.
29. Passow, U., 2002. Transparent exopolymer particles (TEP) in aquatic environments. Prog. Oceanogr. 55 (3e4), 287e333.
30. Reisser, J., Shaw, J., Hallegraeff, G., Proietti, M., Barnes, D.K., Thums, M., Wilcox, C., Hardesty, B.D., Pattiaratchi, C., 2014. Millimeter-sized marine plastics: a new pelagic habitat for microorganisms and invertebrates. PLoS One 9, e100289.
31. Van Sebille, E., England, M.H., Froyland, G., 2012. Origin, dynamics and evolution of ocean garbage patches from observed surface drifters. Environ. Res. Lett. 7, 044040.
32. Windsor, F.M., Durance, I., Horton, A.A., Thompson, R.C., Tyler, C.R., Ormerod, S.J., 2019. A catchment-scale perspective of plastic pollution. Glob. Chang. Biol. 25 (4), 1207e1221.
33. Zettler, E.R., Mincer, T.J., Amaral-Zettler, L.A., 2013. Life in the 'plastisphere': microbial communities on plastic marine debris. Environ. Sci. Technol. 47, 7137e7146.

GENERAL CONCLUSIONS

General considerations

Electron paramagnetic resonance spectroscopy proved a powerful ally, granting to gain unique information on the studied systems.

In drug discovery, we exploited EPR to get a real-time picture of the drug path inside biological systems. We could deeply characterize Cu(II) complexes, which cannot be studied through NMR due to the aforementioned paramagnetic activity. Finally, we could define the kind of interaction of dendrimers and metallodendrimers with both model and real cell membranes, opening the way to a deep understating of the mode of action of such molecules.

Although EPR is applicable to paramagnetic systems only, the spin-probe technique makes this spectroscopy versatile for a wide range of applications. We could in fact study the physical interaction of living cells and microplastics with the help CAT12 radical, in an unprecedented approach to the very urgent issue of bio-pollution.

The main conclusions of the previously exposed works are here reported:

Chapter 1: Carbosilane metallodendrimers as promising antitumoral agents

a. Ru(II)-conjugated carbosilane metallodendrimers show a high degree of interaction with model membranes, highly dependent on dendrimer generation. Generation 1 is internalized by CTAB micelles, while generation 2 prefers to superficially interact with egg lecithin liposomes.
b. -NH_2 terminated heterofunctional metallodendrimers mainly produce electrostatic interaction with model membranes, due to the positive charge of primary amines at physiological pH. Such interaction would probably lead to a high degree of toxicity in-vivo, and such samples were discarded from future experiments.
c. Ru(II) coordination on the carbosilane skeleton slightly lowers the interaction, but improves molecule solubility in water-based mediums.
d. In Cu(II)-conjugated metallodendrimers, copper ligands play a decisive role in the interaction with both tumoral and healthy cells. -Cl produces a long-lasting interaction, makes the molecule more hydrophobic and promotes a penetrative of the molecule into cell membranes. NO_3 has more of a counterion character, making the molecule more hydrophilic and therefore soluble. It promotes more electrostatic interactions with cell membranes.
e. The synthetized carbosilane Cu(II)-conjugated metallodendrimers show a partial degree of selectivity for U937 tumoral cells, with a less toxic effect exerted on PBMC, proving good candidates for *in-vivo* testing.
f. Two different coordination geometries were found for Cu(II)-conjugated metallodendrimers in EPR studies with model membranes. The predominant one for -Cl samples is distorted square planar Cu-N_2O_2, while for nitrate compounds a second geometry arose, Cu-O_4, highlighting the difference in the solubility of the two complexes.
g. *In-vivo* testing of the antitumoral activity of Cu(II) metallodendrimers showed IC_{50} in the low micromolar ranges for many different types of cancer. In particular, results obtained against PC3 cells are superior to those obtained with similar Ru(II) conjugated systems. In general, generation 1, nitrate-coordinated compounds proved the best candidates for ex-vivo testing.
h. An ex-vivo experiments, with mice models of PC3 prostate cancer was conducted, resulting in a 37% tumor size reduction after 55 days of treatment, with no casualties nor significant weight change in the animals.

Chapter 2: A potential Wilson's Disease treatment

a. G4-DOTA-Mal is a promising copper chelator, due to its strong coordination properties. The stability pf the complex is not significantly affected by the interaction with membrane models, making the system suitable for *in-vivo* studies.

b. Two different coordination geometries were found analyzing the glycodendrimer-copper system:

1) A highly distorted square planar Cu-N_2O_2 coordination, with two nitrogens belonging either to the DOTA structure or to the inner nitrogens of the dendritic scaffold, is the predominant geometry of the complex
2) A Cu-O_4 component, with copper surrounded by water molecules, only arises when the system is saturated, indicating a high coordination potential.

c. G4-DOTA-Mal and its Cu(II) complexes are not internalized by the membrane models. This desirable behavior could prevent glycodendrimer toxicity in the future *in-vivo* studies, allowing the molecule to exert its activity in extracellular fluids.

Chapter 3: An environmental pollution case

a. It is possible to monitor the physical interaction between plastics and phytoplankton in synthetic seawater medium *via* electron paramagnetic resonance technique, with the help of CAT12 probes.

b. *S. marinoi* interacts significantly with PET microplastics, showing high adhesion potential and possibly giving birth to a process of biofouling and long-range biological pollution.

c. *L. polyedrum* doesn't show a particular affinity for PET microplastics. EPR data show how this specimen "rolls" on the plastic surface, with no risk of biofouling. The adhesion rate is very little, and the population growing on plastic is neglectable if compared to the free floating one.